



**UNIVERSIDAD NACIONAL  
AUTÓNOMA DE MÉXICO  
FACULTAD DE CIENCIAS**

---

---

**“Estudio de Luminiscencia y  
Fotoconductividad en Películas  
Delgadas de ZnO con Fase Amorfa  
y Fase Wurtzita”**

**TESIS**  
QUE PARA OBTENER EL TÍTULO DE  
**FÍSICO**  
PRESENTA  
**Juan Luis Manríquez Zepeda**



**FACULTAD DE  
CIENCIAS  
UNAM**

**DIRECTORA DE TESIS:  
Dra. Ma. Guadalupe Valverde Aguilar**

**2008**



Universidad Nacional  
Autónoma de México

Dirección General de Bibliotecas de la UNAM

**Biblioteca Central**



**UNAM – Dirección General de Bibliotecas**  
**Tesis Digitales**  
**Restricciones de uso**

**DERECHOS RESERVADOS ©**  
**PROHIBIDA SU REPRODUCCIÓN TOTAL O PARCIAL**

Todo el material contenido en esta tesis esta protegido por la Ley Federal del Derecho de Autor (LFDA) de los Estados Unidos Mexicanos (México).

El uso de imágenes, fragmentos de videos, y demás material que sea objeto de protección de los derechos de autor, será exclusivamente para fines educativos e informativos y deberá citar la fuente donde la obtuvo mencionando el autor o autores. Cualquier uso distinto como el lucro, reproducción, edición o modificación, será perseguido y sancionado por el respectivo titular de los Derechos de Autor.

---

---

1.- Datos del alumno

Manríquez  
Zepeda  
Juan Luis  
59 71 00 56  
Universidad Nacional Autónoma de México  
Facultad de Ciencias  
Física  
097134723

2.- Datos del Tutor

Dr.  
Maria Guadalupe  
Valverde  
Aguilar

3.- Datos del Sinodal 1

Dr.  
Jorge Alfonso  
García  
Macedo

4.- Datos del Sinodal 2

Fis.  
René  
Ortega  
Alvarado

5.- Datos del sinodal 3

Dr.  
Federico  
González  
García

6.- Datos del sinodal 4

Dr.  
Gerardo Jorge  
Vázquez  
Fonseca

7.- Datos del trabajo escrito

Estudio de Luminiscencia y Fotoconductividad  
En Películas Delgadas de ZnO con Fase Amorfa y Fase Wurtzita  
68 p  
2008

---

---

## AGRADECIMIENTOS

Con Especial Afecto a Mis Padres.

A la Dra. Ma. Guadalupe Valverde Aguilar por todo el apoyo brindado a éste proyecto.

Al Dr. Jorge Alfonso García Macedo quien me brindó todos los recursos posibles para la realización de esta tesis.

A mis sinodales, por su apoyo en enriquecer el contenido de este proyecto

Dr. René Ortega Alvarado

Dr. Federico González García

Dr. Jorge Gerardo Fonseca.

Muchas Gracias a los Compañeros Colaboradores del Laboratorio de Rayos X y del Laboratorio de Microscopía Electrónica por Todo el Apoyo Prestado.

Al Profesor José Luis Gutiérrez Sánchez muchas gracias por motivar mi gusto por ésta carrera.

Gracias a los Profesores de Facultad de Ciencias por Dedicarnos un poco de su Tiempo.

A Guíllermína Aguilera muchas Gracias.

A Todos Mis Amigos.

Gracias a la  
Universidad Nacional Autónoma de México

Y a los Proyectos de Investigación apoyados por CONACYT 79781, NSF-CONACYT, PUNTA, ICYTDF y PAPIIT 116506-3.  
Agradezco el apoyo otorgado por las becas DGAPA y CONACYT.

# Índice

Resumen .....	4
Introducción .....	6
<b>Capítulo 1</b> .....	7
1.1. Propiedades del óxido de Zinc (ZnO). .....	8
1.1.1. Aplicaciones Tecnológicas.....	9
1.2 La Fase Cristalina del ZnO: La Wurtzita.....	11
1.3 El Proceso Sol-Gel. ....	12
1.3.1 El Método Alcóxido en el Proceso Sol-Gel.....	13
1.3.2 El Método de las Sales en el Proceso Sol-Gel. ....	15
1.4. Técnica de Spin-Coating .....	16
1.5. Absorción Óptica.....	17
1.6. Luminiscencia.....	22
1.7 Espectroscopia de Infrarrojo.....	24
1.7.1 Usos del Espectro Infrarrojo .....	26
1.7.2 Los Modos de Vibración y Flexión .....	27
1.9 Fotoconductividad .....	27
<b>Capítulo 2</b> .....	33
2.1 Método Experimental.....	34
2.2 Preparación de las Muestras .....	34
2.3 Espectroscopia de Absorción Óptica.....	36
2.4 Espectrometría de Fluorescencia .....	37
2.5 Espectroscopia de Infrarrojo.....	38
2.6 Fotoconductividad .....	39
2.7 Difracción de Rayos X.....	40
2.8. Microscopia Electronica de Barrido (MEB) .....	40
2.9 Microscopia Electrónica de Transmisión (MET) .....	41
<b>Capítulo 3</b> .....	42
3.1 Espectro de Absorción Óptica .....	43
3.2. Calculo del la Energía de Band Gap por el Método Analítico .....	44
3.3 Espectros de Emisión y Excitación .....	45
3.4 Difracción de Rayos X.....	49
3.5 Análisis por Espectrometría Infrarroja.....	50
3.6. Medida del Ancho de la Película .....	54
3.7 Cálculo de Tamaños Promedio de los Cristales de ZnO .....	55
3.8 Fotoconductividad .....	57
<b>Conclusiones</b> .....	62
<b>Apéndice. Validación Experimental</b> .....	64
<b>Bibliografía</b> .....	65

---

---

## Resumen

El presente trabajo se enfoca al estudio de películas delgadas de ZnO con fase amorfa y fase cristalina preparadas por el método sol-gel. Como tal, se incluye desde la búsqueda bibliográfica de los trabajos y avances ya realizados en el tema, así como el estudio y la caracterización de películas delgadas de ZnO, y posteriormente el análisis y presentación de resultados.

Las películas fueron sintetizadas por la técnica sol-gel y depositadas en sustratos de vidrio y cuarzo por la técnica de spin-coating. Y para la producción de las películas cristalinas (fase wurtzita), éstas fueron sometidas a tratamientos de recocido.

En la caracterización de estas películas se emplearon las técnicas de absorción óptica, difracción de rayos X (DRX), luminiscencia, espectroscopia infrarroja (FTIR), fotoconductividad, microscopía electrónica de barrido (MEB) y microscopía electrónica de transmisión de alta resolución (HRTEM).

Por medio de los análisis de DRX se determinó que la fase wurtzita está presente en nuestras películas al recocerlas a 450 °C por 15 minutos. En esta película el espectro de absorción óptica consistió en una banda con un máximo en los 359 nm. Posteriormente mediante los espectros de fotoluminiscencia (PL) se observó que estas muestras tienen bandas de emisión en 409 nm, 455 nm y 576 nm al excitar en la longitud de onda obtenida a partir de los experimentos de absorción o sea en 359 nm; y de los espectros de excitación se obtuvo un poco más de información que permitió confirmar que la absorción en 359 nm es la más indicada para estimular portadores libres en las películas de ZnO con fase wurtzita.

---

---

Mediante los estudios de HRTEM se pudo calcular un tamaño promedio de los cristales de ZnO, el cual está entre 30 y 40 nm. Por medio del estudio de MEB se pudo calcular el espesor de las películas amorfa y con fase cristalina, obteniendo un promedio de  $3.36\mu\text{m}$  y de  $2.36\mu\text{m}$ , respectivamente. Además se determinaron las frecuencias de los modos vibracionales por FTIR, las cuales coinciden muy bien con lo esperado por ser una muestra formada a partir de acetato de zinc y otros compuestos orgánicos que después desaparecen por efecto del tratamiento térmico.

Los estudios de fotoconductividad permiten concluir que las películas con fase cristalina tienen mucho mejor transporte de cargas que las películas amorfas.

---

---

## Introducción

"Hasta hace muy poco el hombre aprovechó los materiales que se encuentran disponibles en la naturaleza; hoy en día este proceso empieza a sufrir un cambio cualitativo: ya no se trata de encontrar usos nuevos para cada material, sino de sintetizar los materiales más adecuados para los nuevos requerimientos de la civilización moderna."

Guillermo Aguilar Sahún

El siglo pasado fue de grandes avances científicos y tecnológicos, entre los que destacan el desarrollo de la teoría cuántica. Los mismos que ayudaron al desarrollo de tecnologías como son las telecomunicaciones, el láser y las primeras computadoras.

Pero quizás el avance más revolucionario de nuestra época ha sido el debido al estudio de los materiales empleando la teoría de la mecánica cuántica.

Un ejemplo de la importancia de esta materia lo vemos en lo sucedido con la televisión, el radio, el radar, etc. Este tipo de electrónica fue construida a base de bulbos. Los límites tecnológicos que presenta el bulbo se alcanzaron muy pronto, el sobrecalentamiento que había que controlar, el alto consumo de energía y la velocidad a la que se podía llegar a procesar datos usando las válvulas termoiónicas (los bulbos) hizo pensar seriamente a la industria tecnológica de los años cuarenta en superar éstos problemas.

Uno de los primeros logros en el estudio de los semiconductores fue la invención del transistor. El transistor

---

---

se convirtió en el sustituto perfecto del bulbo, haciendo mucho más que corregir sus dificultades.

Por otra parte este no ha sido el único logro del estudio de los materiales. El estudio de los nuevos materiales no solo ha permitido la miniaturización de la tecnología. Además, hay materiales que en conjunción con los avances en el área de la química sirven como filtros moleculares, como catalizadores en reacciones químicas, como emisores de luz, etc.

El presente trabajo de tesis expone los resultados obtenidos en la investigación de uno de los más importantes materiales que existen, las películas delgadas de ZnO, que entre sus cualidades tiene la de servir como catalizador en varios procesos, además de ser el mejor prospecto para la producción de emisión estimulada de luz ultravioleta (láser UV).

# **Capítulo 1**

## **Marco Teórico**

## 1.1 Propiedades del óxido de Zinc (ZnO).

El ZnO es un material con un alto punto de fusión de aproximadamente 2000°C, pertenece a la familia II-VI<sup>1</sup>: La diferencia de electronegatividades entre el zinc y el oxígeno produce un alto grado de ionicidad en su enlace. Esto produce una repulsión considerable entre las nubes de carga de átomos vecinos con igual carga eléctrica, haciendo que su estructura cristalina más estable sea la hexagonal tipo wurtzita. La Tabla 1.1.1 presenta algunas de las propiedades físicas más importantes de este material.

Propiedad	Símbolo (unidades)	Valor
Parámetros de red	a,c, (Å)	3.253, 5.213
Temperatura de fusión	T <sub>f</sub> (°K)	>2250
Densidad	ρ(Kg·m <sup>-3</sup> )	5675
Entalpía de formación	ΔH(Jmol <sup>-1</sup> )	6.5x10 <sup>3</sup>
Entropía de formación	ΔS(J·mol <sup>-1</sup> ·°K <sup>-1</sup> )	100
Calor específico	C <sub>p</sub> (J·mol <sup>-1</sup> ·°K <sup>-1</sup> )	41
Coeficiente de expansión térmica	α <sub>a</sub> (°K <sup>-1</sup> )	6.5x10 <sup>-6</sup>
	α <sub>o</sub> (°K <sup>-1</sup> )	3.0x10 <sup>-6</sup>
Conductividad térmica	λ(W·m <sup>-1</sup> ·°K <sup>-1</sup> )	0.6
Módulo de cizalladura	H(GPa)	44
Constantes elásticas (300K , 10 Gpa)	C <sub>11</sub> (Pa)	20.70
	C <sub>12</sub> (Pa)	11.77
	C <sub>13</sub> (Pa)	10.61
	C <sub>33</sub> (Pa)	20.95
	C <sub>55</sub> (Pa)	4.48
	C <sub>66</sub> (Pa)	0.45
Constantes dieléctricas	ε <sub>0  </sub> , ε <sub>0⊥</sub>	8.75, 7.8
	ε <sub>∞  </sub> , ε <sub>∞⊥</sub>	3.75, 3.70
Gap(2K)	E <sub>g</sub> (eV)	3.42
Gap(300K)	E <sub>g</sub> (eV)	3.35
Energía de enlace excitónico	E <sub>b</sub> (meV)	60
Masa efectiva de los electrones	m <sub>η</sub>	0.28·m <sub>0</sub>
Masa efectiva de los huecos	m <sub>ρ</sub>	0.58·m <sub>0</sub>

### 1.1.1. Propiedades físicas del ZnO

### 1.1.1 Aplicaciones tecnológicas.

El ZnO es importante por su amplia gama de aplicaciones industriales, entre las cuales la más extendida y tradicional ha sido su uso en la producción de goma, donde disminuye el tiempo de vulcanización, como pigmento en la producción de pinturas, así como su uso en la industria farmacéutica, en especial en el campo de la cosmetología, donde se utiliza como filtro de radiación ultravioleta en la producción de cremas solares<sup>1</sup>. Pero, han sido otras aplicaciones las que han mantenido el interés y la investigación en dicho material desde principios de la década de los 70's. Dentro de este grupo se incluye su uso en transductores acústicos, en varistores, en sensores de gas, en electrodos transparentes, como ventana óptica en celdas solares, etc.<sup>2, 3</sup>

Merece especial atención su posible aplicación en dispositivos optoelectrónicos. Por un lado, el hecho de poseer la misma estructura cristalina (con una diferencia del 2.0% y del 0.5 % para los parámetros  $a$  y  $c$ , respectivamente) que el GaN<sup>4</sup>, el material más estudiado hasta el momento para esta aplicación, le convierte en un excelente sustrato para su crecimiento heteroepitaxial. Por otro lado, el hecho de poseer un ancho de banda (bandgap) directo de 3.35 eV, a temperatura ambiente, le convierte en uno de los principales candidatos para actuar como elemento activo en el desarrollo de este tipo de dispositivos optoelectrónicos. Su alta energía de enlace excitónico puede permitir la emisión estimulada a temperaturas mayores a los valores ambientales (~550°K). Además, su módulo de cizalladura hace que sea un material mucho más estable que los demás compuestos de la familia II-VI, incluso más que otros semiconductores empleados tecnológicamente como es el GaAs. Todas estas propiedades han hecho que el estudio del ZnO haya crecido exponencialmente en estos últimos años, en especial después de la obtención de emisión estimulada a temperatura ambiente en capas de ZnO.

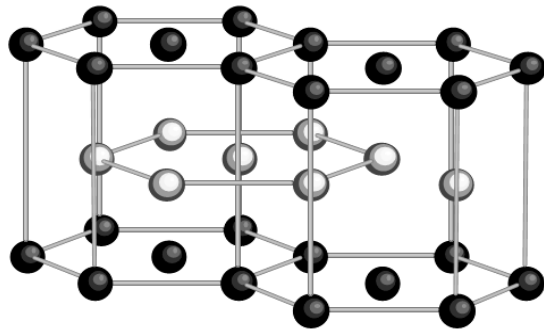
Los compuestos de ZnO contaminados con impurezas son usados como fotoconductores en electrofotografía, varistores cerámicos, elementos sensores en la detección de gases combustibles. En forma de películas delgadas exhiben propiedades piezoeléctricas, las cuales pueden ser usadas en varios transductores de presión y dispositivos acusto-ópticos. Contaminados con Al e I se les utiliza como electrodos conductores transparentes para construir pantallas fluorescentes debido a sus propiedades ópticas no lineales, y en celdas solares, en coloides hechos con ZnO se ven efectos de tamaño cuántico y de luminiscencia. El ZnO también se utiliza en la elaboración de fotodetectores, fotodiodos, diodos emisores de luz, agentes fotocatalíticos, moduladores de guía de ondas. Además, por ser el ZnO un material óxido semiconductor y por su bandgap a temperatura ambiente, se convierte en un potencial emisor de luz ultravioleta a temperatura ambiente (como lo son el ZnSe y el GaN).

Otra de las importantes propiedades de este material es la fotocatalisis, lo que significa que bajo iluminación, este material, puede degradar contaminantes orgánicos, tales como los del agua sucia<sup>5</sup>. En este aspecto el ZnO comparte esta propiedad con el TiO<sub>2</sub> cuyo bandgap también es de 3.2 eV. Pero a diferencia de este último, el ZnO no se degrada por la fotocorrosión. Como sensor de gases, se sabe que el ZnO es un buen sensor de metanol, etanol, alcohol propílico, LPG (por sus siglas en inglés Liquefied petroleum gas), monóxido de carbono, y del hidrógeno. Sin embargo, su preparación en películas presenta grandes ventajas sobre otros sensores, puesto que pueden ser fabricados en pequeñas dimensiones, y a gran escala, a un menor costo, además son altamente compatibles con la tecnología microelectrónica y de circuitos, adicionalmente la incorporación de contaminantes le puede dar mayor sensibilidad a la película de ZnO, por ejemplo contaminado con Al que es un buen detector de trimetilamina<sup>2</sup>.

## 1.2 La fase cristalina del ZnO: La Wurtzita

Originalmente la wurtzita es una de las formas cristalinas que toma el ZnS en estado natural<sup>6</sup>. Posteriormente se le asignó el mismo nombre a la fase cristalina del ZnO. Esta estructura es hexagonal con empaquetamiento compacto; esto es, la disposición de un número infinito de celdas unitarias esféricas de forma que ocupen la mayor fracción posible de un espacio infinito tridimensional (o lo que es lo mismo, que dejen el menor espacio vacío). Y consiste en átomos de zinc y oxígeno coordinados de forma tetraédrica, apilados según la secuencia ABABAB<sup>7</sup>.

En dichas estructuras los átomos se encuentran suficientemente alejados para compensar las repulsiones electrostáticas. Así, cada átomo de zinc se encuentra rodeado por un tetraedro de cuatro átomos de oxígeno y viceversa, lo que se puede apreciar en la figura 1.2.2.



**Estructura Hexagonal Compacta (HCP)**

Red: hexagonal

$$a_1 = a(1,0,0)$$

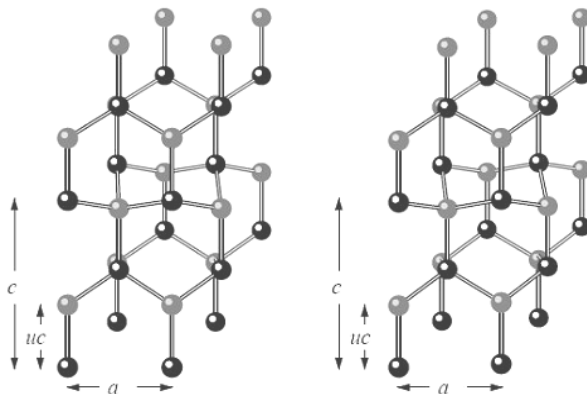
$$a_2 = a(-1/2, 3^{1/2}/2, 0)$$

$$a_3 = c(0,0,1)$$

Base: consiste de 2 átomos

$$(0,0,0)$$

$$(a_1/3, a_2/3, a_3/2)$$



### **Wurtzita**

Red hexagonal +

$$(0,0,0) \left( \frac{a}{2}, \frac{a}{2}\sqrt{3}, \frac{c}{2} \right)$$

(primera especie)

$$(0,0,0) \left( \frac{a}{2}, \frac{a}{2}\sqrt{3}, \frac{c}{2} + cu \right)$$

(segunda especie)

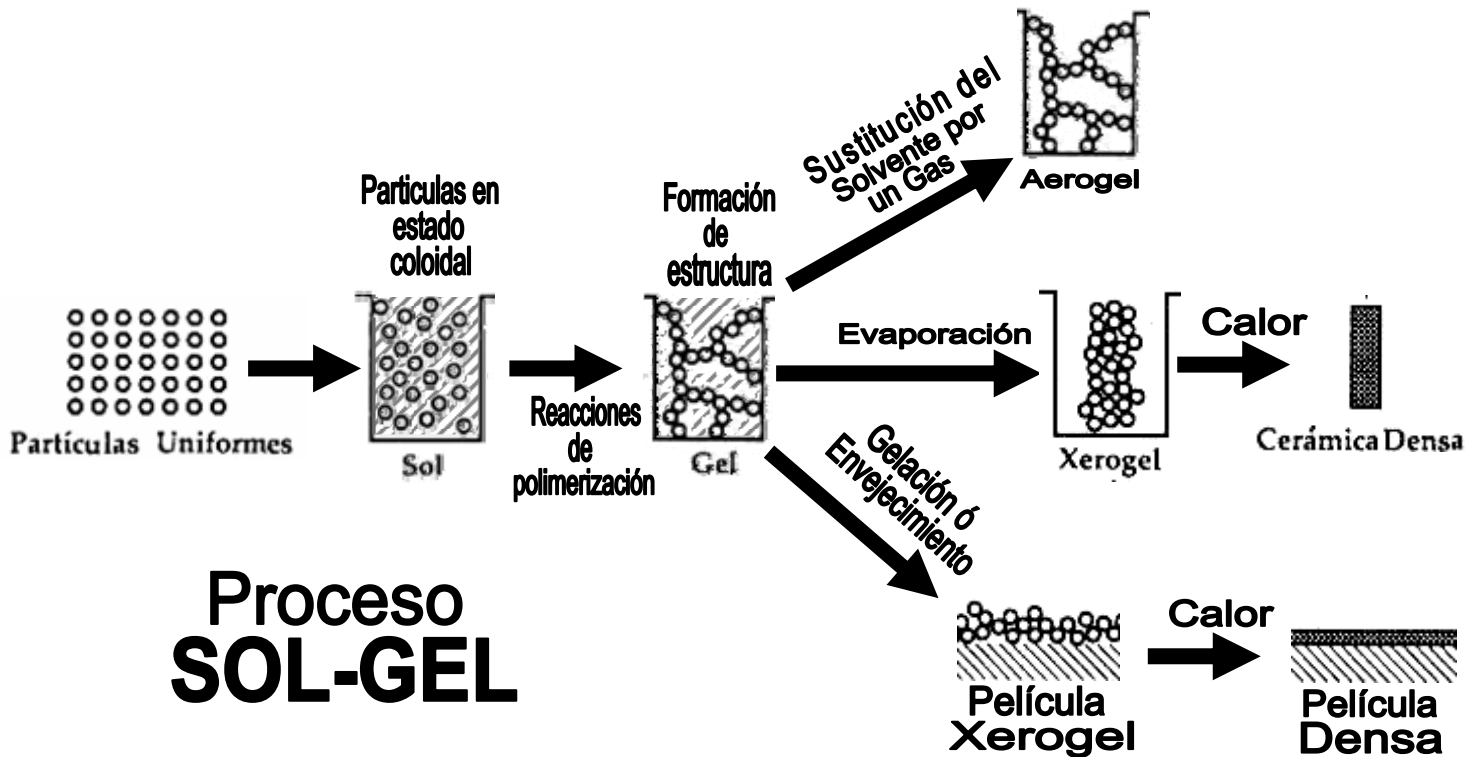
1.2.2. Estructura de la celda unitaria del ZnO. ● Oxígeno, ● Zinc

Los parámetros de la esta celda son:  $a = b = 0,381$  nm y  $c = 0,623$  nm. Esta estructura pertenece al grupo especial  $P6_3mc(C^4_{6v})$  y se puede describir como una combinación alternada de planos de átomos de oxígeno y de planos de átomos de zinc apilados a lo largo del eje  $c$ , con un desplazamiento entre ellos de  $0.38c$ , siendo  $c$  su parámetro de red en la dirección vertical.

### 1.3 El proceso sol-gel.

El proceso sol gel<sup>8</sup> es una ruta química que permite fabricar materiales amorfos y policristalinos de forma relativamente sencilla. Se pueden obtener nuevos materiales que por los métodos tradicionales de fabricación son muy difíciles de obtener, además de poder contaminarlos con iones de tierras raras ó colorantes orgánicos.

El proceso sol-gel permite la fabricación de materiales amorfos y policristalinos con características especiales en su composición y propiedades. El sol-gel es una ruta química que inicia con la síntesis de una suspensión coloidal de partículas sólidas o cúmulos en un líquido (sol) y la hidrólisis y condensación de éste sol para formar un material sólido lleno de solvente (gel). El solvente se le extrae al gel simplemente dejándolo reposar a temperatura ambiente durante un periodo de tiempo llamado envejecimiento, en el cual el gel se encogerá expulsando el solvente y agua residual. Al término del tiempo de envejecimiento por lo general aún se tienen solventes y agua en el material, además de que el tamaño del poro es considerable. Para solucionar esto, el material se somete a un tratamiento térmico, al final del cual obtendremos nuestro material en forma de monolito o de película delgada. El proceso sol-gel se esquematiza en la figura 1.3.1



### 1.3.1 El proceso sol-gel en la fabricación de películas y cerámicas densas.

#### 1.3.1 El método alcóxido en el proceso sol-gel.

En el proceso Sol Gel, el método alcóxido es el más utilizado. En este caso los precursores son alcóxidos metálicos. El proceso inicia con la fabricación de una solución que produce una red porosa por medio de reacciones de hidrólisis y polimerización.

En forma general, la elaboración de la solución se lleva a cabo con tres elementos: un alcóxido metálico, un alcohol y agua. Para geles de titanio o circonio se utiliza isopropóxido, propóxido y alcohol isopropílico.

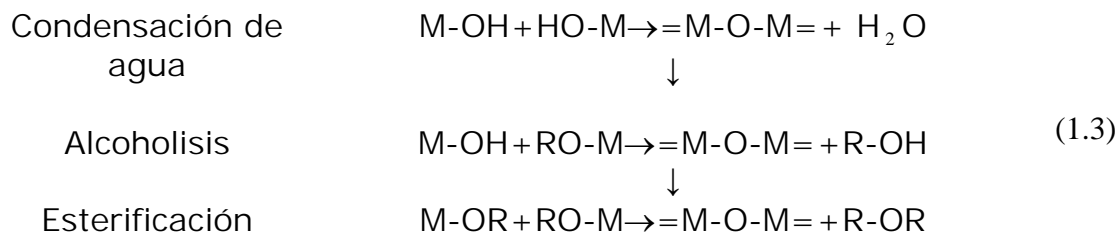
En esta etapa comienzan las reacciones que dan lugar a la gelación: la hidrólisis y la condensación. La ecuación siguiente describe el proceso de hidrólisis.





Donde M es el átomo metálico y R el radical alquilo.

Al mismo tiempo ocurren reacciones de polimerización que se pueden describir de la siguiente forma.



Donde los  $=M-O-M=$  son monómeros que tienen la propiedad de unirse y formar los polímeros. Las moléculas poliméricas pueden a su vez viajar en la solución y formar largas cadenas de polímeros. De tal manera que todas estas cadenas al unirse con otras cadenas dan lugar a la estructura del gel. El proceso es autosostenido por que los productos secundarios de las reacciones son nuevamente  $H_2O$ , OH y el alcohol.

Lo anterior significa que las reacciones de hidrólisis, polimerización y condensación siguen hasta que la viscosidad de la solución es tal que deja de fluir. Un gel se define como un material consistente de fases sólidas y líquidas continuas de dimensiones coloidales<sup>9</sup>, es decir existen polímeros (5-10 nm) a través de las cuales se puede viajar sin nunca entrar en contacto con la fase líquida (poros).

Posteriormente, se lleva a cabo un proceso de secado cuyo objetivo es la reducción y eliminación de los poros dentro del gel que contienen la fase líquida, lo que trae como consecuencia que los poros se vuelvan más pequeños y que el volumen total del disolvente dentro del gel disminuya. Dependiendo de las condiciones bajo las cuales se lleve a cabo el secado, lo que se puede obtener es un xerogel (condiciones normales) o un aerogel (condiciones supercríticas). Todo lo anterior tiene como efecto un

incremento entre las interacciones de las moléculas y la matriz. Finalmente, la densificación del gel puede llevarnos a la elaboración de una película ó una cerámica.

El método alcóxido permite obtener cerámicas como el PZT o PZTL, sin embargo, los alcóxidos de plomo son insolubles e inestables bajo almacenamiento<sup>9</sup>.

### 1.3.2 El método de las sales en el proceso sol-gel.

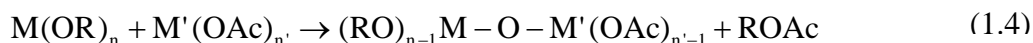
En el proceso sol-gel, también se puede obtener geles reduciendo el número de alcóxidos presente por medio del uso de sales, a condición de que éstas sean solubles en agua. La utilización de sales es muy útil cuando se emplean elementos de los grupos I y II, los cuales forman alcóxidos insolubles. Las sales utilizadas pueden ser las siguientes:

- citratos
- acetatos
- formatos
- tartaratos
- nitratos

La preparación por la vía sol gel utilizando sales consiste en formar una solución con todos los componentes tales como alcóxidos, enseguida se agregan las sales como solución en alcohol o agua. Entonces, toman lugar los procesos anteriormente descritos en el método alcóxido, para finalmente obtener una estructura gel con todos los componentes incorporados.

Dentro del grupo de sales, las que se utilizan principalmente son los acetatos y los nitratos<sup>10</sup>. El uso de estas dos sales es similar; sin embargo, la utilización de los nitratos es particularmente peligrosa por ser altamente oxidables. En lo concerniente a los acetatos, en sistemas de silicatos estos producen una gelación rápida gracias a su pH, la cual puede ser en parte retardada por medio del ácido acético. Una de las desventajas de los acetatos es que éstos no se degradan tan bien como los nitratos, lo cual provoca la existencia de residuos orgánicos.

La preparación por medio del método de sales es más complicada que en el método alcóxido, esto es porque al momento de entrar en contacto el alcóxido con la sal, la hidrólisis del alcóxido se realiza más rápidamente que la correspondiente degradación térmica u oxidativa del acetato. Para evitar la acumulación de grupos acetatos se utiliza el método de Thomas, el cual consiste en producir acetatos alquilo al combinar ciertos acetatos con alcóxidos, la ecuación que describe la reacción es la siguiente:



Donde la nomenclatura Ac representa el grupo  $-\text{COCH}_3$ .

Este proceso se consigue al calentar juntos el alcóxido y el acetato sin la presencia de ningún disolvente, es necesario que la razón entre alcóxido y acetato sea mayor que uno para producir una solución que pueda ser hidrolizada.

Entre los pares alcóxido-acetato que son utilizados en el proceso, algunos de los más conocidos son:

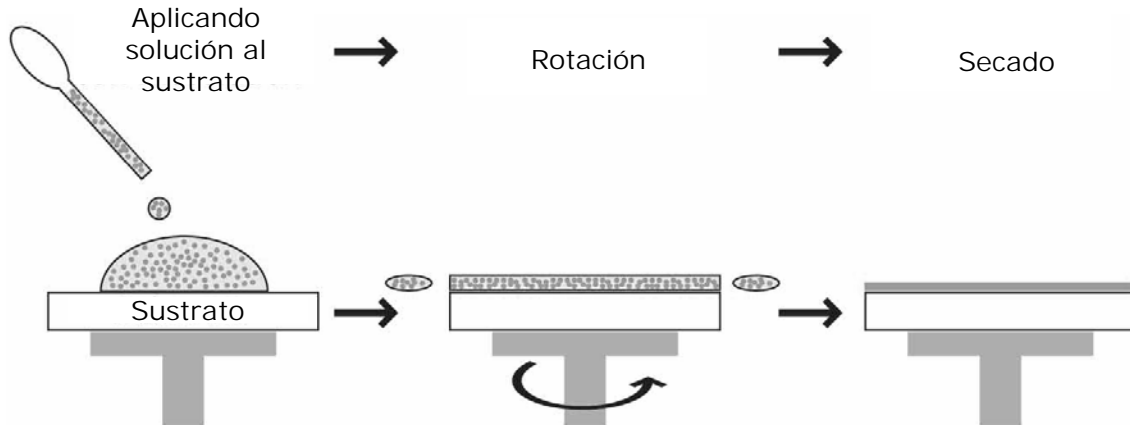
• Acetato de calcio-Alcóxido de aluminio	• Acetato de plomo-Alcóxido de silicio
• Acetato de zinc-Alcóxido de aluminio	• Acetato de plomo-Alcóxido de titanio

#### 1.4 Técnica de spin-coating

La técnica de spin-coating es un procedimiento utilizado para aplicar uniformemente películas delgadas a sustratos planos. Se coloca una gota de solución en un sustrato, el cual rota a altas velocidades de manera que se esparce el fluido por acción de la fuerza centrífuga<sup>11</sup>. A los equipos que realizan esta tarea se les conocen como spin-coater o spinner.

La velocidad de giro y la concentración de solución son determinantes en el espesor de la película resultante.

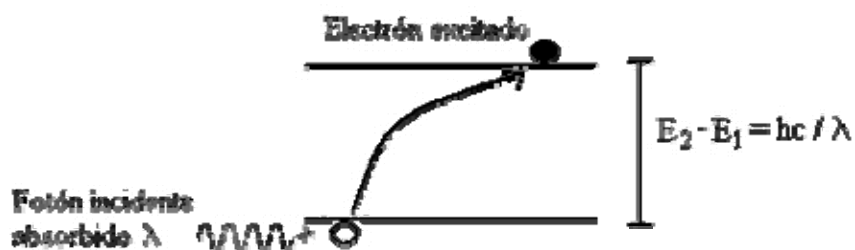
La técnica de spin-coating es ampliamente usada en la fotolitografía, en la fabricación de películas con espesores menores a los 10 nm, y para depositar fotorresistencias de cerca de un micrómetro de ancho.



*1.4.1. Técnica de Spin Coating. En un aparato llamado spinner, es depositada la solución de ZnO, luego la función del spinner es rotar la muestra para que por acción de la fuerza centrífuga ésta se esparza uniformemente formando una película al secarse.*

## 1.5 Absorción Óptica.

La espectroscopía de absorción óptica es muy útil para estudiar las propiedades ópticas de las películas delgadas. Al incidir sobre el sistema radiación electromagnética, los electrones que se encuentren en un estado de energía  $E_1$  pueden ser excitados al siguiente estado energético,  $E_2$ , si y solo si los fotones incidentes tienen una energía tal que  $E_2 - E_1 = \Delta E = hc/\lambda$  donde  $h$  es la constante de Planck,  $c$  es la velocidad de la luz y  $\lambda$  es la longitud de onda de estos fotones. Así, un fotón excita a un electrón llevándolo al estado  $E_2$ , siendo este reabsorbido por el átomo para cumplir con la conservación de la energía. A este proceso se le llama absorción óptica<sup>12</sup>, éste se ilustra en la figura 1.5.1.



### 1.5.1. Proceso de Absorción

Para entender el proceso de absorción se ha usado un modelo cuántico altamente simplificado como lo es el modelo de gas de electrones libres. Este modelo se basa en el hecho de que las moléculas son esencialmente planas, todos los átomos de la cadena conjugada están en un plano común y unidos por enlaces  $\sigma$ ; los electrones  $\pi$ , además de tener un nodo en dicho plano, forman una nube de carga arriba y debajo de él, a lo largo de la cadena conjugada, a una distancia de media longitud de enlace. Esto causa que el potencial electrostático para cualquier electrón  $\pi$  moviéndose en el campo del resto de la molécula pueda considerarse constante<sup>13</sup>.

Además, si se supone que la cadena conjugada, que se extiende una longitud de enlace a la izquierda y una a la derecha más allá de los átomos terminales, tiene longitud  $L$ , entonces la energía del  $n$ -ésimo eigenestado de dicho electrón  $\pi$  está dado por:

$$E_n = \frac{h^2 n^2}{8mL^2} \quad (1.5)$$

Con  $h$  la constante de Planck,  $m$  la masa del electrón y  $n$  el número cuántico que da el número de antinodos de la eigenfunción a lo largo de la cadena. De acuerdo al principio de Pauli, cada estado puede ser ocupado por dos electrones. Si se tienen  $N$  electrones, con  $N$  par que es el caso de las moléculas estables, entonces los  $N/2$  estados más bajos están

lentos y los demás superiores están vacíos. La absorción de un fotón con energía

$$\Delta E = \frac{hc}{\lambda} \quad (1.6)$$

con  $\lambda$  la longitud de onda de la radiación absorbida, excita un electrón de un estado ocupado a uno vacío, y por lo tanto la absorción a la mayor longitud de onda posible, ó lo que es lo mismo la que menos energía requiere para realizarse la transiciones:

$$E_{\min} = \frac{h^2}{8mL^2}(N+1) \quad \text{ó} \quad \lambda_{\max} = \frac{8mcL^2}{h(N+1)} \quad (1.7)$$

Por lo tanto, en primera aproximación, la posición de la banda de absorción solo depende de la longitud de la cadena conjugada  $L$  y el número de electrones  $\pi(N)$ . Para moléculas grandes, se ha encontrado gran concordancia entre las longitudes de absorción calculadas y las observadas, mientras que para moléculas pequeñas se ha tenido que considerar además la repulsión entre los electrones  $\pi^{14}$ .

Cuando sobre la superficie de un material dado incide radiación electromagnética, una parte es reflejada, mientras que la otra atraviesa el material y otra más es absorbida por él. El espectro de absorción es la región del espectro electromagnético que resulta absorbido. Puede ser encontrado con ayuda de un espectrofotómetro, un aparato que mide la cantidad de luz absorbida por la sustancia en cuestión al ser iluminada con diferentes longitudes de onda.

Un espectro de absorción se presenta usualmente como una gráfica de *densidad óptica (O.D., también llamada absorbancia) vs longitud de onda de la iluminación*. La densidad óptica es un parámetro cuyo significado puede

aclararse al considerar el siguiente modelo para la absorción: Supóngase que una muestra de cierto material es iluminada con luz que, en su superficie, tiene una intensidad  $I_0$ . Parte de la luz es reflejada y parte transmitida a través de la muestra.

La intensidad de cualquier onda electromagnética incidente en un medio sigue la ley de Bouguer-Lambert-Beer, de acuerdo a la cual la intensidad dentro del medio está dada por

$$I = I_1 e^{-\alpha(\lambda)d} \quad (1.8)$$

donde  $I_1 = I_0(1-R^2)$  (con  $R$  el coeficiente de reflexión del material) es la intensidad de la luz que logra penetrar en la muestra,  $d$  es la distancia recorrida por la onda electromagnética dentro de ella y  $\alpha(\lambda)$  es su *coeficiente de absorción óptica*, el cual está definido como el cambio relativo de la intensidad de la luz  $L(h\nu)$  a lo largo de la dirección de propagación:

$$\alpha \equiv \frac{1}{L(h\nu)} \bullet \frac{dL(h\nu)}{dx} \quad (1.9)$$

La razón entre la intensidad  $I_1$  que penetra en el material y la intensidad  $I$  que se observa después de recorrida una distancia  $d$  es un parámetro que revela la cantidad de luz absorbida por el objeto iluminado. La *densidad óptica (O.D.)* es el logaritmo de base 10 de este cociente, utilizado por razones de escala<sup>15</sup>. Puede entonces verse fácilmente que la densidad óptica está dada por:

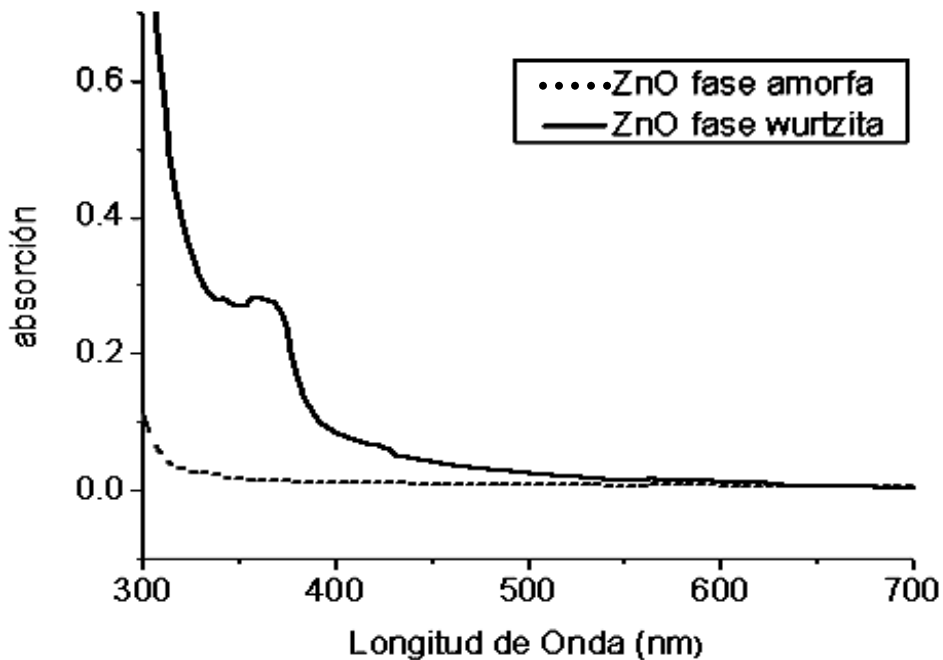
$$O.D. = \log_{10} \left( \frac{I_1}{I} \right) = \alpha d \log_{10}(e) \quad (1.10)$$

de manera que si se conoce el espesor  $d$  de la muestra estudiada, y se cuenta con un espectro en el cual está determinada la densidad óptica absorbida por ella, el

coeficiente de absorción  $\alpha$  se obtiene inmediatamente, despejando de la ecuación (1.10); y queda dado por

$$\alpha = \frac{O.D.}{d \log_{10}(e)} \quad (1.11)$$

En la figura 1.5.2 se aprecia un espectro característico de la absorción óptica. Puesto que la película se halla sobre un sustrato de vidrio, el espectro muestra la absorbancia (O.D.) del sistema película-sustrato, y no puede obtenerse directamente el coeficiente de absorción de la película a partir de él.



1.5.2. Espectros de absorción de una película de ZnO amorfa (línea punteada) y de una película de ZnO cristalina (wurtzita) (línea continua). El segundo espectro muestra una banda centrada en 359 nm.

Ahora bien, la línea sólida de la figura 1.5.2 representa el espectro de absorción óptica correspondiente al sistema ZnO wurtzita, la línea punteada representa el espectro del sistema ZnO amorfo.

## 1.6 Luminiscencia

La luminiscencia es el proceso de emisión de la luz por átomos o moléculas excitadas. Una molécula en el estado base es elevada al estado excitado debido a la absorción de fotones que tienen suficiente energía. Las moléculas excitadas experimentan una relajación vibracional del nivel de energía al que llegaron hacia el nivel más bajo del estado excitado mediante procesos no-radiativos y regresan al estado base emitiendo fotones. De este modo, los fenómenos de fluorescencia y fosforescencia entran dentro de esta definición. Las características de los espectros de ambos fenómenos pueden ser explicadas por medio de consideraciones orbitales moleculares.

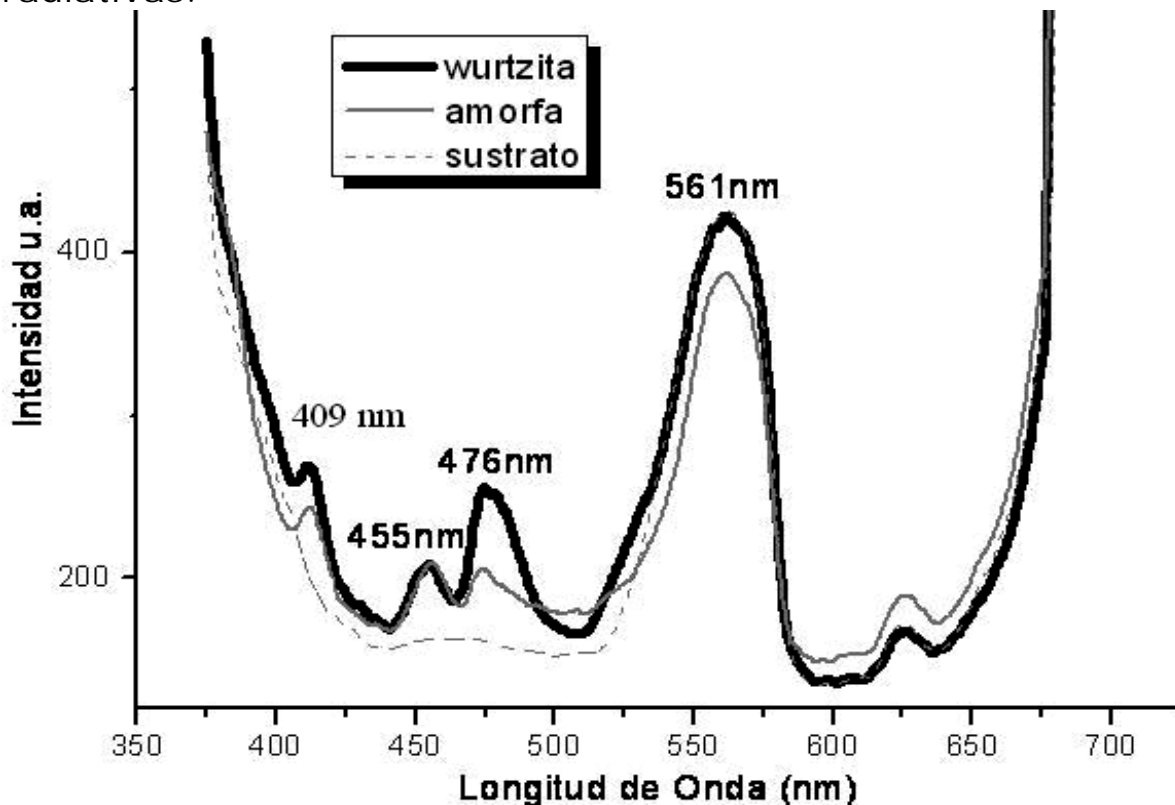
El principio de exclusión de Pauli establece que dos electrones en un átomo no pueden tener el mismo conjunto de los cuatro números cuánticos  $n$ ,  $l$ ,  $m$ ,  $s$ . La restricción requiere que no más de dos electrones pueden estar en un mismo orbital, además, los dos deberán tener los espines opuestos. Bajo estas circunstancias, se dice que los espines están apareados. Un estado electrónico molecular en el cual todos los espines de los electrones están apareados se llama estado singulete, y no se da una división de los niveles de energía cuando la molécula es expuesta a un campo magnético. Cuando uno de los dos electrones en una molécula es excitado a un nivel de energía más alto, un estado singulete o triplete es permitido. En el estado excitado singulete, el espín del electrón promovido está aun apareado con el electrón que está en el estado base; en el estado triplete, sin embargo, los espines de ambos electrones se desaparean.

Ya que las transiciones de absorción de un estado base singulete a un estado triplete son muy improbables, debido a que son espín prohibidas, solo se encuentra un electrón en algún estado triplete cuando decae a él desde el estado excitado de singulete inmediato superior. Este decaimiento llamado cruzamiento de sistemas, también es espín prohibido

por lo que es no radiativo (ocurre mediante fonones) y puede ocurrir debido a los acoplamientos espín-órbita ó a sustituyentes con núcleos más pesados<sup>13</sup>.

En términos de decaimiento se define a la fluorescencia como el decaimiento radiativo del estado singulete  $S_i$  al estado base  $S_0$ . Este decaimiento ocurre muy rápido, en alrededor de 1 ns. Por el contrario, el tiempo de vida media de los estados de triplete es muy grande. Es por esto que su decaimiento al estado base resulta en fosforescencia cuando se produce vía un fotón, pues también puede decaer mediante procesos no radiativos.

Un espectro de fluorescencia es casi igual al espectro de absorción, salvo un corrimiento de Stokes<sup>14</sup> de algunos nanómetros hacia el infrarrojo producto de las pérdidas no-radiativas.



1.6.1 Ejemplo de un espectro de emisión fluorescente realizado con un Fluorómetro Perkin Elmer.

La emisión fluorescente está condicionada por la estructura molecular de la sustancia fluorescente: los tipos de enlace electrónico, la rigidez de la molécula, las estructuras multicíclicas, los arreglos moleculares, la presencia de grupos donadores ó aceptores de electrones, la introducción de un átomo de número atómico elevado, etc.; y por otros factores dependientes del medio con el que interactúa: el tipo de disolvente, el nivel de pH, el oxígeno disuelto, la temperatura, etc.

Los estudios de luminiscencia se diferencian con respecto a los de absorción por<sup>15</sup>:

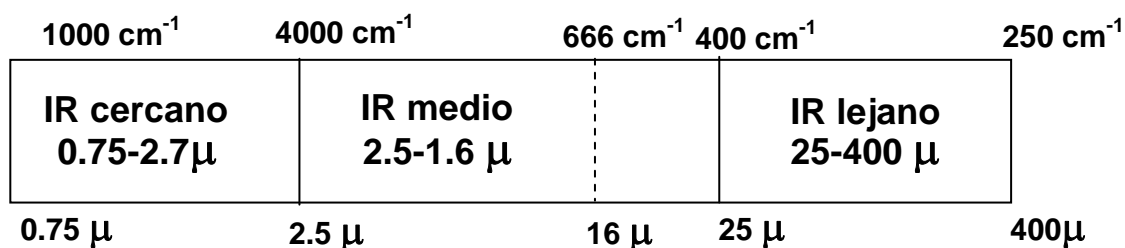
**Sensibilidad.** Los métodos de fluorescencia son más sensibles que los de absorción. En general, los métodos de fluorescencia suelen ser entre 10 y 100 veces más sensibles que los de absorción.

**Selectividad.** La selectividad de los métodos luminiscentes suele ser mayor que la de los de absorción: hay muchas especies capaces de absorber radiación, pero el número de ellas que puede reemitir es mucho menor; además en los métodos de luminiscencia tanto la longitud de onda de excitación, como la de emisión, pueden seleccionarse para minimizar interferencias, mientras que en espectrofotometría, solo la longitud de onda de absorción es seleccionable.

## **1.7 Espectroscopia de infrarrojo**

Casi todos los compuestos, tanto orgánicos como inorgánicos, tienen enlaces covalentes. Estos absorben varias frecuencias de la radiación electromagnética en la región del espectro infrarrojo. El espectro infrarrojo se caracteriza por las longitudes de onda más largas que aquellas del espectro de luz visible (400-800 nm). Pero de menor longitud que aquellas asociadas a las microondas. El espectro infrarrojo está comprendido entre los 0.8 y las 400  $\mu\text{m}$  y se debe a energía absorbida por vibraciones de los enlaces.

Debido a su gran amplitud se suele dividir en tres zonas: El infrarrojo cercano, medio y lejano, así nombrados por su relación con el espectro visible. El infrarrojo lejano (aproximadamente  $400\text{-}10\text{ cm}^{-1}$ ) se encuentra adyacente a la región de microondas, posee una baja energía y puede ser usado en espectroscopia rotacional. El infrarrojo medio (aproximadamente  $4000\text{-}400\text{ cm}^{-1}$ ) puede ser usado para estudiar las vibraciones fundamentales y la estructura rotacional vibracional, mientras que el infrarrojo cercano ( $14000\text{-}4000\text{ cm}^{-1}$ ) puede excitar sobretonos o vibraciones armónicas.



### 1.7.1 Zonas de la radiación infrarroja.

Siendo el IR medio el que generalmente se utiliza en la determinación estructural (2.5 - 16  $\mu$ ).

Debido a consideraciones de tipo histórico la unidad más usada en la espectroscopía infrarroja no es la longitud de onda ( $\lambda$ ) sino el número de onda ( $\kappa = 1/\lambda\text{ cm}^{-1}$ ). Además, esta unidad tiene la ventaja, que es directamente proporcional a la energía.

$$\kappa(\text{cm}^{-1}) = \frac{1}{\lambda(\text{cm})} \quad \nu(\text{Hz}) = \frac{c(\text{cm/s})}{\lambda(\text{cm})}$$

Como en otros tipos de energía, las moléculas son excitadas a estados superiores de energía cuando éstas absorben la radiación infrarroja. La absorción de radiación infrarroja es como otro proceso de absorción, un proceso cuántico<sup>16</sup>. Solo

cantidades discretas de energía de radiación infrarroja serán absorbidas por la molécula. La radiación en este intervalo de energía corresponde a estiramientos y flexiones en los enlaces de la mayoría de las moléculas. En el proceso de absorción, solo aquellas frecuencias de radiación infrarroja que coinciden con la frecuencia normal de vibración o con alguno de los modos normales de vibración de la molécula en cuestión serán absorbidas y la energía absorbida servirá para incrementar la amplitud del movimiento vibracional de los enlaces en la molécula. Debería notarse, sin embargo, que no todos los enlaces en la molécula son capaces de absorber energía infrarroja, aún si la frecuencia de radiación coincide exactamente con el movimiento del enlace. Solo aquellos enlaces que tienen un momento dipolar son capaces de absorber radiación infrarroja. Enlaces simétricos, como los del  $H_2$  o  $Cl_2$ , no absorberán radiación infrarroja. Un enlace debe presentar un dipolo eléctrico que esté a la misma frecuencia que la radiación entrante para que le pueda ser transferida una energía. El dipolo eléctrico del enlace puede acoplarse con el campo electromagnético de la radiación entrante. Los enlaces simétricos que son simétricamente sustituidos no absorberán en el infrarrojo.

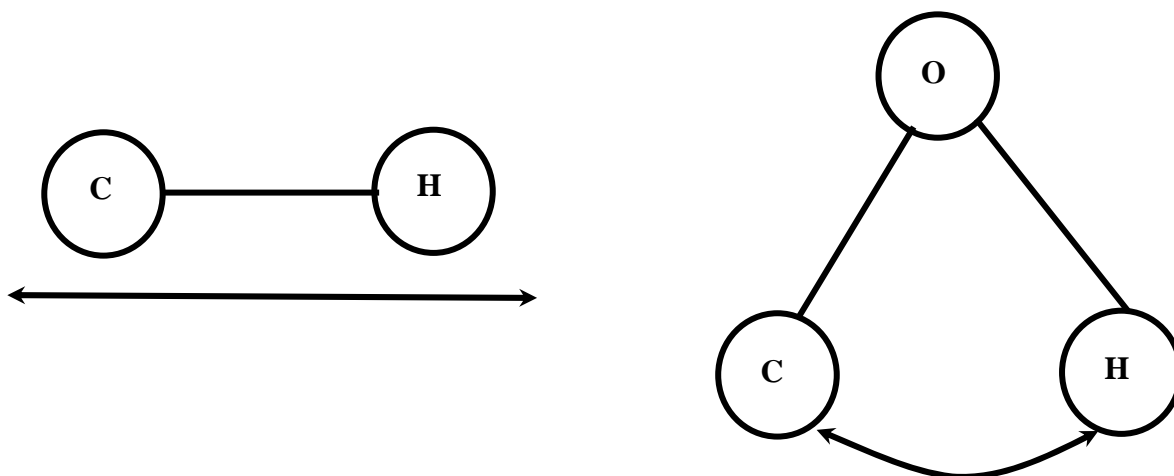
### **1.7.1 Usos del Espectro Infrarrojo.**

Ya que diferentes tipos de enlaces tienen una frecuencia de vibración natural diferente, y ya que el mismo tipo de enlace en dos diferentes compuestos está en un entorno ligeramente diferente, no hay dos moléculas de diferente estructura que tengan exactamente el mismo patrón de absorción infrarroja o mejor dicho el mismo espectro infrarrojo. Además aunque en algunos casos se absorba la misma frecuencia en dos muestras, en ningún caso de dos diferentes moléculas se obtendrá el mismo espectro infrarrojo. Entonces el espectro infrarrojo puede ser usado en moléculas tal como la huella digital en seres humanos.

Un segundo y más importante uso para el espectro infrarrojo es que éste nos da información estructural acerca de la muestra. La absorción de cada tipo de enlace (N-H, C-H, O-H, C-X, C=O, C-O, C-C, C=C, C≡C, C≡N, etc.) solo son encontradas en ciertas pequeñas porciones de la región del espectro vibracional infrarrojo. Un estrecho intervalo de absorción puede ser asociado a cada tipo de enlace. Fuera de este intervalo, cualquier tipo de absorción es debido a algún otro tipo de enlace.

### 1.7.2 Los Modos de Vibración y Flexión.

Hay dos tipos sencillos de movimiento en una molécula activada por absorción infrarroja, y estos son el de estiramiento y el de flexión. Todos los demás modos son combinaciones de estos.



1.7.2 Modos vibracionales de estiramiento y flexión

En general los modos de estiramiento asimétrico son más comunes que los simétricos a altas frecuencias y además los modos de estiramiento ocurren generalmente a mayores frecuencias que los de flexiones.

## 1.8 Fotoconductividad

Se define a la fotoconductividad<sup>17</sup> como el cambio en la conductividad eléctrica de un material como consecuencia de la absorción de fotones de radiación electromagnética<sup>18</sup>. El

fenómeno es el resultado de varios procesos, entre los cuales están la absorción de radiación, la fotogeneración de portadores de carga, la separación y transporte de estos portadores por efecto de un campo eléctrico aplicado, y la recolección de cargas en los electrodos para obtener una corriente.

En oscuridad la conductividad eléctrica está dada por la ecuación 1.12,

$$\sigma = e(n\mu_n + p\mu_p) \quad (1.12)$$

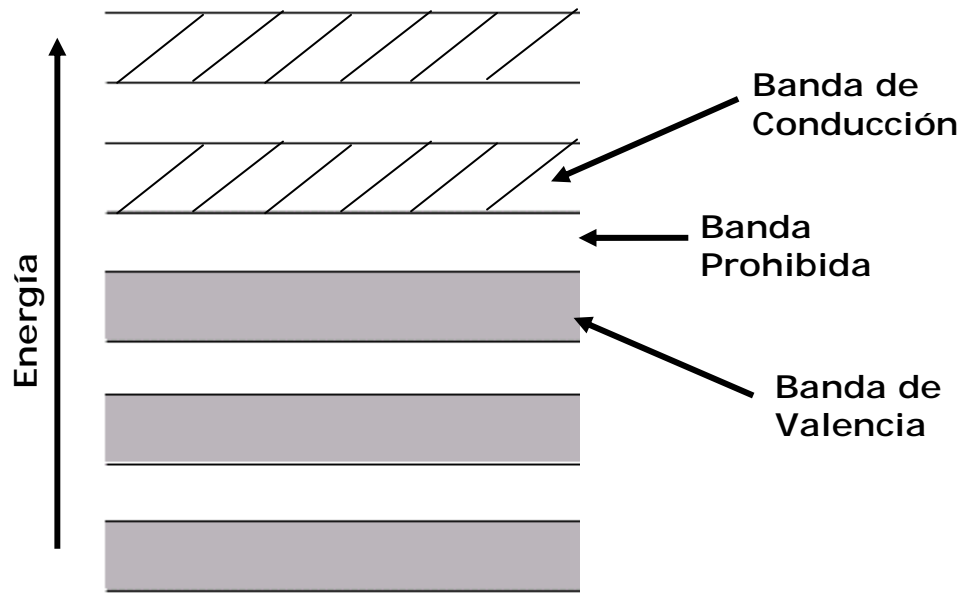
donde,  $n$  es el numero de portadores tipo N;  $\mu_n$ , la movilidad de los portadores tipo N y analogamente  $p$  es el numero de portadores tipo P y;  $\mu_p$ , la movilidad de los portadores tipo P<sup>19</sup>.

Como se hizo ver en la sección anterior, cuando el material es iluminado, la radiación produce carga adicional  $\Delta n$  y  $\Delta p$ , dando una fotoconductividad  $\sigma_{ph}$  expresada como

$$\sigma_{ph} = e(\Delta n\mu_n + \Delta p\mu_p) \quad (1.13)$$

En materiales inorgánicos covalentes la fotoconductividad es descrita con el modelo de bandas.

El modelo de bandas supone que una gran cantidad de átomos se unen, como en las estructuras sólidas donde el número de orbitales debidos a estos átomos es muy grande y la diferencia de energía entre cada uno de ellos es muy pequeña, tanto que, se puede considerar como si los niveles de energía conjunta forman bandas continuas de energía más que niveles discretos como ocurre en los átomos aislados.



*1.8.1. Representación esquemática de las bandas de energía en un sólido. El modelo de bandas en una simplificación ante el hecho de tratar con muchos átomos en un sólido. Los orbitales atómicos se traslapan produciendo un número discreto de orbitales moleculares en forma de bandas angostas de energía.*

Existen dos tipos de bandas, las de conducción y las de valencia, en las primeras se trata de electrones libres dentro de un material dispuestos para participar en la conducción eléctrica; en las de valencia se trata de electrones amarrados al sistema y que están típicamente en la última capa o nivel electrónico del átomo y participan en los enlaces moleculares pero no en la conducción eléctrica. Para que un electrón pase de su banda de valencia (similar al estado base) es necesario aportarle la energía suficiente para cruzar una banda prohibida (conocida como band gap) hasta la banda de conducción.

En fotoconductividad el modelo de bandas considera que existe fotogeneración de carga gracias a que la iluminación excita electrones de la banda de valencia a la de conducción. Pero es posible que en lugar de darse directamente la fotogeneración de portadores ocurran otros fenómenos: la absorción de luz provoca la formación de estados excitados

(conocidos como excitones), sujetos a varios procesos fotofísicos tanto radiativos (fluorescencia y fosforescencia) como no radiativos (conversión interna y cruce entre sistemas). Estos fenómenos se encuentran representados en la figura 1.8.3.

Los excitones pueden también viajar no radiativamente por varias moléculas, antes de ser desactivados en alguna de ellas. La generación de portadores puede ocurrir, por ejemplo, al observar el paso de un electrón de una molécula a otra vecina dando lugar a un estado excitado de transferencia de carga. Haciendo uso de un campo eléctrico externo presente, es posible generar portadores si la atracción coulombiana entre el par electrón-hueco se vuelve más pequeña que la energía térmica  $kT$  (donde  $k$  es la constante de Boltzmann y  $T$  es la temperatura absoluta en grados kelvin). Siendo, pues, la fotogeneración de portadores el resultado de varios procesos en competencia unos con otros.

Es conveniente definir la eficiencia cuántica primaria de fotogeneración ( $\phi$ ) como el número de portadores generados por cuanto de luz absorbido. Así, la eficiencia cuántica puede escribirse como

$$\phi = \frac{k_{ph}}{k_{ph} + k_n + k_{isc} + k_q[Q]} \quad (1.14)$$

donde  $k_{ph}$  es la tasa de producción de portadores,  $k_n$  la de procesos de desactivación no radiativos,  $k_{isc}$  la de transiciones al estado triplete,  $k_q$  la razón de procesos de captura de portadores y  $Q$  la concentración de centros de captura. Se sabe que  $\phi$  depende del coeficiente de absorción, de la temperatura y del campo eléctrico aplicado<sup>18</sup>.

Tomando en cuenta estos conceptos, es posible describir el transporte de carga en materiales aislantes con la ecuación

(1.15), que expresa la densidad de corriente observada bajo el efecto de un campo eléctrico y de una iluminación uniforme a cierta longitud de onda  $\lambda$ . El primer término de (1.15) es el transporte por efecto fotovoltaico, el segundo es la conductividad en la oscuridad y el tercero es la fotoconductividad propiamente dicha<sup>20</sup>:

$$J = \frac{q\phi l_o}{h\nu} \alpha I + \left( qn_o \mu + \frac{q\phi\mu\tau}{h\nu} \alpha I \right) E \quad (1.15)$$

$I$  es la intensidad de la iluminación (cuya energía es  $h\nu = hc/\lambda$ ),  $\phi$  es la eficiencia cuántica para excitar un portador libre,  $\mu$  es la movilidad de los portadores,  $E$  es el campo eléctrico aplicado,  $\alpha$  es el coeficiente de absorción para una longitud de onda dada,  $\tau$  el tiempo de vida media de los portadores excitados,  $n_o$  la densidad de portadores que producen la conductividad en la oscuridad y  $l_o$  es su camino libre medio. Con ayuda de esta ecuación pueden determinarse los parámetros  $\phi l_o$  y  $\phi\mu\tau$ , midiendo únicamente la intensidad de la iluminación, la conductividad en la oscuridad y la fotoconductividad. En efecto: si se realizan experimentos de fotoconductividad en los cuales se obtengan rectas  $E$  vs  $J$  en oscuridad y bajo iluminación (iluminación de longitud de onda e intensidad conocida), se despeja directamente de la ecuación 1.15 se llega a las siguientes expresiones para  $\phi l_o$  y  $\phi\mu\tau$ ,

$$\phi l_o = (b_i - b_d) \frac{hc}{e \alpha \lambda I} \quad (1.16)$$

$$\phi\mu\tau = (m_i - m_d) \frac{hc}{e \alpha \lambda I} \quad (1.17)$$

donde  $b_d$  y  $b_i$  son las ordenadas al origen de las rectas experimentales  $E$  vs  $J$  en oscuridad y bajo iluminación,

respectivamente, y  $m_d$  y  $m_i$  son las pendientes de tales rectas<sup>21</sup>. Se vuelve claro el hecho de que  $\phi I_0$  es proporcional a la diferencia entre la ordenada al origen en oscuridad y la ordenada bajo iluminación ( $b_d - b_i$ ). Mientras que  $\phi\mu\tau$  lo es a la diferencia entre la pendiente en oscuridad y la pendiente bajo iluminación ( $m_d - m_i$ ). Se concluye que  $\phi I_0$  guarda estrecha relación con el carácter fotovoltaico del material (una ordenada al origen bajo iluminación distinta de cero es la manifestación de un efecto fotovoltaico), mientras  $\phi\mu\tau$  depende de sus propiedades fotoconductoras (una pendiente bajo iluminación mayor a la observada en oscuridad indica un aumento de la conductividad en presencia de luz). Así, la magnitud de ambos parámetros revela qué tan fotovoltaico/fotoconductor es el sistema bajo estudio.

## **Capítulo 2**

# **Desarrollo Experimental**

## 2.1 Método Experimental.

A continuación se describe el proceso de síntesis de las películas y los estudios para su caracterización y determinación de sus propiedades luminiscentes y conductivas.

La solución precursora fue preparada por el método sol-gel. Posteriormente esta solución fue depositada sobre sustratos de vidrio o cuarzo por la técnica de *spin-coating* obteniendo películas uniformes y de alta calidad óptica.

El tratamiento térmico realizado sobre una porción del lote de muestras consistió en recocer las muestras a unos 450 °C por unos 15 minutos.

Otro lote de muestras fue preparado para los estudios de fotoconductividad. En la superficie de la película se colocaron electrodos con pintura de plata en los extremos.

Las películas se caracterizaron por absorción óptica, fotoluminiscencia, espectroscopía de Infrarrojo con transformada de Fourier (FTIR) y por difracción de rayos X (DRX). El grosor de la película fue medido por la técnica de microscopía electrónica de barrido (MEB), para ello las películas de ZnO fueron depositadas sobre sustratos de silicio. La rutina experimental incluyó varias repeticiones con el fin de garantizar la reproducibilidad del experimento.

## 2.2 Preparación de las muestras

La solución fue preparada usando acetato de zinc deshidratado ( $\text{Zn}(\text{CH}_3\text{COO})_2 \cdot 2\text{H}_2\text{O}$ ), etilenglicol ( $\text{HOCH}_2\text{CH}_2\text{OH}$ ), etanol ( $\text{CH}_3\text{CH}_2\text{OH}$ ) y glicerol ( $\text{HOCH}_2\text{CH}(\text{OH})\text{CH}_2\text{OH}$ ). En un matraz de Elenmeyer se mezclaron cantidades apropiadas de etilenglicol y de acetato de zinc deshidratado. Se hizo un reflujo de esta solución agitándola y manteniéndola a una temperatura constante de 150 °C por 15 minutos, hasta obtener una solución uniformemente transparente. Se dejó enfriar esta solución obteniendo un sólido quebradizo y transparente.

A este sólido se le agregó glicerol, trietilamina y etanol; y se agitó magnéticamente por dos horas obteniendo una solución incolora y transparente. Para remover polvo e impurezas, esta solución final fue filtrada usando papel filtro de poro grande. Las películas de óxido de zinc fueron depositadas por la técnica de spin-coating sobre sustratos de vidrio, cuarzo y silicio. Para esto, la solución precursora fue depositada sobre un sustrato de vidrio de dimensiones  $2.5 \times 2.5 \text{ cm}^2$  usando una pipeta de plástico y se utilizó una velocidad de 3000 rpm por 20 s. Después las películas fueron mantenidas en aire húmedo ( $\text{RH} = 40\%$ ) por 10 min. para facilitar la hidrólisis.

Se les dio un tratamiento térmico a una parte de las películas, calentándolas a  $450 \text{ }^\circ\text{C}$  por 15 minutos para obtener la fase cristalina wurtzita. La figura 2.2.1 muestra un diagrama de flujo de los pasos para la preparación de la película cristalina.

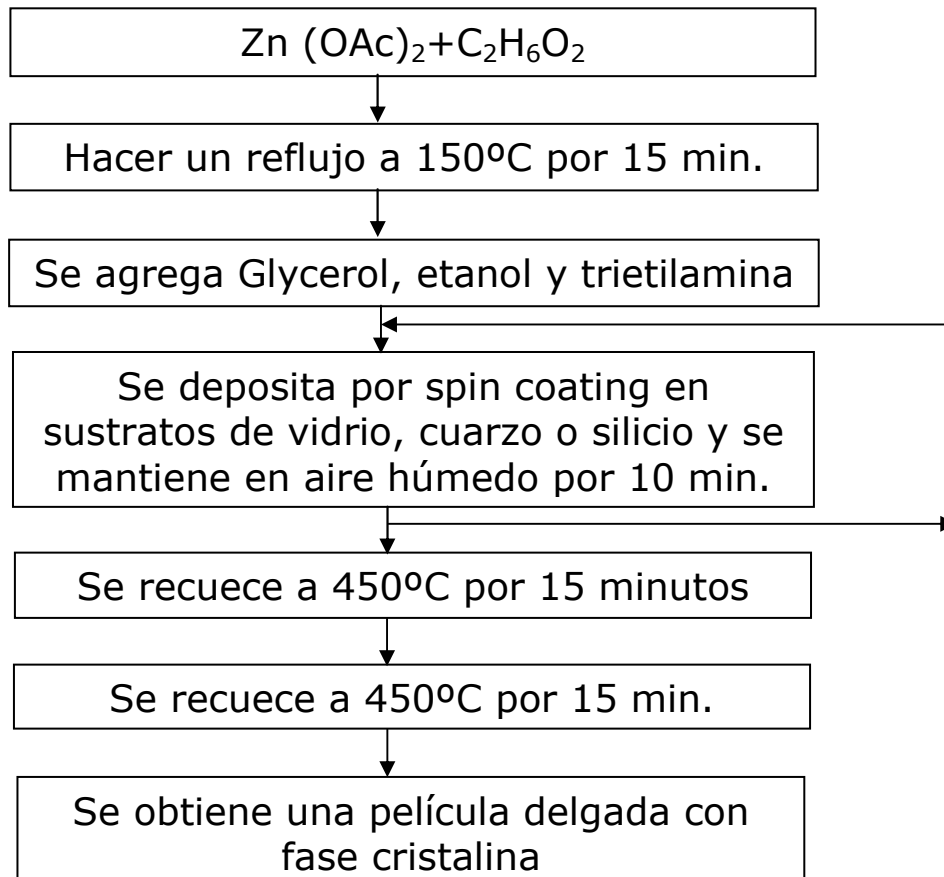
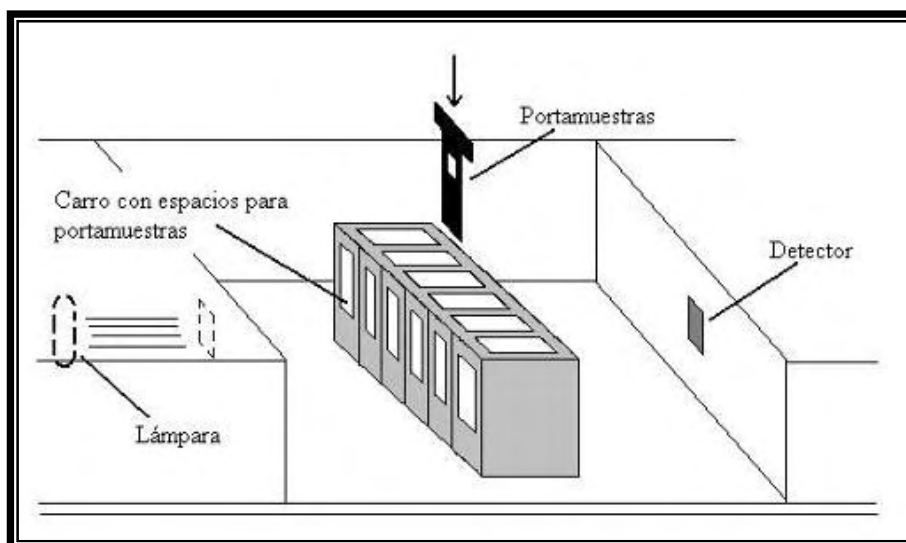


Figura 2.2.1 Esquema de preparación de las películas de ZnO con fase wurtzita.

## 2.3 Espectroscopia de Absorción Óptica

Se realizaron análisis de absorción óptica cada vez que eran sometida a tratamiento alguna de nuestras muestras. Esto con el fin de ver qué cambios se habían producido como resultado del cambio de estructura durante el tratamiento de recocido al que era sometido la muestra.

Para el estudio de absorción, se empleó el espectrofotómetro Genesis 2 y el programa *WinSpec*<sup>22</sup>.



2.3.1. *Esquema del espectrofotómetro Genesis 2. La muestra se coloca en el portamuestras y éste, en su lugar en el carro. Acto seguido, la lámpara emite radiación en las longitudes de onda deseadas y el detector en el otro extremo, registra la radiación transmitida.*

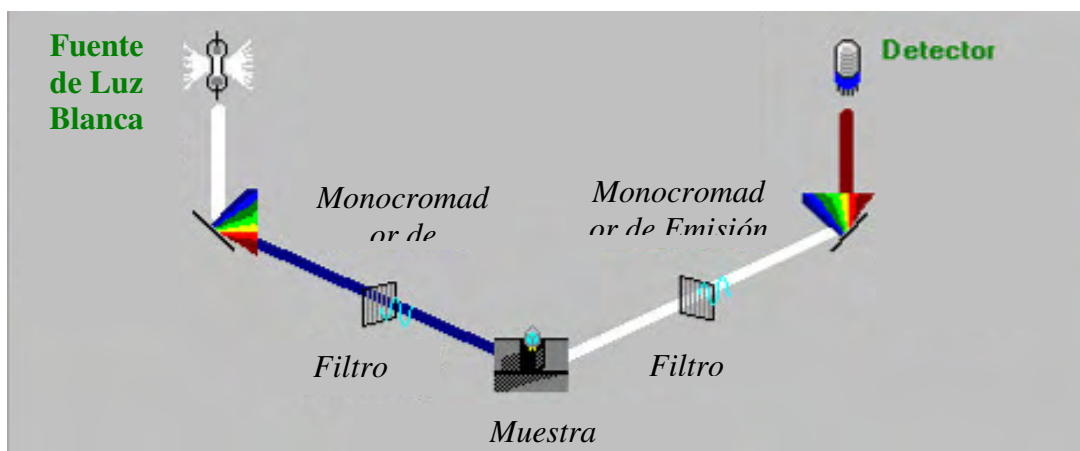


2.3.2 Espectrofotómetro Genesis para medir la absorción óptica.

## 2.4 Espectrometría de Fluorescencia

Para estudiar la luminiscencia, se obtuvieron los espectros de excitación y emisión óptica en el fluorómetro Perkin Elmer LS55, equipado con una lámpara de Xenón de 150 watts, dos monocromadores con intervalo de operación de 220 nm hasta 830 nm, con una resolución de 2 nm, y un fotomultiplicador R372F.

En el fluorómetro el haz de radiación emitido por la lámpara, dirigido a la muestra, pasa a través del monocromador de excitación donde se selecciona la longitud de onda que se desea incida en la muestra. El haz de radiación fluorescente emitido por la muestra, se dirige al monocromador de emisión donde se selecciona la longitud de onda de salida que se requiere monitorear. La señal llega al fotomultiplicador, y finalmente se envía a la computadora (figura 2.4.1).



2.4.1 Esquema del fluorómetro Perkin Elmer LS55.



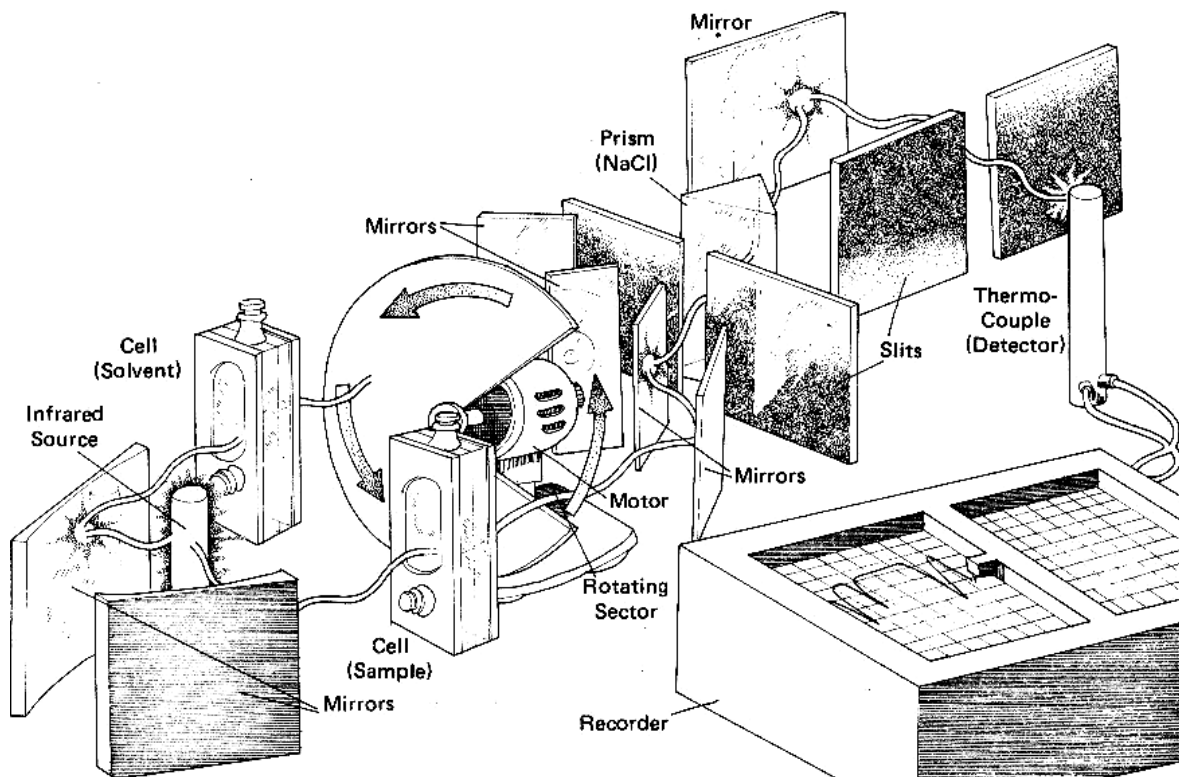
2.4.2 Fluorómetro Perkin Elmer LS55

El fluorómetro tiene un sistema automático que le permite realizar un barrido por las diferentes longitudes de onda, tanto en el monocromador de excitación, como en el de emisión<sup>23, 24</sup>.

## 2.5 Espectroscopia de Infrarrojo

Los estudios de infrarrojo (FTIR) fueron realizados con un espectrofotómetro Bruker Tensor 27 FT-IR con el aditamento de ATR a temperatura ambiente. El Tensor 27 trabaja con un láser de He-Ne de 633 nm de longitud de onda, su intervalo de trabajo es desde el cercano infrarrojo y todo el mediano infrarrojo ( $400$  a  $4000\text{ cm}^{-1}$ )

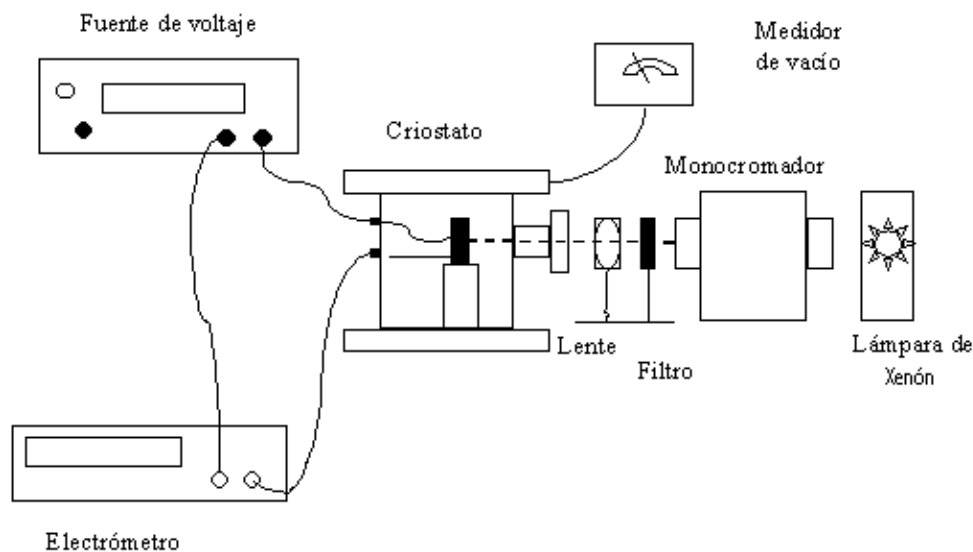
Los estudios de infrarrojo fueron realizados en polvos amorfos de ZnO, en películas delgadas con fase amorfa y wurtzita y se identificaron los modos vibracionales presentes en cada fase.



2.5.1 Diagrama de funcionamiento de un espectrómetro de infrarrojo.

## 2.6 Fotoconductividad

Para medir las corrientes en la oscuridad y bajo iluminación en función del campo aplicado, se utilizó un criostato con ventana de cuarzo donde se introduce la muestra y se hace vacío. Dicho vacío es realizado con ayuda de dos bombas, una bomba mecánica Sargent Welch modelo 1376 con la cual se logran vacíos del orden de  $10^{-3}$  Torr, y una bomba turbomolecular Pfeiffer Blazer modelo TSH190 para alcanzar un vacío del orden de  $10^{-6}$  Torr. El vacío inicial se midió con un termopar Varian 801. Para aplicar el campo eléctrico, se empleó una fuente de alto voltaje Hewlett Packard modelo 6515A con un intervalo de operación de 0 a 1600 V. La corriente fue medida con un electrómetro digital Keithley modelo 642. Para medir las fotocorrientes se iluminó la muestra con una lámpara de Xenón Oriel 66002 de 150 W, usando un monocromador Spex 1680B para seleccionar la longitud de onda en la cual absorbe la muestra. También se usó un filtro adecuado que se colocó en seguida del monocromador para eliminar longitudes de onda no deseadas y eliminar armónicos en el infrarrojo que dan lugar a corrientes piroeléctricas. Además, una lente convergente se colocó entre la ventana del criostato y el monocromador para colimar la luz.



2.6.1 Dispositivo experimental para los estudios de la fotoconductividad.

Es necesario tomar las medidas con un alto vacío pues puede haber riesgo de alcanzar el voltaje de ruptura del aire lo cual arruinaría los resultados obtenidos.

## 2.7 Difracción de Rayos X

Se realizó la difracción de rayos X (DRX) cada vez que se sometió a un tratamiento térmico para ir verificando los cambios de estructura cristalina que sufrieran las películas delgadas de ZnO.

Los análisis de rayos X fueron llevados a cabo en el Laboratorio de Difracción de Rayos X del IFUNAM

## 2.8. Microscopia Electrónica de Barrido (MEB)

El grosor de las películas se midió usando el microscopio electrónico de barrido MEB del Laboratorio Central de Microscopía (LCM) del Instituto de Física de la UNAM (IFUNAM). Para mejorar el contraste de la película respecto al sustrato en el momento de hacer el análisis, la película fue depositada sobre un sustrato de silicio.

Posteriormente con el software DigitalMicrograph se analizaron las fotografías tomando muchas medidas del grosor en distintas partes de la película y se calculó el promedio del grosor de nuestras películas.



2.8.1 Microscopio electrónico de barrido

## 2.9 Microscopia Electrónica de Transmisión (MET)

Este estudio se realizó con el microscopio electrónico de transmisión MET del Laboratorio Central de Microscopía (LCM) en el Instituto de Física de la UNAM (IFUNAM). La muestra fue preparada y analizada por los técnicos del laboratorio de Microscopia Electrónica. Para los estudios de TEM y HRTEM, la muestra en polvo fue suspendida en etanol para dispersarlo.

Una gota de esta solución fue depositada sobre una rejilla de cobre, la cual tiene sobrepuesta una película delgada de colodión y otra película de carbón amorfo que sirve de soporte.

Los resultados obtenidos son fotografías digitalizadas de la muestra.

Posteriormente se uso un software para medir los diámetros de las partículas, censando cientos de cristales de ZnO en distintas partes de la película, y con estos valores se calculó el promedio del diámetro de los cristales de ZnO.



2.9.1 Microscopio electrónico de Transmisión

## **Capítulo 3**

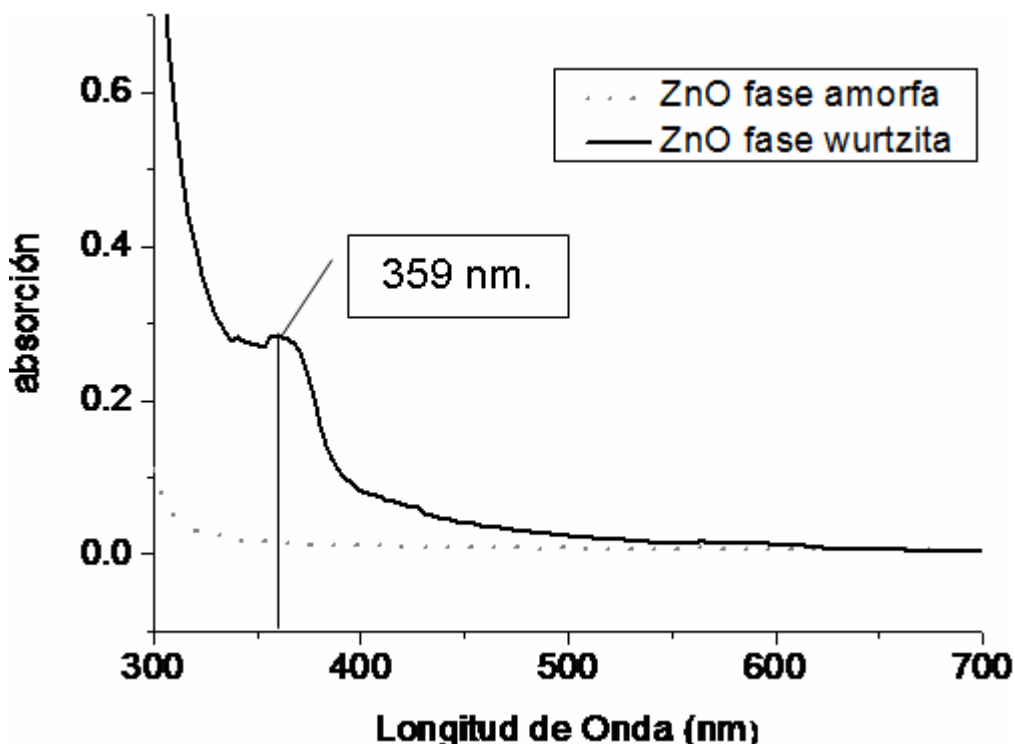
# **Resultados, Análisis y Conclusiones**

A continuación se presentan los resultados del análisis realizado en las películas de ZnO amorfas y cristalinas preparadas en el Laboratorio de Fotónica de Geles del Instituto de Física de la UNAM. Se presentan los resultados obtenidos por absorción óptica, luminiscencia, microscopia de barrido y de transmisión, difracción de rayos X, espectroscopía infrarroja y fotoconductividad. Los ajustes se realizaron con el programa *OriginLab* versión 7.5.

Las gráficas se comentan brevemente, para hacer posteriormente un análisis de los resultados obtenidos en cada etapa.

### 3.1 Absorción Óptica.

Usando el espectrofotómetro Genesys se escaneó el intervalo de longitudes de onda desde los 300 nm hasta los 700 nm y se obtuvieron los siguientes espectros de absorción óptica en las películas delgadas de ZnO para la fase amorfa y la fase wurtzita. Ambos espectros se muestran superpuestos en la gráfica 3.1.1.



3.1.1. Espectros de absorción de las películas delgadas de ZnO amorfa (línea punteada) y wurtzita (línea continua).

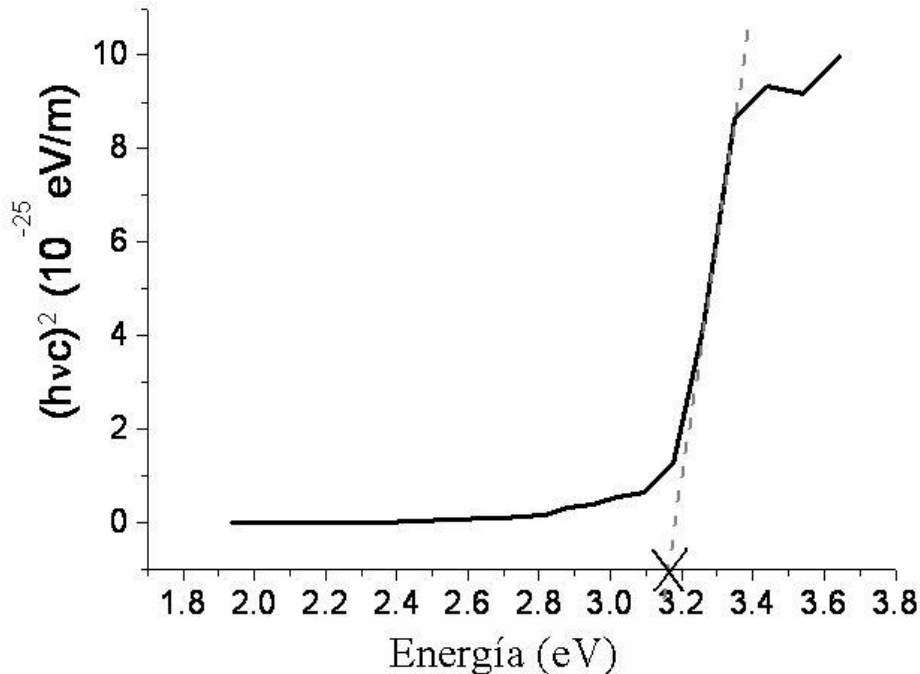
Como se aprecia en la gráfica 3.1.1. la absorción de la película de ZnO de fase amorfa no presenta ninguna banda, mientras que la película de ZnO con fase wurtzita presenta una banda de absorción que va desde los 320 hasta los 450 nm, centrada alrededor de los 359 nm.

### 3.2. Cálculo del la Energía de Band Gap por el Método Analítico.

El Band Gap o energía de transición de la banda de valencia a la banda de conducción es conocido como  $E_g$ , y ésta se obtiene según la ecuación<sup>2, 25</sup>:

$$(\alpha h\nu)^2 = C(h\nu - E_g) \quad (3.2.1)$$

Donde  $\alpha$  es el coeficiente de absorción,  $h\nu$  es la energía de los fotones,  $E_g$  es el band gap óptico y  $C$  es una constante que depende de la movilidad de los excitones. Utilizando la ec. (3.2.1) graficamos  $(\alpha h\nu)^2$  vs  $h\nu$  para obtener el valor de  $E_g$  como se muestra en la Figura 3.2.1.



3.2.1. Gráfica de  $(\alpha h\nu)^2$  vs  $E$ , la recta que interseca el eje de las abscisas corresponde al valor de  $E_g$  del ZnO.

En la literatura se reportan varios valores para la energía del band gap del ZnO, desde los 3.2 eV hasta los 3.36 eV a temperatura ambiente. Haciendo el cálculo, obtenemos una  $E_g$  de 3.18 eV para las películas delgadas de ZnO con fase wurtzita (este valor se marca con una cruz en la Fig. 3.2.1). Lo cual concuerda con los valores reportados en la literatura.

### **3.3 Espectros de Emisión y Excitación**

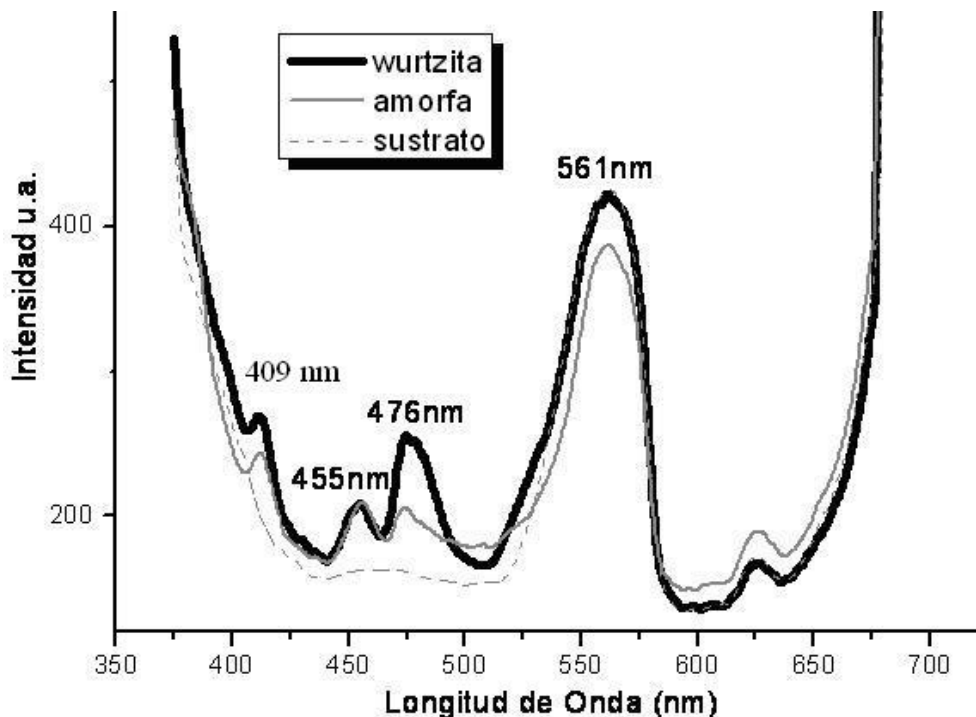
Se utilizó la longitud de onda de absorción más intensa (359 nm.) obtenida del espectro de absorción (fig. 3.1.1) como longitud de onda de excitación ( $\lambda_0$ ) en el análisis de la fluorescencia de las películas de ZnO.

En la gráfica 3.3.1 se encuentran superpuestos tres espectros de emisión tomados a temperatura ambiente. Se presentan los espectros del sustrato de silicio (línea punteada), de la emisión de la película de ZnO amorfa sobre sustrato de silicio (línea delgada) y de la emisión de la película con fase wurtzita (línea gruesa).

Como se puede apreciar, la luminiscencia muestra bandas de emisión en el violeta y en el azul detectadas en 409 nm (3.03 eV) y 455-476 nm (2.72-2.60 eV), respectivamente. La banda localizada a 561 nm claramente corresponde al sustrato de silicio.

Se ha reportado que la emisión fotoluminiscente característica del ZnO depende fuertemente de la calidad cristalina de la muestra<sup>26</sup>.

De la figura 3.3.1 podemos notar el aumento de intensidad de la emisión de la película cristalina con respecto a la intensidad de la película con fase amorfa.



3.3.1 Espectros de emisión de: (a) sustrato de silicio sobre el que está depositada la película (línea punteada), (b) de la película de ZnO fase amorfa (línea delgada), y (c) de la película de ZnO con fase wurtzita (línea gruesa).

Sun<sup>27, 28</sup> calculó los niveles de energía de los defectos intrínsecos en ZnO usando el método orbital muffin-tin de potencial total. De estos niveles calculados para defectos, puede verse que el pico centrado en 409 nm (3.03 eV) es producido por las vacancias del Zn ( $V_{Zn}$ ). De acuerdo a estos cálculos y la figura 3.3.2, el intervalo de energía de la transición de la banda de conducción al nivel de la vacancia Zn ( $V_{Zn}$ ) (3.06 eV) es consistente con la energía (3.03 eV) de la emisión violeta localizada en 409 nm en nuestro espectro. El oxígeno intersticial ( $O_i$ ) y el oxígeno de defecto anti-sitio ( $O_{Zn}$ ) también son defectos favorables para formar un ambiente rico en oxígeno. Jeong et al.<sup>26</sup> también reportaron que este tipo de vacancias son responsables de las emisiones en el violeta. Jin et al.<sup>29</sup> reportaron que esta emisión violeta está probablemente relacionada con defectos radiativos relacionados con las trampas de la interface que se encuentran en las fronteras de grano y emiten radiativamente entre la banda de conducción y estos niveles.

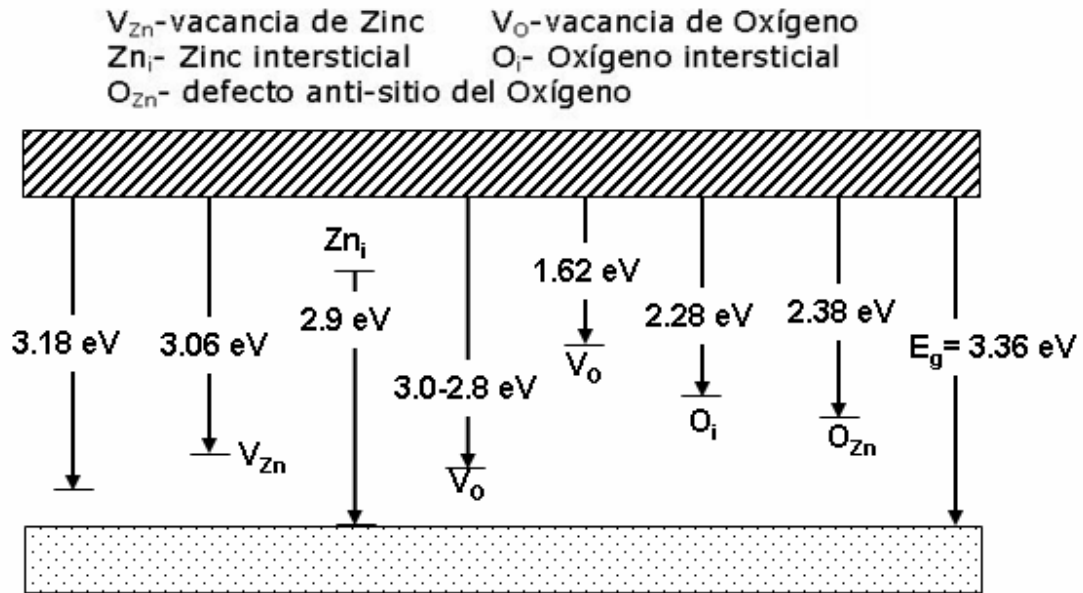


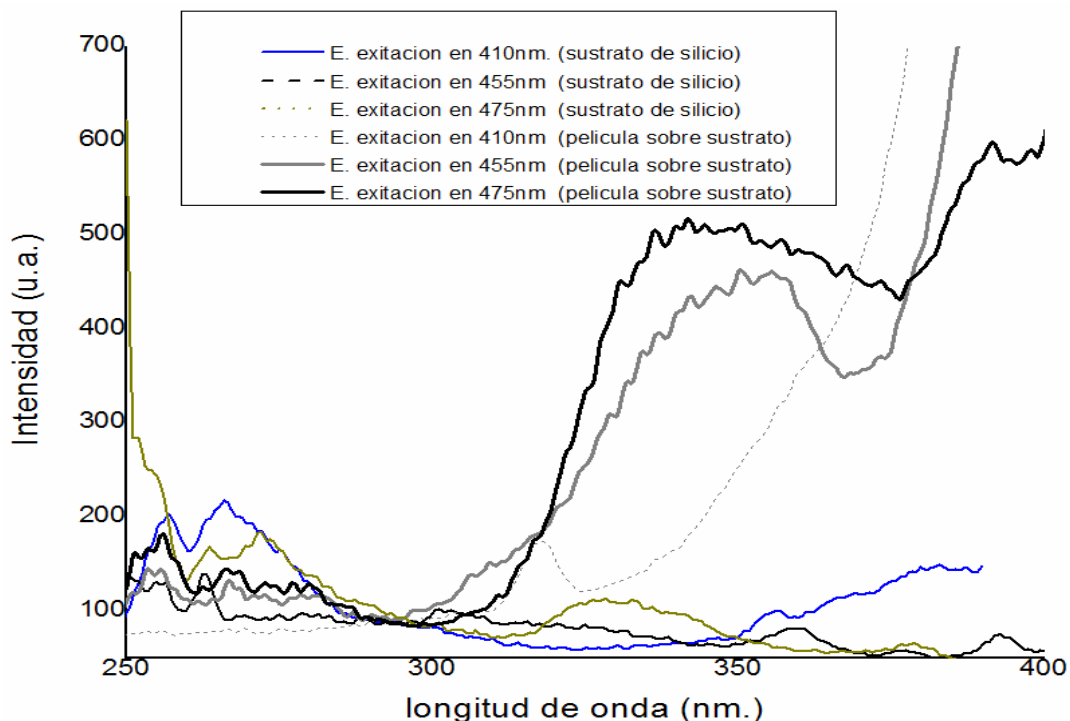
Figura 3.3.2. Representación esquemática de los niveles de defectos calculados en nanoestructuras de ZnO.

En la literatura, la emisión azul en 476 nm (2.60 eV) del ZnO ha sido reportada, pero desafortunadamente el origen exacto no es claro<sup>30-32</sup>. Respecto a la emisión en 455 nm (2.72 eV) se ha reportado que depende fuertemente de la presión del oxígeno<sup>33</sup>. Cuando la presión parcial del oxígeno aumenta, la luminiscencia disminuye. Esta dependencia prueba que el pico de emisión está relacionado con la vacancia del oxígeno en nuestras películas de ZnO. Las vacancias de oxígeno pueden producir dos niveles de defectos donador<sup>33</sup>: uno es el nivel donador profundo localizado entre 1.3-1.6 eV por debajo de la banda conductora, y la otra en el nivel donador superficial localizada a 0.3-0.5 eV. El intervalo de energía del nivel superficial al límite superior de la banda de valencia está cerca de 2.8 eV, lo cual concuerda con la energía de 2.72 eV de la emisión azul observada en la figura 3.2.1. Por ello, la emisión azul en 455 nm es originada por la transición electrónica de las vacancias del oxígeno en el nivel donador superficial a la banda de valencia.

A su vez, los átomos de Zn intersticiales pueden ser producidos en muestras ricas en zinc, los cuales actúan como centros donores. Los cálculos<sup>33</sup> indican que ambos, las vacancias de oxígeno y los Zn intersticiales ( $Zn_i$ ) tienen

energías bajas de formación. El nivel de energía de los  $Zn_i$  es de 2.9 eV por encima de la banda de valencia para muestras con un gap de energía de 3.36 eV. En nuestro caso, el gap de energía es de 3.18 eV (gráfica 3.2.1), el nivel de energía de los  $Zn_i$  deberá ser 2.74 eV por encima de la banda de valencia, lo cual está muy cerca de la energía de 2.72 eV de la emisión azul observada en la fig. 3.3.1. Así, el otro origen de la emisión azul en 455 nm es originada por la transición electrónica de los  $Zn_i$  en el nivel donador superficial a la banda de valencia.

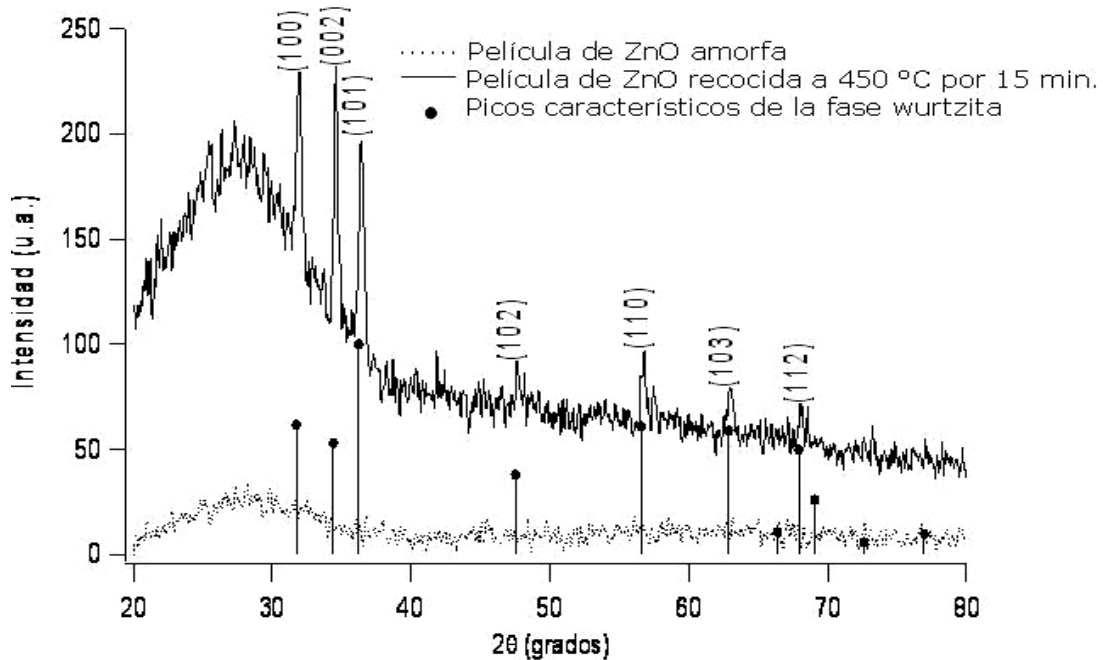
La figura 3.3.3 muestra los espectros de excitación de la película de ZnO con fase wurtzita a diferentes longitudes de onda de observación: 410 nm (línea sólida), 455 nm (línea sólida), y 476 nm (línea sólida). El pico observado en 359 en la absorción está cerca del pico de excitación observado en estos espectros (350 nm), por lo que hay concordancia entre ambas técnicas.



3.3.3 Espectros de excitación de la película de ZnO con fase wurtzita a diferentes longitudes de onda de observación: 410 nm (línea sólida de color gris claro), 455 nm (línea sólida de color gris oscuro), y 476 nm (línea sólida de color negro).

### 3.4 Difracción de Rayos X

La Figura 3.4.1 muestra la difracción de rayos X de las películas de ZnO con fase amorfa y cristalina. El espectro de la película de ZnO con fase amorfa es muy homogéneo y sin picos, esto significa que las moléculas dentro de la película no presentan ningún ordenamiento cristalino preferencial. En cambio, al someter a tratamiento de recocido las películas de ZnO amorfo éstas presentaron cristalinidad. La difracción de rayos X muestra la aparición de picos debido a que el tratamiento térmico induce un reordenamiento en los iones de la película de ZnO, que como resultado de tener una orientación y dirección preferente se forman planos cristalográficos. Se identificó la presencia de los picos ubicados en las direcciones (100), (002), (101), (102), (110), (110), (103), (112) que coinciden con los datos reportados en la carta #05-0664 y que en la literatura es conocida como fase wurtzita. La banda ancha que se observa entre  $2\theta = 20-40^\circ$  corresponde al sustrato de vidrio, sobre el que está depositada la película de ZnO.



3.4.1 Espectros de difracción de rayos X de una película de ZnO con fase amorfa (línea punteada) y de una película de ZnO con fase wurtzita (línea sólida). Los puntos aislados corresponden a los picos característicos de la fase cristalina tipo wurtzita.

Según la fórmula de Sherrer, para calcular el diámetro promedio de los nanocristales de ZnO;

$$d = \frac{0.9\lambda}{B \cos \theta}$$

con  $\lambda=1.54056 \times 10^{-10}$  m. y tomando de la difracción de rayos X  $2\theta=31.95^\circ$  y  $B=0.4^\circ=0.00628$  rad correspondiente al ancho del pico (100), tenemos que  $d= 23$  nm.

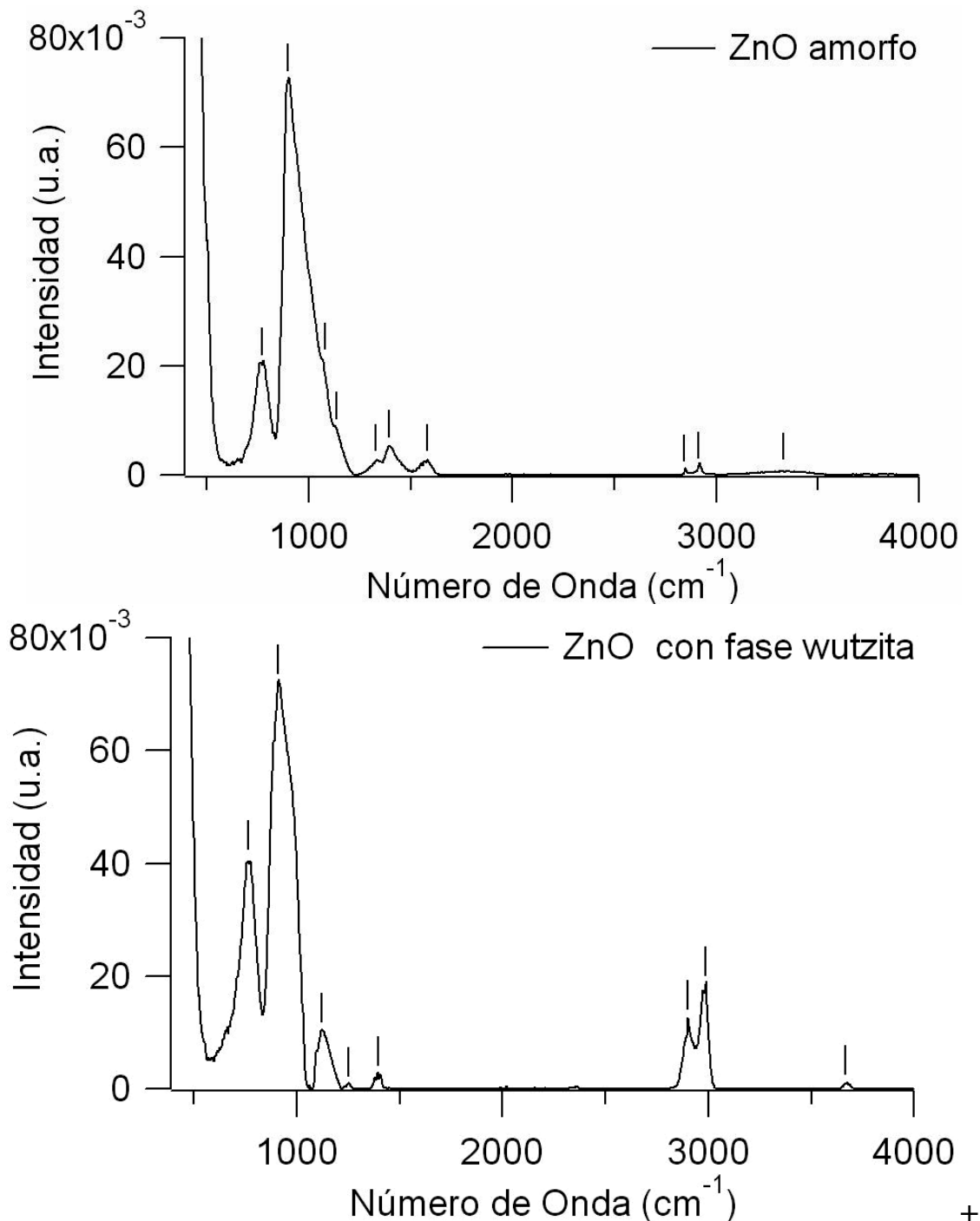
Esto nos muestra la eficiencia del tratamiento de recocido para producir la fase wurtzita en las películas de ZnO aquí preparadas.

### 3.5 Análisis por Espectroscopia Infrarroja

La figura 3.5.1 muestra el espectro de infrarrojo de películas de ZnO con fase amorfa y fase wurtzita depositadas sobre sustrato de vidrio. Las bandas localizadas en  $3341$  y  $3674 \text{ cm}^{-1}$  corresponden a especies O-H en las películas<sup>34</sup>. De aquí se identificó diferentes bandas dentro del rango de  $2800-3000 \text{ cm}^{-1}$  que corresponden a una frecuencia de "stretching" en los enlaces C-H. Para la película amorfa, la banda localizada en  $1335 \text{ cm}^{-1}$  es debida a un enlace débil de la molécula del ácido acético (HOOC-R). Y la banda localizada a  $1582 \text{ cm}^{-1}$  corresponde al enlace del tipo C=O producido por un puente tipo metal acetato (M-OCOO-M) siendo el Zn el metal asociado<sup>34, 36</sup>. Mientras que las bandas localizadas en  $1392 \text{ cm}^{-1}$  (amorfa) y  $1394 \text{ cm}^{-1}$  (fase wurtzita) corresponden a un enlace stretching de C-O. Para la película con fase wurtzita se identificó una banda en  $1450 \text{ cm}^{-1}$ , la cual corresponde a una vibración del tipo scissoring  $\text{CH}_2$ <sup>35, 36</sup>.

Las bandas correspondientes al sustrato de vidrio fueron detectadas en ambas películas, las cuales corresponden a los enlaces  $\nu_s$  (Si-O-Si) en  $775 \text{ cm}^{-1}$  y al  $\nu$  (Si-OH) en  $902-912$

$\text{cm}^{-1}$ . Estas bandas son muy intensas, por lo que deben minimizar la presencia de bandas propias de la película depositada sobre el sustrato de vidrio. Por esta razón, se decidió medir el espectro infrarrojo en muestras de KBr.



3.5.1 Espectros de infrarrojo de películas de ZnO amorfa y cristalina.

La figura 3.5.2 corresponde al espectro de infrarrojo de las pastillas de KBr de ZnO amorfa y con fase wurtzita. El modo stretching del ZnO fue localizado a 471 y 465  $\text{cm}^{-1}$  para la muestra amorfa y con fase wurtzita, respectivamente<sup>36</sup>. Las bandas localizadas a 854  $\text{cm}^{-1}$  y 1042  $\text{cm}^{-1}$  (amorfa), y en 865  $\text{cm}^{-1}$  y 1038  $\text{cm}^{-1}$  (fase wurtzita) son atribuidas a modos de bending y stretching simétricos y antisimétricos de  $\text{ZnO}\cdot\text{H}_2\text{O}$ , respectivamente<sup>36</sup>. La banda localizada a 1557  $\text{cm}^{-1}$  (amorfa) y 1599 (fase wurtzita) corresponde al enlace del tipo C=O producido por un puente tipo metal acetato (M-OCOO-M) siendo el Zn el metal asociado<sup>33, 35</sup>. Las bandas localizadas en 3263 y 3414  $\text{cm}^{-1}$  corresponden a especies O-H en las películas<sup>34</sup>.

Para la muestra amorfa, las bandas localizadas entre 2800-3000  $\text{cm}^{-1}$  corresponden a frecuencias de "stretching" de los enlaces C-H. La banda de 1342  $\text{cm}^{-1}$  corresponde a un enlace débil de la molécula del ácido acético (HOOC-R).

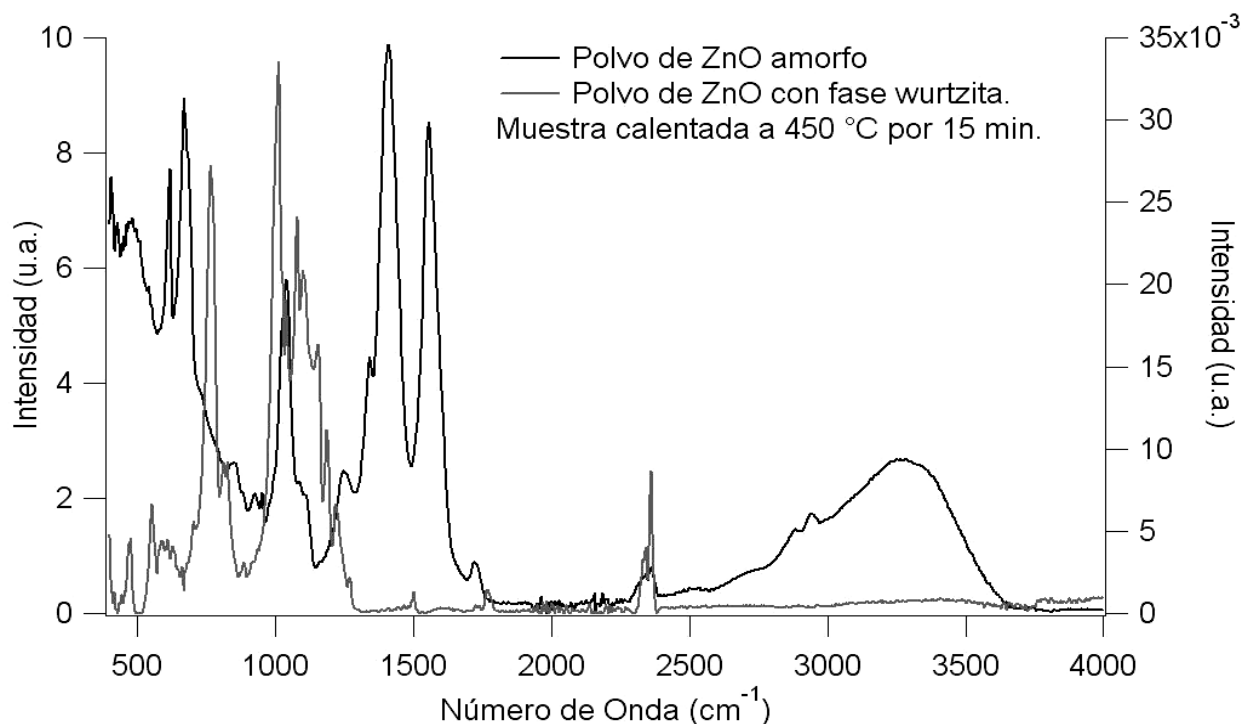


Figura 3.5.2. Espectros infrarrojos de muestras en polvo de ZnO amorfo y con fase wurtzita.

La tabla 3.5.3 contiene los modos vibracionales de las bandas identificadas en las muestras de ZnO amorfa y con fase wurtzita, tanto en pastilla de KBr como en película delgada. La banda correspondiente al disolvente (etanol) fue identificada en  $1068\text{ cm}^{-1}$  en la película amorfa de ZnO. Esta banda no fue encontrada en el espectro de las muestras con fase wurtzita (pastilla de KBr y película). Esto indica que el tratamiento térmico de  $450\text{ }^{\circ}\text{C}$  por 15 minutos eliminó los compuestos orgánicos e hidroxilos.

Pastilla KBr de ZnO amorfa	Pastilla KBr de ZnO con fase Wurtzita	Película de ZnO amorfa	Película de ZnO con fase Wurtzita	
$\bar{\nu}_{\text{exp}}\text{ (cm}^{-1}\text{)}$	$\bar{\nu}_{\text{exp}}\text{ (cm}^{-1}\text{)}$	$\bar{\nu}_{\text{exp}}\text{ (cm}^{-1}\text{)}$	$\bar{\nu}_{\text{exp}}\text{ (cm}^{-1}\text{)}$	descripción
471	465	-	-	ZnO stretching
-	766	775	773	$\nu_s$ (Si-O-Si)
854	865	-	-	symm. bending ZnO
-	-	902	912	$\nu$ (Si-OH)
-	-	1068	-	Etanol
1042	1038	-	-	asymm. stretching ZnO
-	1121	1130	1124	-
1248	-	-	1252	-
1342	-	1335	-	HOOC-R
1410	-	1392	1394	C-O
-	-	-	1450	scissoring de $\text{CH}_2$
1557	1599	1582	-	C=O
-	-	2851	-	C-H stretching
2900	-	2918	2900	C-H stretching
2945	-	-	2988	C-H stretching
3263	3414	3341	3674	H-O especies

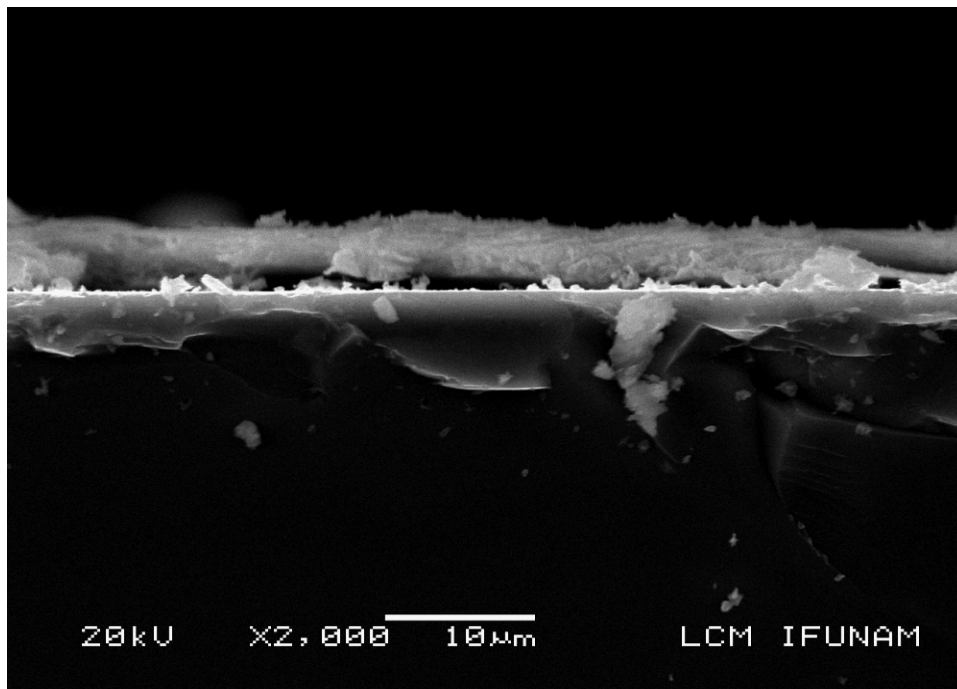
*Tabla 3.5.3 Modos vibracionales identificados en el ZnO, indicando los respectivos cambios que sufre el espectro al cambiar la morfología de la pastilla de KBr a película delgada<sup>33, 34, 35, 36</sup>.*

Las bandas ubicadas en 766, 775, 773, 902 y 912 nm, corresponden al sustrato de vidrio donde fue depositada la película. Las muestras amorfas muestran bandas localizadas

en 1068, 1335, 1582 y 2851 que desaparecen después de tratamiento térmico al que se sometieron las muestras con fase wurtzita. Esto indica que el tratamiento térmico elimino residuos orgánicos.

### 3.6. Medida del Espesor de la Película

Las fotografías digitales que se obtuvieron con la técnica de MEB muestran claramente que se forma una película delgada, y que ésta no reacciona con el sustrato.



*3.6.1. Fotografía del perfil de las muestras de ZnO, la película es la parte grisácea. En los bordes se alcanza a ver un poco el escarapelado del perfil del sustrato de silicio.*

Las fotografías son imágenes de secciones del perfil de la muestra. Estas fueron analizadas con el software DigitalMicrograph tomando medidas en varias partes de película para obtener un promedio del espesor de las películas. A continuación se muestran los resultados:

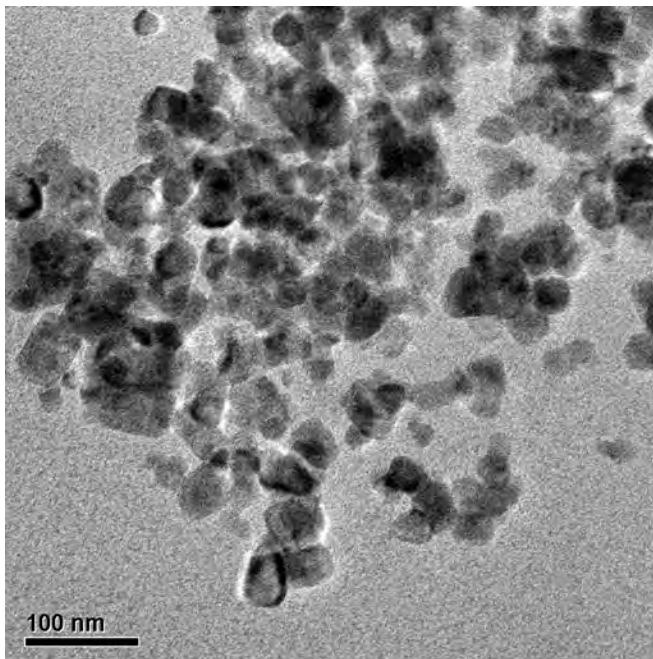
	Espesor	Desviación Estándar
Película de ZnO Amorfa	3.37 $\mu\text{m}$	0.97
Película de ZnO Wurtzita	2.36 $\mu\text{m}$	0.46

*Tabla 3.6.2. Espesor de las películas*

Las películas cristalinas (fase wurtzita) tienen un espesor menor al de las películas amorfas, esto debido a que durante el tratamiento térmico son eliminadas impurezas, moléculas de agua y disolventes que se alojaban dentro de la película, produciendo el adelgazamiento de la misma.

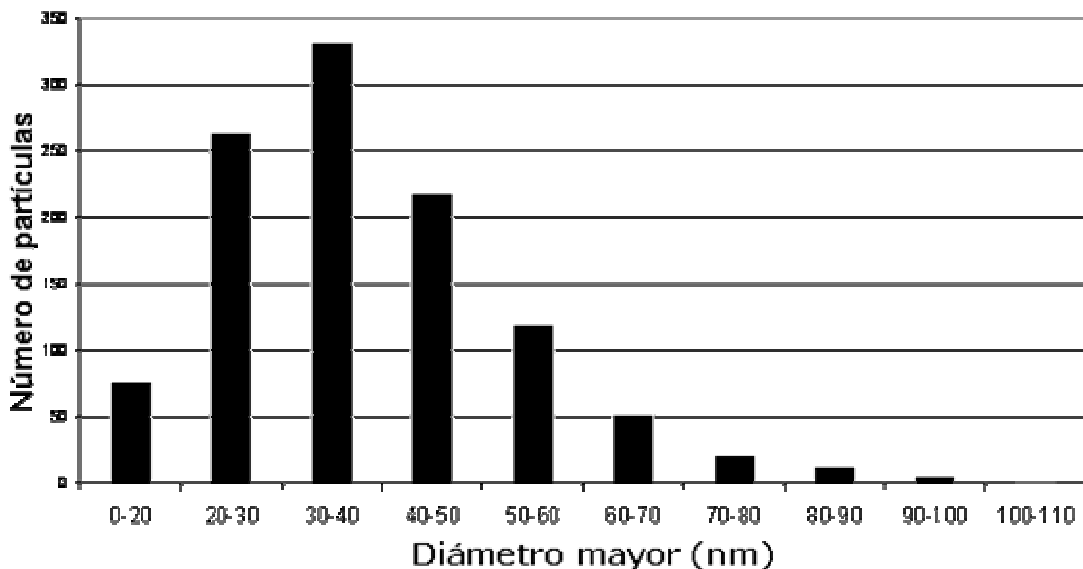
### **3.7 Cálculo de Tamaños Promedio de los Cristales de ZnO**

La Figura 3.7.1 muestra una fotografía digital que corresponde a una muestra de ZnO cristalina. En ella se pueden observar la formación de cristales de varios tamaños.

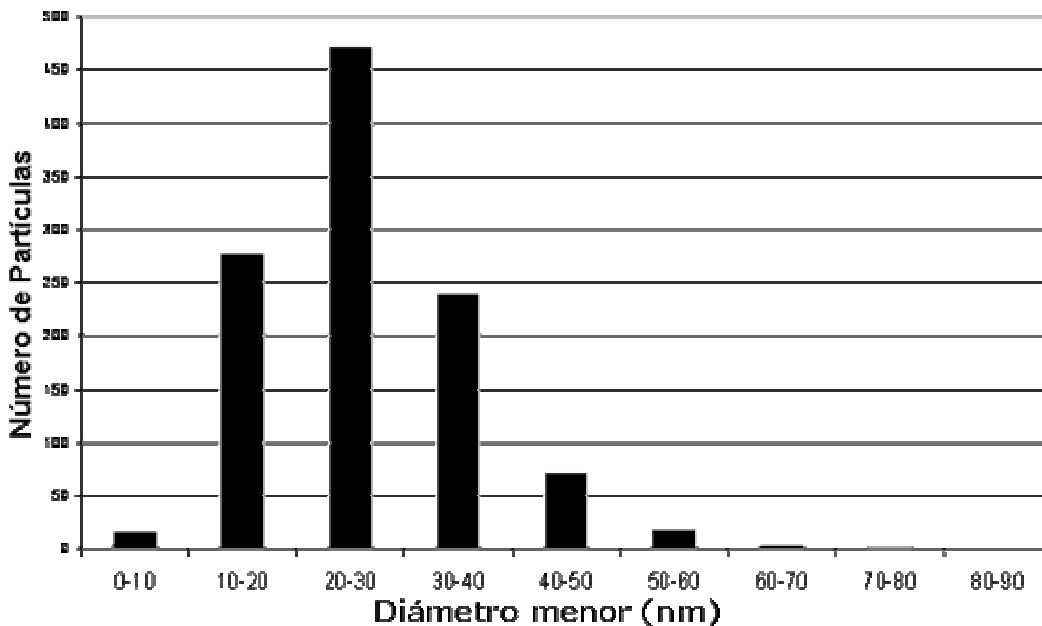


*3.7.1 Fotografía digital. Por microscopía electrónica de transmisión se determinó la formación de cristales en la película de ZnO cristalina (fase wurtzita).*

Utilizando las fotografías obtenidas con la técnica MET (Fig. 3.7.1), se consideraron alrededor de mil partículas para realizar la estadística correspondiente. Las Figs. 3.7.2 y 3.7.3 presentan los histogramas del diámetro mayor y el menor, respectivamente. De la fig 3.7.2 se deduce que los cristales con diámetros entre 30 y 40nm fueron la especie predominante. Otra de las poblaciones abundantes es la de diámetro de entre 20 y 30 nm lo cual concuerda con el resultado obtenido con la formula de Sélter (sección 3.4)



3.7.2. Histograma de frecuencias del diámetro mayor.



3.7.3. Histograma de frecuencias del diámetro menor.

Asimismo, se calculó el diámetro promedio por cristal de nuestras películas de ZnO. La tabla 3.7.1. contiene los resultados obtenidos para el diámetro mayor y menor de los cristales de ZnO.

	<b>Semieje mayor (nm)</b>	<b>Semieje menor (nm)</b>
<i>ZnO cristalino (fase wurtzita)</i>	38.45	26.531
	Desviación estándar 15.00	Desviación estándar 9.54

Tabla 3.7.1. Resultados obtenidos para el diámetro mayor y menor de los cristales de ZnO.

El máximo de absorción localizado a 359 nm (fig. 3.1.1) es un pico excitónico que está relacionado con el efecto de confinamiento cuántico debido al tamaño nanoscópico de los cristalitas de ZnO. La posición de este pico está relacionado al tamaño de grano de acuerdo a la relación<sup>2, 38</sup>:

$$\frac{1240}{\lambda_{1/2}} = a + \frac{b}{D^2} - \frac{c}{D} \quad (3.7.1)$$

Donde  $\lambda_{1/2}$  corresponde a la longitud de onda al 50 % de la intensidad del máximo y las constantes son  $a = 3.301$ ,  $b = 294$ ,  $c = -1.09$ . Estos valores empíricos permiten una descripción adecuada de la relación entre  $\lambda_{1/2}$  y el tamaño del cristalito. Sustituyendo el valor experimental obtenido por MET,  $D = 38.45$  nm, obtenemos de la ec. (3.7.1.) que  $\lambda_{1/2} = 351.4$  nm, que está muy cercano al máximo de absorción de nuestra película cristalina (359 nm).

### 3.8 Fotoconductividad

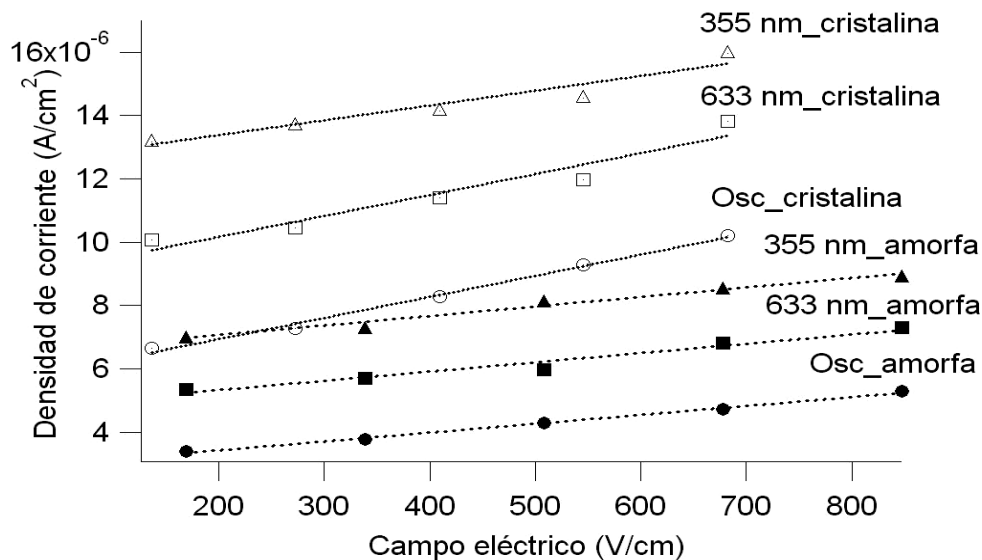
De los experimentos de fotoconductividad se obtuvieron los valores de Corriente (I) y voltaje (V), los cuales tienen que ser convertidos a Campo eléctrico (E) vs Densidad de corriente (J), a fin de volver los resultados independientes de la geometría de las muestras. La corriente se relaciona con la

densidad de corriente  $J$  y el voltaje se relaciona con el campo eléctrico  $E$  de la siguiente forma:

$$J = \frac{I}{A} \quad \text{y} \quad E = \frac{V}{L} \quad (3.8.1)$$

Donde  $A$  es el área de la sección transversal de la película comprendida por la longitud del electrodo  $l$ . Es decir,  $A = l \cdot d$ , con  $d$  el grosor de la película, que en el caso de la película amorfa es de  $3.37 \mu\text{m}$  y para la cristalina es de  $2.36 \mu\text{m}$  (Tabla 3.6.2).  $L$  es la separación entre los dos electrodos.

Después de haber transformado a densidad de corriente y campo eléctrico, los datos registrados se pudieron comparar entre sí. La figura 3.8.1 muestra los datos experimentales para la película amorfa y cristalina en la oscuridad y bajo iluminación a  $355 \text{ nm}$ ,  $633 \text{ nm}$ . La longitud de onda de  $633 \text{ nm}$  se empleó debido a que en el espectro de absorción se observa que no hay bandas de absorción, mientras que la longitud de onda de  $355 \text{ nm}$  corresponde al máximo de absorción de la película. Los puntos experimentales obtenidos mostraron una clara tendencia lineal, por lo que se les ajustaron rectas para unir a cada conjunto de puntos, esto significa que se obtuvo un comportamiento totalmente óhmico.



### 3.8.1 Gráfica de Campo eléctrico ( $E$ ) vs Densidad de corriente ( $J$ ).

En estos experimentos de fotoconductividad se vio reflejado claramente el efecto de la cristalinidad obtenida en las muestras. En las gráficas de  $E$  vs  $J$ , las películas con fase wurtzita tienen una mayor pendiente y ordenada al origen que las películas con fase amorfa, lo cual indica que las películas cristalinas poseen mejores propiedades fotoconductoras y fotovoltaicas que las películas amorfas.

Los ajustes respectivos se incluyen en la tabla 3.8.1.

$\lambda$ (nm)	Película	Pendiente	Ord. Al origen
633	Amorfa	$2.93 \times 10^{-9}$	$4.73 \times 10^{-6}$
	Cristalina	$6.62 \times 10^{-9}$	$8.84 \times 10^{-6}$
355	Amorfa	$2.99 \times 10^{-9}$	$6.46 \times 10^{-6}$
	Cristalina	$4.71 \times 10^{-9}$	$1.24 \times 10^{-5}$
Oscura	Amorfa	$2.82 \times 10^{-9}$	$2.86 \times 10^{-6}$
	Cristalina	$6.69 \times 10^{-9}$	$5.59 \times 10^{-6}$

Tabla 3.8.1. Ajustes lineales de las películas de ZnO amorfas y cristalinas.

De la tabla 3.8.1, la pendiente de los ajustes para las películas cristalinas son mayores que la pendiente de los ajustes para las amorfas, tanto en la corriente oscura como bajo iluminación. La pendiente para las películas cristalinas disminuye al disminuir la longitud de onda, en cambio, la pendiente de las películas amorfas aumenta. En el caso de las películas amorfas este hecho indica un fuerte comportamiento fotoconductor. Por otro lado, la ordenada al origen aumenta al disminuir la longitud de onda en ambos tipos de películas.

De los ajustes de  $J$  en función de  $E$  se obtienen la pendiente ( $m$ ) y la ordenada al origen ( $b$ ) de cada recta. Con estos datos se calcularon los parámetros de transporte de carga tanto para la corriente oscura como bajo iluminación, utilizando las siguientes ecuaciones:

$$\phi l_0 = (b_i - b_d) \frac{hc}{e\alpha\lambda I} \quad (3.8.2)$$

y

$$\phi\mu\tau = (m_i - m_d) \frac{hc}{e\alpha\lambda I} \quad (3.8.3)$$

Los resultados obtenidos se muestran en la tabla 3.8.2.

Película de ZnO	$\lambda$	$\phi l_0$ (cm)	$\phi\mu\tau$ (cm <sup>2</sup> /V)
Amorfa	633nm	$2.5 \times 10^{-6}$	$1.5 \times 10^{-10}$
	355nm	$2.2 \times 10^{-6}$	$1.0 \times 10^{-10}$
Cristalina (wurtzita)	633nm	$8.8 \times 10^{-6}$	$4.6 \times 10^{-13}$
	355nm	$2.1 \times 10^{-7}$	$0.6 \times 10^{-10}$

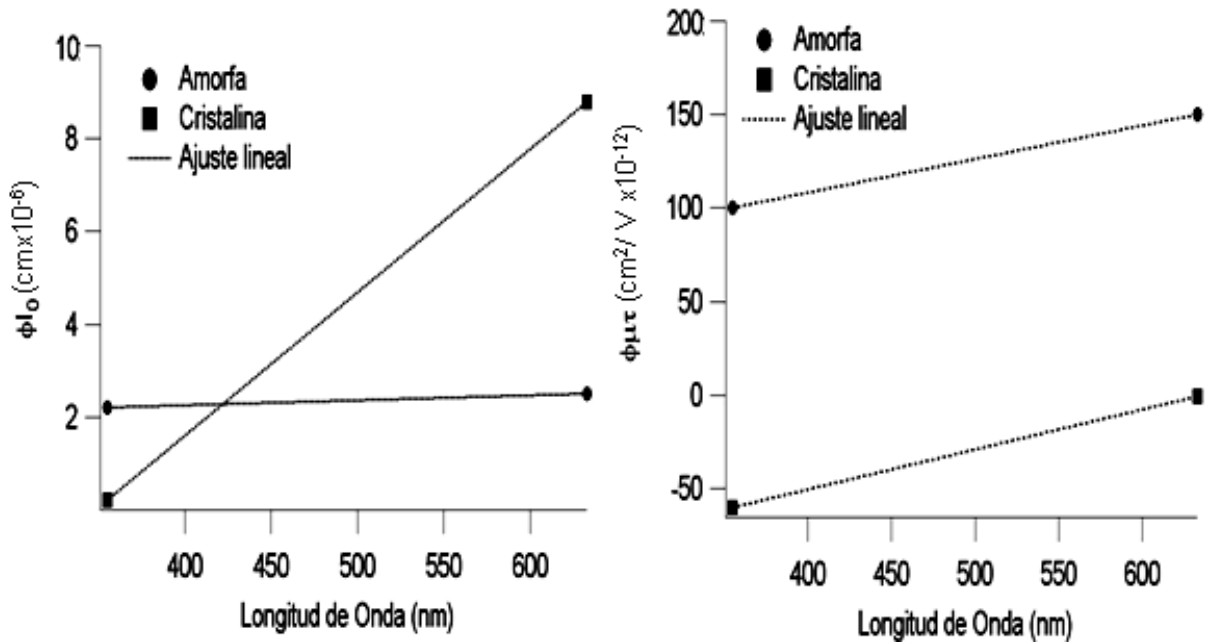
3.8.2 Tabla de resultados obtenidos del experimento de fotoconductividad

De la tabla 3.8.2 se observa que en general el parámetro fotovoltaico ( $\phi l_0$ ) y el parámetro fotoconductor ( $\phi\mu\tau$ ) decrecen al disminuir la longitud de onda en ambas muestras.

Los valores del parámetro fotoconductor resultaron mayores en la muestra amorfa con respecto a la cristalina. Una explicación de esto es que en la muestra amorfa hay más disolvente y agua lo cual aumenta la conductividad.

La figura 3.8.3 muestra las gráficas de ambos parámetros de transporte,  $\phi l_0$  y  $\phi\mu\tau$  en función de la longitud de onda. Solo tenemos dos puntos experimentales, los cuales fueron

ajustados por mínimos cuadrados. Los ajustes se muestran en la tabla 3.8.3.



3.8.2. Gráfica de los parámetros de transporte  $\phi_0$  y  $\phi\mu\tau$  en función de la longitud de onda de excitación de las películas de ZnO amorfa y cristalina.

Parámetro	Película Amorfa	Película cristalina
$\phi_0$	$y = 1.1 \times 10^{-9} X + 1.8 \times 10^{-6}$	$y = 3.1 \times 10^{-8} X - 1.1 \times 10^{-5}$
$\phi\mu\tau$	$y = 1.8 \times 10^{-13} X + 3.6 \times 10^{-11}$	$y = 2.1 \times 10^{-13} X + 1.4 \times 10^{-10}$

Tabla 3.8.3 Ajustes lineales para los parámetros de transporte  $\phi_0$  y  $\phi\mu\tau$ .

## Conclusiones

Se sintetizaron películas de ZnO amorfas y cristalinas homogéneas y de alta calidad óptica mediante la técnica sol-gel.

La cristalinidad obtenida en las películas fue identificada como de fase wurtzita en las muestras que recibieron tratamiento térmico de 450 °C por 15 minutos esto se comprobó por medio de la difracción de rayos X.

Estas películas delgadas así obtenidas presentaban un máximo de absorción óptica en 359 nm.

Las muestras amorfas muestran bandas en el infrarrojo localizadas en 1068, 1335, 1582 y 2851 mismas que desaparecen después del tratamiento térmico al que se sometieron las muestras con fase wurtzita. Esto indica que el tratamiento térmico es efectivo para eliminar residuos orgánicos en dichas muestras.

Las películas con fase wurtzita tienen un espesor menor a las películas amorfas, esto debido a que durante el tratamiento térmico son eliminadas impurezas, disolventes y las moléculas de agua que se alojaban dentro de la película, lo cual produce un adelgazamiento de la misma de 3.37  $\mu$ . a 2.36  $\mu$ .

Mediante mediciones en el microscopio electrónico de transmisión se determinó que la población más abundante de cristales de ZnO tiene diámetros de entre 30 y 40 nm habiendo también una población considerable de entre 20 y 30 nm y que es claramente identificada al usar la fórmula de Sélter.

La emisión fotoluminiscente de las películas de ZnO depende fuertemente de la calidad cristalina de la muestra. Esto se confirmó al observar que la intensidad de la emisión de la película cristalina es mayor que la intensidad de la emisión de

la película con fase amorfa. Se lograron identificar varias transiciones ya reportadas en la literatura; 410 nm. relacionada con las vacancias del Zn ( $V_{Zn}$ ); 455 nm debida a las transiciones electrónicas de las vacancias del oxígeno; y 475 nm.

Las curvas de J vs E mostraron una clara tendencia lineal, esto significa que ambas películas (amorfa y cristalina) tienen un comportamiento totalmente óhmico. En las gráficas de E vs J, las películas con fase wurtzita tienen una mayor pendiente y ordenada al origen que las películas con fase amorfa, lo cual indica que las películas cristalinas poseen mejores propiedades fotoconductoras y fotovoltaicas que las películas amorfas, aún cuando el agua y el disolvente dan lugar a mayor conductividad en las muestras amorfas.

En general, el parámetro fotovoltaico ( $\phi|_0$ ) y el parámetro fotoconductor ( $\phi\mu\tau$ ) decrecen al disminuir la longitud de onda en ambas muestras.

Es un hecho que las propiedades estructurales de una película delgada de ZnO se pueden modificar mediante un tratamiento térmico de recocido, y con ello sus propiedades ópticas y eléctricas, así como también es posible identificar la fase cristalina en películas por medio de análisis ópticos.

## Conclusiones

Se sintetizaron películas de ZnO amorfas y cristalinas homogéneas y de alta calidad óptica mediante la técnica sol-gel.

La cristalinidad obtenida en las películas fue identificada como de fase wurtzita en las muestras que recibieron tratamiento térmico de 450 °C por 15 minutos esto se comprobó por medio de la difracción de rayos X.

Estas películas delgadas así obtenidas presentaban un máximo de absorción óptica en 359 nm.

Las muestras amorfas muestran bandas en el infrarrojo localizadas en 1068, 1335, 1582 y 2851 mismas que desaparecen después del tratamiento térmico al que se sometieron las muestras con fase wurtzita. Esto indica que el tratamiento térmico es efectivo para eliminar residuos orgánicos en dichas muestras.

Las películas con fase wurtzita tienen un espesor menor a las películas amorfas, esto debido a que durante el tratamiento térmico son eliminadas impurezas, disolventes y las moléculas de agua que se alojaban dentro de la película, lo cual produce un adelgazamiento de la misma de 3.37  $\mu$ . a 2.36  $\mu$ .

Mediante mediciones en el microscopio electrónico de transmisión se determinó que la población más abundante de cristales de ZnO tiene diámetros de entre 30 y 40 nm habiendo también una población considerable de entre 20 y 30 nm y que es claramente identificada al usar la fórmula de Sélter.

La emisión fotoluminiscente de las películas de ZnO depende fuertemente de la calidad cristalina de la muestra. Esto se confirmó al observar que la intensidad de la emisión de la película cristalina es mayor que la intensidad de la emisión de

la película con fase amorfa. Se lograron identificar varias transiciones ya reportadas en la literatura; 410 nm. relacionada con las vacancias del Zn ( $V_{Zn}$ ); 455 nm debida a las transiciones electrónicas de las vacancias del oxígeno; y 475 nm.

Las curvas de  $J$  vs  $E$  mostraron una clara tendencia lineal, esto significa que ambas películas (amorfa y cristalina) tienen un comportamiento totalmente óhmico. En las gráficas de  $E$  vs  $J$ , las películas con fase wurtzita tienen una mayor pendiente y ordenada al origen que las películas con fase amorfa, lo cual indica que las películas cristalinas poseen mejores propiedades fotoconductoras y fotovoltaicas que las películas amorfas, aún cuando el agua y el disolvente dan lugar a mayor conductividad en las muestras amorfas.

En general, el parámetro fotovoltaico ( $\phi|_0$ ) y el parámetro fotoconductor ( $\phi\mu\tau$ ) decrecen al disminuir la longitud de onda en ambas muestras.

Es un hecho que las propiedades estructurales de una película delgada de ZnO se pueden modificar mediante un tratamiento térmico de recocido, y con ello sus propiedades ópticas y eléctricas, así como también es posible identificar la fase cristalina en películas por medio de análisis ópticos.

---

---

## Apéndice

### **Validación experimental.**

Los experimentos de absorción, fluorescencia e infrarrojo se realizaron en equipos cuya incertidumbre porcentual es de menos del 1% según manuales, aún así, éstos se realizaron mas de una vez en todos los casos, esto para obtener experiencia en el uso de los dispositivos al mismo tiempo que se corroboraba la reproducibilidad del experimento.

En el caso del experimento de fotoconductividad donde los resultados obtenidos variaban mucho, se tomo un promedio de los datos obtenidos y se les calculó una incertidumbre máxima del 22%.

El resto de los experimentos fue realizado por expertos en el análisis de rayos X y de microscopia electrónica en sus correspondientes laboratorios.

---

---

## Bibliografía

<sup>1</sup> Ramón Tena Zaena, "El óxido de zinc: crecimiento cristalino mediante transporte en fase gaseosa y caracterización de propiedades físicas"; Tesis Doctoral, Universidad de Valencia, España (2004).

<sup>2</sup> G. G. Valle, P. Hammer, S. H. Pulcinelli, C. V. Santilli. "Transparent and conductive ZnO:Al thin films prepared by sol-gel dip-coating", J. of the European Ceram. Soc. **24**, 1009-1013 (2004).

<sup>3</sup> Yu-de Wang, Shuo Zhang, Xing-hui Wu. "Green Light Luminescence from ZnO/Dedecylamine Mesolamellar Nanocomposites synthesized by Self-Assembly", Eur. J. Inorg. Chem. 727-731 (2005).

<sup>4</sup> P. Zu, Z. K. Tang, G.K.L. Wong, M. Kawasaki, A. Ohtomo, H. Koinuma and Y. Sewaga, "Ultraviolet spontaneous and stimulated emissions from ZnO microcrystalline thin films at room temperature", Solid State Commun. **103**, 459-463 (1997).

<sup>5</sup> B. Pal, M. Sharon, "Enhanced photocatalytic activity of highly porous ZnO thin films prepared by sol-gel process", Mater. Chem. and Phys. **76**, 82-87 (2002).

<sup>6</sup> <http://es.wikipedia.org/wiki/Wurtzita>

<sup>7</sup> Charles Kittel; "Introducción a la Física del Estado Sólido", Ed. Reverté S. A.; Barcelona 3<sup>a</sup> ed. (1993).

<sup>8</sup> [www.smf.mx/boletin/2006/Bol-20-1/Articulos/sol-gel.htm](http://www.smf.mx/boletin/2006/Bol-20-1/Articulos/sol-gel.htm)

<sup>9</sup> C. J. Brinker, G. W. Scherer, "Sol-gel Science. The Physics and Chemistry of Sol-Gel processing", Academic Press; E.U.A., 1<sup>a</sup> ed. (1990).

<sup>10</sup> R. W. Jones, "Fundamental Principles of Sol-Gel Technology", 1<sup>st</sup> Ed.; London: Inst. Of Metals (1989).

<sup>11</sup> [http://en.wikipedia.org/wiki/Spin\\_coating](http://en.wikipedia.org/wiki/Spin_coating)

<sup>12</sup> Klingshirn, C.F.; "Semiconductor optics" Springer-Verlag, (1995).

<sup>13</sup> U. R. Torres; "Fotodestrucción de Coumarina 440 en geles de SiO<sub>2</sub> expuestos a un láser entonable de Nitrógeno"; Tesis de Licenciatura; Facultad de Ciencias; UNAM (1998)

# NANOTECH 2008



24 - 26 Noviembre  
2008

Torre de Ingeniería  
UNAM

## INVITED LECTURES

Gerardo Goya

INA - Universidad de Zaragoza - Spa

Ricardo Guirado López

IF - UASLP - MEX

Brad Chmelka

Chem - Eng - UCSB - USA

Rodolfo Zanella

CCADET - UNAM - MEX

Ricardo F. Aroca

University of Windsor - CAN

Edilso Reguera Ruiz

CICATA - Legaria - MEX

Massimo Guglielmi

University of Padua - ITA

Tessy Lopez

UAM - Xochimilco - MEX

Gerko Oskam

CINVESTAV - Merida - MEX

## SHORT COURSES

X ray diffraction

X. Bokhimi, IF - UNAM

SEM and TEM Microscopy

Patricia Santiago IF - UNAM

## CONFERENCE CHAIRMEN

David Diaz, FQ - UNAM, MEX

Jorge Garía, IF - UNAM, MEX

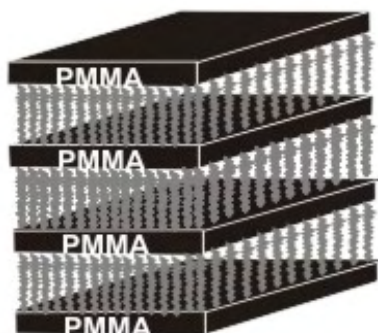
Elder De la Rosa, CIO, MEX

## INFORMATION AND REGISTRATION

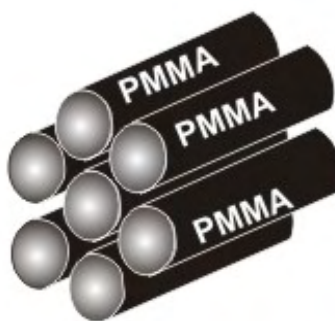
<http://www.cio.mx/NANOTECH2008/1.html>



4nm



5nm



# NANOTECH 2008

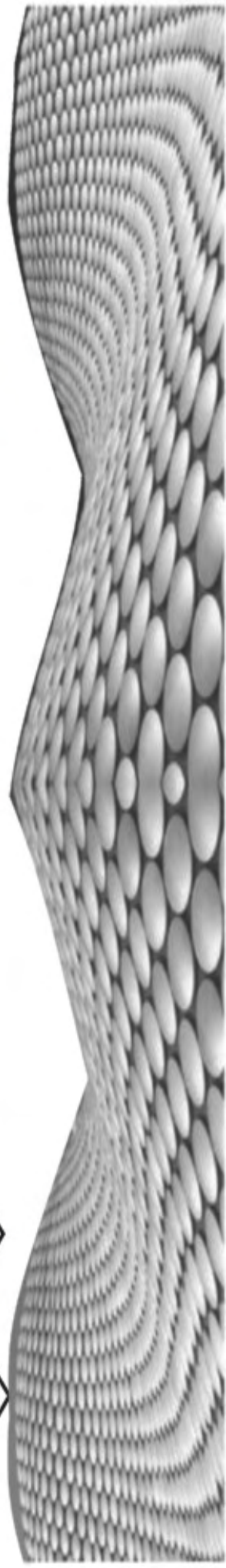


24-26 Noviembre 2008

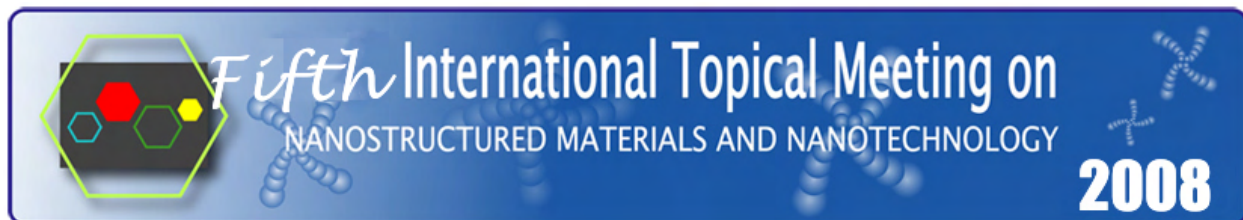
Torre de Ingeniería  
UNAM

CONFERENCE CHAIRMEN

David Díaz, FQ-UNAM, MEX.  
 Jorge García Macedo, IF-UNAM, MEX.  
 Elder de la Rosa, CIO, MEX.



**PROGRAM**



**FIFTH INTERNATIONAL TOPICAL MEETING ON  
NANOSTRUCTURED MATERIALS AND NANOTECHNOLOGY  
NANOTECH 2008**

**November 24-26, 2008, Cd. de México, D.F., México**

**Torre de Ingeniería, UNAM, CU**

**Chairs: Jorge García Macedo (IF-UNAM, MEX)  
David Díaz (FCQ-UNAM, MEX)  
Elder de la Rosa (CIO, MEX)**

**GENERAL PROGRAM**

**Monday (Nov/24/2008)**

**8:00 to 11:00.a.m. - Registration.**  
**Auditorium, Torre de Ingeniería**

**9:00-9:20. - Inauguration by** Dr. Eduardo Bárzana García, Director de la Facultad de Química UNAM; Dr. Guillermo Monsiváis Galindo, Director del Instituto de Física UNAM; Dr. José Manuel Saniger Blesa, Director del Centro de Ciencias Aplicadas y Desarrollo Tecnológico UNAM; Dr. Alipio G. Calles Martínez, Coordinador de la Investigación en Facultades y Escuelas de la UNAM.

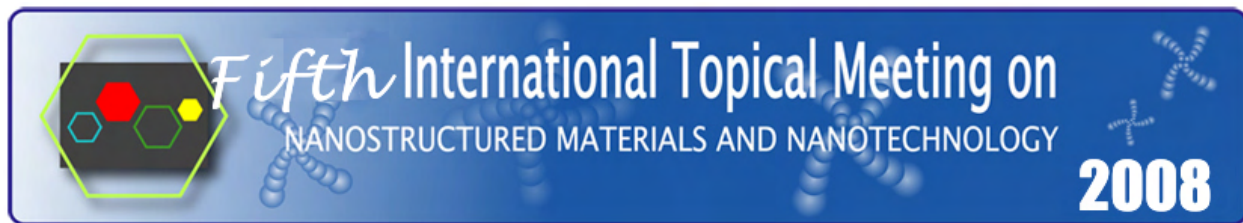
Session Chairman: Professor Massimo Guglielmi

**9:30-10:15 (Invited talk)** *The sol-gel method: a versatile soft chemistry tool for nanotechnology*  
Massimo Guglielmi, Dipartimento di Ingegneria Meccanica – Settore Materiali

**10:15-10:35 (Invited talk)** *Catalytic Nanomedicine: Cancer,*  
Tessy López<sup>1,2,3</sup>, <sup>1</sup>Health Department Universidad Autónoma Metropolitana-Xochimilco. Calzada del Hueso 1100, México D.F. 04960, México. <sup>2</sup>Nanotechnology Laboratory. National Institute of Neurology and Neurosurgery, Insurgentes 3877, México DF 14279, México. <sup>3</sup>Department of Chemical and Biomolecular Engineering, Tulane University, New Orleans, LA 70118, United States.

**10:35-10:55** *Strontium Aluminates (SrAl<sub>2</sub>O<sub>4</sub>:Eu<sup>2+</sup>, Dy<sup>3+</sup>) Nanophosphors by Combustion Synthesis.*  
R. García<sup>1,2</sup>, F. A. Ponce<sup>1</sup> and M. Barboza-Flores<sup>2</sup>, <sup>1</sup>Department of Physics, Arizona State University, Tempe, AZ 85281-1504, USA. <sup>2</sup>Centro de Investigación en Física, Universidad de Sonora, P.O. Box 5-088, Hermosillo, Sonora, 83190 México.

**10:55-11:15** *Synthesis and Characterization of Fe<sub>3</sub>O<sub>4</sub> inserted in SiO<sub>2</sub> and TiO<sub>2</sub> matrices*  
Guadalupe Valverde - Aguilar<sup>1</sup>, Jorge García - Macedo<sup>1\*</sup>, Raúl W. Gómez<sup>2</sup>, José L. Pérez - Mazariego<sup>2</sup>, and Vivianne Marquina<sup>2</sup>. <sup>1</sup>Departamento de Estado Sólido. Instituto de Física, Universidad Nacional



Autónoma de México. México D. F. C. P. 04510. <sup>2</sup>Facultad de Ciencias. Universidad Nacional Autónoma de México. Av. Universidad 3000, Copilco el Bajo. Coyoacán . México D. F., 04510.

**11:15-11:35 Amorphous Carbon - Silver Nanocomposites**

O. García - Zarco, S.E. Rodil, S. Muhl, Instituto de Investigaciones en Materiales, UNAM, Circuito Exterior s/n Ciudad Universitaria, 04510, México, D.F

**11:35-11:55 Coffee Break.**

Session Chairman: Edilso Reguera

**11:55-12:40 (Invited talk) The Hydrogen Storage in Nanocavities**

E. Reguera, Centro de Investigación en Ciencia Aplicada y Tecnología Avanzada del IPN, Unidad Legarí, Legarí 694, México, D.F.; e Instituto de Ciencia y Tecnología de Materiales, Universidad de La Habana, Cuba

**12:40-13:00 Diffuse Reflectance study of the photoactivation kinetics of TiO<sub>2</sub> (Degussa P25) in a polyacrylic acid gel matrix;** R. Trejo - Tzab, J.J. Alvarado - Gil, P. Quintana, CINVESTAV - Unidad Mérida, Depto. de Física Aplicada, A.P. 73, Cordemex, Mérida, Yuc. México. C.P. 97310

**13:00-13:20 Crystallite Dimensions, Morphology, and Microstrain of Nanocrystalline Materials obtained by using X-ray powder diffraction;** Xim Bokhimi, Universidad Nacional Autónoma de México, A.P. 20-364, 01000 México D. F., Mexico

**13:20-13:40 Transmission electron microscopy on the characterization of photonics nanomaterials.**

C. Angeles - Chavez<sup>1</sup>, E. de la Rosa - Cruz<sup>2</sup>, L. A. Díaz - Torres<sup>2</sup>, P. Salas<sup>3</sup>

<sup>1</sup>Programa de Ingeniería Molecular. Instituto Mexicano del Petróleo, Eje Central Lazaro Cardenas No. 152, Mexico D.F.C.P. 07730 Mexico, cangeles@imp.mx

<sup>2</sup>Centro de Investigaciones en Optica A.C. León, Guanajuato, C.P. 37150, Mexico.

<sup>3</sup>Centro de Física Aplicada y Tecnología Avanzada, Universidad Nacional Autónoma de México, A. P. 1-1010, Querétaro 76000, MEXICO.

**13:40-16:00 Lunch Break**

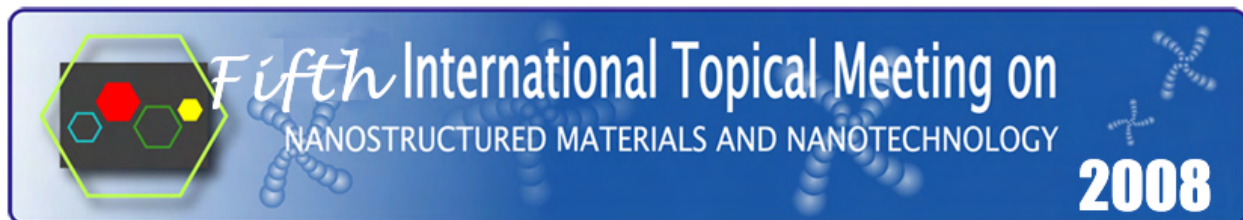
Session Chairman: Elder de la Rosa

**16:00-16:45 (Invited talk) Fullerenes, nanotubes, and nanoparticles: properties and possible applications;** Ricardo Guirado López, Instituto de Física, Universidad Autonoma de San Luis Potosí

**16:45-18:30** Poster session. Terrace Floor.

**Tuesday (Nov/25/2008)**

**9:00 to 10:00.a.m Registration.**



Session Chairman: Bradley Chmelka

**9:00-9:45 (Invited Talk)** *Heterogeneities in Semiconducting Nano-crystals': Surface Influences on Macroscopic Properties.* Bradley F. Chmelka,<sup>1</sup> Sylvian Cadars,<sup>1</sup> Benjamin Smith,<sup>1</sup> Jan D. Epping,<sup>1</sup> Yuval Golan,<sup>2</sup> Geoffrey Strouse<sup>3</sup>. <sup>1</sup>Dept. of Chemical Engineering, University of California, Santa Barbara, California, U.S.A. <sup>2</sup>Dept. of Materials Engineering, Ben-Gurion University, Beer-Sheva, Israel <sup>3</sup>Dept. of Chemistry, Florida State University, Tallahassee, Florida, U.S.A.

**9:45-10:05** *Structural characterization of one dimension nanostructures using transmission electron microscopy and associated techniques.* Patricia Santiago Jacinto, Departamento de Materia Condensada, Instituto de Física, Universidad Nacional Autónoma de México, Coyoacan, 04510, A.P. 20-364, C.P. 01000, Mexico City, Mexico.

**10:05-10:25** *Electrical Conductivity of Nanostructured Ce(1-x) Sm(x) O(2-δ).* R.Vilchis-Morales\*, E. Ruiz-Trejo. Facultad de Química, Departamento de Física y Química Teórica, Universidad Nacional Autónoma de México, 04510, México D.F.

**10:25-10:45** *Nanotechnology in Mexico: Societal Implications and Technology Assessment.* Zachary Tyler Gallagher Pirtle. Fulbright-García Robles Scholar 2008-9, Center for Nanotechnology in Society at ASU. M.S. Student in Department of Civil and Environmental Engineering, Arizona State University

**10:45-11:05** *Second Harmonic Generation of Nano-Spheres.* Bernardo S. Mendoza. Department of Photonics, Centro de Investigaciones en Optica, León, Guanajuato, México

#### **11:05-11:25 Coffee Break**

Session Chairman: Ricardo Aroca

**11:25-12:10 (Invited Talk)** *Effect of temperature and pH on the morphology, crystallinity and vibrational properties of hydrothermally grown SnO<sub>2</sub> nanostructures.* U. Pal, and A. Escobedo Morales Instituto de Física, Universidad Autónoma de Puebla, Apdo. Postal J - 48, Puebla, Pue. 72570, Mexico.

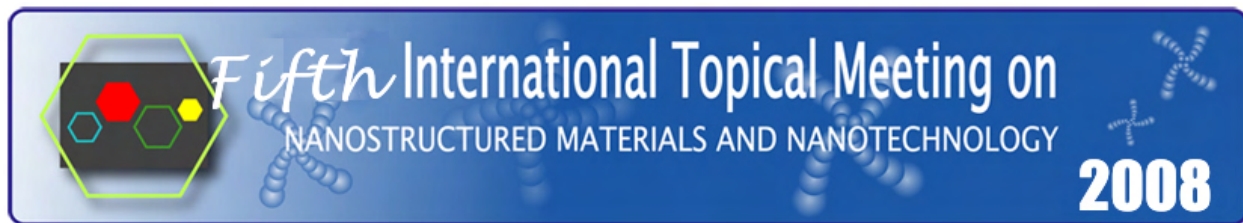
**12:10-12:55 (Invited Talk)** *SER(R)S, Plasmonics and Single Molecule Detection.* Ricardo F. Aroca. Materials and Surface Science Group, Department of Chemistry and Biochemistry, University of Windsor, Windsor, ON, Canada, N9B 3P4.

**12:55-13:15** *Optically Active Nanoparticles* Cecilia Noguez, A. Sánchez-Castillo, Francisco Hidalgo, Ignacio L. Garzón. Instituto de Física, Universidad Nacional Autónoma de México, Apartado Postal 20-364, México D. F. 01000 MÉXICO

**13:15-13:35** *Flatness Approach to Optimal Particle Steering by Optical Traps.* A. Barrañón<sup>(1)</sup>; C. Aguilar - Ibáñez<sup>(2)</sup>; H. Sira - Ramírez<sup>(3)</sup>; L.I. Rosas - Soriano<sup>(2)</sup>. <sup>(1)</sup>Dep. Basic Sciences, UAM - A, Mexico City. <sup>(2)</sup>Dep. of Physics, U. Texas. El Paso. <sup>(3)</sup>Centro de Investigación en Computación, IPN, Mexico City. <sup>(3)</sup>Dep. Ingeniería Eléctrica, CINVESTAV - IPN, Mexico City.

#### **13:35-16:00 Lunch Break**

Session Chairman: Gerko Oskam



**16:00-16:45 (Invited Talk)** *Preparation of gold nanoparticles supported on oxides. Reactivity in oxidation reactions.* Rodolfo Zanella. CCADET-UNAM. Ciudad Universitaria, México D. F. 04510

**16:45-17:05** *Small and Wide Angle X-ray Scattering (SAXS and WAXS), with the NANOSTAR of BRUKER AXS solution.* Juan Jacobo Miranda, Bruker Mexicana S.A. de C.V.

**17:20-19:30** Poster Session. Terrace Floor

## Wednesday (Nov/26/2008)

Session Chairman: Gerko Oskam

**9:00-9:45 (Invited Talk)** *Synthesis and characterization of nanomaterials for application in dye - sensitized solar cells.* Gerko Oskam, Departamento de Física Aplicada, CINVESTAV - IPN, Carr. Ant. a Progreso km 6, A.P. 73 "Cordemex", Mérida, Yuc. 97310, MEXICO.

**9:45-10:05** *Structural, magnetic and optical study of ZnO and Fe(II) doped ZnO nanoparticles.* América Vázquez - Olmos<sup>1</sup>, Jazmín Matamoros - Contreras<sup>1</sup>, Roberto Sato - Berrú<sup>1</sup>, Ana L. Fernández - Osorio<sup>2</sup> and Esther Mata - Zamora<sup>1</sup>. <sup>1</sup>Centro de Ciencias Aplicadas y Desarrollo Tecnológico and <sup>2</sup>Facultad de Estudios Superiores Cuautitlán, Universidad Nacional Autónoma de México.

**10:05-10:25** *Passive and iontophoretic transdermal penetration of triclosan nanoparticles through human skin.* I. M. Rodríguez Cruz<sup>a,b</sup>, C.L. Domínguez Delgado<sup>a</sup>, G. Leyva Gómez<sup>a</sup>, A. Ganem-Quintanar<sup>a</sup>, V. Merino-Sanjuán<sup>b</sup>, D. Quintanar-Guerrero<sup>a</sup>. <sup>a</sup>División de Estudios de Posgrado (Tecnología Farmacéutica), Facultad de Estudios Superiores Cuautitlán, Universidad Nacional Autónoma de México, Av. 1° de Mayo s/n, Cuautitlán Izcalli, C.P. 54740, México. <sup>b</sup>Departamento de Farmacia y Tecnología Farmacéutica, Universidad de Valencia. Avda. Vicente Andrés Estellés s/n, 46100 Burjassot, Valencia, España.

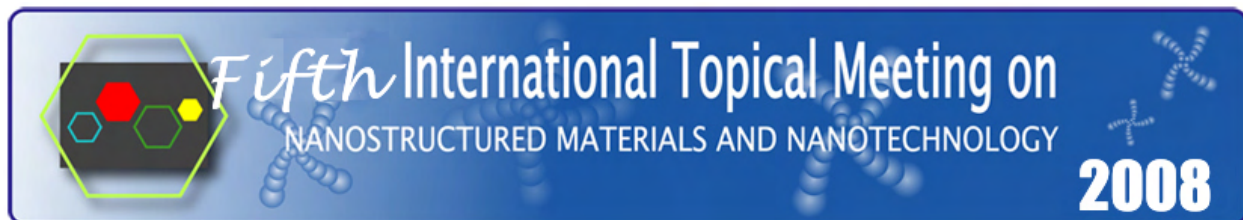
**10:25-10:45** *Optical response of silver-gold nano-shells.* Carlos E. Román-Velázquez and Cecilia Noguez. Instituto de Física, Universidad Nacional Autónoma de México, Apartado Postal 20-364, México DF 01000, México.

### 10:45-11:05 Coffee Break

Session Chairman: Professor Gerardo Goya

**11:05-11:50 (Invited Talk)** *Magnetic Nanoparticles as Heating Agents for Biomedicine.* G. F. Goya<sup>1</sup>, I. Marcos - Campos<sup>2</sup>, T. Torres<sup>1</sup>, L. Asín<sup>1</sup>, A. Tres<sup>2</sup>, C. Marquina<sup>1,3</sup> and M. R. Ibarra<sup>1,3</sup>  
<sup>1</sup> Nanoscience Institute of Aragon (INA), University of Zaragoza, Pedro Cerbuna 12, Zaragoza, Spain.  
<sup>2</sup> Hospital Clínico Universitario "Lozano Blesa", San Juan Bosco 15, Zaragoza, Spain.  
<sup>3</sup> Instituto de Ciencia de Materiales de Aragon (ICMA), Pedro Cerbuna 12, Zaragoza, Spain.

**11:25-11:45** *Molecular modeling of high-nitrogen content compounds*  
Tenorio, F. J., Merino G., Villanueva García M.  
<sup>1</sup>Centro Universitario de los Lagos, Universidad de Guadalajara. Enrique Díaz de León 1144.



Paseos de la Montaña, Lagos de Moreno, Jalisco. 2Facultad de Química, Universidad de Guanajuato. Noria Alta S/N. CP 36050. Guanajuato México.

**11:45-12:05** *Spectroscopic and Structural characterization of nanodendrites Yb<sup>3+</sup>-Er<sup>3+</sup> codoped YAG particles prepared by glycolate assisted with PVA and UREA.* R.A. Rodríguez<sup>a</sup>, H. Desirena<sup>b</sup>, E.H. Tobar<sup>a</sup>, L.A. Díaz-Torres<sup>b</sup>, P. Salas<sup>c</sup>, C. Angeles<sup>d</sup> and E. de la Rosa<sup>b</sup>. (a) Universidad de Guadalajara, CULAGOS, Lagos de Moreno, Jal. 47460, México. (b) Centro de Investigaciones en Óptica, A.P. 1-948, León, Gto. 37150, México. (c) Centro de física aplicada y tecnología avanzada-UNAM, A. P. 1-1010, Qro. México. d Instituto Mexicano del Petróleo, Eje Central Lázaro Cárdenas 152, C.P. 07730, D.F, México.

**12:05-12:25** *Studies on performance of polystyrene-brushes of CN<sub>x</sub> carbon nanotubes synthesized by NMRP in PS matrixes.* Mariamne Dehonor,<sup>a,b,c</sup> Karine Masenelli-Varlot,<sup>b</sup> Alfonso González-Montiel,<sup>c</sup> Catherine Gauthier,<sup>b</sup> Jean-Yves Cavallé,<sup>b</sup> Mauricio Terrones<sup>a</sup>. <sup>a</sup>Advanced Materials Department, IPICT, Sn. Luis Potosi, Mexico. <sup>b</sup>MATEIS, INSA de Lyon, France. <sup>c</sup>CID, Centro de Investigación y Desarrollo Tecnológico S.A. de C.V., Lerma, Mexico.

**12:25-12:40 Coffee Break**

**12:40-14:10 Mesa Redonda:** Hacia la construcción de una Red de Redes de Nanociencia y Nanotecnología en México

**14:10 Concluding Remarks**

## MONDAY POSTER TITLES

**(P001) A General Vision about Nano-science and Nano-technology**

*E.E. Hernández-Vázquez, H.H. Cerecedo-Núñez, P. Padilla-Sosa. Facultad de Física e Inteligencia Artificial Universidad Veracruzana Xalapa, Ver. Mex.*

**(P002) SHG of Poled Liquid Crystalline Azo-Dye Doped Hybrid Thin Films Prepared by the Sonogel Method**

*V. Torres-Zúñiga, O. G. Morales-Saavedra, E. Rivera, and R. Ortega-Martínez. Centro de Ciencias Aplicadas y Desarrollo Tecnológico, Universidad Nacional Autónoma de México, CCADET-UNAM. A. P. 70-186, Coyoacán, 04510, México, D. F. MEXICO.*

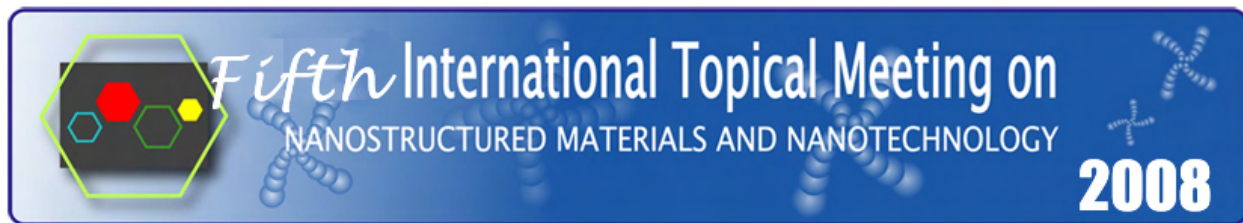
**(P003) Biodegradable nanoparticles as carrier for brain drug delivery**

*Gerardo Leyva Gómez, Marlen Rodríguez Cruz, Clara Domínguez Delgado, Celene Lozano Rivas, Adriana Ganem Rondero and David Quintanar Guerrero. División de Estudios de Posgrado (Tecnología Farmacéutica), Facultad de Estudios Superiores Cuautitlán- Universidad Nacional Autónoma de México, Estado de México, C. P. 54740, México.*

**(P004) Triclosan nanoparticles, a novel delivery system intended to be used in acne treatment.**

**Effect of sucrose laurate as skin pretreatment** *Domínguez Delgado Clara Luisa, Leyva Gómez Gerardo, Rodríguez Cruz Isabe Marlen, David Quintanar Guerrero, Ganem Rondero Flora Adriana División de Estudios de Posgrado (Tecnología Farmacéutica), Facultad de Estudios Superiores Cuautitlán, Universidad Nacional Autónoma de México, Av. 1º de Mayo s/n, Cuautitlán Izcalli, Estado de México, México. C.P. 54740, Tel.+52 55 56 23 20 65*

**(P005) High-dose TL properties of nanostructured ZnO:Yb**



E. Cruz-Zaragoza<sup>1</sup>, U. Pal2, V. Chernov<sup>3</sup>, M. Barboza-Flores<sup>3</sup>. <sup>1</sup>Instituto de Ciencias Nucleares, Universidad Nacional Autónoma de México, A.P. 70 543, México 04510 D.F. <sup>2</sup>Instituto Física, Universidad Autónoma de Puebla, A.P. J-48, Puebla, 72570 México <sup>3</sup>Centro de Investigación en Física, Universidad de Sonora, A.P. 5-088, Hermosillo, Sonora, 83190 México.

**(P006) Complex Dispersion Relation of a Dielectric Stack with Thin Metallic Layers**

A. Alejo-Molina<sup>1</sup>, J. J. Sánchez-Mondragon<sup>1</sup>, D. A. May-Arrijo<sup>1</sup>, D. Romero-Antequera<sup>1</sup>, J. Escobedo-Alatorre<sup>2</sup> and O. Ibarra-Manzano<sup>3</sup>. <sup>1</sup>Instituto Nacional de Astrofísica Óptica y Electrónica, Puebla, México, CP 72840 <sup>2</sup>Center for Research in Engineering and Applied Sciences, UAEM, Mor., México, CP 62209 <sup>3</sup>Nanophotonics Group, University of Guanajuato, Salamanca, Guanajuato, México

**(P007) Spherical 3D Photonic Crystal with a Conducting Nanoparticle Core**

A. Zamudio-Lara<sup>1</sup>, J. Sanchez-Mondragon<sup>2</sup>, R. Jaime-Rivas<sup>3</sup>, M. Torres-Cisneros<sup>3</sup>, E. Aguilera-Gómez<sup>3</sup> and S. Ledezma-Orozco<sup>3</sup>. <sup>1</sup>Center for Research in Engineering and Applied sciences. UAEM, Cuernavaca, Mexico. <sup>2</sup> INAOE/Photonics and Physical Optics Lab., Puebla, México. <sup>3</sup> NanoBioPhotonics Group, University of Guanajuato, Salamanca, Gto, México

**(P008) Synthesis of Colloidal Titanium, Tin and Zinc Oxides Nanoparticles Under Normal Reaction Conditions with Electronic Quantum Confinement**

I. Zumeta, D. Díaz. Universidad Nacional Autónoma de México, Facultad de Química, Coyoacán, C. P. 04510, México DF, México.

**(P009) Synthesis and application of carbon nanotubes by floating catalyst method using a matrix of hybrid material SBA-16/CMK**

Portales. M. B.<sup>1</sup>, Domínguez E. J. M.<sup>2</sup>, Reyes T. A. I.<sup>2</sup>, Cortés E. C. A.<sup>1</sup>, Melo B. J. A.<sup>3</sup>, Menendez. A. V. M.<sup>2</sup>. <sup>1</sup> Centro de Investigación e Innovación Tecnológica (CIITEC) <sup>2</sup>Instituto Mexicano del Petróleo, Área de Ingeniería Molecular, México D. F., México. <sup>3</sup>Instituto Tecnológico de Cd. Madero, División de Estudios de Posgrado e Investigación.

**(P010) Two-photon Lithography for Nanofabrication of Electromechanical Devices**

Naser Qureshi, Jesus Garduño-Mejía and Roberto Ortega-Martínez. Centro de Ciencias Aplicadas y Desarrollo Tecnológico, Universidad Nacional Autónoma de México, Circuito Exterior S/N, Ciudad Universitaria, México DF 04510

**(P011) Viral nanostructures: in vitro self-assembly of Parvovirus B19-like particles**

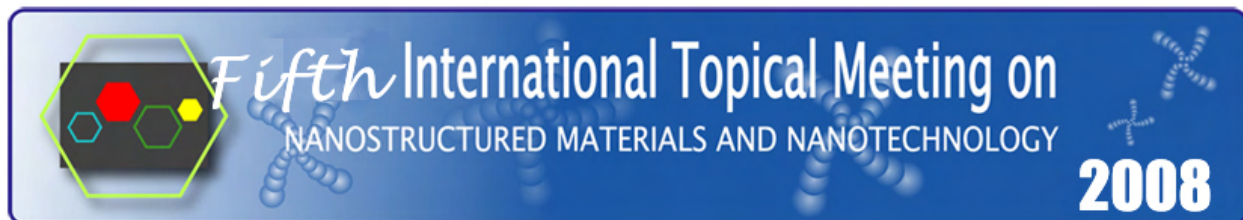
S.P. Sánchez-Rodríguez<sup>1</sup>, L. Munch-Anguiano<sup>1</sup>, O. Echeverría<sup>2</sup>, G. Vázquez-Nin<sup>2</sup>, I. Bustos-Jaimes<sup>1</sup>. <sup>1</sup> Laboratorio de Físicoquímica e Ingeniería de Proteínas, Departamento de Bioquímica, Facultad de Medicina, P.O. Box 70-159, Ciudad Universitaria, México DF 04510, México. <sup>2</sup> Laboratorio de Microscopía Electrónica, Departamento de Biología Celular, Facultad de Ciencias, Ciudad Universitaria, México DF 04510, México.

**(P012) Thermal and optical characterization of solutions containing Au nanoparticles at different pH values**

E. Navarro Cerón Juárez<sup>1</sup>, J.L. Jiménez Perez<sup>1,a</sup>, J.F. Sanchez Ramirez<sup>1</sup>, A. Cruz Orea<sup>2</sup>, J.A. Pescador Rojas<sup>1</sup>, D. Cornejo Monroy<sup>1</sup>, J.L. Herrera Pérez<sup>1</sup>. <sup>1</sup>CICATA-IPN, Legaria 694, Col. Irrigación, 11500 México D.F., México <sup>2</sup>Physics Department, CINVESTAV-IPN, A.P. 14-740, 07360 México D.F., México

**(P013) Thermal lens technique applied to the study of degradation, by UV light irradiation, of rhodamine R6G dye solutions containing TiO<sub>2</sub> nanoparticles**

S. A. Lozano Morales<sup>1</sup>, A. Cruz-Orea<sup>2</sup>, J.L. Jiménez-Pérez<sup>1,a</sup>, J.F. Sanchez Ramirez<sup>1</sup>, C. J. da Silva<sup>3</sup>, R. Saavedra<sup>4</sup>, F. Sanchez Sinencio<sup>2</sup> <sup>1</sup>CICATA-IPN, Legaria 694, Col. Irrigación, 11500 México D.F., México <sup>2</sup>Physics Department, CINVESTAV-IPN, A.P. 14-740, 07360 México D.F., México <sup>3</sup>Universidad Federal de Alagoas, UFAL, Campus A.C. Simões, BR. 104 Km. 14 Tabuleiro dos Martins CEP 57072-970. Maceió, Al, Brasil <sup>4</sup>Universidade de Concepcion, FCFM, Av. Esteban Iturra s/n, Casilla 160-C Correo 3, Concepción-Chile



**(P014) Experimental characterization of Fe(OH)<sub>2</sub> and  $\alpha$ -Fe<sub>2</sub>O<sub>3</sub> thin films prepared by the sol-gel technique.** A.E. Jiménez González, Edith Nestor Chamu and Ariatna Maldonado Abarca. Departamento de Materiales Solares, Centro de Investigación en Energía, Universidad Nacional Autónoma de México, Temixco, Morelos CP 62580, Mexico

**(P015) Study of blue, green and red emission of ZrO<sub>2</sub>:Tb<sup>3+</sup>, Tm<sup>3+</sup> and Eu<sup>3+</sup> nanocrystals respectively as function of ion concentration, H<sub>2</sub>O/EtoH and Pluronic P-127 as dispersant** T. López-Luke<sup>a</sup>, V. H. Romero<sup>a</sup>, E. De La Rosa<sup>a</sup>, Pedro Salas<sup>b</sup>, C. Angeles-Chavez<sup>b</sup>. <sup>a</sup>Centro de Investigaciones en Optica A. C. A. P. 1-948 371590 León Gto. México. <sup>b</sup>Fata, UNAM, Querétaro, Qro. 76000, México. <sup>c</sup>Instituto Mexicano del Petróleo, A. P. 14-805 07730 México D.F.

**(P016) Size and shape effect on the visible and NIR fluorescence lifetimes of nanocrystalline upconversion phosphors.** O. Meza, and L. A. Díaz-Torres. Centro de Investigaciones en Optica, A. P. 1-948, León Gto. 37160, Mexico

**(P017) Atomic Structure of Small and Intermediate-Size Silver Nanoclusters**  
Alí Michel Angulo Martínez, Cecilia Noguez. Instituto de Física, Universidad Nacional Autónoma de México, Apartado Postal 20-364, México D. F. 01000 MÉXICO

**(P018) Synthesis of carbon nanomaterials using different methods and dextrose as carbon source**  
E. Hernández<sup>a</sup>, J.A. Melo<sup>a</sup>, J. M. Domínguez<sup>b</sup>, A.I.Reyes<sup>b</sup>. <sup>a</sup>Instituto Tecnológico de Cd. Madero, División de Estudios de Posgrado e Investigación, Juventino Rosas y Jesús Urueta S/N, C. P. 89440 Tel y Fax (+52 833)215-85-44, Col. Los Mangos, Cd. Madero, Tamps, México. <sup>b</sup>Instituto Mexicano del Petróleo, Área de Ingeniería Molecular, Eje Central Lázaro Cárdenas 152, C.P. 07730, México D. F., México.

**(P019) Photoluminescence instability in Porous Silicon**  
T. Flores-Arroyo, A. Mendez-Blas, and U. Pal. Instituto de Física, Benemérita Universidad Autónoma de Puebla, Apdo. Postal J 48, C.P. 72570, Puebla, Pue., México

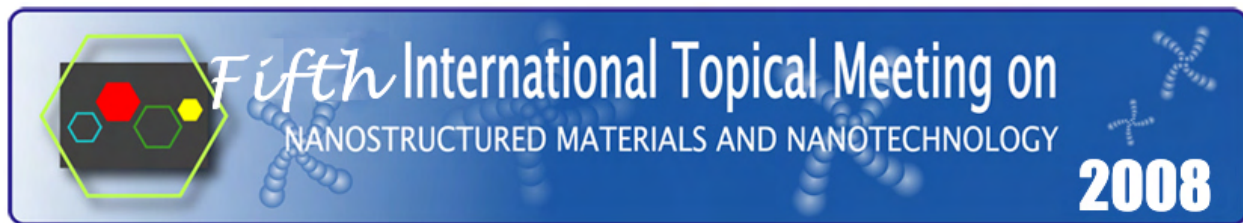
**(P020) Layered cylinders in 2D photonic crystals**  
D.L. Romero-Antequera, A. Alejo-Molina, J.J. Sánchez-Mondragón. Instituto Nacional de Astrofísica, Óptica y Electrónica Luis Enrique Erro #1, Tonantzintla, Puebla. México, C.P. 72000

**(P021) Self- organization of Cholesterol molecules on the Au (111): An STM study**  
Aristeo Segura<sup>a,b</sup>, and Nikola Batina<sup>b</sup>. a) Facultad de Ciencias Químicas. Universidad Autónoma Benito Juárez de Oaxaca, Av. Univ. S/N, Col. 5 Señores. C.P. 68120. Oaxaca, Oax., México. b) Laboratorio de Nanotecnología e Ingeniería Molecular, Depto. de Química, UAM-I, Av. San Rafael Atlixco No. 186, Col. Vicentina, Del. Iztapalapa, C.P. 09340. México, D.F., México

**(P022) Interaction of porphyrin molecules with metallic and semiconductor Nanoparticles**  
Rita Patakfalvi<sup>1,2</sup>, Donaji Velasco-Arias<sup>2</sup>, Víctor Fabián Ruiz-Ruiz<sup>2</sup>, Monica Castillo-Guevara<sup>2</sup>, Héctor García-Ortega<sup>2</sup>, David Díaz<sup>2</sup>. <sup>1</sup>Universidad de Guadalajara, Centro Universitario de los Lagos, Lagos de Moreno, México, <sup>2</sup>Universidad Nacional Autónoma de México, Facultad de Química, México.

**(P023) Preparation and Optical Evaluation of Au-Nanoparticles Based SiO<sub>2</sub> Sonogel Hybrid Composites** O. G. Morales-Saavedra, R. Zanella-Specia, J. Garduño-Mejía, F. G. Ontiveros-Barrera, V. Torres-Zuñiga, J. O. Flores-Flores and R. Ortega- Martínez.

**(P024) Novel Photochromic Effect Amplified by the Nanosize of Titania Particles of a composite with Organic Polymers** LI. M. Flores Tandy<sup>1</sup>, J. J. Perez Bueno<sup>1</sup>, Y. Meas Vong<sup>1</sup>. <sup>1</sup>Centro de Investigación y Desarrollo Tecnológico en Electroquímica, S.C. Parque Tecnológico Querétaro-Sanfandila, Pedro Escobedo, Querétaro, México. CP. 76703



**(P025) Sensibilization with Metallic Nanoparticles and Low Power Laser Treatment for Selective Modification of ABS Surfaces for Plating** Loreña Magallón Cacho<sup>1,2</sup>, José de Jesús Pérez Bueno<sup>1</sup> Yunny Meas Vong<sup>1</sup>, Guy Stremmsdoerfer<sup>2</sup>. <sup>1</sup>Centro de Investigación y Desarrollo Tecnológico en Electroquímica, S.C. Parque Tecnológico Querétaro Sanfandila, Pedro Escobedo Querétaro, México. CP. 76703 <sup>2</sup>Laboratory of Tribology and Dynamics of the Systems UMR 5513 Ecole Central de Lyon, 36 Avenue Guy de Collongue B P 163 69131 Ecully Cedex, France.

**(P026) Chemical synthesis and characterization of nanostructured hydroxyapatite Powder** A.B. Martínez-Valencia<sup>1,2</sup>, G. Carvajal-De la Torre<sup>2</sup>, H.E. Esparza-Ponce<sup>1</sup>, J. Ortiz-Landeros<sup>3</sup>. <sup>1</sup> Centro de Investigación en Materiales Avanzados CIMAV, Ave. Miguel de Cervantes 120 C.P. 31109 Complejo Industrial Chihuahua, Chihuahua, México. <sup>2</sup>Universidad Michoacana de San Nicolás de Hidalgo UMSNH, Facultad de Ingeniería Mecánica, Santiago Tapia 403. Centro C.P. 58000. Morelia Michoacán, México. <sup>3</sup> Escuela Superior de Ingeniería Química e Industrias Extractivas, Instituto Politécnico Nacional, U. P. Adolfo López Mateos, CP. 07730, México D.F., México.

**(P027) Synthesis of Nanosized Beta-Eu8Ga16Ge30 Clathrate via Calciothermic Reduction.** L. Tepech-Carrillo<sup>1,2</sup>, V. Pacheco<sup>2</sup>, W. Carrillo-Cabrera<sup>2</sup>, Yu. Grin<sup>2</sup>. <sup>1</sup> Instituto de Física, Benemérita

Universidad Autónoma de Puebla, Apdo. Postal J-48, C.P. 72570, Puebla, Pue., México. <sup>2</sup> Max-Planck-Institut für Chemische Physik fester Stoffe, Nöthnitzer Str. 4001187 Dresden, Germany

**(P028) Electronic Circular Dichroism of Single-Wall Carbon Nanotubes**

A. Sánchez-Castillo, Cecilia Noguez. Instituto de Física, Universidad Nacional Autónoma de México, Apartado Postal 20-364, México D.F.

**(P029) Optical Circular Dichroism of Bare and Passivated Au Nanoclusters**

Francisco Hidalgo and Cecilia Noguez. Instituto de Física, Universidad Nacional Autónoma de México, Apartado Postal 20-364, México D. F. 01000 MÉXICO

**(P030) Synthesis and characterization of Mg(OH)<sub>2</sub> and Ca(OH)<sub>2</sub> nanoparticles under mild reaction conditions.** Silvia Castillo - Blum<sup>1</sup>, Yolia León - Paredes<sup>1</sup>, Alicia Díaz<sup>2</sup>, and David Díaz<sup>1</sup>. <sup>1</sup> Facultad de Química. Universidad Nacional Autónoma de México. México D. F., CP 04510, México. <sup>2</sup> Facultad de Química. Universidad de La Habana, CP 10400, C. Habana. Cuba.

**(P031) A dynamic study of interaction between fragments unit (CH<sub>2</sub>) ions and fullerene (C<sub>60</sub>) molecule.** Irineo Pedro Zaragoza<sup>4</sup>, Roberto Salcedo<sup>1</sup>. Instituto de Investigaciones en Materiales,

Departamento de Polímeros, Universidad Nacional Autónoma de México, Circuito exterior s/n, Ciudad Universitaria, Coyoacán 04510, México D.F., México.

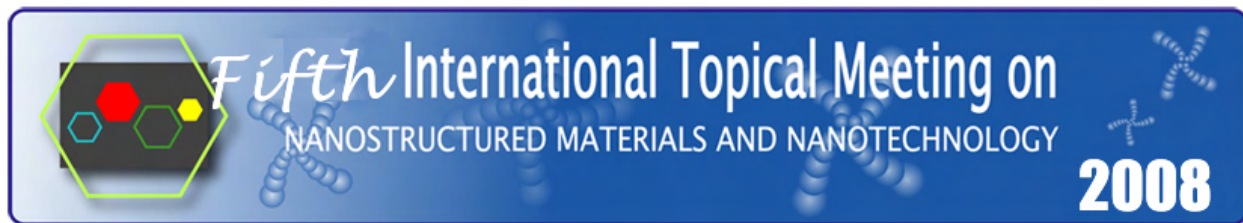
**(P032) Synthesis of Carbon Nanotubes Via Microwave Heating**

G. Rueda - Morales, G. Ortega - Cervantez, J. Ortiz - López and J.J. Vivas - Castro. Escuela Superior de Física y Matemáticas, Instituto Politécnico Nacional Edificio 9, UPALM - Zacatenco, 07738 México D.F., Mexico.

**(P033) Gd<sub>2</sub>O<sub>3</sub>:Eu<sup>3+</sup>/SiO<sub>2</sub> thick films elaborated by sol-gel process**

Juan C. Badillo Aviles<sup>1</sup>, A. García Murillo<sup>1</sup>, F. Carrillo Romo<sup>1</sup>, V. H. Romero<sup>2</sup>, E. de la Rosa<sup>2</sup>, J. Duval Lara<sup>1</sup> <sup>1</sup>Centro de Investigación en Ciencia Aplicada y Tecnología Avanzada U Altamira IPN, Km 14.5 Carr. Tampico-Pto. Industrial, C.P.89600 Altamira, Tamps, México. <sup>2</sup>Centro de Investigaciones en Óptica A.P. 1-948, 37000 León, Gto., México

**(P034) Properties of Gd<sub>2</sub>O<sub>3</sub>:Eu<sup>3+</sup>, Tb<sup>3+</sup> nanopowders obtained by the sol - gel process**



A. de J. Morales Ramírez<sup>2</sup>, A. García Murillo<sup>1</sup>, F. de J. Carrillo Romo<sup>1,2</sup>, M. García Hernández<sup>2</sup>, J. Moreno Palmerín<sup>2</sup>. 1CICATA, Unidad Altamira – Instituto Politécnico Nacional. 2Depto. de Ingeniería Metalúrgica - ESIQIE - Instituto Politécnico Nacional

**\*(P035) Synthesis and structural characterization of Ni-TR (TR = La, Ce) nanocrystalline.**

C. E. Yañez-Zamora, S. B. Brachetti-Sibaja, M. A. Domínguez-Crespo, A. M. Torres-Huerta. Km. 14.5 carretera Tampico - Puerto Industrial. Altamira, Tamaulipas. CP 89600. Fax (833) 264 93 01 CICATA IPN UNIDAD ALTAMIRA

**(P036) Effect of Optoelectronic Doping on the Phononic modes of ZnO Nanostructures:**

**Correlation between Structural and Vibrational Properties.** A. Escobedo - Morales and U. Pal.

Instituto de Física, Benemérita Universidad Autónoma de Puebla, Apdo. Postal J - 48, CP, 72570, Puebla, Pue., México.

**(P037) Synthesis of LiCoO<sub>2</sub> compound nanoparticulated by sol-gel acrylamide polymerization and microwave.** V. H. Ortiz-Iturbe, A. Ibarra-Palos, E. Chavira, C. Flores-Morales. Instituto de Investigaciones en Materiales, Universidad Nacional Autónoma de México, Circuito Exterior s/n, Ciudad Universitaria, Coyoacán, Apdo. Postal 70-360, México D.F. 04510.

## TUESDAY POSTER TITLES

**(P038) Synthesis of metallic bismuth nanoparticles by colloidal dispersion**

Selene R. Islas-Sánchez, Silvia E. Castillo-Blum, David Díaz. Depto. de Química Inorgánica, Facultad de Química, Universidad Nacional Autónoma de México, Coyoacan, Mexico D.F. 04510 Mexico.

**(P039) Synthesis of nanofibers of carbides Ni - Mo in mesoporous silicates**

Adriana Isabel Reyes de la Torre<sup>1</sup>, Benjamín Portales Martínez, José Manuel Domínguez Esquivel<sup>1</sup>, Nicolás Cayetano Castro<sup>1</sup>, Carlos Ángeles Chávez<sup>1</sup>, José Aarón Melo Banda<sup>2</sup>. 1Instituto Mexicano del Petróleo, Programa de Ingeniería Molecular, 152 Eje Central L. Cárdenas, C.P. 07730 México D. F. 2Instituto Tecnológico de Ciudad Madero, Juventino Rosas y Jesús Urueta S/N Col. Los Mangos, C.P. 89440, Cd. Madero, Tamps.

**(P040) A Novel bionanotechnological Method To Eliminate Fluorine From Water**

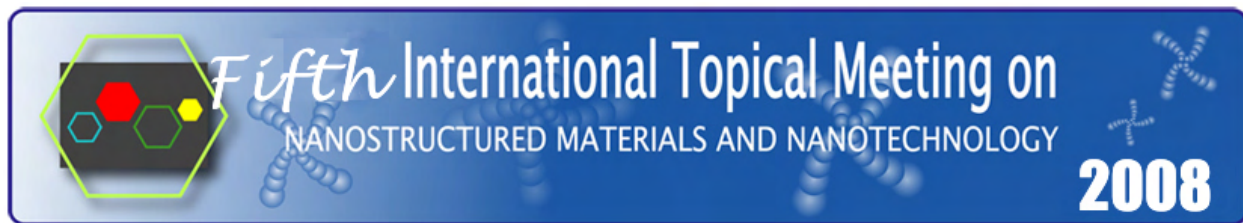
Emilio Segovia, Carlos Enrique Muñoz Brambila y Francisco Mendoza Barajas Laboratory of Bionanotechnology, Departamento de Ciencias de la Tierra y de la Vida Centro Universitario de Los Lagos, Universidad de Guadalajara, Lagos de Moreno, Jal.

**(P041) Toward solid-state molecular machines: crystalline steroid-based rotors**

Rodríguez-Molina B.<sup>1</sup>; Pozos A.<sup>2</sup>; Cruz R.<sup>2</sup>; Farfán N.<sup>2</sup>; Romero M.<sup>2</sup>; Méndez-Stivalet J. M.<sup>2</sup>; García-Garibay M.A.<sup>3</sup>; Santillan R.<sup>1</sup>. 1Departamento de Química, Centro de Investigaciones y Estudios Avanzados del IPN, México, DF. 2Facultad de Química, Universidad Nacional Autónoma de México, México, DF. 3Departamento de Química y Bioquímica, Universidad de California, Los Angeles, USA

**(P042) Structural and morphological properties of polycrystalline BaTiO<sub>3</sub>:Er<sup>3+</sup>, Yb<sup>3+</sup> ceramics synthesized by the sol-gel route: Influence of chelating agents.**

J. Duval Lara<sup>1</sup>, J. C. Badillo Avilés<sup>1</sup>, García Hernández<sup>1</sup>, A. García Murillo<sup>1</sup>, F. Carrillo Romo<sup>1</sup>, J. Ramírez Salgado<sup>2</sup>, H. Terrones<sup>3</sup>. 1Centro de Investigación en Ciencia Aplicada y Tecnología Avanzada, U. Altamira-IPN Km. 14.5 Carretera Tampico-Puerto Industrial, C.P. 89600, Altamira, Tamaulipas, México. 2 Programa de Ingeniería Molecular, Instituto Mexicano del Petróleo, Eje Lázaro Cárdenas No. 152, CP 07730, México D.F., México



3Instituto Potosino de Investigación Científica y Tecnológica, Camino a la Presa San José 2055. Col. Lomas 4 sección San Luis Potosí, S.L.P. México.

**(P043) Sol-gel synthesis and Structural Properties of Europium Doped Gadolinium Oxide Glass Nanoceramic Powders.** I. Ponce<sup>1</sup>, A. Murillo<sup>1</sup>, F. Carrillo<sup>1</sup>, E. de la Rosa<sup>2</sup>, H. Terrones<sup>3</sup>. 1Centro de Investigación en Ciencia Aplicada y Tecnología Avanzada-Instituto Politécnico Nacional, Km 14.5 Carr. Tampico-Pto. Industrial, C.P.89600 Altamira, Tamps, México. 2Centro de Investigaciones en Óptica, A. C., Loma del Bosque 115, Col. Lomas del Campestre, C. P. 37150, León, Gto., México. 3Instituto Potosino de Investigación Científica y Tecnológica, Camino a la Presa San José 2055. Col. Lomas 4 sección C. P. 78216, San Luis Potosi. S.L.P., México

**(P044) Sol-gel BaTiO<sub>3</sub>: Er<sup>3+</sup> and BaTiO<sub>3</sub>:Yb<sup>3+</sup> powders and films: Chemical and structural studies** M. García Hernández, A. García Murillo, F. de J. Carrillo Romo, L. A. Cruz Santiago, A. Garrido Hernández. Centro de Investigación en Ciencia Aplicada y Tecnología Avanzada (CICATA) Unidad Altamira – IPN Altamira, Tamaulipas; México CP 89600

**(P045) Influence of Precursor Chemistry on the Formation of BaTiO<sub>3</sub> Ceramic Powders** C. Damiani, A. García Murillo, F. Carrillo Romo, M. García Hernández. Centro de Investigación en Ciencia Aplicada y Tecnología Avanzada-Instituto Politécnico Nacional, Km 14.5 Carr. Tampico-Pto. Industrial, C.P.89600 Altamira, Tamps, México.

**(P046) Characterization and CO oxidation on silver-SiO<sub>2</sub> film-like and powder-like catalysts prepared by dip-coating method** Jorge García-Macedo, Guadalupe Valverde-Aguilar, Miguel A. Ríos-Enríquez, Víctor M. Rentería, Alfredo Franco. Departamento de Estado Sólido. Instituto de Física, Universidad Nacional Autónoma de México. México D. F. C. P. 04510

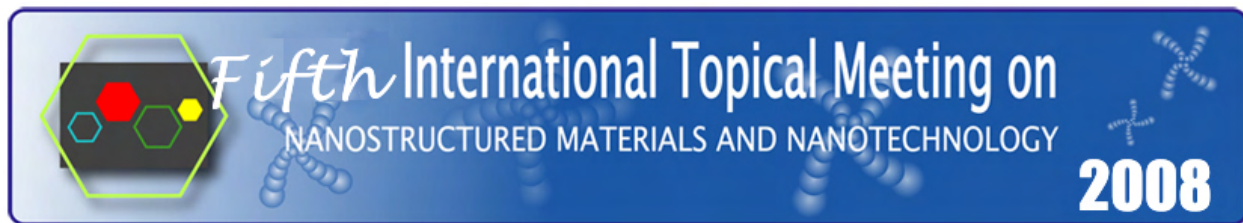
**(P047) New relationships between optical and dielectric properties of core-shell nanostructures** Víctor M. Rentería-Tapia<sup>1</sup>, Jorge A. García-Macedo<sup>1, 2</sup>. Departamento de Estado Sólido. Instituto de Física, Universidad Nacional Autónoma de México. México D.F. C.P. 04510, Ciudad Universitaria, Coyoacán, México, D.F.

**(P048) An implantable Tio<sub>2</sub> - DA complex could lead to improved motor deficits of hemiparkinsonism induced by 6 - OHDDA.** P. Vergara-Aragon<sup>1</sup>, R. Martínez-Vega<sup>2</sup>, P. Ibarra<sup>1</sup>, G. Valverde-Aguilar<sup>3</sup>, D. R Acosta<sup>3</sup>, J.A.García-Macedo<sup>3</sup>. 1 Physiology Department, Faculty of Medicine, UNAM), 2 Mathematics Academy, UACM, Sn Lorenzo Tezonco, Mexico. 2Academia de Matemáticas, UACM, México DF. 3 Departamento de Estado Sólido. Instituto de Física, Universidad Nacional Autónoma de México. México D. F. C. P. 04510

**(P049) Upconversion dynamics of the red and green emissions in ZrO<sub>2</sub>:Er-Yb nanocrystals** O. Meza,<sup>1</sup> D. Solís,<sup>1</sup> E. de la Rosa,<sup>1</sup> L. A. Díaz-Torres,<sup>1</sup> P. Salas,<sup>2</sup>. 1Centro de Investigaciones en Óptica, A. P. 1-948, León Gto. 37160, Mexico. 2Centro de Física Aplicada y Tecnología Avanzada, Universidad Nacional Autónoma de México, A.P. 1- 1010, Querétaro, Qro. 76000, Mexico

**(P050) Upconversion characterization of ZrO<sub>2</sub>:Yb<sup>3+</sup> – Tm<sup>3+</sup> nanocrystals** D. Solís<sup>1,\*</sup>, T. López-Luke<sup>2</sup>, P. Salas<sup>3</sup>, E. De la Rosa<sup>1</sup>. <sup>1</sup> Centro de Investigaciones en Óptica, A. P. 1-948, León Gto., 37160, México. <sup>2</sup> IIM, UMSNH, C.U., Morelia Mich., 58060, México. <sup>3</sup> Centro de Física Aplicada y Tecnología Avanzada, Universidad Nacional Autónoma de México, A. P. 1-1010, Querétaro, Qro., 76000, México. "MVS", Insurgentes Sur 3877, Col La Fama, C.P. 14269, D.F. México. 3Departament of Chemical Engineering, Tulane University, New Orleans, LA 70118

**(P051) Nanofluids Containing Monodisperse SiO<sub>2</sub> Nanospheres with Different Concentrations** D. Cornejo Monroy<sup>1</sup>, J. A. Balderas-López<sup>2</sup>, J. F. Sánchez Ramírez<sup>1\*</sup>, J. L. Herrera-Pérez<sup>1</sup>, U. Pal3, J. Mendoza Álvarez<sup>4</sup>. 1 Centro de Investigación en Ciencia Aplicada y Tecnología Avanzada del Instituto



Politécnico Nacional, Legaria 694. Colonia Irrigación, 11500 México D. F. 2 Unidad Profesional Interdisciplinaria de Biotecnología del IPN, Av. Acueducto S/N, Col. Barrio la Laguna, Del. Gustavo A. Madero, C.P. 07340, México, D.F., México. 3 Instituto de Física, Universidad Autónoma de Puebla, Apdo. Postal J-48, Puebla, Pue. 72570, México. 4 Departamento de Física, CINVESTAV, A. P. 14-740, México D. F. 07360, México.

**(P052) Optical and Photoacoustic Detection of Europium Nanostructures Size**

E.V. Mejía-Urriarte<sup>1</sup>, R. Huitrón-Aguilar<sup>1</sup>, J. G. Bañuelos<sup>2</sup>, O. Kolokol'tsev<sup>1</sup> and H. Murrieta S<sup>3</sup>. 1Laboratorio de Fotónica de Microondas, CCADET, AP 70-186 C.P. 04510, Universidad Nacional Autónoma de México, D.F. México. 2Laboratorio de Materiales y sensores, CCADET, AP 70-186 C.P. 04510, Universidad Nacional Autónoma de México, D.F. México. 3 Instituto de Física, AP 20-364, C.P. 01000, Universidad Nacional Autónoma de México, D.F. México.

**(P053) Development of immobilized nanostructured iron oxide catalysts and its application in the photocatalytic degradation of textile dyes.**

A.E. Jiménez González, E. Nestor Chamú and A. Maldonado Abarca. Departamento de Materiales Solares, Centro de Investigación en Energía, Universidad Nacional Autónoma de México, Temixco, Morelos CP 62580, Mexico

**(P054) Mode-Locked Fiber Laser based on Nitrogen Doped Carbon Nanotubes**

I. Hernandez-Romano<sup>1</sup>, E. E. Garcia-Espino<sup>2</sup>, D. Hernandez-Cruz<sup>2</sup>, D. A. May-Arrijoa<sup>1</sup>, M. Terrones<sup>2</sup>, and J. J. Sanchez-Mondragon<sup>1</sup>. 1 INAOE, Optics Dept., Apdo. Postal 51 y 216, Tonantzintla, Puebla 72000, Mexico. 2 Advanced Materials Department, IPICYT, San Luis Potosí 78216, México

**(P055) Free solvent synthesis of Iridium(0) nanoparticles**

Rocío Redón<sup>1</sup>, Fermín Ramírez<sup>1</sup>, Ana L. Fernández-Osorio<sup>2</sup>. 1 CCADET, Universidad Nacional Autónoma de México, Cd. Universitaria, A.P. 70-186, C.P. 04510 México D. F. 2 FES, Cuautitlán, Universidad Nacional Autónoma de México, Edo. de México.

**(P056) Synthesis and characterization of Bismuth zero-valent nanoparticles and Bismuth oxide in colloidal dispersion**

Donaji Velasco Arias<sup>1</sup>, David Díaz<sup>1\*</sup>, Patricia Santiago Jacinto<sup>2</sup>, Luis Rendón<sup>2</sup>, <sup>1</sup>Departamento de Química Inorgánica y Nuclear, Facultad de Química. <sup>2</sup>Instituto de Física UNAM. Av. Universidad 3000, Coyoacán, 04510, Mexico City, Mexico.

**(P057) Beta and UV radiation induced thermoluminescence in nanocrystalline zirconia**

V. Chernov<sup>1</sup>, F. Ramos-Brito<sup>2</sup>, T. M. Piters<sup>1</sup>, R. Meléndrez<sup>1</sup>, M. Barboza-Flores<sup>1</sup>. 1 Departamento de Investigación en Física, Universidad de Sonora, A. P. 5-088. Hermosillo, Sonora 83190, México. 2 Centro de Ciencias de Sinaloa, Av. de las Américas 2771 Norte, Culiacán, Sinaloa, 80010 México

**(P058) Electrical conductivity anomaly in single wall carbon nanotubes induced by water**

D. Mendoza. Instituto de Investigaciones en Materiales, Universidad Nacional Autónoma de México.

**(P059) Calculation of the dielectric function of zigzag (6,0) boron nitride nanotubes with adsorption of molecular hydrogen.**

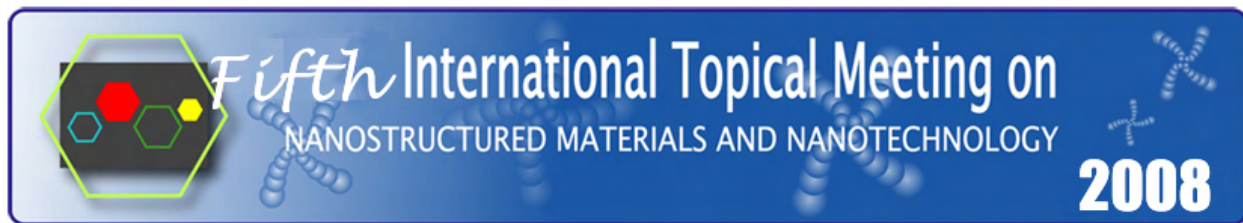
N. Arzate, R. A. Vázquez-Nava, and J. E. Mejía

**(P060) Empirical approach to calculate the number of atoms in column-domains by HAADF-STEM analysis: A binary approximation in the Nb<sub>16</sub>W<sub>18</sub>O<sub>94</sub> ternary system.**

L. Rendón and P. Santiago. 1 Departamento de Materia Condensada, Instituto de Física, Universidad Nacional Autónoma de México, Coyoacan, 04510, A.P. 20-364, C.P. 01000, Mexico City, Mexico.

**(P061) Controlled Manipulation and Transport of Vanadium Oxide Nanotubes with Optical Tweezers**

José Luis Hernández-Pozos<sup>\*†</sup>, W.M. Lee<sup>§</sup>, L. Irais Vera-Robles<sup>‡</sup>, Antonio Campero<sup>‡</sup>, and Kishan Dholakia<sup>§</sup>. <sup>†</sup> Departamento de Física, Universidad Autónoma Metropolitana-Iztapalapa (UAM-I).



Av. San Rafael Atlixco No 186. Col Vicentina. Mexico City. México. ‡ Departamento de Química, Universidad Autónoma Metropolitana-Iztapalapa, PO Box 55-534, México, DF 09340, Mexico § SUPA, School of Physics and Astronomy, University of St Andrews, North Haugh, St. Andrews KY16 9SS. United Kingdom.

**(P062) Electroluminescence in Porous Silicon whit SnO<sub>2</sub> coating**

F. Severiano-Carrillo<sup>1</sup>, G. G. Salgado<sup>2</sup>, A. Méndez-Blas<sup>1</sup>, J.M. Gracia y Jimenez<sup>1</sup> Instituto de Física, Benemérita Universidad Autónoma de Puebla, Apdo. Postal J-48, C.P. 72570, Puebla, Pue., México. Instituto de Semiconductores, Benemérita Universidad Autónoma de Puebla, C.P. 72570, Puebla, Pue., México

**(P063) Europium doped Yttrium Oxide glass ceramic nanopowders elaborated by sol-gel process: Structural and luminescent characteristics**

D. López Torres<sup>1</sup>, A. García Murillo<sup>1</sup>, F. Carrillo Romo<sup>1</sup>, N. Cayetano Castro<sup>3</sup>, V. H. Romero<sup>2</sup>, E. de la Rosa<sup>2</sup>, V. Garibay Febles<sup>3</sup>. 1Centro de Investigación en Ciencia Aplicada y Tecnología Avanzada Unidad Altamira IPN, Km 14.5 Carr. Tampico-Pto. Industrial, C.P.89600 Altamira, Tamps, México. 2Centro de Investigaciones en Óptica A.P. 1-948, 37000 León, Gto., México. 3 Programa de Ingeniería Molecular, Instituto Mexicano del Petróleo, Eje Lázaro Cárdenas No. 152, CP 07730, Mexico D.F., Mexico

**(P064) Anchoring of Bismuth Sulfide Nanoparticles on Graphite Surface**

Coraabdi Pérez Luna and David Díaz\* Universidad Nacional Autónoma de México, Facultad de Química, Ciudad Universitaria Coyoacán, CP 04510, México DF, México.

**(P065) Non-linear optical studies on amorphous and nanostructured PMMA and SiO<sub>2</sub> films doped with DO3.**

Jorge Garcia-Macedo<sup>1\*</sup>, Guadalupe Valverde-Aguilar<sup>1</sup>, Laura A. Romero Miranda<sup>1</sup>. 1 Departamento de Estado Sólido. Instituto de Física, Universidad Nacional Autónoma de México. México D. F. C. P. 04510

**(P066) Photoconductivity on amorphous and nanocrystalline sol-gel ZnO-TiO<sub>2</sub> samples**

R. Juárez-Arenas<sup>1</sup>, J. A. García-Macedo<sup>1\*</sup>, G. Valverde-Aguilar<sup>1</sup>. 1 Departamento de Estado Sólido. Instituto de Física, Universidad Nacional Autónoma de México. México D.F. C.P. 04510

**(P067) Adsorption sites for the first CO molecule on Au<sub>n</sub>+1, n=18, 19, 20: a theoretical study.**

B. Molina, J. R. Soto, and A. Callesa Facultad de Ciencias, Universidad Nacional Autónoma de México, Apartado Postal 70-646, 04510 México D. F., México. All authors are members of UNAM Nanotechnology Project (PUNTA).

**(P068) Computational Study of silicon-doped fullerenes**

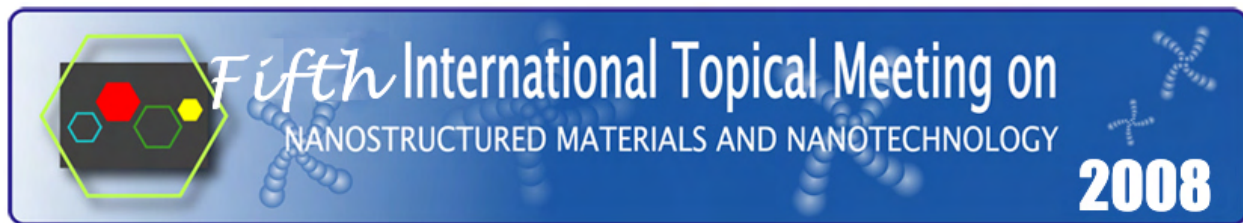
Francisco J. Tenorio<sup>1</sup>, J. G. Rodríguez Zavala<sup>1</sup>, Juvencio Robles<sup>2</sup>. 1Centro Universitario de los Lagos, Universidad de Guadalajara. Enrique Díaz de León 1144 Col. Paseos de la Montaña. Lagos de Moreno, Jalisco. CP47463. 2 Facultad de Química, Universidad de Guanajuato. Noria Alta S/N. CP36050. Guanajuato, Gto.

**(P069) B Hybrid epoxy resin –silica coatings**

E. Rubio - Rosas, Itzcua G., Varela J. and V. Rodríguez - Lugo. 1Centro Universitario de Vinculación, BUAP, Ciudad Universitaria, 72570, Puebla, Puebla, MÉXICO.

**(P070) Silver-Carbon Nanoparticles Produced By Highcurrent Pulsed Arc**

F. Maya<sup>\*1,2</sup>, M. Yoshida<sup>1</sup>, S. Muh<sup>2</sup> And O. Peña<sup>2</sup>. 1 Centro de Investigación en Materiales Avanzados (CIMAV) Chihuahua, Av Miguel de Cervantes #120, Complejo Industrial Chihuahua, C. P. 31109, Chihuahua México. 2 Instituto de Investigaciones en Materiales, Universidad Nacional Autónoma de México, Circuito Exterior S/N, Ciudad Universitaria, Coyoacan, C. P. 04510, México, D. F.



**(P071) Design of superplasticity equipment to deform Zr-base ceramic nanomaterial**

S.R. Casolco<sup>1</sup>, S. Valdez, UNAM, Av. Universidad s/n, Col. Chamilpa, Cuernavaca, Morelos, 62210. 3 Department of Mechanical Engineering, University of California, Riverside, USA

**(P072) Influence of alloying and inoculants element on the Al-Mg nanocrystalline Ribbon**

<sup>1</sup>S.R. Casolco, <sup>2</sup>M. Aguilar, <sup>3</sup>S. Valdez. 1 Tecnológico de Monterrey, Campus Puebla, Vía Atlixcáyotl 2301, Puebla, Pue. México. C.P. 72800. 2 Instituto de Física, Circuito escolar S/N, Cd. Universitaria, 04515, México, D.F., México. 3 Instituto de Ciencias Físicas-UNAM, P.O Box 48-3, Av. Universidad S/N, Col. Chamilpa, 062210, Cuernavaca, Morelos, México.\*

**(P073) Molecular hydrogen storage in nanoporous hexacyanocobaltates by means of  $\sigma$ -bond**

Cristina Pérez Krap, Luis Felipe del Castillo Dávila, Jorge Balmaseda Era Departamento de polímeros, Instituto de Investigaciones en Materiales, Universidad Nacional Autónoma de México, D.F. C.P. 04510.

**(P074) Optical shift- and injection-current response of boron nitride nanotubes**

N. Arzate, R.A. Vázquez-Nava, C.M. González, and B.S. Mendoza Centro de Investigaciones en Óptica, A.C., México. F.Nastos and J.E. Sipe Department of Physics, University of Toronto, Canada

**(P075) Sizing metallic nanoparticles by optical extinction spectroscopy**

Ovidio Peña,<sup>1</sup> \* Luis Rodríguez-Fernández,<sup>2</sup> Vladimir Rodríguez-Iglesias,<sup>2</sup> Guinther Kellermann,<sup>3</sup> Alejandro Crespo-Sosa,<sup>2</sup> Juan Carlos Cheang-Wong,<sup>2</sup> Héctor Gabriel Silva-Pereyra,<sup>2</sup> Jesús Arenas-Alatorre,<sup>2</sup> and Alicia Oliver<sup>2</sup>. 1 Instituto de Investigaciones en Materiales, Universidad Nacional Autónoma de México, Circuito Exterior S/N, Ciudad Universitaria, Coyoacan, C.P. 04510, México, D.F., México. 2 Instituto de Física, Universidad Nacional Autónoma de México, Apartado Postal 20-364, México, D.F., 01000, México. 3 Laboratório Nacional de Luz Síncrotron (LNLS), Campinas, SP, Brazil

**(P076) Au/TiO<sub>2</sub> and Au/SiO<sub>2</sub> systems as SERS active substrates**

R. Sato Berrú, V. Maturano Rojas, R.Zanella Specia, J. Saniger Blesa Centro de Ciencias Aplicadas y Desarrollo Tecnológico, Universidad Nacional Autónoma de México, Circuito Exterior s/n, C.U., Apdo. Postal 70-186, C.P. 04510, México, D.F.

**(P077) Segregation and Chemical ordering in bimetallic nanoclusters**

J. A. REYES-NAVA<sup>1,2</sup>, J. L. Rodríguez López<sup>3</sup>, U. PAL<sup>1</sup>, H. B. Liu<sup>4</sup>. <sup>1</sup>Instituto de Física, Benemérita Universidad Autónoma de Puebla, Av. San Claudio y Blvd. 18 Sur Col. San Manuel, Ciudad Universitaria C.P. 72570, Puebla, Pue., México. <sup>2</sup>Universidad Politécnica de Chiapas, Calle Eduardo J.Selvas S/N entre Manuel de J.Cancino y Enriqueta Camarillo, Col. Magisterial, C.P.29010, Tuxtla Gutiérrez, Chiapas, México. <sup>3</sup>Advanced Materials Department, IPICYT; San Luis Potosí, S.L.P, México. <sup>4</sup>Instituto Mexicano del Petróleo, Eje Central Lázaro Cárdenas No. 152, Col. San Bartolo Atepehuacan, C.P. 07730, México D.F., México

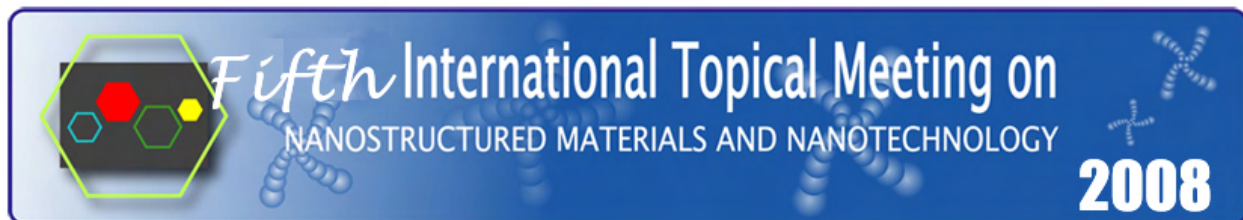
**(P078) SERS Properties Of Gold Nanoparticles In Ordered And Not Ordered Systems.**

José Juan Francisco Castillo Rivera<sup>1</sup>, Ma<sup>3</sup>. de Lourdes González González<sup>2</sup>, Elías Pérez López<sup>2</sup>, Elder de la Rosa Cruz<sup>1</sup>. Centro de investigaciones en óptica, Loma del Bosque #115 Colonia Lomas del Campestre 1, Instituto de Física, Universidad Autónoma de San Luis Potosí, Av. Manuel Nava #6 Zona Universitaria. C.P 782902.

**(P079) One Dimensional Photonic Crystal with Conducting Nanoparticles Classical Composite**

J. Sánchez-Mondragon<sup>1</sup>, J. Escobedo-Alatorre<sup>2</sup>, M. Basurto-Pensado<sup>2</sup>, A. Alejo-Molina<sup>1</sup>, J. O. Vázquez Buenos Aires<sup>3</sup> and D. A. May-Arrijo<sup>1</sup>. 1 INAOE/Photonics and Physical Optics Lab., Puebla, México. 2 Center for Research in Engineering and Applied sciences. UAEM, Cuernavaca, Mexico. 3 Universidad del Papaloapan, Loma Bonita Oaxaca, México.

**(P080) Sensibilization with Metallic Nanoparticles and Low Power Laser Treatment for Selective**



**Modification of ABS Surfaces for Plating** Lorena Magallón Cacho<sup>1,2</sup>, José de Jesús Pérez Bueno<sup>1</sup> Yunny Meas Vong<sup>1</sup>, Guy Stremmsdoerfer<sup>2</sup>. <sup>1</sup>Centro de Investigación y Desarrollo Tecnológico en Electroquímica, S.C. Parque Tecnológico Querétaro Sanfandila, Pedro Escobedo Querétaro, México. CP. 76703 <sup>2</sup>Laboratory of Tribology and Dynamics of the Systems UMR 5513 Ecole Central de Lyon, 36 Avenue Guy de Collongue B P 163 69131 Ecully Cedex, France.

**(P081) Study of layer defect in 1-D omnidirectional mirrors based in Porous Silicon Multilayers** J. O. Estevez<sup>1</sup>, J. Arriaga<sup>1</sup>, A. Mendez-Blas<sup>1</sup>, V. Agarwal<sup>2</sup>. <sup>1</sup>Instituto de Física, Benemérita Universidad Autónoma de Puebla, Apdo. Postal J-48, C.P. 72570, Puebla, Pue., México. <sup>2</sup>CIICAP, Universidad Autónoma del Estado de Morelos, C.P. 62209, Cuernavaca Mor., México

**(P082) Estudio de optimización de nanoestructuras de CeO<sub>2</sub>, La<sub>2</sub>O<sub>3</sub> y fases mixtas obtenidas aplicando la síntesis hidrotérmica.** R. Rangel<sup>1</sup>, K. Arreola<sup>1</sup>, P. Bartolo-pérez<sup>2</sup>. <sup>1</sup>Facultad de ingeniería química, Universidad Michoacana de San Nicolás de Hidalgo, Edificio "K", Ciudad Universitaria. 58060, Morelia, Michoacán, México. <sup>2</sup>CINVESTAV-IPN unidad Mérida, Departamento de Física de Materiales. Mérida, Yuc. México

**(P083) Influence of the Ethanol in the formation of Vanadium Oxide Nanotubes** L. Irais Vera-Robles, Antonio Campero Universidad Autónoma Metropolitana-Iztapalapa, Departamento de Química.

**(P084) A general and easy colloidal method for the synthesis of small and stable zerovalent Fe, Co, Ni and Cu nanoparticles** Maiby Valle-Orta<sup>1</sup>, David Díaz<sup>1\*</sup>, Patricia Santiago-Jacinto<sup>2</sup>, América R. Vazquez-Olmos<sup>3</sup>, Roberto Sato-Berrú<sup>3</sup> and Edilso Reguera Ruiz<sup>4</sup>. <sup>1</sup>Facultad de Química; <sup>2</sup>Instituto de Física; <sup>3</sup>Centro de Ciencias Aplicadas y Desarrollo Tecnológico de la Universidad Nacional Autónoma de México, Ciudad Universitaria, Coyoacán, CP 04510; <sup>4</sup>CICATA U Legaria, Instituto Politécnico Nacional, Legaria 694, Colonia Irrigación, Miguel Hidalgo, CP 11500, México D. F., México

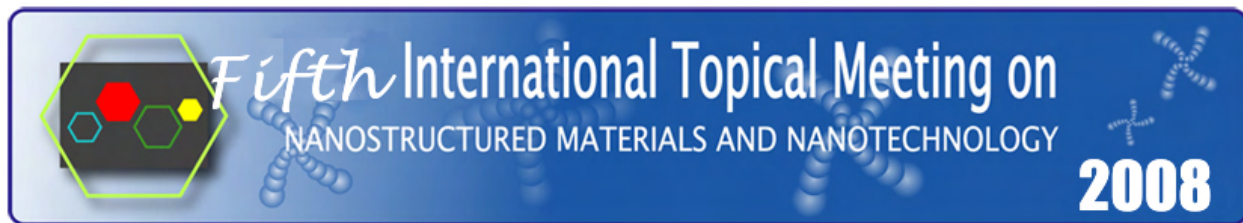
**(P085) Nano-pigments: synthesis, characterization and performance** A. Fernández-Osorio<sup>1</sup>, L. Serrano<sup>2</sup>. <sup>1</sup>FES Cuautitlán Universidad Nacional Autónoma de México. <sup>2</sup>Ferro Mexicana, S.A. de C.V.

**(P086) Chemical reactivity study of Fe<sub>2</sub>O<sub>3</sub> and Fe<sub>3</sub>O<sub>4</sub> nanoestructures by DFT** B. Ruiz - López<sup>1</sup>, R. Esparza<sup>2</sup>, E. Rubio - Rosas<sup>1</sup>, R. Pérez<sup>2</sup> y V. Rodríguez - Lugo<sup>1</sup>  
<sup>1</sup>Centro Universitario de Vinculación, BUAP, Ciudad Universitaria, 72570, Puebla, Puebla, MÉXICO. <sup>2</sup>Instituto de Ciencias Físicas, UNAM, P. O. Box 48 - 3, 62251, Cuernavaca, Mor., MÉXICO.

**(P087) Molecular simulation of thiol - functionalized carbon nanotubes** R. Rivera<sup>1</sup>, R. Esparza<sup>2</sup>, E. Rubio - Rosas<sup>1</sup>, R. Pérez<sup>2</sup> y V. Rodríguez - Lugo<sup>1</sup>. <sup>1</sup>Centro Universitario de Vinculación, BUAP, Ciudad Universitaria, 72570, Puebla, Puebla, MÉXICO. <sup>2</sup>Instituto de Ciencias Físicas, UNAM, P. O. Box 48 - 3, 62251, Cuernavaca, Mor., MEXICO.

**(P088) Nonlinear Pulse Propagation in an Optical Fiber Doped with Conducting Nanoparticles** J. Sanchez-Mondragon<sup>1</sup>, M. Torres-Cisneros<sup>2</sup>, C. Velásquez-Ordoñez<sup>3</sup>, M. Tecpoyotl-Torres<sup>4</sup>, E. Pérez-Careta<sup>2</sup> and J. O. Vázquez Buenos Aires<sup>5</sup>. <sup>1</sup>INAOE/Photonics and Physical Optics Lab., Puebla, México. <sup>2</sup>NanoBioPhotonics Group, University of Guanajuato, Salamanca, Gto, México. <sup>3</sup>Universidad de Guadalajara, Guadalajara, Jalisco, México. <sup>4</sup>Center for Research in Engineering and Applied Sciences. UAEM, Cuernavaca, Mexico. <sup>5</sup>Universidad del Papaloapan, Loma Bonita Oaxaca, México.

**(P089) Adsorption and separation of linear and branched hydrocarbons by nanoporous pyrazine**



**pillared tetracyanonickelate** P. Vera-Cruz<sup>1</sup>, A. A. Lemus-Santana<sup>1</sup>, B. Torruco<sup>1</sup>, L. F. del Castillo<sup>1</sup>, J. Balmaseda<sup>1</sup>. Departamento de polímeros, Instituto de Investigaciones en Materiales, Universidad Nacional Autónoma de México, D.F. C.P. 04510.

**(P090) Reactive block copolymers as versatile compatibilizers for polymer-clay nanocomposites** Leticia Flores-Santos, Alberto Rosas-Aburto, Alfonso González-Montiel, María Dolores Baeza-Alvarado, Edgar Espinoza-Rodríguez and Pablo Esparza-Hernández. CID, Centro de Investigación y Desarrollo Tecnológico S.A. de C.V., Lerma, Mexico.

**(P091) A comparative study of nano - structured iron oxide films prepared by spray pyrolysis and laser ablation.** M.A. García - Lobato<sup>1</sup>, A.I. Martínez<sup>1</sup>, R. Castro - Rodríguez<sup>2</sup>, D. Bueno - Baques<sup>3</sup>  
<sup>1</sup> Cinvestav Unidad Saltillo, Carr. Saltillo - Mty Km 13, Ramos Arizpe Coahuila 25900, México.  
<sup>2</sup> Departamento de Física Aplicada, Cinvestav Unidad Mérida, 97310 Mérida Yucatán, México.  
<sup>3</sup> Centro de Investigación en Química Aplicada, Blvd. Enrique Reyna Hermosillo 140, Apto, Postal 379, Saltillo, Coah, 25100, México.

**(P092) Detection and Light Enhancement by means of Porous Silicon Devices**  
 G. Palestino<sup>a</sup>, V. Agarwal<sup>b</sup>, E. Pérez<sup>c</sup>, C. Gergely<sup>d</sup>. a Facultad de Ciencias Químicas, Universidad Autónoma de San Luis Potosí, México; b CIICAP-UAEM, Av. Universidad 1001, Col Chamilpa, Cuernavaca, Mor., México; c Instituto de Física, Universidad Autónoma de San Luis Potosí, SLP, México d GES-UMR 5650, CNRS- Université Montpellier II, Montpellier Cedex 5, France;

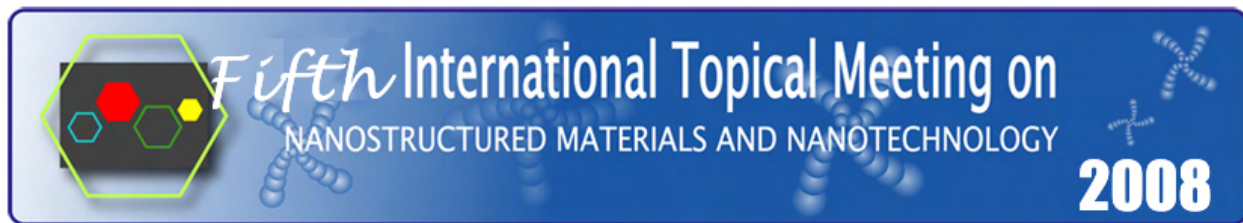
**(P093) Effect of water concentration in dopamine occluded in nanostructured silica reservoirs to Parkinson treatment.** T. López<sup>1,2,3</sup>, D. Esquivel<sup>4</sup>, E. Ortiz<sup>2</sup>, A. Miguel<sup>1,2</sup>, I. Sánchez-Jerónimo<sup>1,2</sup>.  
<sup>1</sup>Universidad Autónoma Metropolitana- Xochimilco. Health Attention Department. Calzada del Hueso 1100, C.P. 04960, Tlalpan, México D.F. <sup>2</sup>Instituto Nacional de Neurología y Neurocirugía "MVS". Nanotechnology-Nanomedicine Laboratory. Insurgentes Sur 3877, Col. La Fama, Tlalpan México D.F. <sup>3</sup>CIQI, Guanajuato University. Noria Alta s/n, C.P. 36050. Guanajuato, México.

**(P094) Structural and Electronic Properties of Au and Au<sub>2</sub> on an MgO(100) Surface: Nature of the Bonding, Surface Relaxation and Charge Transfer.** Alicia Ayala<sup>1</sup>, Reyna Caballero,<sup>1</sup> Andreas M. Köster,<sup>2</sup> Shiv N. Khanna,<sup>3</sup> and J. Ulises Reveles,<sup>3</sup> and Carlos Quintanar,<sup>1</sup>. <sup>1</sup>Facultad de Ciencias, Universidad Nacional Autónoma de México, Ciudad Universitaria, 04510 México, D.F., México. <sup>2</sup>Departamento de Química, Cinvestav, Avenida Instituto Politécnico Nacional 2508, A.P. 14-740, México, D.F., 07000, México. <sup>3</sup>Physics Department, Virginia Commonwealth University, Richmond, Virginia, 23284-2000, USA.

**(P0095) Activity of nanostructured TiO<sub>2</sub> or SiO<sub>2</sub> based biocatalysts over DNA fragmentation**  
 T. López<sup>1,2,3</sup>, J. Bustos<sup>1</sup>, M. Alvarez<sup>2</sup>, V. Coria<sup>1</sup>, I. Meza-Mena<sup>1</sup>. <sup>1</sup> Departamento de Atención a la Salud, Universidad Autónoma Metropolitana-Xochimilco, Calz. Del Hueso 1100, Col. Villa Quietud, Coyoacán, C. P. 04960, D.F. México. <sup>2</sup> Laboratorio de Nanotecnología, Instituto Nacional de Neurología y Neurocirugía

**(P096) Molecular dynamic study of the interaction vanadium oxide-HY zeolite**  
 Maricela Arroyo<sup>1</sup>, I. Pedro Zaragoza<sup>1</sup> and Ruben Santamaria<sup>2</sup>. <sup>1</sup>Instituto de Investigaciones en Materiales, Polímeros, Universidad Nacional Autónoma de México, A.P. 70-360, D.F. 045510, México <sup>2</sup>Instituto de Física, Universidad Nacional Autónoma de México, A.P. 20-364, 01000, D.F. México

**(P097) Stabilization of metotrexato in sol-gel biocompatible sol-gel silica to treat brain gliomas**  
 T. López<sup>1,2,3</sup>, M. Alvarez<sup>1,2</sup>, E. Ortiz-Islas<sup>2</sup>, A. Miguel<sup>2</sup>, I. Sanchez-Jerónimo<sup>2</sup>. <sup>1</sup> Universidad Autonoma Metropolitana-Xochimilco. Departamento de Microbiología, Calzada del Hueso 1100, Col. Villa Quietud, Coyoacán, C. P. 04960, México D.F, <sup>2</sup> Instituto Nacional de Neurología y Neurocirugía "MVS", Laboratorio de Nanotecnología. Av. Insurgentes Sur 3877, Col. La Fama, Tlalpan, 14269, México, D.F. <sup>3</sup> Department of Chemical and Biomolecular Engineering, Tulane University, New Orleans LA 70118 USA.



**(P098) Biocompatibility analysis nanostructured Pt/TiO<sub>2</sub> by histological techniques of nanostructured titania microinjection in the central nervous system.** T. López<sup>1,2,3</sup>, P. Arteaga-López<sup>1</sup>, L. Aguirre<sup>2</sup>, A. Arellano<sup>2</sup>, J. Avilés<sup>2</sup> and D. Molina<sup>2</sup>. 1Universidad Autónoma Metropolitana - Xochimilco, Health Department. Calzada del Hueso 1100, Col. Villa Quietud, Coyoacán, México, 04960. 2Nanotechnology Laboratory, National Institute of Neurology and Neurosurgery "Manuel Velasco Suárez". Insurgentes Sur 3877, Col. La Fama, Tlalpan, México, 14279. 3Department of Chemical and Biomolecular Engineering, Tulane University, New Orleans, LA 70118.

**(P099) Biocompatibility study of criptomelane vs functionalized criptomelane implants in rat brain** T. Lopez<sup>(a,b,c)</sup>, E. Ortiz-Islas<sup>(a)</sup>, P. Arteaga-López<sup>(b)</sup>, J. Manjarrez<sup>(a)</sup>, R. Arroyo<sup>(b)</sup>, M. Alvarez<sup>(a)</sup>, M. Montes<sup>e</sup>, P. Navarro<sup>e</sup>, J. A. Odriozola<sup>f</sup>. (a) Instituto Nacional de Neurología y Neurocirugía "MVS", México, DF, México. (b) Depto. Ciencias Biológicas y de la Salud. Universidad Autónoma Metropolitana-Xochimilco, México. (c) Department of Chemical and Biomolecular Engineering, Tulane University, New Orleans. (e) Universidad del País Vasco. Departamento de Química aplicada, España. (f) Instituto de Ciencia de Materiales US-CSIC. Sevilla, España.

**(P100) Biocompatibility and efficiency of nanocatalysts M/TiO<sub>2</sub> implanted in brain glioma using stereotaxic surgery.** T. López<sup>1,2,3</sup>, J. Manjarrez<sup>4</sup>, M. Calvillo<sup>5</sup>, E. Martínez<sup>1,2</sup>. 1Universidad Autónoma Metropolitana - Xochimilco, Health Department. Calzada del Hueso 1100, Col. Villa Quietud, Coyoacán, México, 04960. 2Nanotechnology Laboratory, National Institute of Neurology and Neurosurgery "Manuel Velasco Suárez". Insurgentes Sur 3877, Col. La Fama, Tlalpan, México, 14279. 3Department of Chemical and Biomolecular Engineering, Tulane University, New Orleans, LA 70118. 4Reticular Formation Physiology Laboratory, National Institute of Neurology and Neurosurgery "Manuel Velasco Suárez". Insurgentes Sur 3877, Col. La Fama, Tlalpan, México, 14279. 5Neurodegenerative Diseases Laboratory, National Institute of Neurology and Neurosurgery "Manuel Velasco Suárez", Insurgentes Sur 3877, Col. La Fama, Tlalpan, México, 14279.

**(P101) Catalytic Nanomedicine: Dispersed Cis-Pt/TiO<sub>2</sub> activity and of support super acid in the model C6 rat Wistar.** T. López<sup>1,2,4</sup>, P. Guevara<sup>3</sup>, I. Sánchez-Jeronimo<sup>2</sup>, J. A. Odriozola<sup>5</sup>. 1Universidad Autónoma Metropolitana-Xochimilco. Dept. Atención a la salud. Calzada del hueso 1100, C. P. 04960, Tlalpan, México, D. F. 2Laboratorio de Nanotecnología and, 3Departamento de Neuroinmunología, Instituto Nacional de Neurología y Neurocirugía "MVS". Insurgentes Sur 3877, México D. F. C. P 14269, México. 4 Chemistry Department and Biochemical Engineering, Tulane University, New Orleans U.S.A. 5 Departamento de Química Inorgánica e Instituto de Ciencia de Materiales de Sevilla, Centro Mixto Universidad de Sevilla-CSIC, Av. Américo Vespucio 49, Sevilla, Spain.

**TALKS**

# The sol-gel method: a versatile soft chemistry tool for nanotechnology

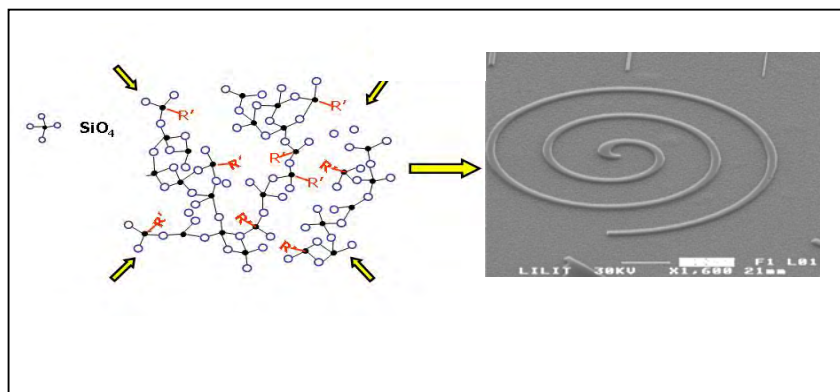
*Massimo Guglielmi*

Dipartimento di Ingegneria Meccanica – Settore Materiali

[massimo.guglielmi@unipd.it](mailto:massimo.guglielmi@unipd.it)

## INVITED TALK

The sol-gel method was continuously growing in both scientific fundamentals and industrial applications since the seventies, when it started to interest the community of glass researchers as an innovative method to prepare glasses at low temperature. During its evolution it was employed to prepare glasses, glass-ceramics, ceramics and, finally, hybrid organic-inorganic materials in the shape of dense or porous (aerogel) bulks, thin films, nanoparticles. Nowadays, that nanotechnologies are capturing an enormous amount of activity in many scientific and technological fields, sol-gel is proving a powerful, versatile and soft chemistry tool. This is due to the possibility to synthesise different materials with different properties and to tailor them to specific and sophisticated needs. Few examples to prove this statement will be given, related to different applications: films containing chromophores with large dipolar moments for second order non-linear optical applications, hybrid materials specifically designed for direct nanopatterning, porous materials doped with semiconductor nanoparticles for gas-sensing applications, multifunctional nanocomposite materials for LED encapsulation.



**Example of patterned film achieved in a hybrid O/I material by EBL**

# Catalytic Nanomedicine: Cancer

Tessy López<sup>1,2,3</sup>

<sup>1</sup>Health Department Universidad Autónoma Metropolitana-Xochimilco. Calzada del Hueso 1100, México D.F. 04960, México [tessy3@prodigy.net.mx](mailto:tessy3@prodigy.net.mx) <sup>2</sup>Nanotechnology Laboratory. National Institute of Neurology and Neurosurgery, Insurgentes 3877, México DF 14279, México. <sup>3</sup>Department of Chemical and Biomolecular Engineering, Tulane University, New Orleans, LA 70118, United States.

## INVITED TALK

Cytostatic drugs are important compounds used in chemotherapeutic treatment of cancer, autoimmune diseases, and bacterial or viral infection. They are also used in immuno-suppression therapies to reduce transplant rejection. Most of them are extremely active compounds, highly toxic and are used in micro-quantities. They are divided in different categories according to their mechanism of action or chemical nature. Glioblastoma multiforme (GBM) is by far the most common and most malignant of the glial tumors. It is composed of a heterogeneous mixture of poorly differentiated neoplastic astrocytes. These tumors may develop from lower-grade astrocytomas (World Health Organization [WHO] grade II) or anaplastic astrocytomas (WHO grade III). The treatment of glioblastomas is palliative and includes surgery, radiotherapy, chemotherapy and recently gliadel® local PLGA implants with carmustine. The kind of chemotherapeutics use in these patients is alkylating agents like temozolamide or cis-platinum based drugs, due to their relative efficacy against GBM. However, blood brain barrier (BBB) is the main obstacle to reach damaged areas. In our laboratory has been developed a neurological nanostructured biocatalyst using 1% of  $\text{H}_2\text{PtCl}_6 \cdot 6 \text{H}_2\text{O}$  supported on a solid acid and brain tissue biocompatible sol-gel titania or silica. The results show nanostructured solids with elevated quantity of Lewis sites and the presence of the  $1450 \text{ cm}^{-1}$  characteristic Brönsted sites. A  $\text{C}_6$  glioma model in Wistar rats was used. These solid materials are effective for the reduction of tumors. A strong dependence of platinum particle size and dispersion, as well, support hydroxylation and functionalization grade in the reduction of the tumor was observed. The acid sites of nanostructured biomaterial will be coordinated to C-N basic sites in DNA. Subsequently, the platinum cross-links two bases via displacement of the chloride ligand. Dispersed  $\text{H}_2\text{PtCl}_6$  link DNA in several different ways, interfering with cell division by mitosis. The damaged DNA elicits was bonded to the octahedral metal ligands, which in turn activate cell apoptosis.

## Strontium Aluminates ( $\text{SrAl}_2\text{O}_4:\text{Eu}^{2+}, \text{Dy}^{3+}$ ) Nanophosphors by Combustion Synthesis

R. García<sup>1,2</sup>, F. A. Ponce<sup>1</sup> and M. Barboza-Flores<sup>2</sup>

<sup>1</sup> *Department of Physics, Arizona State University,  
Tempe, AZ 85281-1504, USA.*

<sup>2</sup> *Centro de Investigación en Física, Universidad de Sonora, P.O. Box 5-088,  
Hermosillo, Sonora, 83190 México.*

[rafael.garcia@asu.edu](mailto:rafael.garcia@asu.edu)

$\text{Eu}^{2+}$ -doped phosphors usually show intense broad band luminescence with a short decay time of the order of tens nanoseconds. The emission of  $\text{Eu}^{2+}$  is very strongly dependent on the host lattice and can occur from the ultraviolet to the red region of the electromagnetic spectrum. This is because the  $5d \leftrightarrow 4f$  transition is associated with a change in the electric dipole and the  $5d$  excited state is affected by crystal field effects. The  $\text{Eu}^{2+}$  emission from many phosphor hosts is sufficiently intense for important lighting and display applications. An important class of phosphors is based on  $\text{Dy}^{3+}$ - $\text{Eu}^{2+}$ -codoped aluminates of alkaline earth metals. Strontium aluminates codoped with  $\text{Dy}^{3+}$  and  $\text{Eu}^{2+}$  have very high quantum efficiency, long persistence and better stability than the other alkaline earth aluminates. In this presentation, we report a two-step method to synthesize strontium aluminates codoped with  $\text{Eu}^{2+}$  and  $\text{Dy}^{3+}$  nanopowders. This phosphor was prepared via a novel synthesis technique based on combustion synthesis and a subsequently annealing in ammonia at  $1000\text{ }^\circ\text{C}$ . The combustion synthesis involves a highly exothermic redox reaction between metal nitrates and an organic fuel to produce nanosized particles. With this two-step method is possible to control the particle size from the few nanometers to micrometers through the fuel-to-oxidizer ratio and the later annealing process under an ammonia atmosphere. Studies of cathodoluminescence and photoluminescence show that the spectra of the as-synthesized nano-powder present the main electronic transitions of each ion present in the host, while the annealed powders show only a broad intense peak centered at  $528\text{ nm}$  that is related to the  $\text{Eu}^{2+}$  ion. The luminescence of this powders is at least two order of magnitude more intense than the luminescence of the as-synthesized powder.

# Synthesis and Characterization of Fe<sub>3</sub>O<sub>4</sub> inserted in SiO<sub>2</sub> and TiO<sub>2</sub> matrices

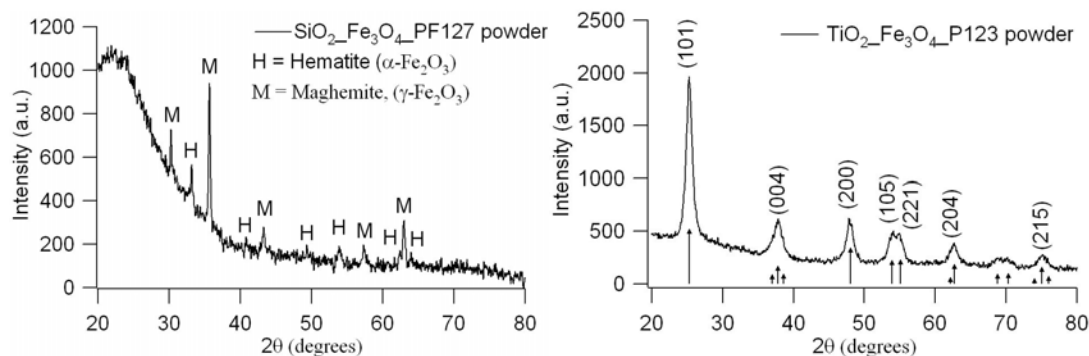
Guadalupe Valverde-Aguilar<sup>1</sup>, Jorge Garcia-Macedo<sup>1\*</sup>, Raúl W. Gómez<sup>2</sup>, José L. Pérez- Mazariego<sup>2</sup>, and Vivianne Marquina<sup>2</sup>

3. *Departamento de Estado Sólido. Instituto de Física, Universidad Nacional Autónoma de México. México D. F. C. P. 04510*

2. *Facultad de Ciencias. Universidad Nacional Autónoma de México. Av. Universidad 3000, Copilco el Bajo. Coyoacán . México D. F., 04510.*

E-mail: valverde@fisica.unam.mx

A study of sol-gel embedded Fe<sub>3</sub>O<sub>4</sub> nanoparticles into silica (SiO<sub>2</sub>) and titanium dioxide (TiO<sub>2</sub>) is presented. In order to avoid agglomeration of the nanoparticles into the matrices, block copolymers were added to the precursor solution (described below): Pluronic F127 to SiO<sub>2</sub> and Pluronic P123 to TiO<sub>2</sub>. Both kinds of Fe<sub>3</sub>O<sub>4</sub>-doped matrices were annealed at 450 °C for 2 h. X-ray diffraction (XRD) was used to determine the structures of these matrices: Optical absorption, infrared spectroscopy and high resolution transmission electronic microscopy (HRTEM) were used to characterize the films. Room temperature transmission Mössbauer spectra were also obtained to determine the ionic state of the Fe atoms and also to establish if the heat treatment modified its original state.



XRD patterns of SiO<sub>2</sub>:Fe<sub>3</sub>O<sub>4</sub> powders (Left) and TiO<sub>2</sub>:Fe<sub>3</sub>O<sub>4</sub> powders (Right) recorded at room temperature.

\* CONACYT 79781, NSF-CONACYT, PUNTA, PAPIIT 116506-3 and DGAPA UNAM IN123804 supported this work. GVA is grateful for a ICyTDF postdoctoral fellowship.

# The Hydrogen Storage in Nanocavities

E. Reguera

*Centro de Investigación en Ciencia Aplicada y Tecnología Avanzada del IPN, Unidad Legaríá, Legaríá 694, México, D.F.; e Instituto de Ciencia y Tecnología de Materiales, Universidad de La Habana, Cuba.*

Email: [ereguera@yahoo.com](mailto:ereguera@yahoo.com)

**INVITED TALK**

The development of the human civilization is closely related to the availability of energy sources. From the first industrial activity for exploitation of petroleum, in 1859, and then its processing to obtain different derivatives, practically all of the known technological advances have been linked to the use of this fossil fuel. Petroleum and other fossil fuels are nonrenewable energy resources, and for the next decades a definitive decline in their availability and production are expected. The energy accumulated by nature as fossil fuel during millions of years is being consumed by the human kind in scarcely three centuries. In addition, the combustion of fossil fuels leads to CO<sub>2</sub> emission, which is responsible for the global warming and of the related climate changes. From these facts, the research and development activities on renewably energy sources have received increasing attention in the last decades. In this sense, sunlight harvesting appears to be most attractive solution. However, for applications like automotive vehicles, and also as an energy storage medium, a secondary energy bearer is required. Hydrogen is a promising secondary-energy bearer related to its clean combustion (produces water as byproduct) and high heating value (572 kJ/mol). For such applications, the main fundamental and technological challenge is to find appropriate methods for hydrogen storage. Hydrogen, in its molecular form, H<sub>2</sub>, can only be maintained in liquid state below 32.7 K (the H<sub>2</sub> critical temperature), independent of the applied pressure, and the liquefaction process consumes about 40% of the energy to be generated. H<sub>2</sub> storage at high pressure appears to be impractical, for a pressure of 345 atm. a density of 15/g is obtained, relatively low compared with 70 g/L for liquid state. An attractive option is the physical adsorption due to its reversibility, but with the inconvenience, to date, of relatively low gravimetric density of adsorbed hydrogen. Such possibility has stimulated the development of new porous solids with high potential for hydrogen adsorption. This supposes an appropriate understanding on the driving forces that determine the stability of the hydrogen molecule within nanometric size cavities. The challenges for the H<sub>2</sub> storage by physical adsorption are derived from the properties of this molecule. It has only two electrons involved in a  $\sigma$  bond and from this feature participates in relatively weak dispersive interactions. This explains its low critical temperature (32.7 K). H<sub>2</sub> has quadrupole moment related to its non-spherical shape and, in consequence, it is sensible to interact with an electric field gradient. These are the physical interactions available for the H<sub>2</sub> physical adsorption. However, the paradigm for the H<sub>2</sub> storage is probably found in its coordination chemistry. The H<sub>2</sub> binds side-on to the metal center through  $\sigma$ -donation to a vacant metal d orbital to form a coordination bond. This interaction is stabilized when a fraction of the metal electrons populates the H<sub>2</sub>  $\sigma^*$  orbital by means of a back-bonding interaction. The hydrogen molecule behaves as a donor-acceptor ligand. In this short lecture the role of these possible interactions for the hydrogen storage in nanocavities will be discussed, with emphasis on the cavity properties and their contribution to the adsorption potential for the hydrogen molecule. The results to be discussed contribute to shed light on the available routes for the materials design oriented to obtain porous frameworks appropriate to satisfy the technological requirements related with the applications of hydrogen as a secondary energy bearer, instead of gasoline for automotive vehicles, for instance.

# **Diffuse Reflectance study of the photoactivation kinetics of TiO<sub>2</sub> (Degussa P25) in a polyacrylic acid gel matrix**

R. Trejo-Tzab, J.J. Alvarado-Gil, P. Quintana

CINVESTAV-Unidad Mérida, Depto. de Física Aplicada, A.P. 73, Cordemex, Mérida, Yuc. México. C.P. 97310

**E-Mail: [rtrejo@mda.cinvestav.mx](mailto:rtrejo@mda.cinvestav.mx)**

## Abstract

It has been shown that nanostructured titania is photoactivated when it is illuminated with UV radiation. This has been related to Ti<sup>3+</sup> formation as a consequence of the induction of hole-electron pairs in the sample [1,2,3]. A change of color of titania from its original white to blue grayish color has been reported in solutions of alcohol [4]. However, the photoactivation process of nanoparticles of TiO<sub>2</sub> in water-alcohol mixture was difficult to analyze, requiring a long sonication process, which in our case is not necessary.

In this work the photoactivation of titania Degussa P25 powder into a carbopol 940 (polyacrylic acid) gel matrix is studied by diffuse reflectance. Carbopol is dispersed in a mixture of water-alcohol (60-40%) forming a gel matrix. Alcohols used were ethanol, methanol, and a mixture of ethanol-methanol (50-50%). The samples are diffusely illuminated with a Xe lamp and the change of the reflectance spectra is measured with a spectrophotometer during the photoactivation process. Using the Kubelka-Munk approach, the ratio between the absorption (S) and scattering (K) coefficients are obtained. It is shown that the kinetics of the photoactivation is stronger for large wavelengths and it is weaker for shorter wavelengths. The significant changes in optical absorption in the red region of the optical spectra allow to understand the coloration evolution and the availability of the modified interband states in titania due to the photoactivation processes.

## References

1. Z. Zhang, P. A. Maggard, *J. of Photochem. and Photobio A: Chemistry* 186 (2007) 8-13.
2. Z. Yu and S. C. Chuang, *J. Catal.*, 246 (2007)118-126.
3. J. Marugán, D. Hufschmidt, M.J. Lopez-Muñoz, V. Selzer, D. Bahnemann, *J. Appl. Catal. B: Environmental*, 62 (2006) 201-207.
4. R. Trejo-Tzab, J. J. Alvarado-Gil, P. Quintana, T. Lopez, *J. Mol. Cat. A. Chemical* 281 (2007) 113-118.

# Crystallite Dimensions, Morphology, and Microstrain of Nanocrystalline Materials obtained by using X-ray powder diffraction

*Xim Bokhimi*

*Universidad Nacional Autónoma de México, A.P. 20-364, 01000 México D. F., Mexico*

*E-mail: [bokhimi@fisica.unam.mx](mailto:bokhimi@fisica.unam.mx)*

Soon after the discovery of X-rays by W. Roentgen in 1895, M. von Laue showed in 1912 that they can be used to determine the atom distribution in solids. In 1913 P. Debye and P. Scherrer showed that X-rays can be used to analyze powders, and in 1918 Paul Scherrer showed that the width of the diffraction peak of a cubic system is equal to  $K\lambda/(D \cos\theta)$ , where  $2\theta$  is the angle between the X-ray source and the detector,  $\lambda$  is the X-ray wavelength; D represents an isotropic average dimension of the crystallites and K is related with their morphology. The relationship reported by Scherrer in 1918 is known nowadays as the Debye-Scherrer formula, and is the basic relationship used to determine the dimensions and morphology of the average crystallite in nanocrystalline materials. During the last 90 years scientists have been interested into using this formula to determine crystallite dimensions and morphology: in 1930 Laue showed that the peak width depended not only on crystallite dimensions but also in their morphology. In 1939 A. L. Patterson calculated the K for crystallite with the morphology of an ellipsoid, while, in 1942 P. M. De Wolff obtained the K value when the average crystallite was a parallelepiped. In 1950 B. E. Warren and B. L. Averbach showed that the width of the diffraction peaks was determined not only by the crystallite dimensions and morphology but also by the lattice deformations. In the same year E. F. Bertaut showed that this width is also affected by the distribution of the crystallite dimensions. In 1998 N. C. Popa modeled crystallite morphology with an expansion of symmetrical spherical harmonics, and in 2008 he also considered the distribution of crystallite dimensions. In 1999 P. W. Stephens modeled lattice deformations with a multidimensional distribution of lattice metrics. The improvement of the quality of the experimental X-ray diffraction patterns after 1970 and the introduction of the refinement of the crystalline structure of the phases in powder samples by H. Rietveld made it possible to incorporate these models in the simulation of the diffraction patterns. Therefore using this technique it is possible to obtain the crystallite dimensions and morphology as well as the lattice deformations (microstrain). The analysis also supplies information about the concentration of the phases in the sample and their crystallography.

# Transmission electron microscopy on the characterization of photonics nanomaterials

C. Angeles-Chavez<sup>1</sup>, E. de la Rosa-Cruz<sup>2</sup>, L. A. Díaz-Torres<sup>2</sup>, P. Salas<sup>3</sup>

<sup>1</sup>Programa de Ingeniería Molecular. Instituto Mexicano del Petróleo, Eje Central Lazaro Cardenas No. 152, Mexico D.F.C.P. 07730 Mexico, [cangeles@imp.mx](mailto:cangeles@imp.mx)

<sup>2</sup>Centro de Investigaciones en Optica A.C. León, Guanajuato, C.P. 37150, Mexico.

<sup>3</sup>Centro de Física Aplicada y Tecnología Avanzada, Universidad Nacional Autónoma de México, A. P. 1-1010, Querétaro 76000, MEXICO.

## Abstract

Recent advances in electron microscopy provide a number of new analytical techniques that expands its application in studies of new materials. High angle annular dark field scanning transmission electron microscopy (HAADF-STEM), STEM-energy dispersive X-ray spectrometry (EDXS), and energy filtered TEM (EFTEM) can be effectively used to identify and characterize nanoparticles. The image contrast in HAADF-STEM is strongly correlated to the atomic mass: heavier elements contribute to brighter contrast while high-resolution transmission electron microscopy (HRTEM) image provide very reliable information about the crystallography of the specimen in chosen crystallographic orientation. Together provide invaluable information about of the chemical composition and structural characteristics of the sample. In the past decade, 1-D nanostructures such as rods, wires, belts, ribbons and tubes have become the focus of intensive research owing to their fascinating applications in mesoscopic physics and fabrication of nanodevices. In the optical field the nanosize of the new materials promises to improve the performance in photonics application. Therefore, new characterization techniques are required to explain the increase or decrease of the properties generated by the nanosize and morphology effect. In this work, characterization of ZrO<sub>2</sub> nanocrystals doped with Er and Yb atoms are investigated by electron microscopy analyzing the crystalline structure, the crystallite size, and chemical composition The crystalline phase is controlled by the active ion concentration and the size by synthesis conditions. For some cases the average crystallite size is around 80 nm and is possible to see some nanocrystals faceted, generally with truncated-octahedral geometry. Monoclinic and tetragonal zirconia phases in different directions were identified by analyzing HR-TEM image. Homogeneous distribution of the rare earths in the nanocrystals was observed in the chemical mapping and the HAADF-STEM images.

# **Fullerenes, nanotubes, and nanoparticles: properties and possible applications**

**Ricardo Guirado López**

Instituto de Física, Universidad Autónoma de San Luis Potosí  
[guirado@dec1.ifisica.uaslp.mx](mailto:guirado@dec1.ifisica.uaslp.mx)

## **INVITED TALK**

In this work, we present extensive ab-initio density functional theory calculations, within the ultra-soft pseudopotential plane-wave method, in order to analyze the electronic and structural properties of some relevant nanostructured materials. We analyze first the stability and electronic behavior of highly hydroxylated fullerenes containing an encapsulated La-atom. We will show how the entrapped metal ion can have different spatial locations within the cavities by simply controlling the structure of the adsorbed molecular over layer. This complex dynamics of the confined species leads to strong variations in the charge transfer, optical properties, and spin magnetization of the molecular compounds, which are all facts that could be used to better identify the structure of these highly relevant fullerene structures. Second, we will discuss the structural properties and reactivity of nitrogen molecules confined in spheroidal and tube-like carbon nanostructures. We will demonstrate how, by increasing the N<sub>2</sub> gas pressure within the cavities, it is possible to induce chemical reactions between the encapsulated nitrogens, leading to the formation of various types of nitrogen clusters. We define thus these kinds of nano-containers as non ideal storage materials for molecular nitrogen. Finally, we will present the structural properties of Co nanoparticles and nanowires with complex morphologies. We will analyze surface reconstruction processes and will present some preliminary results concerning the simulation of transmission electron microscopy images that reveal interesting features that could be used to characterize the structure of these magnetic materials.

# Heterogeneities in Semiconducting Nano'crystals':

## Surface Influences on Macroscopic Properties

Bradley F. Chmelka,<sup>1</sup> Sylvian Cadars,<sup>1</sup> Benjamin Smith,<sup>1</sup> Jan D. Epping,<sup>1</sup>  
Yuval Golan,<sup>2</sup> Geoffrey Strouse<sup>3</sup>

<sup>1</sup> *Dept. of Chemical Engineering, University of California, Santa Barbara, California, U.S.A.*

<sup>2</sup> *Dept. of Materials Engineering, Ben-Gurion University, Beer-Sheva, Israel*

<sup>3</sup> *Dept. of Chemistry, Florida State University, Tallahassee, Florida, U.S.A.*

### INVITED TALK

Nanoparticles have been the focus of intense research interest, because their size-dependent properties are generally different from bulk materials with similar compositions. Recent advances in chemical syntheses of nanoparticles allow their sizes, shapes, morphologies, and overall chemical compositions to be controlled within narrow distributions that have enabled fundamental studies and comparisons of their physicochemical properties. In particular, numerous semiconducting compounds and metals have been prepared with high degrees of 'nanocrystalline' order, as evidenced by scattering and electron microscopy measurements. Resulting applications often benefit from more uniform macroscopic properties that are not complicated by otherwise broad distributions of nanoparticle sizes, shapes, and/or atomic disorder. Nanoscale materials are, nevertheless, inherently heterogeneous systems that lack the long-range three-dimensional periodic ordering that is characteristic of bulk crystalline solids. Surface effects, in particular, can exert important influences on size-dependent nanoparticle properties, due to heterogeneous distributions of species and/or of local bonding environments near nanoparticle peripheries that have been difficult to characterize. Solid-state nuclear magnetic resonance (NMR) spectroscopy can provide detailed insights on local nanoparticle compositions and structures, new results and analyses of which will be presented for size-controlled Group II-VI ZnSe and Group III-V InGaP nanoparticles. In these systems, despite high extents of atomic positional order, large size- and surface-dependent variations in local <sup>77</sup>Se, <sup>67</sup>Zn, <sup>71</sup>Ga, <sup>115</sup>In, and/or <sup>31</sup>P electronic environments are manifested by broad distributions in their respective NMR signals, which increase with decreasing nanoparticle size. First-principles calculations of NMR parameters distinguish between atomic positional and electronic disorder near the nanoparticle surfaces and yield insights on the nature of the order present. These insights are being used to understand and optimize the effects of different synthesis and processing conditions on the compositions, structures and properties of semiconducting nanoparticles for different applications.

# **Structural characterization of one dimension nanostructures using transmission electron microscopy and associated techniques.**

Patricia Santiago Jacinto

*Departamento de Materia Condensada, Instituto de Física, Universidad Nacional Autónoma de México, Coyoacan, 04510, A.P. 20-364, C.P. 01000, Mexico City, Mexico.*

[paty@fisica.unam.mx](mailto:paty@fisica.unam.mx)

Recent progress in nanoscience and nanotechnology have been produced the interest on controlling the size, shape and composition of tiny structures. While the physical and chemical characteristics of the nanostructures are defined by controlling these parameters it is very important to count on techniques of highly precision. Meanwhile the composition of bulk materials can be estimated by conventional techniques such as XR-D, EDS, SIMS and XPS, the local composition and structure are evaluated by high resolution transmission electron microscopy (HRTEM).

HRTEM technique allows us to analyze individual nanocrystals and specific crystal planes with their corresponding orientation, however, the phase-contrast imaging, associated with HRTEM, complicates the image interpretation and the poor contrast generated by light materials produce missing information. Also, soft matter structures are not able to study by HRTEM.

On the other hand, there are other associated techniques to HRTEM that can give us the information that we lose by the phase-contrast phenomenon. For example, Z-contrast or scanning transmission electron microscopy (STEM) uses a high angle annular dark field detector to collect the incoherent electron beams and this signal strongly depends on the atomic number  $Z$  of the sample. Therefore it is possible to understand directly the chemical composition of binary nanotubes, nanowires or nanorods.

Nanotubes, nanowires and nanorod are studied by HRTEM and associated techniques such as electron energy loss spectroscopy (EELS), HAADF, image filtering by EELS (Gatan Image Filter- GIF), electron diffraction techniques and most recently electron holography. We will present the advance characterization techniques applied on specific one dimension nanostructures.

# Electrical Conductivity of Nanostructured $\text{Ce}_{(1-x)}\text{Sm}_{(x)}\text{O}_{(2-\delta)}$

R. Vilchis-Morales<sup>\*</sup>, E. Ruiz-Trejo

*Facultad de Química, Departamento de Física y Química Teórica, Universidad Nacional Autónoma de México, 04510, México D.F.*

## Abstract

In this work, we present our results on nanoceramics of  $\text{Ce}_{(1-x)}\text{Sm}_{(x)}\text{O}_{(2-\delta)}$ . Samples of samaria doped ceria (SDC) were prepared by the combustion route  $x = 0.20$  and co-precipitation method  $x = 0.05, 0.10, 0.20, 0.30$ . The powders show a fluorite structure and a particle size around 8 nm. The nanopowders were pressed uniaxially and sinterized in air at 1200°C for 1 and 1.5 hours respectively. The sintered bodies had particle sizes around 50 nm and a density around 96%. The conductivity was measured on the denser samples of 5% SDC and 20% SDC. For the 20 % SDC impedance spectroscopy was performed in atmospheric air. For the 5% SDC the impedance spectroscopy were performed on dry and wet  $\text{N}_2$  ( $p_{\text{H}_2\text{O}}$  from 0.0010 to 0.022 atm.). The striking results show practically no change in the bulk response independent of dopant amount, grain size, preparation method and atmosphere; however, the grain boundary impedance response different at this conditions.

Key words: Ceria, Nanostructured doped Ceria, SDC nanostructured electrolyte, SDC electrical conductivity, Oxygen conductor nanostructured ceramic.

---

<sup>\*</sup>Corresponding author. Laboratorio de Materiales de Alta Temperatura (F-103), Facultad de Química, Departamento de Física y Química Teórica, UNAM, México, D.F., 04510. T: +52-55-5622-3831, F: +52-55-5679-9936. vilchisruben@gmail.com

# Nanotechnology in Mexico: Societal Implications and Technology Assessment

Zachary Tyler Gallagher Pirtle

*Fulbright-García Robles Scholar 2008-9*

*Center for Nanotechnology in Society at ASU*

*M.S. Student in Department of Civil and Environmental Engineering*

*Arizona State University*

*zachpirtle@gmail.com*

In addition to creating knowledge and new economic innovation, research in science and technology should do as much as possible to solve societal problems. For developing countries like Mexico, the imperative to connect research to social outcomes is heightened by both its own pressing social, environmental and health problems, as well as by the disparities in research budgets between it and developed countries. A more strategic approach to academic research could enable Mexico to both better serve its people and to make the best use of its smaller research budgets.

But what strategy for science policy can best help Mexico? No one has developed a strong approach for the analysis of the impacts of science on society, but it is increasingly becoming clear that the old linear model for science, the idea that funding of research automatically attains social outcomes, is insufficient. As one possible source of inspiration, research in nanotechnology in the United States is currently being examined by a process called Real-Time Technology Assessment (RTTA) (1).

RTTA is currently in use at the Center for Nanotechnology in Society at Arizona State University. At CNS-ASU, social scientists work with scientists engaged in nanotechnology at ASU's BioDesign Institute, talking through design decisions, developing plausible scenarios for the outcomes of scientific research, and getting public input on what kinds of research in nanotechnology raise concerns or could have desirable consequences. RTTA could enable universities to better connect their research to specific societal outcomes, and can generate valuable information for policymakers.

For scientists working with nanotechnology, I will present some of the useful insights of the societal implications research in the US brought forward by RTTA. However, I will argue that RTTA is not sufficient in scope to help give Mexico the strategic guidance in research it needs to maximize benefit for Mexican society. RTTA focuses at the institutional level of the university, Mexico could benefit more from TA at broader levels of the government and of CONACYT, with tools to help Mexico determine the impacts of funding certain kinds of research, allowing it to prioritize funding both for different kinds of research but also between funding social or technological programs for solving societal problems (For recent efforts, see 3). In order to develop a broader TA approach, it is important to survey and exactly understand how Mexican researchers attempt to connect their work with societal problems.

My research project aims to seek information needed to make this type of TA. My project will involve interviews with Mexican researchers in nanotechnology, to get their insights about how they try to connect their research with societal outcomes, and to solve problems related to Mexican society.

[1] Guston, D. and D. Sarewitz. 2001. "Real-Time Technology Assessment." *Technology in Society* 24(1-2) pp. 93-109. [2] Pirtle, Zachary. 2006. "Nanotechnology: Constructing a Proactive Science Policy Towards Democracy." *The Triple Helix*. Volume 3, Number 1, ASU. Available at [<http://www.cspo.org/documents/pirtletriplehelix.pdf>] [3] Bozeman, B. & Sarewitz, D. (2005, April). Public values and public failure in US science policy. *Science and Public Policy*, 32(2), 119-136.

## **Second Harmonic Generation of Nano-Spheres**

Bernardo S. Mendoza

Department of Photonics, Centro de Investigaciones en Optica,  
León, Guanajuato, México

Optical second-harmonic generation (SHG) is used as a noninvasive probe of the interfaces of Si nanocrystals (NCs) embedded uniformly in an SiO<sub>2</sub> matrix. Measurements of the generated SH mode verify that the second-harmonic polarization has a nonlocal dipole form proportional to  $(\mathbf{E} \cdot \nabla)\mathbf{E}$  that depends on inhomogeneities in the incident field  $\mathbf{E}$ , as proposed in recent models based on a locally noncentrosymmetric dipolar response averaged over the spherical NC interfaces. A two-beam SHG geometry is found to enhance this polarization greatly compared to single-beam SHG, yielding strong signals useful for scanning, spectroscopy, and real-time monitoring. This configuration provides a general strategy for enhancing the second-order nonlinear response of centrosymmetric samples, as demonstrated here for both Si nanocomposites and their glass substrates.

# Effect of temperature and pH on the morphology, crystallinity and vibrational properties of hydrothermally grown SnO<sub>2</sub> nanostructures

U. Pal<sup>\*</sup>, and A. Escobedo Morales

*Instituto de Física, Universidad Autónoma de Puebla, Apdo. Postal J-48, Puebla, Pue. 72570, Mexico.*

\*upal@sirio.ifuap.buap.mx

## INVITED TALK

SnO<sub>2</sub> nanostructures of different sizes and morphologies were grown by hydrothermal technique at different pH values and at different temperatures. It has been observed that the size and morphology of the nanostructures depend strongly on these two parameters. The nanostructures were characterized by X-ray diffraction (XRD), transmission electron microscopy (TEM), Fourier transform infrared (FT-IR) spectroscopy and Raman spectroscopy techniques. While the nanostructures grown at lower temperature and with low pH values of the reaction mixture produce nanoparticles of size ~ 5.0 nm, at higher temperature of hydrothermal treatment and high pH values, they transform to uniform one-dimensional rod-like structures. As the width of the rod-like nanostructures are same as that of the diameter of initially grown nanoparticles, it is believed that the 1D nanostructures are grown by interconnecting the primary nanoparticles through Ostwald ripening process at high temperature.

SnO<sub>2</sub> nanoparticles were also doped with indium at different concentrations. The doping affected drastically the crystallinity, and size of the nanoparticles. Degradation of crystal quality and incorporation of lattice defects in the nanostructures affect strongly their photoluminescent (PL) properties.

*\*The work was partially supported by VIEP-BUAP (Grant # 93/EXC/2008-1), Mexico.*

# SER(R)S, Plasmonics and Single Molecule Detection

*Ricardo F. Aroca*

Materials and Surface Science Group, Department of Chemistry and Biochemistry, University of Windsor, Windsor, ON, Canada, N9B 3P4.

## INVITED TALK

The coupling of the molecular excitations to localized surface plasmon resonances (LSPR) in silver or gold nanostructures is at the centre of the single molecule detection<sup>1, 2</sup> (SMD) using surface-enhanced Raman scattering (SERS) and surface-enhanced resonance Raman scattering (SERRS).<sup>3</sup> SERS and SERRS are powerful analytical techniques used in such frontier areas of research as ultra-sensitive chemical analysis, the characterization of nanostructures, the development of biosensors, and SMD. The detection of a single molecule using metal colloidal nanostructures and metal island covered with a single Langmuir-Blodgett (LB) monolayer has been reported.<sup>3</sup> The enhancement is attributed to the elastic scattering by nanostructures at molecular frequencies when there is coupling with the surface plasmons of the metal. However, the most efficient coupling is attained when the excitation is in resonance with the electronic absorption of the molecule and the nanostructure's plasmon resonance, the case of SERRS. The dispersion of the SERRS spectrum can be followed with different laser lines to obtain the spectra of the chromophore in and out of resonance. Here we present results using monomolecular layers containing a chromophore that dominates the Raman when the laser is in resonance with its absorption. The target molecule is incorporated, at varying concentrations, into single fatty acid and transferred onto a silver nanoparticle film to form a Langmuir-Blodgett monolayer. It is demonstrated that using LB, Raman-microscopy and mapping, single-molecule detection is achieved. The efficiency of several SERRS substrates and the corresponding enhancement factors are also discussed.

1. K. Kneipp, Y. Wang, H. Kneipp, L. T. Perelman and I. Itzkan, *Physical Review Letters*, 1997, **78**, 1667-1670.
2. S. Nie and S. R. Emory, *Science*, 1997, **275**, 1102-1106.
3. R. Aroca, *Surface-enhanced Vibrational Spectroscopy*, John Wiley & Sons, Chichester, 2006.

## Optically Active Nanoparticles

Cecilia Noguez\*, A. Sánchez-Castillo, Francisco Hidalgo, Ignacio L. Garzón  
*Instituto de Física, Universidad Nacional Autónoma de México, Apartado Postal 20-364,  
México D. F. 01000 MÉXICO*

\*email: [cecilia@fisica.unam.mx](mailto:cecilia@fisica.unam.mx)      web: <http://www.fisica.unam.mx/cecilia>

Chirality plays a major role in biochemistry and the pharmaceutical industry, and now it becomes an important issue in nanoscience and nanotechnology [1,2]. For instance, chiral nanoparticles can be used for asymmetric catalysis, enantiomeric analysis, and enantioselective separation. Other examples of these types of materials are chiral supramolecules, chiral fullerenes, and chiral carbon nanotubes, which have potential applications in molecular electronics and DNA technology. In fact, nearly all aspects of chiral technology including synthesis, separation, and analysis, have already seen nanoscale approaches. Whether the goal is to use nanostructures for new approaches to solve problems in chiral technology or to use molecular chirality to engineering useful properties in nanoscale materials, this area is fruitful and exciting, and certainly to continue to attract interest for the years to come.

In this talk, we present new insights into this fundamental problem, where a time-perturbed first-principles formalism is developed to study the optical activity of nanostructures, making large-scale calculations of the circular dichroism feasible. Expressions to calculate circular dichroism using density functional theory for molecules and periodic systems are obtained. To show the versatility and applicability of the method, the circular dichroism of ligand-protected nanoclusters, fullerenes and nanotubes are studied. The results show good consistency with previous time-dependent density functional theory calculations, and an excellent agreement with available experiments [3,4]. This methodology provides theoretical support for the quantification, understanding, and prediction of chirality and its measurement in nanostructures. It is expected that this information would be useful to motivate further experimental studies and the interpretation of natural optical activity in terms of the electronic circular dichroism.

- [1] J. Zhang, M. T. Albelda, Y. Liu, J. W. Canary, *Chirality* **17**, 404 (2005).
- [2] C. Noguez and I. L. Garzón, *Chem. Soc. Rev.* (2008) in press.
- [3] F. Hidalgo, A. Sánchez-Castillo, I. L. Garzón and C. Noguez, *Euro Phys. J. D*, submitted (2008).
- [4] F. Hidalgo, A. Sánchez-Castillo, and C. Noguez, *Phys. Rev. B*, submitted (2008).

## Flatness Approach to Optimal Particle Steering by Optical Traps.

A. Barrañón (1); C. Aguilar-Ibáñez (2); H. Sira-Ramírez (3); L.I. Rosas-Soriano (2).

(1) *Dep. Basic Sciences, UAM-A, Mexico City. Dep. of Physics, U. Texas. El Paso. email:*

*bca@correo.azc.uam.mx*

(2) *Centro de Investigación en Computación, IPN, Mexico City.*

(3) *Dep. Ingeniería Eléctrica, CINVESTAV-IPN, Mexico City.*

Based on the fact that the optical tweezers system is a flat system, with flat outputs given by their horizontal and vertical positions, a flatness based control approach for the manipulation of a microscopical particle is presented in this paper. The control strategy is derived under the assumption that the particle is suspended in a frictionless medium, obtaining a simple controller with a relatively simple stability analysis. A differential flatness approach for the manipulation of a particle by means of optical tweezers is presented. The fact that the optical tweezers system is a flat system with a flat output, given by their vertical and horizontal positions, allows us to systematically solve the tracking control problem. Our control strategy uses a saturation function in conjunction with the poles placement controller to overcome the low reach ratio of the optical tweezers due to its light potential field weakness problem. Physically the strategy consists of placing the optical tweezers close enough to the position of the particle, then, little by little, the optical tweezers drag the particle to the desired tracking trajectory. In order to accomplish this task, a nonlinear system of algebraic equations have to be solved in order to obtain the needed controllers. This is successfully solved using the well-known Newton-Rapson numerical method. The control strategy is tested by tracking a straight line, an elliptic curve, and carrying out the rest-to-rest transfer maneuver task by using a smooth trajectory. A.B. acknowledges financial funding from CONACYT-75722 Grant.

## Preparation of gold nanoparticles supported on oxides. Reactivity in oxidation reactions.

Rodolfo Zanella

CCADET-UNAM. Ciudad Universitaria, México D. F. 04510

e-mail: [rodolfo.zanella@ccadet.unam.mx](mailto:rodolfo.zanella@ccadet.unam.mx)

### INVITED TALK

Among the various methods developed for the synthesis of gold based supported catalysts, the deposition-precipitation with NaOH (DP NaOH), which leads to small metallic gold particle, is easy to handle. However, most of the gold present in solution (~60%) is not deposited on the support. We developed another method of deposition-precipitation with urea (CO(NH<sub>2</sub>)<sub>2</sub>) (DP Urea) to prepare Au/TiO<sub>2</sub> catalysts [1,2]. In contrast to the DP NaOH method, we observed that the DP Urea method permits the deposition of all gold present in solution, which corresponds to a gold loading of 8 wt % instead of 3 wt % for DP NaOH. This higher gold content does not lead to larger gold particles after calcination. They are similar for both preparations (~2 nm after calcination at 300°C). On the other side, deposition-precipitation, co-precipitation, and impregnation have not been effective to support small gold particles on SiO<sub>2</sub>. The difficulty to deposit highly dispersed gold nanoparticles on SiO<sub>2</sub>, by liquid phase methods, arise from the fact that the point of zero charge (PZC) for SiO<sub>2</sub> surfaces is close to pH=2. This fact means that the SiO<sub>2</sub> surface becomes negatively charged above pH=2, making difficult the deposition of anionic gold species. We have showed that it is possible to prepare small particles of gold on the surface of SiO<sub>2</sub> based on the adsorption of cationic Au(en)<sub>2</sub><sup>3+</sup> complex [3]. We have previously reported that cation adsorption of the [Au(en)<sub>2</sub>]<sup>3+</sup> complex could also produce small gold particles on TiO<sub>2</sub> [1,2]. In this way a new and simple liquid phase method for the preparation of gold nanoparticles is available, allowing a more reliable comparison of the activities of gold nanoparticles supported on reducible and inert supports. These Au supported samples have been evaluated in CO oxidation at low temperature. A summary of the obtained results will be presented. These results suggest that the catalytic activity of gold based catalysts is mainly controlled by the gold and the oxide particle size, and by their morphology. On the other side, an emerging application for the water gas shift reaction is the production of hydrogen for proton exchange membrane (PEM) fuel cells. This reaction is important because it removes CO, a poison to the fuel cell electrocatalysts, which is produced during the steam reforming and/or partial oxidation reactions. Moreover WGS reaction is one of the key steps involved in the automobile exhaust processes, converting CO and water to hydrogen and CO<sub>2</sub> and including the produced hydrogen as a very effective reductant for NO<sub>x</sub> removal. We have compared the catalytic behavior of gold supported on reducible (TiO<sub>2</sub> and CeO<sub>2</sub>) and non-reducible (SiO<sub>2</sub> and Al<sub>2</sub>O<sub>3</sub>) oxides for the WGS reaction in order to determine the role of the support on the catalytic activity and stability of the gold particles. The activity of gold nanoparticles on the reducible supports was much higher than the one observed on Al<sub>2</sub>O<sub>3</sub> and SiO<sub>2</sub> and varied as follows for reaction temperatures below 200°C TiO<sub>2</sub>>CeO<sub>2</sub>>>Al<sub>2</sub>O<sub>3</sub>>>>SiO<sub>2</sub> [4]. Deactivation runs at 200°C after 24h on stream showed practically no deactivation of the Au/TiO<sub>2</sub>, Au/CeO<sub>2</sub> and Au/Al<sub>2</sub>O<sub>3</sub> catalysts. CO and CO/H<sub>2</sub>O adsorption was followed by DRIFTS, the results obtained will be discussed. Recent results about the preparation, characterization and catalytic evaluation of bimetallic gold based samples will be presented.

[1] R. Zanella, S. Giorgio, C.R. Henry, C. Louis, J. Phys. Chem. B *106* (2002) 7634.

[2] R. Zanella, L. Delannoy, C. Louis, Appl. Catal. A *291* (2005) 62.

[3] R. Zanella, A. Sandoval, P. Santiago, V.A. Basiuk, J.M. Saniger, J. Phys. Chem. B *110* (2006) 8559.

[4] A. Sandoval, A. Gómez-Cortés, R. Zanella, G. Díaz, J.M. Saniger, J. Mol. Catal. A *278* (2007) 200.

## **Small and Wide Angle X-ray Scattering (SAXS and WAXS), with the NANOSTAR of BRUKER AXS solution.**

**Juan Jacobo Miranda**

**[juan.jacobo@bruker.com.mx](mailto:juan.jacobo@bruker.com.mx)**

**Bruker Mexicana S.A. de C.V.**

In the research and characterization of tridimensional structures, liquid or solid samples by X-ray diffraction method in transmission mode, the Bruker AXS - NANOSTAR system is a powerful and superior tool to analyze and measure phase arrangements and/or nano particles with dimensions from 1 to 100 nm.

The techniques of SAXS (small angle X-ray scattering) and WAXS (wide angle X-ray scattering) are reliable and non destructive methods for the analysis of nano structural materials. The range of applications is wide for example: polymer analysis, metallic materials, ceramics, biological materials, fibers, nano particles, complex fluids, food technology, etc. with a minimum of simple preparation.

It will be showed the basis of both techniques of characterization, the accessories that comes with the system and the software of evaluation as the most versatile tool.

# Synthesis and characterization of nanomaterials

## for application in dye-sensitized solar cells

Gerko Oskam

*Departamento de Física Aplicada, CINVESTAV - IPN, Carr. Ant. a Progreso km 6,*

*A.P. 73 "Cordemex", Mérida, Yuc. 97310, MEXICO. [oskam@mda.cinvestav.mx](mailto:oskam@mda.cinvestav.mx)*

### INVITED TALK

The dye-sensitized solar cell (DSC) is a third generation photovoltaic device based on inexpensive materials and simple fabrication processes, which could lead to a significant reduction in the cost of the conversion of solar energy to electricity. The light absorbing electrode consists of a mesoporous, nanostructured metal oxide film, sensitized to visible light by an adsorbed molecular dye. The dye absorbs sunlight, and injects an electron from the excited state into the metal oxide conduction band. The electron is transported to the external circuit, and the dye is regenerated by an electron donor in the electrolyte solution. The electron donor is, in turn, regenerated at the counter electrode by an electron from the external circuit, thus closing the loop [1]. The cell is regenerative, hence, no net chemical changes occur during operation. The current record efficiency of the DSC at  $100 \text{ mW cm}^{-2}$ , AM 1.5 simulated sun light is 11.1% [2], and further improvements are still expected. The structural, morphological, and electronic properties of the nanostructured metal oxide film strongly affect the performance of the solar cell, hence, it is essential to have a good control over the materials properties. The  $\text{TiO}_2$  films are generally cast from a paste of nanoparticle aggregates prepared by solution-phase processing. In this presentation, the nucleation and growth kinetics of  $\text{ZnO}$  and  $\text{TiO}_2$  nanoparticles from solution are discussed in detail. We have prepared phase-pure  $\text{TiO}_2$  nanoparticles with control over the particle size in the three common crystalline structures: rutile, anatase, and brookite. Formation mechanisms for the three phases will be discussed.  $\text{ZnO}$  is an interesting alternative to  $\text{TiO}_2$ , and results will be presented on the nucleation, growth and aging kinetics for the synthesis of  $\text{ZnO}$  nanoparticles. The  $\text{TiO}_2$  and  $\text{ZnO}$  nanomaterials have been applied in dye-sensitized solar cells, and preliminary results for both oxides will be presented.

1. M. Grätzel, *Inorg. Chem.* **44**, 6841-6851 (2005).
2. Y. Chiba, A. Islam, Y. Watanabe, R. Komiya, N. Koide, L. Y. Han, *Jap. J. Appl. Phys. Part 2 - Letters & Express Letters* **45**, L638-L640 (2006).

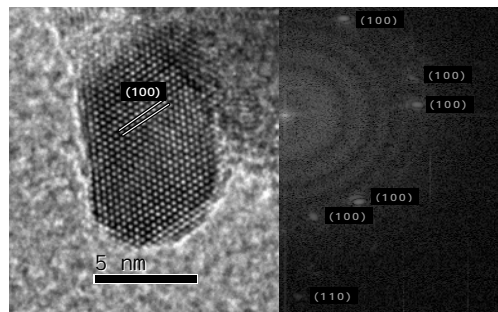
# Structural, magnetic and optical study of ZnO and Fe(II) doped ZnO nanoparticles

América Vázquez-Olmos<sup>1</sup>, Jazmín Matamoros-Contreras<sup>1</sup>, Roberto Sato-Berrú<sup>1</sup>,  
Ana L. Fernández-Osorio<sup>2</sup> and Esther Mata-Zamora<sup>1</sup>

<sup>1</sup>Centro de Ciencias Aplicadas y Desarrollo Tecnológico and <sup>2</sup>Facultad de Estudios Superiores  
Cuatitlán, Universidad Nacional Autónoma de México.

america.vazquez@ccadet.unam.mx

Spintronics, also known as magnetoelectronics is a new research field, which studies possible application of electron spin in electronic devices. In this sense, diluted magnetic semiconductors (DMS), materials based on the conventional semiconductors as GaN, GaAs, ZnO, TiO<sub>2</sub> etc. doped with transition metals, are promising candidates for spintronics. In particular, ZnO is the most widely studied oxide semiconductor for DMS materials. This is a direct wide band-gap semiconductor (~3.3 eV) with applications in UV photonics and transparent electronics. However, the experimental results on transition metal doped ZnO are very controversial, because of some authors have observed room temperature ferromagnetism while others observed paramagnetism in the same systems. This work focuses on the one step room temperature mechano-synthesis of ZnO nanoparticles and 5% and 10% Fe(II) doped ZnO Nps. Their structural, magnetic and optical properties were studied by UV-visible electronic absorption and emission spectroscopies as well as Raman dispersion. The average diameter of ZnO (12 nm) and Fe(II) ZnO (15 nm) doped nanoparticles, were determined from HR-TEM images. We have found that the 5% and 10% Fe(II) doped ZnO nanocrystallites exhibit superparamagnetism at room temperature.



HR-TEM micrograph of a Zn<sub>0.9</sub>Fe<sub>0.1</sub>O nanoparticle and  
its corresponding electron diffraction pattern

## PASSIVE AND IONTOPHORETIC TRANSDERMAL PENETRATION OF TRICLOSAN NANOPARTICLES THROUGH HUMAN SKIN

**I. M. Rodríguez Cruz**<sup>a,b</sup>, C.L. Domínguez Delgado<sup>a</sup>, G. Leyva Gómez<sup>a</sup>, A. Ganem-Quintanar<sup>a</sup>, V. Merino-Sanjuán<sup>b</sup>, D. Quintanar-Guerrero<sup>a</sup>

<sup>a</sup>División de Estudios de Posgrado (Tecnología Farmacéutica), Facultad de Estudios Superiores Cuautitlán, Universidad Nacional Autónoma de México, Av. 1° de Mayo s/n, Cuautitlán Izcalli, C.P. 54740, México. E. mail: isabelmarlen@yahoo.com.mx

<sup>b</sup>Departamento de Farmacia y Tecnología Farmacéutica, Universidad de Valencia. Avda. Vicente Andrés Estellés s/n, 46100 Burjassot, Valencia, España.

**Introduction:** Several drugs are used by topical application in the treatment of skin diseases (i.e., acne) obtaining a local effect. However, the skin provides an excellent barrier (stratum corneum), which limits percutaneous transport of several drugs into the skin. Thus, the aim of this work was to prepare and characterize triclosan (TCL) nanoparticles (NP's) to evaluate the *in vitro* passive and iontophoretic delivery through human skin to improve the accumulation of TCL to the upper layers of the skin with the idea to obtain a local effect.

**Experimental methods:** TCL-NP's were prepared by emulsification-diffusion by the solvent displacement technique using Eudragit RL100 as matrix polymer. The average size and  $\Psi_z$  were determined by the laser light scattering technique (Coulter N4 Plus) and by electrophoretic mobility using a Laser Doppler Velocimetry (Zetasizer ZEN 3600), respectively. The *in vitro* passive and iontophoretic permeation studies were performed using Franz-type glass diffusion cells. The human skin was excised (500  $\mu\text{m}$  thickness) with an electrodermatome with an available area of 0.6  $\text{cm}^2$ . TCL concentration was analyzed using high performance liquid chromatography (HPLC-UV,  $\lambda=280$  nm). All the experiments were performed by quadruplicate. The amount of the TCL retained within the skin was extracted of the skin using the same HPLC mobile phase (MeOH/H<sub>2</sub>O, 90:10) and analyzed by the same way.

**Results and discussion:** The emulsification-diffusion by the solvent displacement technique allowed the preparation of positively charged TCL-NP's with a  $\Psi_z$  of +26 mV. SEM showed solid polymeric submicron spherical particles which were less than ~300 nm in size for all the batches prepared. The process efficiency was higher than 99.0 %. Drug loading and entrapment efficiency were 62 and 68%, respectively. The cumulative amount permeated of free-TCL was of 31  $\mu\text{gcm}^{-2}$  with a flux of 1.11  $\mu\text{g}\cdot\text{cm}^{-2}\cdot\text{h}^{-1}$ . The cumulative amount retained within of the skin after of the permeation experiments (32 h) was of 187  $\mu\text{g}$ . Nevertheless, the cumulative amount permeated and the flux of TCL loaded into of NP's were of 19  $\mu\text{g}\cdot\text{cm}^{-2}$  and 0.6  $\mu\text{g}\cdot\text{cm}^{-2}\cdot\text{h}^{-1}$ , respectively. As expected, the amount retained within of the skin after of the permeation experiments (iontophoresis: 8 h and passive diffusion: 24 h) was increased 8.5 times more than free-TCL. It is clear that the use of NP's increased the amount retained in the skin. This was due to the high attraction between the NP's (positively charge) and the skin (negatively charge) and on the other hand, the iontophoresis improved the diffusion of charged NP's by electroosmotic transport.

**Conclusions:** Results demonstrated that TCL-NP's were able to increase the accumulation and targeting of TCL to the upper layers of the skin. The combination of iontophoresis and TCL-NP's is an excellent alternative to dermal drug delivery systems.

**References:** Y.B. Schuetz, et al. Pharm, Res 22 (2005)1305-1312. R. Alvarez-Roman, et al. J. Controll Rel. 99 (2004) 53-62. T.W. Lee, et al. Eur. J. Pharm. and Biopharm. 56 (2003) 407-412.

## **Optical response of silver-gold nano-shells**

Carlos E. Román-Velázquez and Cecilia Noguez

*Instituto de Física, Universidad Nacional Autónoma de México, Apartado Postal 20-364,  
México DF 01000, México.*

e-mail: cecilia@ifisica.unam.mx

A theoretical formalism was developed to study the optical response of metallic bishells of nanometric sizes. The Mie theory was generalized and employed, as well as the discrete dipolar approximation (DDA), to determine the effects and importance of the different parameter of the system such as thickness, size and material properties. The manipulation of those parameters allowed a good fitting with several experimental data [1], with parameter values that coincide with those of measurements performed in the systems. This study will allow synthesise nanoparticles with required surface plasmons properties.

[1] T. Y. Olson, A. M. Schwartzberg C. A. Orme, Chad E. Talley, B. O'Connell and J. Z. Zhang, *J. Phys. Chem. C* 112, 6319-6329 (2008).

# Magnetic Nanoparticles as Heating Agents for Biomedicine

G. F. Goya<sup>1,1</sup>, I. Marcos-Campos<sup>2</sup>, T. Torres<sup>1</sup>, L. Asín<sup>1</sup>,  
A. Tres<sup>2</sup>, C. Marquina<sup>1,3</sup> and M. R. Ibarra<sup>1,3</sup>

<sup>1</sup> Nanoscience Institute of Aragon (INA), University of Zaragoza, Pedro Cerbuna 12, Zaragoza, Spain.

<sup>2</sup> Hospital Clínico Universitario "Lozano Blesa", San Juan Bosco 15, Zaragoza, Spain.

<sup>3</sup> Instituto de Ciencia de Materiales de Aragon (ICMA), Pedro Cerbuna 12, Zaragoza, Spain.

## INVITED TALK

Magnetic hyperthermia is the process of killing cells targeted with magnetic nanoparticles by submitting them to a magnetic field, which locally releases energy as heat in their microenvironment.[1] This strategy has been applied recently to achieve cytolysis of tumor cells [2], raising interesting perspectives for cancer therapy. Injection of MNP-charged Dendritic cells (DCs) into the blood system appears as a valuable MNP-delivery strategy for tumor targeting, since DCs have been found to participate in tumoral vasculogenesis in animal models [3]. In this strategy the cargo (i.e., the magnetic particles) is delivered inside a 'biological' unit from the same organism (the DCs), and therefore no immune response against these carriers is expected. The MNPs vectorized in this way could be used as heating agents for magnetic hyperthermia (MHT) therapy, and efficiently kill tumors to which a sufficient numbers of MNPs have been delivered. At the Nanoscience Institute of Aragon (INA), we have explored the use of MHT to approach a possible therapy on unicellular organisms. The models include *Crithidia fasciculata*, a protozoan belonging to the Trypanosomatidae family, and human Dendritic Cells. The particles used consisted of a magnetic core of Fe<sub>3</sub>O<sub>4</sub> (Magnetite) with sizes ranging from 5 to 30 nm, and functionalized with different organic polymers. Experiments were performed in order to assess a) the final location of the particles; b) the toxicity of MNPs with different functional coatings, and c) the effectiveness of alternating magnetic fields as source of intracellular heat for MHT *in vitro* protocols. As a general result, we found that magnetite nanoparticles of 20-40 nm were efficiently incorporated showing minimum effects on their viability. After separating the MNPs/loaded cells the analysis by electron microscopy and magnetic measurements showed that NPs are internalized in lysosomes, providing a large magnetic signal. Using Fe<sub>3</sub>O<sub>4</sub> nanoparticles of 20-30 nm, we found that mature DCs are able to incorporate magnetic material in the range of 10 pg/cell after 24 h of incubation, depending on particle surface. Applying 30 minutes of AC magnetic field on magnetite-charged DCs cells resulted in 40 % of cell death, as reflected by flow cytometry (anexine-propidium iodide staining) analysis. These results suggest that loading eukariotic cells with specific MNPs could be a promising strategy for improved vectorization and hyperthermia therapy in the field of biomedical applications.

[1] G.F. Goya, V. Grazú and M.R. Ibarra, Current Nanoscience, 4 (2008), 1-16.

[2] C. Wilhelm, J.P. Fortin, and F. Gazeau, J.Nanosci. Nanotech., 7 (2007) 1–5.

[2] J.I. Mayordomo, T. Zorina, W.J. Storkus, C.M. Celluzzi, L.D. Falo, S.T. Ildstad, M.W. Kast, A.B. DeLeo and M.T. Lotze. Nature Med. 1 (1995) 1297.

## Molecular modelling of high-nitrogen content compounds

Tenorio, F. J.<sup>1,2</sup>, Merino, G.<sup>2</sup>, Villanueva García, M.<sup>2</sup>

<sup>1</sup>Centro Universitario de los Lagos, Universidad de Guadalajara. Enrique Díaz de León 1144. Paseos de la Montaña, Lagos de Moreno, Jalisco. <sup>2</sup>Facultad de Química, Universidad de Guanajuato. Noria Alta S/N. CP 36050. Guanajuato México.

E-mail: [ftenorio@culagos.udg.mx](mailto:ftenorio@culagos.udg.mx)

Energetic materials include propellants, explosives, and pyrotechnics. Modern energetic materials derive most of their energy either from oxidation of the carbon backbone, or from their very high positive heat of formation. High-nitrogen content molecules have been the subject of many studies because of their potential as high energy density materials, and are frequently used as propellants [1-3]. An example is  $N_3^-$  anion, which is a propellant in airbags that can be easily produced with salts like sodium azide,  $NaN_3$  [3]. Another example is  $N_5^+$ , that has been stabilized with  $AsF_6^-$  as a counter ion. Gagliardi and Pyykko [4] have found a list of ring complexes with five or seven nitrogen atoms, stabilized with a metal atom. Among their results, they concluded that a local minimum with  $C_{7v}$  symmetry,  $ScN_7$ , has high possibilities to being experimentally detected [4c].

In this work, electronic structure calculations under Density Functional Theory framework were performed for several  $N_nM_m$  systems, where  $n=7, 10$ ;  $m=1, 2$  and  $M$ =metal atom. Full geometry optimizations with no symmetry restrictions were performed. Every stationary point was characterized with harmonic analysis.

The role of alkali and alkaline earth metal atoms in the stabilization of high nitrogen molecules as well as the electronic structure of these materials is discussed.

### References:

- [1] (a) Haiges R., Schneider S., Schroer T., Christe K.O., *Angew Chem Intl Ed* 43, 2004, 4919. (b) Huynh MH V., Hiskey M.A., Hartline E.L., Montoya D.P. Gilardi R., *Angew Chem Intl Ed* 43, 2004, 4924.
- [2] (a) Leininger M.L., Van Huis, T.J., Schaefer H.F., *J Phys Chem A*, 101, 1997, 4460. (b) Strout D.L., *J Phys Chem A*, 2002, 106, 816.
- [3] Christe K.O. Wilson W.W., Sheehy J.A., Boatz J.A., *Angew Chem Intl Ed. Engl* 38, 1999, 2004.
- [4] Gagliardi L, Pyykko P., *J Phys Chem A*, 106, 2002, 4690. (b) Gagliardi L, Pyykko P., *J Phys Chem A*, 106, 2002, 8491. (c) Gagliardi L, Pyykko P., *J Am Chem Soc*, 123, 2001, 9700.

# “Spectroscopic and Structural characterization of nanodendrites Yb<sup>3+</sup>-Er<sup>3+</sup> codoped YAG particles prepared by glycolate assisted with PVA and UREA”

R.A. Rodriguez<sup>a,\*</sup>, H. Desirena<sup>b</sup>, E.H. Tobar<sup>a</sup>, L.A. Díaz-Torres<sup>b</sup>, P. Salas<sup>c</sup>, C. Angeles<sup>d</sup>  
and E. de la Rosa<sup>b,\*</sup>

<sup>a</sup> Universidad de Guadalajara, CULAGOS, Lagos de Moreno, Jal. 47460, México.

<sup>b</sup> Centro de Investigaciones en Óptica, A.P. 1-948, León, Gto. 37150, México.

<sup>c</sup> Centro de física aplicada y tecnología avanzada-UNAM, A. P. 1-1010, Qro. México.

<sup>d</sup> Instituto Mexicano del Petróleo, Eje Central Lázaro Cárdenas 152, C.P. 07730, D.F, México.

\* email: [fifu2004@yahoo.com.mx](mailto:fifu2004@yahoo.com.mx), [elder@cio.mx](mailto:elder@cio.mx)

## ABSTRACT

The Photoluminescence (PL), XRD and TEM characterization of Yb<sup>3+</sup> and Er<sup>3+</sup> codoped YAG nanocrystals (Y<sub>3</sub>Al<sub>5</sub>O<sub>12</sub>:Yb<sup>3+</sup>-Er<sup>3+</sup>) prepared by glycolate method with surfactant assistant as PVA and UREA is reported. The XRD spectra show the typical cubic crystalline phase of YAG. The TEM images show mainly the formation of nanoparticles agglomerated using PVA or UREA. Nanodendrites are observed when the samples were prepared with PVA and UREA at the same time. Several concentrations of the Yb<sup>3+</sup>-Er<sup>3+</sup> were prepared and the spectroscopic properties were studied as function of Yb<sup>3+</sup> concentration. Emission spectra and fluorescence lifetime in the near infrared and visible upconversion were measured. Strong upconversion emission was observed readily with the naked eye, particularly red increase faster than green emission with the increase of Yb<sup>3+</sup> concentration. The energy transfer from Yb<sup>3+</sup> to Er<sup>3+</sup> and back transfer efficiency from Er<sup>3+</sup> to Yb<sup>3+</sup> were calculated using the fluorescence lifetime of Yb<sup>3+</sup> and Er<sup>3+</sup> respectively. The emission mechanisms involved are explained with the help of energy level diagram. Luminescence results show that both PVA and UREA do not modify the emission properties but control the morphology.



## Studies on performance of polystyrene-brushes of CN<sub>x</sub> carbon nanotubes synthesized by NMRP in PS matrixes

*Mariamne Dehonor*<sup>a,b,c</sup>, *Karine Masenelli-Varlot*<sup>b</sup>, *Alfonso González-Montiel*<sup>f</sup>, *Catherine Gauthier*<sup>b</sup>, *Jean-Yves Cavallé*<sup>b</sup>, *Mauricio Terrones*<sup>a</sup>

<sup>a</sup> *Advanced Materials Department, IPICYT, Sn. Luis Potosi, Mexico.*

<sup>b</sup> *MATEIS, INSA de Lyon, France.*

<sup>c</sup> *CID, Centro de Investigación y Desarrollo Tecnológico S.A. de C.V., Lerma, Mexico.*

Polymer composites of carbon nanotubes dispersed in a polymer matrix are efficiently prepared by chemical functionalization but also by polymer grafting reactions on the nanotube surface<sup>1,2</sup>. Radical functionalization of carbon nanotubes is a novel method proposed here to create controlled-living macroinitiators using the radical uptake and scavenging properties of CN<sub>x</sub> (recently observed and according to previous results in CB<sup>3</sup> and SWNT<sup>4</sup>) without extended surface structural modifications. The obtained controlled-living macroinitiators could begin *in situ* radical polymerization, as Nitroxide-Mediated Radical Polymerization (NMRP)<sup>6</sup>. This work propose to take advantage of the N-doped carbon nanotubes (CN<sub>x</sub>) recognized properties as their reactivity, mechanical and electronic properties<sup>7</sup> to synthesize polymer brushes of CN<sub>x</sub> and polystyrene by (i) the CNT free radical functionalization using an initiator-controller molecule per site (reactive and/or defective) and ii) the *in situ* polymerization of radical functionalized CN<sub>x</sub> using NMRP. In addition to synthesize PS nanocomposites using PS-grafted and un-grafted CN<sub>x</sub> evaluating their electrical properties. In summary, we demonstrated using several characterization techniques that CN<sub>x</sub> can be functionalized using radicals (e.g. BPO and several nitroxides) and that the *in situ* controlled polymerization and the grafting from techniques proceeds successfully over CN<sub>x</sub> when the method NMRP is used. Also, that the dispersion and interface strength were improved for the case of PS-grafted CN<sub>x</sub> and that low electrical percolation threshold values and enhance conductivity was achieved.

### References

1. P.J.F. Harris. *Int. Mat. Rev.* **2004**, 49, 31.
2. O. Breuer and U. Sundararaj. *Polym. Composites.* **2004**, 25, 630.
3. J.B. Donnet, *Carbon*, **1982**, 20, 267.
4. M.S.P. Shaffer and K. Koziol. *Chem. Comm.*, **2002**, 2074.
5. Y. Liu, *et al*, *Macromol.* **2005**, 38, 1172.
6. S.M. Ramirez and Y. Sogah, *Polym.Mater.Sci.Eng.*,**2004**, 91, 493.
7. M. Terrones, *Annu. Rev. Mater. Res.*, **2003**, 33, 419.

**POSTERS**

# **Molecular hydrogen storage in nanoporous hexacyanocobaltates by means of $\sigma$ -bond**

Cristina Pérez Krap, Luis Felipe del Castillo Dávila, Jorge Balmaseda Era

Departamento de polímeros, Instituto de Investigaciones en Materiales, Universidad Nacional Autónoma de México, D.F. C.P. 04510.

balmaseda@iim.unam.mx

Tel: (52) (55) 562 24718

FAX: (52) (55) 561 6 1201

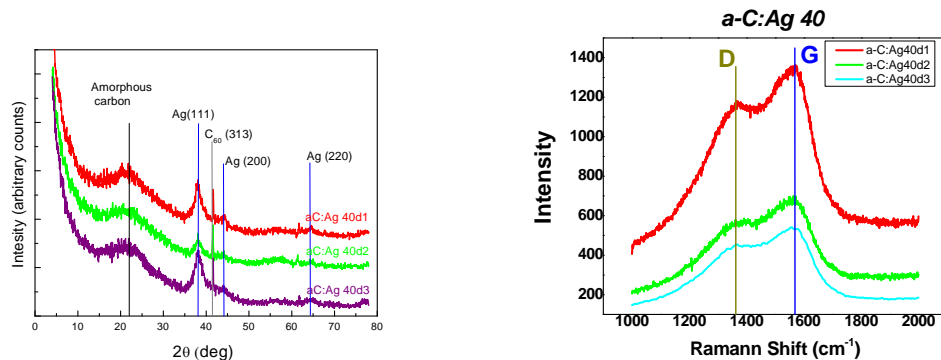
Hexacyanometallates of divalent transition metals has nanoporous frameworks with tridimensional system of channels. The divalent transition metal cations are located in the channel surface and have an incomplete coordination sphere, that allow  $\sigma$  lateral bond of hydrogen molecules. The adsorption of molecular hydrogen on nickel and cooper hexacyanometallates was studied at boiling points of nitrogen and argon. Evidences of  $\sigma$ -H<sub>2</sub> binding between nickel and cooper atoms and hydrogen molecules are given. The magnitude of isosteric heats are explained based on this kind of bond. Quadropole and van der Waals interactions influence is discussed. The  $\sigma$ -H<sub>2</sub> binding strength is controlled by electron density transfer through C≡N ligands from carbon to nitrogen coordinated metals. It is demonstrated that the increase in electron density around divalent transition metal is positive correlated to the  $\sigma$ -H<sub>2</sub> bond strength. In this contribution we propose mechanism to increase H<sub>2</sub> delivery and storage capacity via  $\sigma$  bond.

# Amorphous Carbon-Silver Nanocomposites

O. García-Zarco, S.E. Rodil, S. Muhl

Instituto de Investigaciones en Materiales, UNAM, Circuito Exterior s/n Ciudad Universitaria, 04510, México, D.F. [oscar@graef.fciencias.unam.mx](mailto:oscar@graef.fciencias.unam.mx)

Amorphous carbon (a-C) films are established as very important engineering materials. Metal-containing a-C films gained recently special attention as a way to control the stress and adhesion of the films, as well as due to their potential for biomedical and optical applications. Composites of Amorphous carbon films and silver were deposited by co-sputtering, where the target (10 cm diameter) was of pure graphite with small inclusion of pure silver.(less than 1 cm<sub>2</sub>). The films were deposited under different power, from 40 to 250 W, and different target-substrate distances. The substrate was earthed and rotating in order to obtain an uniform distribution of the silver content (less than 10 at%). The addition of the Ag piece into the target increased the deposition rate of the carbon films, which could be related to the higher sputter yield of the silver. The conditions that lead to the a-C:Ag nanocomposite were the low power (40 W) and the shortest distance (28 mm). Scanning electron micrographs acquired using backscattered electrons showed that the silver was segregated from the carbon matrix, forming nanoparticles or larger clusters as the power was increased. The X-ray diffraction pattern showed that silver was crystalline and the carbon matrix remains amorphous, although for certain conditions a peak attributed to fullerene-like structures was obtained. Finally, we used Raman spectroscopy to understand the bonding characteristics of the carbon-silver composites, finding that there are variations in the D/G ratio, which can be correlated to the observed structure and X-ray diffraction results.



[1]. G. Matenoglou, G. A. Evangelakis, C. Kosmidis, S. Foulis, D. Papadimitiou, P. Patsalas.

Applied Surface Science 253 (2007) 8155 - 8159.

[2]. A. C. Ferrari, Diamond and Related Materials 11 (2002) 1053 – 1061.

# Nanofluids Containing Monodisperse SiO<sub>2</sub> Nanospheres with Different Concentrations

D. Cornejo Monroy<sup>1</sup>, J. A. Balderas-López<sup>2</sup>, J. F. Sánchez Ramírez<sup>1\*</sup>, J. L. Herrera-Pérez<sup>1</sup>, U. Pal<sup>3</sup>, J. Mendoza Álvarez<sup>4</sup>,

<sup>1</sup> *Centro de Investigación en Ciencia Aplicada y Tecnología Avanzada del Instituto Politécnico Nacional, Legaria 694. Colonia Irrigación, 11500 México D. F.  
e-mail: jfsanchez@ipn.mx*

<sup>2</sup> *Unidad Profesional Interdisciplinaria de Biotecnología del IPN, Av. Acueducto S/N, Col. Barrio la Laguna, Del. Gustavo A. Madero, C.P. 07340, México, D.F., México.*

<sup>3</sup> *Instituto de Física, Universidad Autónoma de Puebla, Apdo. Postal J-48, Puebla, Pue. 72570, México.*

<sup>4</sup> *Departamento de Física, CINVESTAV, A. P. 14-740, México D. F. 07360, México.*

## Abstract

Size selective colloidal SiO<sub>2</sub> nanospheres were prepared through hydrolysis of tetraethyl orthosilicate (TEOS). Ammonia is used as morphological catalyst and as a size controller of the silica (SiO<sub>2</sub>) particles. Obtained silica particles were in the size range 20 to 320 nm in diameter. High homogeneity and fine spherical shape were obtained in bigger particles. To determine the effect of particle size and concentration (0.1, 0.3, 0.6, 0.10 and 0.12 % w/w) on the thermal properties of the nanofluids (water, containing SiO<sub>2</sub> nanospheres), the thermal diffusivity of nanofluids were measured using the inverse photopyroelectric technique. The thermal properties of the nanofluids are seen to be strongly dependent on the concentration of the SiO<sub>2</sub> nanospheres. The maximum diffusivity was achieved for the nanofluids containing nanospheres with higher concentrations. Fourier transform infrared (FTIR) spectra, Micro-Raman spectroscopy, TEM and SEM techniques were used to characterize the SiO<sub>2</sub> nanospheres.

## Optical and Photoacoustic Detection of Europium Nanostructures Size

E.V. Mejía-Urriarte<sup>1</sup>, R. Huitrón-Aguilar<sup>1</sup>, J. G. Bañuelos<sup>2</sup>, O. Kolokoltsev<sup>1</sup> and H. Murrieta S<sup>3</sup>.

<sup>1</sup>*Laboratorio de Fotónica de Microondas, CCADET, AP 70-186 C.P. 04510, Universidad Nacional Autónoma de México, D.F. México.*

<sup>2</sup>*Laboratorio de Materiales y sensores, CCADET, AP 70-186 C.P. 04510, Universidad Nacional Autónoma de México, D.F. México.*

<sup>3</sup>*Instituto de Física, AP 20-364, C.P. 01000, Universidad Nacional Autónoma de México, D.F. México.*

elsi.mejia@ccadet.unam.mx - rober\_ha70@hotmail.com

The present work reports a relationship between the luminescence and photoacoustic response of the nanostructures size of europium ions in KBr single crystals in Suzuki phase<sup>1</sup>. The shape and size of nanostructures formed by the precipitation have been previously studied by luminescence and atomic force microscopy (AFM)<sup>2</sup>. The AFM images show that the precipitates have circular shape and ~ 20 to 400 nm diameter according to the position of emission band peak. The shift of the  $t_{2g}$  absorption band towards longer wavelengths and a larger  $10Dq$  value reveals the growth of the nanostructures. The emission peak is shifted (429 → 433 nm) toward infrared wavelength when the nanostructures diameter is increased and the photoacoustic response is shifted (2.5 → 2.4 MHz) to minor frequencies. These systems can be candidates for optoelectronics devices due to the nanostructures dimensions and its capacity for self-assembled<sup>3</sup>.

**Acknowledgements** This work is supported by CONACYT (J51441-F) and PFAMU-DGAPA program of UNAM (México).

### References.

- 1 E. V. Mejía-Urriarte, R. Castañeda-Guzmán, M. Villagrán-Muniz, E. Camarillo, J. Hernández A, H. Murrieta S y M. Navarrete. (2003) “Studies of the thermal dissolution process of the Suzuki phase of the  $\text{Eu}^{2+}$  ion in KBr single crystals by analysis of the photoacoustic signals” *J. Phys.: Condens. Matter* **15** No. 40 p.p 6889-6898.
  - 2 E.V. Mejía-Urriarte, J. Bañuelos, O. Kolokoltsev, M. Navarrete, F. Jaque, E. Camarillo, J. Hernández A. y H. Murrieta S. “Influence of europium nanostructure size on the emission of  $\text{KBr:Eu}^{2+}$ ”. **Solid State Communications, 2008. Submitted.**
- E.V. Mejía-Urriarte, J. Bañuelos O. Kolokoltsev, M. Navarrete, F. Jaque, E. Camarillo, J. Hernández A. y H. Murrieta S. “Self-assembled  $\text{EuBr}_2$  nanostructures” **Materials Letters, 2008. Accepted.**

# **Experimental characterization of Fe(OH)<sub>2</sub> and α-Fe<sub>2</sub>O<sub>3</sub> thin films prepared by the sol-gel technique**

A.E. Jiménez González, Edith Nestor Chamu and Ariatna Maldonado Abarca.

Departamento de Materiales Solares, Centro de Investigación en Energía,  
Universidad Nacional Autónoma de México, Temixco, Morelos CP 62580, Mexico

E-mail: [ajg@mazatl.cie.unam.mx](mailto:ajg@mazatl.cie.unam.mx)

## **Abstract**

During this work, it has been possible to prepare thin films of Fe(OH)<sub>2</sub> and α-Fe<sub>2</sub>O<sub>3</sub> on Pyrex glass by chemical deposition technique sol-gel. The Fe(OH)<sub>2</sub> films were found to be amorphous at room temperature and below 500 °C. FTIR studies show that when the films of Fe(OH)<sub>2</sub> are thermally treated up to 500 °C in air, there is a loss of OH groups and an amorphous-crystalline phase transition to a rhombohedral structure (α-Fe<sub>2</sub>O<sub>3</sub>), as confirmed by X-ray Diffraction analysis. Iron oxide films treated at 500 °C present a nanometric crystal size. Through UV-VIS spectrophotometry and energy band gap studies carried out on α-Fe<sub>2</sub>O<sub>3</sub>, it was determined that the films present a energy band gap of 2.17 eV. Making use of the sol-gel technique, thin films of iron oxide were deposited on different polymeric substrates (acetate, polycarbonate and PET). The possible application of the iron oxide films in photocatalytic processes is discussed.

**Development of immobilized nanostructured iron oxide catalysts  
and its application in the photocatalytic  
degradation of textile dyes.**

A.E. Jiménez González, E. Nestor Chamú and A. Maldonado Abarca.

Departamento de Materiales Solares, Centro de Investigación en Energía,  
Universidad Nacional Autónoma de México, Temixco, Morelos CP 62580, Mexico

E-mail: [ajg@mazatl.cie.unam.mx](mailto:ajg@mazatl.cie.unam.mx)

**Abstract**

Fenton and photo-Fenton processes have been proved to be very useful in the photocatalytic degradation of a large amount of organic compounds for which the use of iron salts (Fenton's reactive) as catalysts are very common. During these processes, the catalysts as well as pollutants are dissolved in a homogeneous solution, so that after the photoreaction is impossible to recover the catalyst. As an alternative to Fenton's processes carried out in homogeneous phase, during this work iron oxide catalysts have been immobilized. Using the sol-gel chemical deposition technique, it was possible to immobilize the iron oxide catalysts on glass as well as on polymeric substrates. Finally, the photocatalytic degradation of blue and red AZO textile dyes was carried out using the iron oxide immobilized catalysts. It was also demonstrated that the heterogeneous photocatalytic degradation of textil dyes using the immobilized system is catalytically as efficient as the iron salts used in the homogeneous phase.

## “Free solvent synthesis of Iridium(0) nanoparticles”

Rocío Redón<sup>1</sup>, Fermín Ramírez<sup>1</sup>, Ana L. Fernández-Osorio<sup>2</sup>

<sup>(1)</sup>CCADET, Universidad Nacional Autónoma de México, Cd. Universitaria, A.P. 70-186, C. P. 04510 México D. F.

<sup>(2)</sup>FES, Cuautitlán, Universidad Nacional Autónoma de México, Edo. de México.  
rredon@servidor.unam.mx

### Abstract

Nanoscale materials have been widely studied because of their particular properties and potential applications. In particular, noble metal nanoparticles have been used as catalysts [1,2] and photocatalysts in solution for many years. The activity of these materials is controlled by their size, crystal structure and the nature of the stabilizer. Nevertheless, metal nanoparticles in solution are hard to maintain on zero oxidation state, thus there have been some tries to obtain nanoparticles without the use of solvents. In this paper we present the results on the free solvent synthesis of iridium(0) nanoparticles and the interaction with zero generation dendrimer using as central molecule cyanuric chloride. The synthesis of iridium(0) was carried out using two different methodologies. First; reagents were milled to obtain a fine powder, after heat. In the second one, products of the milling were washed before heat. In both cases we study the effect of the change in the concentration of reducing agent used. The synthesis of iridium(0) with the first methodology produces, in some cases, impurities of NaBH<sub>4</sub> and IrO<sub>2</sub>. By the second procedure the powder was obtained free of impurities. In all cases the calculated particle size is less than 10 nm

**Acknowledgements.** Rocío Redón wants to acknowledge PAPIIT (IN101308) project for financial support.

### Bibliography

- 1 H. Yee, R. W. J. Scott, R. M. Crooks, *Langmuir*, **20**, 2915-2920 (2004).
- 2 Y. M. Chung, H. K. Rhee, *Catalysis Surveys from Asia*, **8**, 211-223 (2004).

## Beta and UV radiation induced thermoluminescence in nanocrystalline zirconia

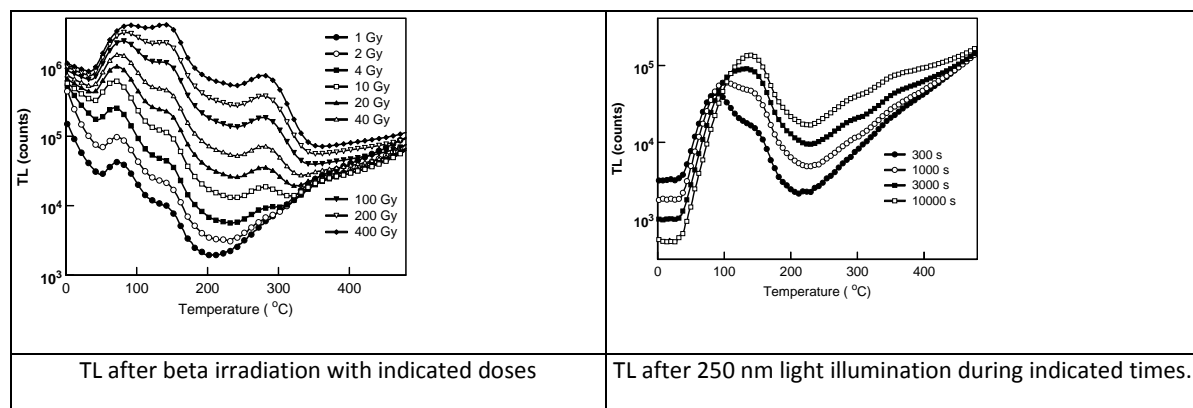
V. Chernov<sup>1</sup>, F. Ramos-Brito<sup>2</sup>, T. M. Píters<sup>1</sup>, R. Meléndrez<sup>1</sup>, M. Barboza-Flores<sup>1</sup>

<sup>1</sup>Departamento de Investigación en Física, Universidad de Sonora, A. P. 5-088. Hermosillo, Sonora  
83190, México

<sup>2</sup>Centro de Ciencias de Sinaloa, Av. de las Américas 2771 Norte, Culiacán, Sinaloa, 80010 México

*E-mail:* mbarboza@cajeme.cifus.uson.mx

ZrO<sub>2</sub> is considered nowadays one of the most important ceramic materials, which can be used in a wide range of industrial applications. Luminescence studies can provide important information about intrinsic and impurity defects. In particular, the thermoluminescence (TL) phenomenon is widely used for determination of kinetic parameters of electron and hole traps. In this work we report TL properties of undoped nanocrystalline ZrO<sub>2</sub> powder prepared by crystallization of a saturated solution followed by a post annealing treatment at 950 °C.



Immediately after beta irradiation or UV illumination the samples exhibit persistence luminescence due to thermal emptying of shallow traps (initial part of the curves up to 30 °C). The glow curves exhibit 3 pronounced TL peaks with maxima at about 75, 140 and 280 °C and unstructured TL between 170 and 250 °C, which looks like a TL peak overlapped by the tails of the 140 and 280 TL peaks. The 75 °C TL peak decay partially during long time irradiation (fading) that causes the change of the low temperature region of the glow curves. The glow peak intensities were found to be dependent lineary-sublinearly on beta dose or UV illumination time. The TL creation spectrum of UV exposed samples spans the 200-450 nm range with maxima around 230 and 300 nm. The non-irradiated sample preliminary heated up to 500 °C and stored in dark exhibits a pronounced TL between 200 and 500 °C, whose intensity increases linearly with the storage time.

## Calculation of the dielectric function of zigzag (6,0) boron nitride nanotubes with adsorption of molecular hydrogen.

*N. Arzate, R. A. Vázquez-Nava, and J. E. Mejía*

We present *ab initio* calculations for the dielectric function of single wall zigzag (6,0) boron nitride nanotubes as a function of the molecular hydrogen adsorption. The *ab initio* calculations are performed within Density Functional Theory. We consider different nanotube-structures adsorbed with different coverage of molecular hydrogen. We find optimized atomic coordinates for such structures and calculate binding energies for the molecule of hydrogen on the nanotube. We also present the energy loss function spectra of the considered structures.

This work has been partly supported by CONACYT, México, grants: SEP-2004-C01-48142, SEP-2003-C02-42576, and SEP-2005-C01-49678-F.

**Empirical approach to calculate the number of atoms in column-domains by  
HAADF-STEM analysis: A binary approximation in  
the Nb<sub>16</sub> W<sub>18</sub> O<sub>94</sub> ternary system.**

*L. Rendón and P. Santiago*

[rendon@fisica.unam.mx](mailto:rendon@fisica.unam.mx)

<sup>1</sup>*Departamento de Materia Condensada, Instituto de Física, Universidad Nacional Autónoma de México, Coyoacan, 04510, A.P. 20-364, C.P. 01000, Mexico City, Mexico.*

In the present work, an ultra thin sample of the complex oxide Nb<sub>16</sub> W<sub>18</sub> O<sub>94</sub> was observed using a high-angle annular dark field detector. An atomic column-domains, produced by non-uniformity intercalation of W and Nb atoms along the [001] projection was observed and studied. An empirical calculation was developed to quantify the number of W atomic sites in excess at the specific column using a binary approximation in the ternary system Nb<sub>16</sub> W<sub>18</sub> O<sub>94</sub>. This theoretical calculation is based on the fact that the profile line intensity in a HAADF image strongly depends on  $Z^\alpha$ , where the  $\alpha$  coefficient is between 1.5 to 2 (named: Z-contrast) and this effect generates observable column domains in the HAADF image recorder. The study was developed along the [001] zone axis projection. Some atomic columns observed by STEM-HAADF technique showed an excess of W atoms, this effect is directly related to the intensity distribution in the image generated by the HAADF scintillation detector.

# Controlled Manipulation and Transport of Vanadium Oxide Nanotubes with Optical Tweezers

José Luis Hernández-Pozos<sup>\*,†</sup>, W.M. Lee<sup>§</sup>, L. Irais Vera-Robles<sup>‡</sup>, Antonio Campero<sup>‡</sup>, and Kishan Dholakia<sup>§</sup>.

<sup>†</sup> *Departamento de Física, Universidad Autónoma Metropolitana-Iztapalapa (UAM-I). Av. San Rafael Atlixco No 186. Col Vicentina. Mexico City. México.*

<sup>‡</sup> *Departamento de Química, Universidad Autónoma Metropolitana-Iztapalapa, PO Box 55-534, México, DF 09340, Mexico*

<sup>§</sup> *SUPA, School of Physics and Astronomy, University of St Andrews, North Haugh, St. Andrews KY16 9SS. United Kingdom.*

\* E-mail: [jlhp@xanum.uam.mx](mailto:jlhp@xanum.uam.mx)

**ABSTRACT:** We present a direct nanotube-microsphere tagging technique for the controlled three dimensional (3D) manipulations and transportation of vanadium oxide nanotubes (VOx-NTs) with optical tweezers. The high scattering and absorptive nature of the VOx-NTs preclude the 3D optical trapping of such nanostructures. VOx-NTs are directly adhered to 3 amino-propylethoxysilane functionalized silica microspheres, which acts as handles for indirectly manipulating and transporting the nanotubes in 3D with optical tweezers. The optical tweezers can operate as an optical scissors that remove the dielectric handles and trim these nanotubes. This technique may be extended to the optical control of nanotubes of any materials.

# Influence of the Ethanol in the formation of Vanadium Oxide Nanotubes

L. Irais Vera-Robles, Antonio Campero

*Universidad Autónoma Metropolitana-Iztapalapa, Departamento de Química.*

E-mail: [live@xanum.uam.mx](mailto:live@xanum.uam.mx), [acc35@xanum.uam.mx](mailto:acc35@xanum.uam.mx),

Vanadium oxide nanotubes VO<sub>x</sub>-NTs were synthesized utilizing a novel approach by the oxidation of a vanadium (IV) species i.e., vanadyl (IV) acetate (VO(Ac)<sub>2</sub>). This compound was mixed with dodecylamine, acting as template, forming a layer precursor with amine molecules intercalated in the vanadium-oxide network [1]. This composite precursor was then subjected to a hydrothermal treatment which gives way to the scrolling of the layers forming the tubular structure. These nanotubes are completely similar to those obtained with vanadium (V) oxide (V<sub>2</sub>O<sub>5</sub>) [2]. In both cases the VO<sub>x</sub>-NTs contain vanadium as a mixture with a molar V<sup>4+</sup>/V<sup>5+</sup> ratio equal to one [3,4] (Figure 1). Due the importance of the layer precursor this was characterized, thus allowing us to suggest a mechanism for the formation of the tubular nanostructures. The influence of the role of EtOH in the formation of the nanotubes was ascertained and it was found that its presence is absolutely necessary only in case that the formation of VO<sub>x</sub>-NTs of top quality is required.

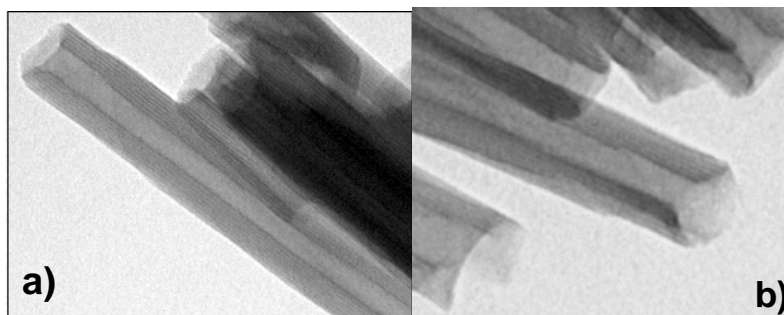


Figure 1. TEM images of the VO<sub>x</sub>-NTs from a)V<sub>2</sub>O<sub>5</sub>, b)VO(Ac)<sub>2</sub>

[1] Vera-Robles L.I.; Campero A. *J. Phys. Chem. C* in press

[2] Niederberger, M.; Muhr, H.-J.; Krumeich, F.; Bieri, F.; Günther, D.; Nesper, R. *Chem. Mater.* **2000**, *12*, 1995.

[3] Sunn, D.; Kwon, C. W.; Baure, G.; Richman, E.; MacLean, J.; Dunn, B.; Tolbert, S.H. *Adv. Funct. Mater.* **2004**, *14*, 1197.

[4] Krumeich, F.; Muhr, H.-J.; Niederberger, M.; Bieri, F.; Schnyder, B.; Nesper, R. *J. Am. Chem. Soc.* **1999**, *121*, 8324.

# Study of layer defect in 1-D omnidirectional mirrors based in Porous Silicon Multilayers

**J. O. ESTEVEZ<sup>1</sup>, J. ARRIAGA<sup>1</sup>, A. MENDEZ-BLAS<sup>1</sup>, V. AGARWAL<sup>2</sup>**

<sup>1</sup>*Instituto de Física, Benemérita Universidad Autónoma de Puebla, Apdo. Postal J-48,*

*C.P. 72570, Puebla, Pue., México*

<sup>2</sup>*CIICAP, Universidad Autónoma del Estado de Morelos,*

*C.P. 62209, Cuernavaca Mor., México*

jestev@sirio.ifuap.buap.mx

Photonic crystals (PC) are artificial periodic structures. When an electromagnetic wave falls into one dimensional (1-D) PC with a frequency in the range of frequencies of the photonic band gap (PBG), all the radiation will be reflected independent on its polarization and incidence angle. Localized modes can be obtained inside the omnidirectional region by introducing a defect on the structure, this means, breaking the periodicity in the PC with a layer with different parameters (thickness and refraction index) than the layers that compose the PC structure. In this work we calculate the band structure for a 1-D PC taking into account a defect in the system. The structure is obtained by using porous silicon (PS) technology. The PC is analyzed from a theoretical and experimental point of view in the near infra red region. Each unit cell of the PC is composed by two layers *A* and *B*, with thickness  $d_A$  and  $d_B$  respectively. The refraction index in part *A* varies according to the envelope of a Gaussian function [1], and the part *B* is a layer with a constant refractive index  $n_B$ . The defect layer has a refractive index  $n_B$  with a different width than layer *B* [2]. These devices can be used as TM/TE filter, splitters [3] and bio-sensors [4].

[1] J. Arriaga and X. I. Saldaña, J. Appl. Phys., **100**, 044911 (2006)

[2] J. D. Joannopoulos, R. D. Meade, and J. N. Winn, "Photonic Crystals: Molding the flow of light", Princeton University Press, (1995)

[3] Hyun-Yong Lee and T. Yao, J. Appl. Phys., **93**, No. 2 (2003)

[4] Michael J. Sailor et al., Science, 278, 5339 (1997)

## Electroluminescence in Porous Silicon with SnO<sub>2</sub> coating

F. Severiano-Carrillo<sup>1</sup>, G. G. Salgado<sup>2</sup>, A. Méndez-Blas<sup>1</sup>, J.M. Gracia y Jimenez<sup>1</sup>

*Instituto de Física, Benemérita Universidad Autónoma de Puebla, Apdo. Postal J-48,*

*C.P. 72570, Puebla, Pue., México.*

*Instituto de Semiconductores, Benemérita Universidad Autónoma de Puebla, C.P. 72570,*

*Puebla, Pue., México*

Porous Silicon (PS) is highly luminescent in the visible spectral range at room temperature<sup>1</sup>, in contrast to bulk crystalline silicon. Electroluminescence (EL), which offers greater potential for device applications, has been obtained from porous silicon in solid-state structures. The electroluminescence was obtained in different current conditions

In this work, we report the fabrication and characterization of a device with visible EL. Porous silicon is formed by anodization of p-type (100) silicon samples in hydrofluoric acid (HF) aqueous solution using a classical experimental setup. We have prepared PS layers of different porosities using p-type silicon wafers of 5 - 10 Ω·cm resistivities by anodizing them at different current density in the electrolyte. The electroluminescence behavior of the PS layers was studied by EL spectroscopy of CCD (Charge-coupled devices) at room temperature. We report the preparation of silicon-based visible light-emitting devices, configured as junctions between PS and n-type tin oxide and fluorine doped (SnO<sub>2</sub>:F). The transparent SnO<sub>2</sub>:F film allows light emission through the top surface of the device, under a forward electrical bias of several volts across the junction.

1. Leigh T. Canham, *Appl. Phys. Lett.* **57**, 1096 (1990).

## Europium doped Yttrium Oxide glass ceramic nanopowders

### elaborated by sol-gel process: Structural and luminescent characteristics

D. López Torres<sup>1</sup>, A. García Murillo<sup>1</sup>, F. Carrillo Romo<sup>1</sup>, N. Cayetano Castro<sup>3</sup>,  
V. H. Romero<sup>2</sup>, E. de la Rosa<sup>2</sup>, V. Garibay Febles<sup>3</sup>

<sup>1</sup>Centro de Investigación en Ciencia Aplicada y Tecnología Avanzada Unidad Altamira IPN,  
Km 14.5 Carr. Tampico-Pto. Industrial, C.P.89600 Altamira, Tamps, México.

<sup>2</sup>Centro de Investigaciones en Óptica A.P. 1-948, 37000 León, Gto., México

<sup>3</sup>Programa de Ingeniería Molecular, Instituto Mexicano del Petróleo, Eje Lázaro Cárdenas  
No. 152, CP 07730, Mexico D.F., Mexico

E-mail: [angarciam@ipn.mx](mailto:angarciam@ipn.mx)

Eu<sup>3+</sup> activated Y<sub>2</sub>O<sub>3</sub>/SiO<sub>2</sub> were synthesized using yttrium oxide and TEOS in order to produce glass ceramic nanoparticles. The glass ceramic phosphor system was prepared taking into account two methodologies, the first one (PS) using the crystallized ceramic added into the SiO<sub>2</sub> sol, and the second one (SS) crystallizing directly the Y<sub>2</sub>O<sub>3</sub>:Eu<sup>3+</sup> into the glass matrix, the Y<sub>2</sub>O<sub>3</sub>:Eu<sup>3+</sup> pure system was also prepared as a reference. Glass ceramic systems were characterized by means of X-ray diffraction, IR spectroscopy, SEM, CTEM and HRTEM. The structural studies suggest the formation of cubic Y<sub>2</sub>O<sub>3</sub>:Eu<sup>3+</sup> annealed at 500 °C for 1 h for PS and SS powders. However, a thermal treatment of 700 °C allows the formation of Y<sub>2</sub>O<sub>3</sub>:Eu<sup>3+</sup>/SiO<sub>2</sub> nanoparticles with an average size between 30-80 nm and nanocrystals with a size of 10 nm for the PS and SS powders respectively. The luminescent properties were measured for ceramic, PS and SS powders heat-treated at 700 °C showing the characteristic <sup>5</sup>D<sub>0</sub> → <sup>7</sup>F<sub>j</sub> emissions of Eu<sup>3+</sup> ions in yttrium oxide glass ceramics. These PL spectra revealed in some extent the local environment Eu<sup>3+</sup> around the Y<sub>2</sub>O<sub>3</sub>, PS and SS nanoparticles, indicating that the (SS) powder exhibited greatest luminescence properties in comparison with (PS) and Y<sub>2</sub>O<sub>3</sub>:Eu<sup>3+</sup>, this could be probably related with europium environment being much symmetrical for the (SS) glass ceramic constituted with yttrium oxide nanocrystals comparatively with (PS) nanopowders.

# Anchoring of Bismuth Sulfide Nanoparticles on Graphite Surface

**Coraabdi Pérez Luna** and David Díaz\*

*Universidad Nacional Autónoma de México, Facultad de Química, Ciudad Universitaria  
Coyoacán, CP 04510, México DF, México.*

[coraabdi@gmail.com](mailto:coraabdi@gmail.com), [david@servidor.unam.mx](mailto:david@servidor.unam.mx) Tel/fax 56223813

Bismuth Sulfide is a type “n” semiconductor, it is found in nature as *bismuthinite*, and it has a crystalline orthorhombic structure<sup>1</sup>. On the other hand, graphite has demonstrated singular properties when present in alloys or composites, due to its multi-layered structure. Some applications of graphite include composite materials for the aerospace industry such as airplane fuselages. Our principal motivation is the study of novel chemical and electronic properties of anchored Bi<sub>2</sub>S<sub>3</sub> on graphite surface composites. Our group has recently anchored Ag NPs onto the surface of graphite successfully<sup>2</sup>. It was decided to test that method in the synthesis Bi<sub>2</sub>S<sub>3</sub>-graphite composites. In this work we used an easy, fast and inexpensive colloidal method for obtaining the Bi<sub>2</sub>S<sub>3</sub> NPs-graphite composites. Graphite powders were suspended in dimethylsulphoxide (DMSO, a polar solvent) and disrupted using a high power sonicator. The graphite supported Bi<sub>2</sub>S<sub>3</sub> NPs were prepared using sodium-citrate (stabilizing agent) and bismuth nitrate (salt precursor) solution dissolved in DMSO with vigorous stirring at room temperature. An aliquot of sodium sulfide was added to the suspension; the color of the brownish suspension indicated that Bi<sub>2</sub>S<sub>3</sub> NPs were formed; finally the sonicated graphite was added. The stirring was continued for 4 days under the same experimental conditions. During this time, the suspensions were protected from the light to avoid the photochemical oxidation of the nanoparticles.

The particles were characterized by Absorption Spectroscopy, X-ray Diffraction; Transmission Electron Microscopy (TEM) and an additional High-Resolution TEM analysis will be made to complete the characterization. The electrical surface potential was also measured.

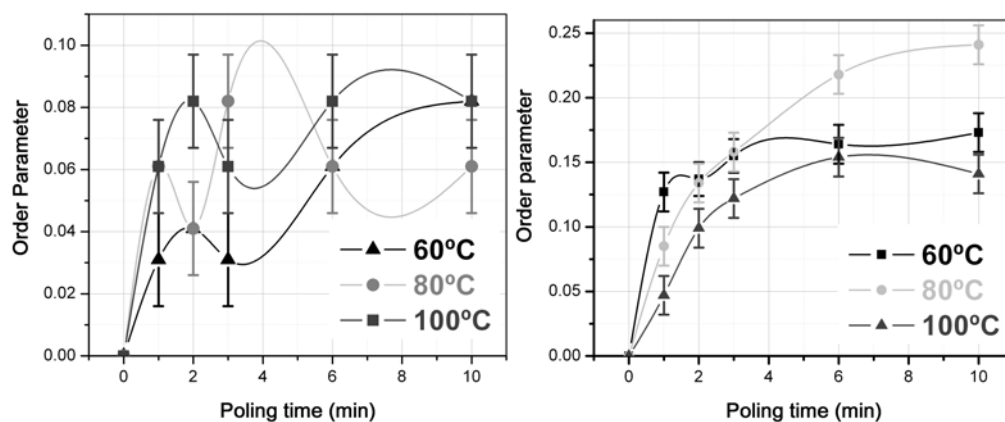
# Non-linear optical studies on amorphous and nanostructured PMMA and SiO<sub>2</sub> films doped with DO3.

Jorge Garcia-Macedo<sup>1\*</sup>, Guadalupe Valverde-Aguilar<sup>1</sup>, Laura A. Romero Miranda<sup>1</sup>

1. Departamento de Estado Sólido. Instituto de Física, Universidad Nacional Autónoma de México.  
México D. F. C. P. 04510

E-mail: gamaj@fisica.unam.mx

Polymethylmethacrylate (PMMA) and silica (SiO<sub>2</sub>) amorphous and nanostructured films were obtained by sol-gel route. Nanostructure was got by the incorporation of the anionic surfactant, Sodium Dodecyl Sulfate (SDS). A lamellar nanostructure in the films was identified by X-ray diffraction (XRD). The orientation kinetics of Disperse Orange 3 (DO3) molecules embedded in amorphous and nanostructured films was studied under the effect of an intense constant Corona electric poling field. Non-centrosymmetric chromophore orientation distributions were obtained by the poling field. These distributions depend on the Corona poling time. The changes in the orientation of the DO3 molecules were followed by Second Harmonic Generation (SHG) and the order parameter measurements. The SHG signal was recorded as function of time at three different temperatures: 60 °C, 80 °C, 100 °C and 120 °C. Results were fitted as a function of the Corona poling time, with a model that takes into account the matrix-chromophore interactions. Nanostructured films showed more stable behaviour.



Order parameter as function of poling time for (Left) amorphous PMMA/DO3 film, and nanostructured PMMA/DO3 film (Right).

CONACYT 79781, NSF-CONACYT, PUNTA, PAPIIT 116506-3 and DGAPA UNAM IN123804 supported this work. GVA is grateful for the ICyTDF postdoctoral fellowship. LRM is grateful for CONACyT fellowship.

# Photoconductivity on amorphous and nanocrystalline sol-gel ZnO-TiO<sub>2</sub> samples

R. Juárez-Arenas<sup>1</sup>, J. A. García-Macedo<sup>1\*</sup>, G. Valverde-Aguilar<sup>1</sup>

1. *Departamento de Estado Sólido. Instituto de Física, Universidad Nacional Autónoma de México. México D.F. C.P. 04510*

E-mail: [gamaj@fisica.unam.mx](mailto:gamaj@fisica.unam.mx)

We report results on the synthesis, characterization and photoconductivity behaviour of amorphous and nanocrystalline ZnO-TiO<sub>2</sub> thin films and powders. The films were produced by the sol-gel process at room temperature by using the spin-coating method and deposited on glass substrates. The ZnO-TiO<sub>2</sub> samples were synthesized by using tetrabutyl orthotitanate and zinc nitrate hexahydrate as the inorganic precursors. The samples were sintered at 520°C for 1 hour. The obtained films were characterized by X-ray diffraction, optical absorption, FTIR and TEM studies. Photoconductivity studies were performed on amorphous and nanocrystalline (anatase phase) films. For amorphous and crystalline films, the experimental data were fitted by least-squares with straight lines at darkness and under illumination at 310 nm, 439 nm and 633 nm. It indicates an ohmic behaviour. Transport parameters were calculated. The  $\phi\mu\tau$  and  $\phi I_0$  parameters were fitted by least-squares with straight lines (nanocrystalline films) and polynomial fits (amorphous films). The anatase phase obtained in the ZnO/TiO<sub>2</sub> matrix provides more stability to improve the photoconductivity.

\* The authors acknowledge the financial supports of CONACYT 79781, NSF-CONACYT, PUNTA, PAPIIT 116506-3 and DGAPA UNAM IN123804. RJA and GVA are grateful for a ICyTDF postdoctoral fellowship and DGAPA fellowship, respectively. The authors are thankful to M. in Sci. Manuel Aguilar-Franco (XRD) for technical assistance.

# Synthesis of Nanosized Beta-Eu<sub>8</sub>Ga<sub>16</sub>Ge<sub>30</sub> Clathrate via Calciothermic Reduction.

L. Tepech-Carrillo<sup>1-2</sup>, V. Pacheco<sup>2</sup>, W. Carrillo-Cabrera<sup>2</sup>, Yu. Grin<sup>2</sup>.

<sup>1</sup>*Instituto de Física, Benemérita Universidad Autónoma de Puebla, Apdo. Postal J-48,*

*C.P. 72570, Puebla, Pue., México*

<sup>2</sup>*Max-Planck-Institut für Chemische Physik fester Stoffe, Nöthnitzer Str. 4001187 Dresden, Germany*

E-mail: ltepech@sirio.ifuap.buap.mx

Eu<sub>8</sub>Ga<sub>16</sub>Ge<sub>30</sub> Clathrate is an interesting material because of its potential thermoelectric applications. The figure of merit may improve for nanocrystalline or amorphous sample<sup>1</sup>. We synthesized Eu<sub>8</sub>Ga<sub>16</sub>Ge<sub>30</sub> clathrate through the reduction of their precursors metal oxides. These precursors were produced by sol-gel-calcination route. The morphology of the particles shows the spheric (10 nm) and thin plates (thickness ~ 20 nm). The subsequent reduction of the oxides with CaH<sub>2</sub> produced intermetallic compounds embedded in a by-product CaO matrix. The XRD pattern of sample shows the reflection of β-Eu<sub>8</sub>Ga<sub>16</sub>Ge<sub>30</sub> clathrate, EuGa<sub>2</sub>Ge<sub>4</sub> and Eu<sub>3</sub>Ga<sub>4</sub>Ge<sub>6</sub> materials. Refined lattice parameters ( $a = 10.710(2)$  Å;  $a = 4.161(4)$  Å,  $b = 11.278(5)$  Å,  $c = 13.159(8)$  Å;  $a = 23.996(6)$  Å,  $b = 4.1316(1)$  Å,  $c = 10.967(3)$  Å,  $\beta = 91.72(2)^\circ$ , respectively) are in agreement with the reported values<sup>2,4</sup>. TEM investigations show nanospheres (~ 50 nm) and bulk material. SAED patterns confirm the presence of β-Eu<sub>8</sub>Ga<sub>16</sub>Ge<sub>30</sub> and Eu<sub>3</sub>Ga<sub>4</sub>Ge<sub>6</sub>.

<sup>1</sup> G. S. Nolas and H. J. Goldsmid. *Pys. Stat. Sol. (a)* **194**, No. 1, 271–276 (2002).

<sup>2</sup> V. Pacheco, A. Bontien, W. Carrillo-Cabrera, S. Paschen, F. Steglich and Yu. Grin. *Phys. Rev. B* **71**, 165205 (2005).

<sup>3</sup> W. Carrillo-Cabrera, S. Paschen and Yu. Grin. *J. Alloys Compd.* **333**, 4-12, (2002).

# Adsorption sites for the first CO molecule on $\text{Au}_n^{+1}$ , $n=18, 19, 20$ : a theoretical study.

B. Molina, J. R. Soto, and A. Calles<sup>a</sup>

*Facultad de Ciencias, Universidad Nacional Autónoma de México, Apartado Postal 70-646, 04510  
México D. F., México.*

*All authors are members of UNAM Nanotechnology Project (PUNTA).*

E-mail: mlnbrt@yahoo.com

Experimental adsorption studies at liquid nitrogen temperature have showed that  $\text{Au}_{18}^{+1}$  and  $\text{Au}_{19}^{+1}$  clusters are very reactive towards the first CO molecule, while  $\text{Au}_{20}^{+1}$  can adsorb until four CO molecules. On the other hand, vibrational and electron spectroscopy and theoretical studies suggest a  $C_{2v}$  (a cage structure),  $C_{3v}$  and  $T_d$  (a pyramidal structures) as lowest-energy symmetries for these clusters respectively. In this work we carried out functional density calculations to identify the adsorption sites for the first CO molecule on the  $\text{Au}_n^{+1}$ ,  $n=18, 19, 20$  clusters and the symmetries above mentioned. The GGA (Gradient Generalized Approximation)-PW91 functional was used for exchange and correlation terms. The 6-311G\*\* basis were used for the carbon and oxygen atoms and LANL2DZ relativistic effective core potential for the gold atoms. Our results showed a high fluxionality in the  $C_{2v}$   $\text{Au}_{18}^{+1}$  cluster when the CO molecule is adsorbed on any site except on a cluster apex, while the  $C_{3v}$   $\text{Au}_{19}^{+1}$  and  $\text{Au}_{20}^{+1}$  clusters exhibit a greater rigidity. However, the apex sites in the  $C_{2v}$   $\text{Au}_{18}^{+1}$  cluster are not the sites with the biggest energy adsorption, conversely to  $C_{3v}$   $\text{Au}_{19}^{+1}$  cluster. In this work, the charge transferences and bond length Au-C and C-O are also analyzed.

# SILVER-CARBON NANOPARTICLES PRODUCED BY HIGH-CURRENT PULSED ARC

F. MAYA<sup>\*1,2</sup>, M. YOSHIDA<sup>1</sup>, S. MUHL<sup>2</sup> AND O. PEÑA<sup>2</sup>

*1 Centro de Investigación en Materiales Avanzados (CIMAV) Chihuahua, Av Miguel de Cervantes # 120, Complejo Industrial Chihuahua, C. P. 31109, Chihuahua México.*

*2 Instituto de Investigaciones en Materiales, Universidad Nacional Autónoma de México, Circuito Exterior S/N, Ciudad Universitaria, Coyoacan, C. P. 04510, México, D. F.*

\*fermin.maya@cimav.edu.mx

Great interest has been focused on Ag-Carbon material systems due to the possibility of obtaining Ag nanoparticles encapsulated by crystalline or amorphous carbon. Silver exhibits excellent thermal and electrical conductivity and has been extensively used in catalysis, electronics, photonics, photography, biological labeling, and surface-enhanced Raman scattering. Composite nanostructures using nanoscale silver as the core have been prepared by many research groups. For example, Ag/C nanocables and Ag/C nanoparticles have been synthesized in the presence of PVP; silver/cross-linked poly (vinyl alcohol) coaxial nanocables have also been prepared. In this work we have used a High-Current Pulsed electric arc in Argon between 3.3mm graphite and 1.5mm silver electrodes to produce silver-carbon nanoparticles at different gas pressures. These nanoparticles were analyzed by TEM, SEM, Optical absorption and XRD. Firstly, we measured the relation between the deposition rate and pressure and found that the deposition rate increased when the pressure decrease. The XRD analysis showed that the silver is crystalline; to confirm this the nanoparticles were analyzed by TEM. The Electron Diffraction again showed that the silver part of the nanoparticle is crystalline. Furthermore, it was established that the particles consisted of a crystalline silver nucleus coated with amorphous carbon. The size of the particles varied from ~150nm to less than 5nm depending on the gas pressure (800-100 Torr). Additionally, small quantities of crystalline graphite and amorphous carbon were found in the produced deposits. By EDS we studied the composition and structure of the deposits as a function of the gas pressure, as well as, the duration of the arc.

Finally, the analysis of the optical absorption spectra showed that the nanoparticles are not spheres but rather spheroids (an ellipsoid with two equal axes). Both, the aspect ratios  $\epsilon$  (the ratio of the largest to the smallest axes) and the equivalent radii  $r_v$  (radius of a sphere having the same volume) are dependant on the gas pressure. This is interesting since by changing the aspect ratios, it is possible to tune the frequency of the surface plasmon resonance (SPR). This SPR tunability makes these nanoparticles potentially interesting for many optical and optoelectronic applications.

# Design of superplasticity equipment to deform Zr-base ceramic nanomaterial

*S.R. Casolco<sup>1</sup>, S. Valdez<sup>2</sup>, J. Garay<sup>3</sup>.*

<sup>1</sup> Tecnológico de Monterrey, Campus Puebla, Vía Atlixcáyotl 2301, Puebla, Pue. México.  
C.P. 72800

<sup>2</sup> Instituto de Ciencias Físicas, UNAM, Av. Universidad s/n, Col. Chamilpa, Cuernavaca,  
Morelos, 62210.

<sup>3</sup>Department of Mechanical Engineering, University of California, Riverside, USA

**Key words:** Zr-base ceramic nanomaterial, Superplasticity

**Abstract.** Nanostructured materials exhibit novel an excellent mechanical and physical properties compared with their microcrystalline counterparts. Nanostructured ceramic materials are also attractive due to their strength at high temperatures, their chemical inertness (as compared with metals) and their resistance to erosion and abrasion [1], low-temperature high-strain-rate formable nanocrystalline superplastic ceramic [2]. However the machinability of bulk nanomaterials has been probed to be very difficult. [2], specially to the ceramic nanomaterials case [2,3]. When bulk ceramic nanosized is deformed, an important factor is to maintain a homogeneous behaviour with their chemical and physical properties constant in high range and with their tension-deformation independently to the direction under study. In order to characterize mechanically bulk nanocrystalline materials of Zirconia-Yttria, a superplastic deformation machine has been designed. Conceptual design is based in a test Instron machine. The subjection equipment was realized by means of Software Solid Edge, whereas Software ADAM™ Graphic Design was used to simulate the test in order to identify the maximum stress points and to verify the design efficiency. The prototype was manufactured in high temperature steel by means of CNC Hass equipment. In addition, the rugosity of steel and nanoceramic was carried out by a rugosimeter SURFCOM 130A – Tokyo Seimitsu. The results showed the friction relationship between the steel and Zirconia- Yttria nanomaterial in order to avoid defects during the test. The analysis and simulations show us the excellent characteristics of equipment designed to deform superplastically a nanocrystalline Zirconia-Yttria nanoceramic.

## ACKNOWLEDGMENTS

The authors would like to thank at DGAPA-UNAM-PAPIIT and CONACyT Grant No. IN105708 and 83164 respectively, for their financial support of this research project..

## References:

- [1] S.R. Casolco, J. Xu, J.E. Garay. *Scrip. Mater.* 58-6, 2008-516-519.
- [2] Dustin M. Hulbert, Dongtao Jiang, Joshua D. Kuntz, Yasuhiro Kodera and Amiya K. Mukherjee. *Scripta Materialia* 55 (2006) 215–217.

# Influence of alloying and inoculants element on the Al-Mg nanocrystalline ribbon

<sup>1</sup>S.R. Casolco, <sup>2</sup>M. Aguilar, <sup>3\*</sup>S. Valdez

<sup>1</sup> Tecnológico de Monterrey, Campus Puebla, Vía Atlixcáyotl 2301, Puebla, Pue. México. C.P. 72800.

<sup>2</sup>Instituto de Física, Circuito escolar S/N, Cd. Universitaria, 04515, México, D.F., México.

<sup>3</sup>Instituto de Ciencias Físicas-UNAM, P.O Box 48-3, Av. Universidad S/N, Col. Chamilpa, 062210,

Cuernavaca, Morelos, México. \*[svaldez@fis.unam.mx](mailto:svaldez@fis.unam.mx), 01 55 56 22 77 85

**Abstract.** The AlMgSiTi nanocrystalline ribbon was obtained by the melt-spinning technique at high cooling rates and with improved mechanical properties. This ribbon was compared with AlMg, AlMgTi and AlMgSi alloys in order to identify the influence of Si alloying element and also the Ti as inoculant element. AlMgSiTi ribbons of  $\approx 40 \mu\text{m}$  thick were obtained with a solidification time of  $5.57 \times 10^{-5} \text{ s}$  and  $1.09 \times 10^6 \text{ }^\circ\text{C/s}$  cooling rate. The microstructure resulting of AlMgSiTi nanocrystalline ribbon was carried out by scanning and high resolution transmission electron microscopes, which reported the formation of  $\alpha$ -Al nanometric grains and precipitates nanosized of  $\text{Al}_3\text{Ti}$ . The Ti addition limits the grain growth due to the increase of nucleus. The cooling rate is an important parameter for the microstructure resulting. In addition, with the combination of high subcooling and high cooling rates, was possible to obtain a fine microstructure with improved hardness and mechanical resistance relationship. With the rapid solidification process was possible to get high cooling rates and a nanocrystalline AlMgSiTi alloys.

## Acknowledgments

The authors would like to thank at DGAPA-PAPIIT and CONACyT, Grants No IN105708 and 89981 for their financial support of this research project.

# **Optical shift- and injection-current response of boron nitride nanotubes**

N. Arzate, R.A. Vázquez-Nava, C.M. González, and B.S. Mendoza

*Centro de Investigaciones en Optica, A.C., México.*

F.Nastos and J.E. Sipe

*Department of Physics, University of Toronto, Canada*

E-mail: narzate@cio.mx

We present the frequency dependence of the electrical shift and injection currents optically generated on boron nitride nanotubes. The shift and injection currents are a second order effect that is associated to a divergence of the nonlinear susceptibility at zero frequency. The shift current is generated with linearly polarized light and the injection current can be generated with circularly polarized light. We make use of density functional theory and pseudopotentials to calculate the nanotube structures and their electronic states. The current coefficient calculations are done in optical rectification, within the independent particle approximation and within a full-band electronic structure scheme. We also obtain the frequency dependence for the shift distance that the center of electron charge moves in the shift-current process and for the maximum swarm velocity acquired by the electrons in the injection process.

This work has been partly supported by CONACYT, México, grants: SEP-2004-C01-48142, SEP-2003-C02-42576, SEP-2005-C01-49678-F and 48915-E.

## Sizing metallic nanoparticles by optical extinction spectroscopy

Ovidio Peña,<sup>1,\*</sup> Luis Rodríguez-Fernández,<sup>2</sup> Vladimir Rodríguez-Iglesias,<sup>2</sup>  
Guinther Kellermann,<sup>3</sup> Alejandro Crespo-Sosa,<sup>2</sup> Juan Carlos Cheang-Wong,<sup>2</sup>  
Héctor Gabriel Silva-Pereyra,<sup>2</sup> Jesús Arenas-Alatorre,<sup>2</sup> and Alicia Oliver<sup>2</sup>

<sup>1</sup>*Instituto de Investigaciones en Materiales, Universidad Nacional Autónoma de México, Circuito Exterior S/N, Ciudad Universitaria, Coyoacan, C.P. 04510, México, D.F., México*

<sup>2</sup>*Instituto de Física, Universidad Nacional Autónoma de México, Apartado Postal 20-364, México, D.F., 01000, México*

<sup>3</sup>*Laboratório Nacional de Luz Síncrotron (LNLS), Campinas, SP, Brazil*

\*Corresponding author: [ovidio@bytesfall.com](mailto:ovidio@bytesfall.com)

Metallic nanoparticles (NPs) embedded in glass matrices present linear and non-linear optical properties which are very promising for technological applications in different fields such as catalysis, optoelectronics and biomedical diagnosis using dark field light microscopy. Nevertheless, technological applications require reliable methods to produce the NPs under controlled conditions because their optical properties depend on several factors like size, shape, spatial distribution and interaction with the host matrix, being the average size and size dispersion some of the most influencing (and hardest to study/control) of these factors. Therefore, it is of paramount importance to be able to determine the size distribution of NPs in an easy and reliable way.

In this work, a method is proposed to estimate the size distribution of nearly spherical metallic nanoparticles from Optical Extinction Spectroscopy (OES) measurements, based in Mie's theory and an optimization algorithm. The described method is compared against two of the most widely used techniques for the task: Transmission Electron Microscopy (TEM) and Small-Angle X-ray Scattering (SAXS). The average radius (AR) obtained by all the three techniques was almost the same for the two studied metals. Concerning the radius dispersion (RD), OES and GISAXS give very similar results, while TEM considerably underestimates the RD of the distribution.

## Synthesis and structural characterization of Ni-TR (TR = La, Ce) nanocrystalline.

C. E. Yañez-Zamora, S. B. Brachetti-Sibaja, M. A. Domínguez-Crespo, A. M. Torres-Huerta.

*Km. 14.5 carretera Tampico - Puerto Industrial. Altamira, Tamaulipas. CP 89600. Fax (833) 264 93 01*

CICATA IPN UNIDAD ALTAMIRA

[cynthiayz80@hotmail.com](mailto:cynthiayz80@hotmail.com), [bbrachetti@hotmail.com](mailto:bbrachetti@hotmail.com), [adcrespo2000@yahoo.com](mailto:adcrespo2000@yahoo.com),  
[atohuer@hotmail.com](mailto:atohuer@hotmail.com).

Ni-based alloys have been extensively investigated as hydrogen electrodes in water electrolysis, and they are often reported to be more active than Ni for the HER [1,2]. The electrodeposited binary Ni-Mo and Co-Mo materials considerably enhanced the HER as compared with Ni and Co and the improvement of the electrocatalytic behaviour was not only attributed to the synergetic composition, but also to the increased surface of the electrodes [3]. The mechanochemical method is promising in the synthesis of equilibrium and metastable phases, supersaturated solid solutions and amorphous phases. Compounds prepared by this method are characterised by high dispersity (in most cases, nanosized particles are obtained), which affects the physicochemical properties of these compounds [4]. In this work, Ni-TR (TR = La, Ce) compounds by mechanochemical method have been synthesised. Metal-acetylacetonates have been used as starting raw materials; the acetylacetonates were mixed and hand-milled in agate mortar, and thermally treated at 795 °C, 1000 °C and 1200 °C, for 3 H, each temperature. The powders obtained at 1200 °C, were analysed by X-ray diffraction (XRD) in order to determine their structure. Ni-Ce system results showed a mixture of NiO-CeO<sub>2</sub>, while the Ni-La system showed NiO-LaNiO<sub>3</sub>. NiO and CeO<sub>2</sub> have an FCC structure (Fm-3m) and LaNiO<sub>3</sub> has a primitive structure (Pm-3m) according to PDF Nos. 00-047-1049, 01-071-4199 and 00-033-0710, respectively. Ni-TR compounds are intended to be used as electrocatalysts in fuel cell anodes, and these compounds will be tested electrochemically by cyclic voltametry, Tafel techniques and ac impedance spectroscopy. Keywords: NiO-CeO<sub>2</sub>, NiO-LaNiO<sub>3</sub>, mechanochemical method.

### Bibliografía:

- [1] E.M. Arce, V.M. Lopez, L. Martínez, H.J. Dorantes, M.L. Saucedo, F. Hernández. *Journal of Materials Science*. 38 (2003) 275-278.
- [2] M.A. Domínguez, M. Plata, A.M. Torres, I.A. Ortiz, C. Ramírez, E.M. Arce. *Materials Characterization*. 56 (2006) 138-146.
- [3] Chonglun Fan, D.L. Piron and P. Paradis. *Electrochimica Acta*. 39 (1994) 2715-2722.
- [4] T.F. Grigorieva, A.P. Barinova, N.Z. Lyakhov. *Russian Chemical Reviews*. 70 (2001) 45-63.

## Au/TiO<sub>2</sub> and Au/SiO<sub>2</sub> systems as SERS active substrates

R. Sato Berrú, V. Maturano Rojas, R. Zanella Specia, J. Saniger Blesa

Centro de Ciencias Aplicadas y Desarrollo Tecnológico, Universidad Nacional Autónoma de México,  
Circuito Exterior s/n, C.U., Apdo. Postal 70-186, C.P. 04510, México, D.F.

E-mail: roberto.sato@ccadet.unam.mx

Noble metal nanostructures attract much interest as efficient media for surface-enhanced Raman scattering (SERS). Significant development has been made on the synthesis of metal nanoparticles with different shapes and controlled plasmonic properties, both of them critical for an efficient SERS response [1,2]. In this work, we present and evaluate as SERS substrates two nanostructured systems which are commonly used as catalytic support. The Au/TiO<sub>2</sub> and Au/SiO<sub>2</sub> composites were prepared respectively by the deposition-precipitation technique with urea or sodium hydroxide and cationic adsorption of Au(en)<sub>2</sub><sup>3+</sup> [3]. We show that these systems present very interesting behavior as SERS substrates. Caffeine, phenylalanine, valine and asparagine were used as probe molecules. Figure 1 shows the analysis of caffeine with these systems.

**Acknowledgements:** The authors acknowledge PAPIIT IN120508, IMPULSA 01(PUNTA) projects and the Fondo de Fomento a la Investigación Científica y Tecnológica del Gobierno del D.F. (ICyT-DF).

[1] M. Banholzer, J. Millstone, L. Qin, C. Mirkin, *Chem. Soc. Rev.*, 37 (2008) 885.

[2] R. Sato, R. Redón, A. Vázquez, O. Flores, R. Zanella, J. Saniger, *AIP Conf. Proc.* 992 (2007) 1232.

[3] R. Zanella, S. Giorgio, C. Henry, C. Louis, *J. Phys. Chem. B* 106 (2002) 7634.

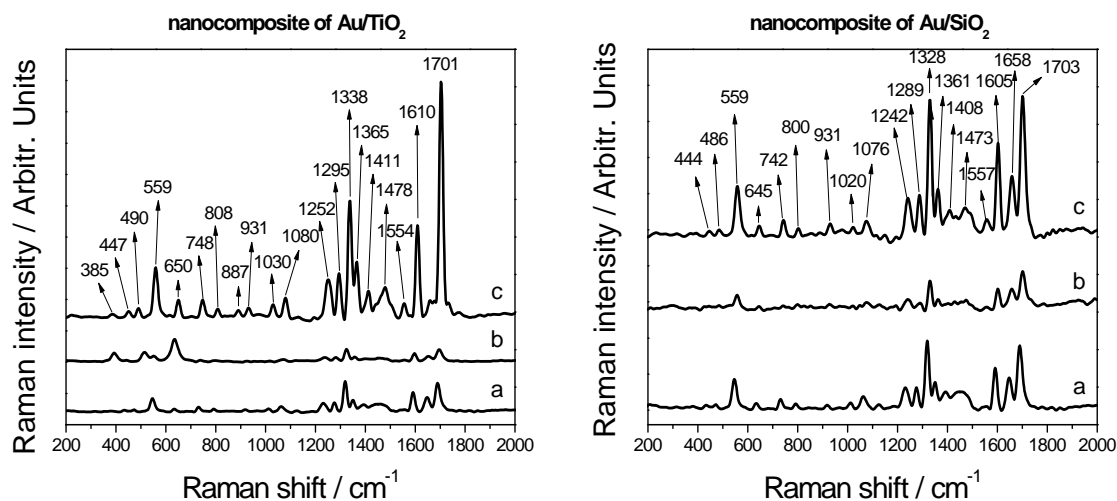


Figure 1: Raman spectra of pure caffeine (a), supports + caffeine (b) and composites + caffeine (c)

# SERS PROPERTIES OF GOLD NANOPARTICLES IN ORDERED AND NOT ORDERED SYSTEMS.

José Juan Francisco Castillo Rivera<sup>1</sup>, Ma. de Lourdes González González<sup>2</sup>, Elías Pérez López<sup>2</sup>, Elder de la Rosa Cruz<sup>1,\*</sup>.

Centro de investigaciones en óptica, Loma del Bosque #115 Colonia Lomas del Campestre<sup>1</sup>, Instituto de Física, Universidad Autónoma de San Luis Potosí, Av. Manuel Nava #6 Zona Universitaria. C.P 78290<sup>2</sup>.

\* elder@cio.mx

In this work, we propose the formation of gold nanostructures onto silicon substrate via self-assembly. We synthesize gold nanoparticles and silica particles with size of 20 and 100 nm respectively to formation of gold monolayer and a structure of mixed gold and silica particles. In the second case the silica template was removed to obtain a porous structure. This structure was characterized using Scanning electron microscopy. The figure 1a show SEM images of gold nanoparticles adsorbed onto a silicon substrate and 1b show the Raman spectra of Rhodamine 6G adsorbed on gold nanostructure.

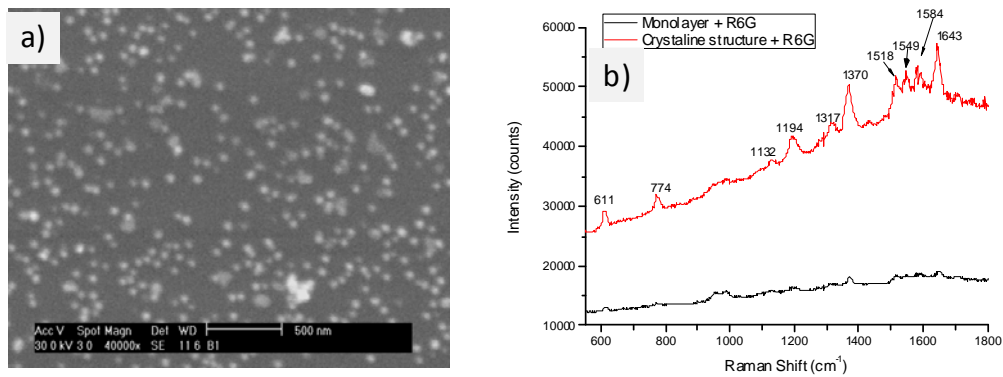


Figure 1. a) SEM image of gold nanoparticles onto a substrate. B) Raman of R6G adsorbed onto gold nanoparticles.

The figure 1b show that the response of the raman monolayer of gold nanoparticles with R6G is more weak compared with the response of the cristaline estructura with R6G.

The importance of the study of these structures is the potential application like biosensores, allowing this way the detection of proteins or compounds in low concentrations.

# A NOVEL BIONANOTECHNOLOGICAL METHOD TO ELIMINATE FLUORINE FROM WATER

Emilio Segovia, Carlos Enrique Muñoz Brambila y Francisco Mendoza Barajas

*Laboratory of Bionanotechnology, Departamento de Ciencias de la Tierra y de la Vida*

*Centro Universitario de Los Lagos, Universidad de Guadalajara, Lagos de Moreno, Jal.*

[emiliosegovia@gmail.com](mailto:emiliosegovia@gmail.com)

The presence of Fluorine compounds in tap water is a naturally occurring fact in many countries in the world. The main source of exposure to Fluoride is tap water. Fluoride exposure is an important public health problem in several Mexican regions. Fluorine in drinking or cooking water causes a wide-spread illness called *chronic fluorosis*. This is why countries without fluoridation have shown an equal improvement in dental health as those with fluoridation. Municipal water supply for domestic and industrial purposes in Lagos de Moreno is provided by 23 wells distributed along the Lagos de Moreno territory. The chemical analysis of the water supplied by all these wells shows these waters fulfil the requirements of the Official Mexican Norm regarding mineral salts, organic substances and microbiological content. All except for the Fluorine content which exceeds this norm (1.5 mg/ml) by SIX TIMES the upper limit. In our laboratory we are actually carrying out studies to find alternative methods to deal with this problem. These methods consist in treating fluoridated water with some amount of milled nopal cladodes (*Opuntia spp.*). Detailed technique consisted of adding 100 g of ground nopal cladodes to one litre of water samples containing several concentrations (1,2,3,4,5,6,7,8,9 and 10 mg/L) of Sodium Fluoride and further stirring it at RT for 10 min. Solids were allowed to sediment for one hour. The mixture was centrifuged at 1,500 RPM and the resulting liquid was then analysed by IR spectroscopy to determine the amount of Fluorine present in the sample. All water samples treated showed a dramatic decrease (60%) in the content of Fluorine. The results obtained so far have proven the described method to be quite promising in fulfilling the main purpose of this study. It is considered to be a practical and reproducible method by the fact that these cactuses are readily available in the regions where fluoridated water is present. The results obtained so far have proven the described method to be suitable for reducing the amount of Fluorine in water in 60%. The present study has not been finished yet, there are still a number of questions to be answered. Amongst them, a proposal as the mechanism of Fluorine entrapment by the *Opuntia cladodes*.

## **AN IMPLANTABLE TiO<sub>2</sub>-DA COMPLEX COULD LEAD TO IMPROVED MOTOR DEFICITS OF HEMIPARKINSONISM INDUCED BY 6-OHDDA.**

P. VERGARA-ARAGON<sup>1</sup>, R. MARTÍNEZ-VEGA<sup>2</sup>, P. IBARRA<sup>1</sup>, G. VALVERDE-AGUILAR<sup>3</sup>, D. R ACOSTA<sup>3</sup>,  
J.A.GARCIA-MACEDO<sup>3</sup>

*1 Physiology Department, Faculty of Medicine, UNAM), 2Mathematics Academy, UACM, Sn Lorenzo Tezonco, Mexico. 2Academia de Matemáticas, UACM, México DF. 3 Departamento de Estado Sólido. Instituto de Física, Universidad Nacional Autónoma de México. México D. F. C. P. 04510*

E mail: [paty\\_ver@hotmail.com](mailto:paty_ver@hotmail.com)

Dopamine (DA) is an important neurotransmitter in the mammalian central nervous system and low levels of it have been found in Parkinson's disease patients. The purpose of the study was to examine its effectiveness on the reversion of the gross motor alterations and the histological changes induced by the capsule on the zone of the implant. Material and method: TiO<sub>2</sub>.DA complex was prepared as follows: Tetrabutylorthotitanate (8.5 ml) and diethanolamine (2.4 ml) were dissolved in 34 ml of ethanol. After stirring vigorously for 2h at room temperature, a mixed solution of deionized water and ethanol is added dropwise slowly to the above described solution with a pipette under stirring. Finally, Tetraethyleneglycol (TEG) (5g) was added to the resulting solution. The resultant alkoxide solution is kept standing at room temperature to perform hydrolysis reaction for 2h, resulting in the TiO<sub>2</sub> sol. DA was added at the final stage. Gross motor behavior was registered on the Open Field Test (OF) for 5 min.; ladder rung walking test (RW) for 2 min and Girus behavior (GB), induced by apomorphine, was registered for 50 minutes. 32 Wistar rats (250g) were divided into four experimental groups (8 rats each) as follows: 1) Control group, no treatment and sham surgery; 2) Unilateral lesioned rats (6-OHDA); 3) Unilateral lesioned rats with nanoparticles implanted without treatment; 4) Unilateral lesioned rats with nanocarriers implanted with DA. Every group was examined on the behavioral tests listed above. Conclusions: The results showed that the rats treated with DA didn't have significant differences with the control group on the RW and GB. While the group with nanoparticles implanted without DA showed no difference from the group with unilateral lesioned rats, however both groups were significant different from the other two (control and DA nanocarriers). It is probable that the continuous release of dopamine through the nanocarriers is capable of reversing the motor deficit observed on the lesioned group. This type of reservoir can be a promising controlled drug delivery system to treat the Parkinson disease.

*Support Contributed By: DGAPA IN-221507, CONACyT 79781, NSF-CONACYT, PUNTA, PAPIIT 116506-3 and DGAPA UNAM IN123804 supported this work. GVA is grateful for a ICyTDF postdoctoral fellowship.*

## Spherical 3D Photonic Crystal with a Conducting Nanoparticle Core

A. Zamudio-Lara<sup>1</sup>, J. Sanchez-Mondragon<sup>2</sup>, R. Jaime-Rivas<sup>3</sup>, M. Torres-Cisneros<sup>3</sup>, E. Aguilera-Gómez<sup>3</sup> and S. Ledezma-Orozco<sup>3</sup>

<sup>1</sup> Center for Research in Engineering and Applied sciences. UAEM, Cuernavaca, Mexico

<sup>2</sup> INAOE/Photonics and Physical Optics Lab., Puebla, México

<sup>3</sup> NanoBioPhotonics Group, University of Guanajuato, Salamanca, Gto, México

Email: azamudio@uaem.mx

Dielectric and Metallo Dielectric Photonic Crystals (PC) have shown common but distinctive characteristics of their own. The scattering by bare metallic nanoparticles has been explored in detail [1], however, the assumption made in those conditions can not be applied to the core of the Photonic Crystal formed by a metallic core and dielectric layers and a spherical layered Photonic Crystal covered with a metallic shell. By using the Transfer Matrix method we analyze the transmission in both cases for few and many dielectric layers.

For a metallic core, we describe it in terms of the size of the conducting nanoparticle, as well as the frequency dependence introduced by the conducting nanoparticles. Ours first results demonstrate a near factorization of both dielectric and metallic transmission behaviour, as a function of their angular dependence. We compare these results with the dependence of layers created by composites of dielectrics and conducting nanoparticles [2].

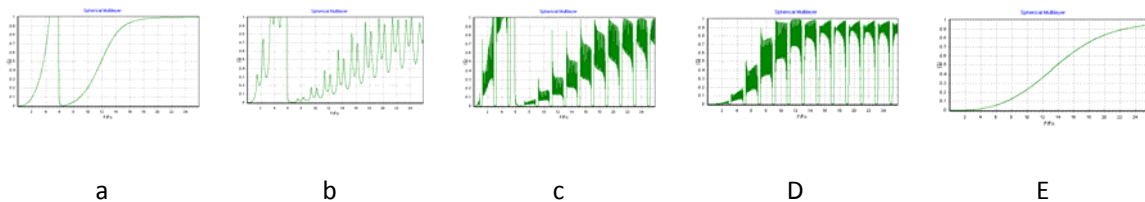


Fig.1 Transmission for Metallic and Dielectric cores bare and covered with dielectric layers in the lowest angular order for a core of  $.01\mu\text{m}$  and  $\frac{1}{4}\lambda$  dielectric layers (a) bare metallic core, (b) covered with a layer, (c) covered with 20 layers; (d) dielectric core covered with 20 layers, (e) bare dielectric core.

### References

[1] Maier, S. A., Plasmonics Fundamentals and Applications Springer, 2007

[1] Panasyuk G. Y., J. C. Schotland, and V. A. Markel. PRL 100, 047402 (2008)

# One Dimensional Photonic Crystal with Conducting Nanoparticles Classical Composite

J. Sánchez-Mondragon<sup>1</sup>, J. Escobedo-Alatorre<sup>2</sup>, M. Basurto-Pensado<sup>2</sup>, A. Alejo-Molina<sup>1</sup>, J. O. Vázquez Buenos Aires<sup>3</sup> and D. A. May-Arrijo<sup>1</sup>

<sup>1</sup> INAOE/Photonics and Physical Optics Lab., Puebla, México

<sup>2</sup> Center for Research in Engineering and Applied sciences. UAEM, Cuernavaca, Mexico

<sup>3</sup> Universidad del Papaloapan, Loma Bonita Oaxaca, México.

Email: [jsanchez@inaoep.mx](mailto:jsanchez@inaoep.mx)

The engineering of nanocomposite materials, metallic nanoparticles embedded in substratums, offers the opportunity of creating new devices with the nanoparticles properties. In particular conducting nanoparticles have been observed to enhance size dependent nonlinearities [1]. Quantum Mechanical confinement in conducting nanoparticle produces a Kerr nonlinearity [2] while a classical composite approach produces a refraction index [3] with an amplitude dependent nonlinearity [4]. We have previously studied stack characterized by a Kerr nonlinearity and demonstrated: a shift in the Photonic Band Gap, Power dependent switching, chirping and bistability. In this work, we discuss those phenomena for such classical nano nonlinearity.

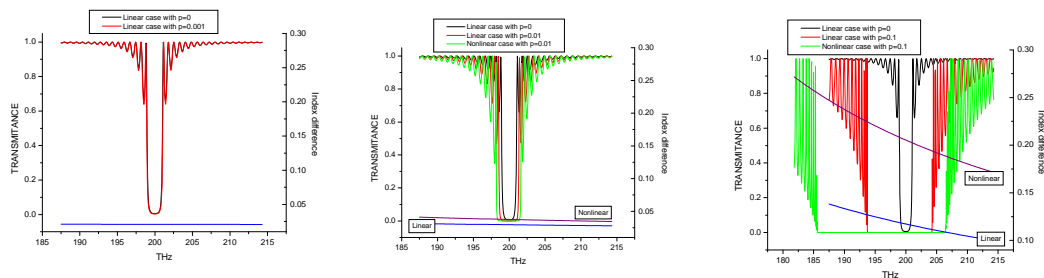


Fig. 1. Band gap curves for a stack. Black is the basic dielectric Photonic Crystal. Red is the doped linear case ( $p \neq 0$ ,  $\beta = 0$ ) and Green is the doped nonlinear case ( $p \neq 0$ ,  $\beta \neq 0$ ).

## References

- [1] K. Uchida et al., J. Opt. Soc. Am. B **11**, 1236 (1994).
- [2] F. Hache, D. Richard and C. Flyzanis, J. Opt. Soc. Am. B **3** 1647 (1986).
- [3] S.G. Rautian, J. Exp Theor. Phys. **85**, 451(1997).
- [4] Panasyuk G. Y., J. C. Schotland, and V. A. Markel. PRL **100**, 047402 (2008).

# Nonlinear Pulse Propagation in an Optical Fiber Doped with Conducting Nanoparticles

J. Sanchez-Mondragon<sup>1</sup>, M. Torres-Cisneros<sup>2</sup>, C. Velásquez-Ordoñez<sup>3</sup>,  
M. Tecpoyotl-Torres<sup>4</sup>, E. Pérez-Careta<sup>2</sup> and J. O. Vázquez Buenos Aires<sup>5</sup>

<sup>1</sup> INAOE/Photonics and Physical Optics Lab., Puebla, México

<sup>2</sup> NanoBioPhotonics Group, University of Guanajuato, Salamanca, Gto, México

<sup>3</sup> Universidad de Guadalajara, Guadalajara, Jalisco, México

<sup>4</sup> Center for Research in Engineering and Applied Sciences. UAEM, Cuernavaca, Mexico

<sup>5</sup> Universidad del Papaloapan, Loma Bonita Oaxaca, México.

Email [jsanchez@inaoep.mx](mailto:jsanchez@inaoep.mx)

Metallic nanoparticles, of a few nanometers radii, show nonlinearities [1] due to the plasmon enhancement and are the object of active experimental and theoretical studies, in particular in the framework of composites. A quantum mechanical analysis of such structures predict a Kerr type nonlinearity [2], however quite a recent publication has shown that a nano metal nanoparticles composite shows a classical nonlinearity proportional to the electric field amplitude [3]. The classical refraction index of a metallic composite is given by

$$n^2 = n_0^2 \left[ 1 + 3p \frac{\omega_F^2}{\omega_F^2 - \omega^2 - i\gamma\omega} \left( 1 + \frac{8\beta}{3\pi} \right) \right],$$

that describes a transparent medium of refractive index  $n_0$  doped with randomly distributed

metal nanospheres, where  $p$  is the volume fraction of the metal and  $\beta$  is proportional to the field amplitude. An optical fiber with metal nanoparticles raises the question if such fibers support a new kind of stable pulse. We have assumed long pulses and have shown a positive answer, demonstrating that exist a modulated stable pulse whose profile, to an incident Gaussian pulse (Blue), corresponds a sharper stable pulse (red), a reminiscent of the *Sech* soliton pulse.

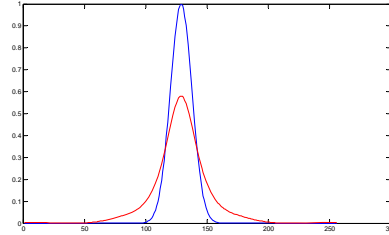


Fig. 1. Gaussian Input Pulse (blue) vs output Pulse (red) in the absence of Kerr nonlinearity alter  $100 L_D$

## References

1. K. Uchida *et al.*, J. Opt. Soc. Am. B 11, 1236 (1994).
2. F. Hache, D. Ricard and C. Flytzanis, J. Opt. Soc. Am. B 3, 1674 (1986). S. G. Rautian, J. Exp. Ther. Phys. 85, 451 (1997).
3. Panasyuk G. Y., J. C. Schotland, and V. A. Markel. "Classical Theory of Optical Nonlinearity in Conducting Nanoparticles", PRL 100, 047402 (2008).

## **Gd<sub>2</sub>O<sub>3</sub>:Eu<sup>3+</sup>/SiO<sub>2</sub> thick films elaborated by sol-gel process**

Juan C. Badillo Aviles<sup>1</sup>, A. García Murillo<sup>1</sup>, F. Carrillo Romo<sup>1</sup>,

V. H. Romero<sup>2</sup>, E. de la Rosa<sup>2</sup>, J. Duval Lara<sup>1</sup>

<sup>1</sup>Centro de Investigación en Ciencia Aplicada y Tecnología Avanzada U Altamira IPN,  
Km 14.5 Carr. Tampico-Pto. Industrial, C.P.89600 Altamira, Tamps, México.

<sup>2</sup>Centro de Investigaciones en Óptica A.P. 1-948, 37000 León, Gto., México

E-mail: jbadilloa0800@ipn.mx

### ABSTRACT

Europium gadolinium oxide glass ceramic films were synthesized from gadolinium acetate, acetic acid, methanol, water, europium nitrate and PVP. SiO<sub>2</sub> matrix was prepared by sol-gel method using TEOS, ammonia and water as precursors. Ceramic sol and silica sol were mixed in a molar ratio 4:1 in order to obtain Gd<sub>2</sub>O<sub>3</sub>:Eu<sup>3+</sup>/SiO<sub>2</sub> stable sol. SiO<sub>2</sub> substrates were used to coat by the transparent precursor sol by means of dip-coating technique. Transparent and optical thick films were produced after a 700 °C heat-treatment for 10 min. In this work, we report the synthesis, structure and optical properties of Gd<sub>2</sub>O<sub>3</sub>:Eu<sup>3+</sup> (5% mol)/SiO<sub>2</sub> using IR, DRX and PL measurements.

# New relationships between optical and dielectric properties of core-shell nanostructures

Víctor M. Rentería-Tapia<sup>1</sup>, Jorge A. García-Macedo<sup>1\*</sup>

2. *Departamento de Estado Sólido. Instituto de Física, Universidad Nacional Autónoma de México. México D.F. C.P. 04510, Ciudad Universitaria, Coyoacán, México, D.F.*

The dipolar Mie theory extended to concentric spherical shells (core-shell model) was used to calculate the variations of the optical shift of the absorption peak from metallic nanoparticles (gold and silver) covered with several shells and dispersed in several dielectric environments. Similar calculations were obtained replacing the refractive index of the dielectric medium  $n_m$  by a local refractive index  $n_{\text{local}}$  (originated of the refractive indexes of the shell and the medium) in the Mie theory for uncoated nanoparticles. The analysis of these results suggested that the variations of the optical shift calculated with the core-shell model are the same as that from a uniform sphere with a local refractive index. It is found that this index depends exponentially on the volume fraction of the shell. Using this function it is possible to calculate the maximal spectral shift, the sensitivities of the wavelength maximum to variations in the refractive index of the environment, the volume fraction and the thickness of the shell. These new relationships describe the local refractive index model and they are directly related with the peak position of the surface plasmon resonance and dielectric properties of both the metallic core and the shell. Furthermore, for evaluating the accuracy of the local refractive index model, experimental data were included in the new relationships and these calculations were compared to the predictions done by the core-shell model. It is concluded that the first model is in better agreement with the experimental data than the core-shell model.

## ACKNOWLEDGMENTS

The authors acknowledge the financial supports of CONACYT 43226-F, NSF-CONACYT, PUNTA, ICYTDF and PAPIIT 116506-3. VMRT is grateful for PUNTA postdoctoral fellowship.

# Characterization and CO oxidation on silver-SiO<sub>2</sub> film-like and powder-like catalysts prepared by dip-coating method

Jorge Garcia-Macedo, Guadalupe Valverde-Aguilar, Miguel A. Ríos-Enríquez,  
Víctor M. Rentería, Alfredo Franco

*Departamento de Estado Sólido. Instituto de Física, Universidad Nacional Autónoma de México.  
México D. F. C. P. 04510*

E-mail: [gamaj@fisica.unam.mx](mailto:gamaj@fisica.unam.mx).

## ABSTRACT

Silver catalysts supported SiO<sub>2</sub> were synthesized as film by sol-gel method. The characterization was performed by X-ray diffraction (XRD), transmission electronic microscopy (TEM) and high resolution transmission electron microscopy (HRTEM). 2d- hexagonal mesophase was provided to the SiO<sub>2</sub> matrix using the neutral surfactant Brij 58 (C<sub>16</sub>EO<sub>20</sub>). The diblock copolymer Brij58 produced channels into the film, which house the silver nanoparticles. These metallic nanoparticles were obtained by spontaneous reduction of Ag<sup>+</sup> ions to Ag<sup>0</sup>. An absorption band located at 438 nm was detected by optical absorption; it corresponds to the plasmon surface. Fit to this band with modified Gans theory is presented. It shows two main peaks, one of them is related to the metallic silver particles and the other one is related to the copolymer shell around nanoparticles. A comparative study of Ag-SiO<sub>2</sub> catalyst powder-like vs film-like has been carried out during CO oxidation. The film-like catalyst showed a very similar catalytic activity in comparison to the powder-like one. Both catalysts reached the total CO conversion at 350°C, using comparable amounts of catalyst.

**Keywords:** CO oxidation, film-like catalysis, Gans theory, silver nanoparticles, surfactant

This work was supported by the following grants: CONACYT 79781, NSF-CONACYT, PUNTA, ICyTDF and PAPIIT 116506-3. The authors GVA and MARE grateful for the postdoctoral fellowships.

# TRICLOSAN NANOPARTICLES, A NOVEL DELIVERY SYSTEM INTENDED TO BE USED IN ACNE TREATMENT. EFFECT OF SUCROSE LAURATE AS SKIN PRETREATMENT

Domínguez Delgado Clara Luisa, Leyva Gómez Gerardo, Rodríguez Cruz Isabel  
Marlen, David Quintanar Guerrero, Ganem Rondero Flora Adriana

*División de Estudios de Posgrado (Tecnología Farmacéutica), Facultad de Estudios Superiores Cuautitlán, Universidad Nacional Autónoma de México, Av. 1º de Mayo s/n, Cuautitlán Izcalli, Estado de México, México. C.P. 54740, Tel.+52 55 56 23 20 65*

e-mail: Clara\_LDD@yahoo.com.mx

## Abstract

Triclosan (TS) loaded nanoparticles (NPs) were prepared by the emulsification-diffusion solvent displacement process, using Eudragit E<sup>®</sup> 100 as the polymeric matrix and poly (vinyl alcohol) as stabilizer. NPs were characterized by their size and charge. The results showed that both the size and charge of NPs were affected by the incorporation of sucrose laurate decreasing their stability. Therefore, a pretreatment of the skin with sucrose laurate in Transcutol<sup>®</sup> (2 % w/v) was performed. *In vitro* permeation studies revealed that the TS does not permeate through the skin (TS was not found in the receptor solution of Franz diffusion cells), but it was retained in the skin. On the contrary, the quantity of TS extracted from the skin without pretreatment with sucrose laurate, was higher than in the pretreated skin (Fig. 1). Of all formulations, NPs and an aqueous dispersion of TS showed the greatest retention in the skin. NPs represent a novel drug target strategy, which would be applicable to facial skin for acne treatment, in order to provide a controlled delivery system contrary to the aqueous dispersion of TS, or to the commercially available solutions.

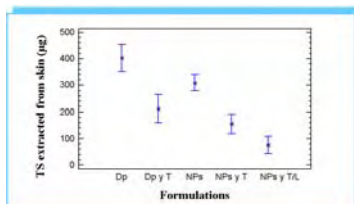


**Fig. 1 TS extracted from skin (P < 0.5, n=6)**

**Dp:** Dispersion of TS in water

**Dp y T:** Dispersion of TS in water, pretreating the skin with sucrose laurate.

**References:** 1) J. Cázares-Delgadillo, et.al. Int. J. Pharm. 297 (2005) 204–212; 2) E.Touitou, B. W. Barry, Enhancement in drug delivery. CRC Press, Taylor & Francis Group. United States of América, 2007, pp 215; 3) Ayala-Bravo, et.al. Pharm. Res. 20-8, (2003) 1267-1273; 4) C. L. Domínguez, Estudio comparativo de la absorción percutánea *in vitro* de triclosán a partir de un sistema nanoparticulado y dos formas comerciales, destinados al tratamiento de acné. Thesis. FES-C, UNAM (2006), pp 157.

**Study of blue, green and red emission  
of ZrO<sub>2</sub>:Tb<sup>3+</sup>, Tm<sup>3+</sup> and Eu<sup>3+</sup> nanocrystals  
respectively as function of ion concentration,  
H<sub>2</sub>O/EtoH and Pluronic-127 as dispersant**

T. López-Luke<sup>a</sup>, V. H. Romero<sup>a</sup>, E. De La Rosa<sup>a</sup>,  
Pedro Salas<sup>b</sup>, C. Angeles-Chavez<sup>b</sup>.

<sup>a</sup>)Centro de Investigaciones en Optica A. C. A. P. 1-948 371590 León Gto. México.

<sup>b</sup>)Fata, UNAM, Querétaro, Qro. 76000, México.

<sup>c</sup>)Instituto Mexicano del Petróleo, A. P. 14-805 07730 México D.F.

email: vicromare@cio.mx , elder@cio.mx

**ABSTRACT.-** Blue, green and red emissions of ZrO<sub>2</sub>:Tb<sup>3+</sup>, Tm<sup>3+</sup> and Eu<sup>3+</sup> nanophosphors were obtained respectively. The structure and morphology of the nanophosphors were studied as a function of ion concentration, surfactant (Pluronic F-127) and the ratio H<sub>2</sub>O/EtoH. We found the optimum concentrations of these three factors to obtain small nanoparticles (18nm) and rods with strong luminescence. The FT-IR results suggest that surfactant helps to reduce contaminants of organic compounds. We have demonstrated that with the combination of proportional red, green and blue is possible to produce white light with ZrO<sub>2</sub> nanocrystals.

## Upconversion characterization of $\text{ZrO}_2:\text{Yb}^{3+} - \text{Tm}^{3+}$ nanocrystals

D. Solís<sup>1,\*</sup>, T. López-Luke<sup>2</sup>, P. Salas<sup>3</sup>, E. De la Rosa<sup>1</sup>

<sup>1</sup> Centro de Investigaciones en Óptica, A. P. 1-948, León Gto., 37160, México

<sup>2</sup> IIM, UMSNH, C.U., Morelia Mich., 58060, México

<sup>3</sup> Centro de Física Aplicada y Tecnología Avanzada, Universidad Nacional Autónoma de México, A. P. 1-1010, Querétaro, Qro., 76000, México.

\* Contact e-mail: dsolis@cio.mx

### ABSTRACT

In many applications, interactions between the rare earth ion and the electronic states of the host material can enhance or inhibit performance and provide mechanisms for manipulating the material's optical properties. Although the general properties of the rare earths' electronic states and transitions are well understood and their theoretical description is well established, much less is known regarding the relationships between the energy levels of the rare earth ions and the electronic band states of the crystal lattice. Special attention has received rare earth doped nanophosphors emitting in the visible range by upconversion process. Upconversion (UPC) is the generation of visible or UV light by the excitation with larger wavelengths usually NIR and IR, through the use of trivalent rare earth ions supported into a solid-state host material. These doped materials have been sensitized with  $\text{Yb}^{3+}$  ion taking advantage of its mayor absorption cross section and that the only excited state matches perfectly the emission of a Laser Diode (LD).

In this work,  $\text{Yb}^{3+}$  codoped  $\text{ZrO}_2:\text{Tm}^{3+}$  nanocrystals were prepared by sol-gel and intense blue emission under IR (968 nm) excitation were observed. The concentration effect of dopant and codopant in the luminescence is analyzed. Visible emission is the effect of the upconversion process by energy transfer from  $\text{Yb}^{3+}$  to  $\text{Tm}^{3+}$  ion. Experimental results show that Yb ion enhances the blue emission by an efficient energy transfer and the reduction of Tm clusters and their inter-ionic relaxation process.

## A general and easy colloidal method for the synthesis of small and stable zerovalent Fe, Co, Ni and Cu nanoparticles

**Maiby Valle-Orta**<sup>1</sup>, David Díaz<sup>1\*</sup>, Patricia Santiago-Jacinto<sup>2</sup>, América R.

Vazquez-Olmos<sup>3</sup>, Roberto Sato-Berrú<sup>3</sup> and Edilso Reguera Ruiz<sup>4</sup>

<sup>1</sup>Facultad de Química; <sup>2</sup>Instituto de Física; <sup>3</sup>Centro de Ciencias Aplicadas y Desarrollo Tecnológico de la Universidad Nacional Autónoma de México, Ciudad Universitaria, Coyoacán, CP 04510; <sup>4</sup>CICATA U-Legaria, Instituto Politécnico Nacional, Legaria 694, Colonia Irrigación, Miguel Hidalgo, CP 11500, México D. F., México e-mail: [david@servidor.unam.mx](mailto:david@servidor.unam.mx)

The preparation of nanoparticles (NPs) of the zerovalent first transitional metals (Fe, Co, Ni and Cu, ZVM NPs) has been widely studied. The colloidal methods are one of the more simple and inexpensive among the synthesis methods more commonly used. However, the stabilization of these metallic NPs is difficult because they are easily oxidized<sup>2</sup>. Then, it is necessary to use capping agents to stabilize them. The most employed in the literature are voluminous and hinder the particle surface, disabling their surface; thus, restricting their catalytic capacity<sup>3</sup>.

In this contribution a new colloidal method for obtaining stable copper, iron, nickel, and cobalt nanoparticles will be discussed. This method involves the precursor metallic salt reduction to the corresponding zerovalent metal with sodium borohydride (NaBH<sub>4</sub>), employing triethylamine (TEA) as capping agent and ethylene glycol (EG) as dispersing medium. These reactions take place instantaneously, at room temperature. The system constituted by EG and TEA is an excellent combination for the stabilization of these metallic nanoparticles. All particles were characterized by X-RD, FT-IR, Raman, Z-Contrast and HR-TEM. The electric potential on the surface of the suspended nanoparticles was measured as well. The average diameter of these nanostructured particles were 9.5±2.5, 10.2±3.3, 4.1±1.0 and 4.4±1.7 nm for Cu, Fe, Ni, and Co, respectively. In the case of the iron NPs, they were characterized by Mössbauer and EELS spectroscopies too.

---

<sup>2</sup> Vitulli, G.; Bernini, M.; Bertozzi, S.; Pitzalis, E.; Salvadori, P.; Coluccia, S. and Martra, G. *Chem. Mater.* **2002**, *14*, 1183

<sup>3</sup> Kanninen, P.; Johans, C.; Merta, J. and Kontturi, K. *J. Colloid Interf. Sci.* **2008**, *318*, 88.

# Thermal lens technique applied to the study of degradation, by UV light irradiation, of rhodamine R6G dye solutions containing TiO<sub>2</sub> nanoparticles

S. A. Lozano Morales<sup>1</sup>, A. Cruz-Orea<sup>2</sup>, J.L. Jiménez-Pérez<sup>1, a</sup>, J.F. Sanchez Ramirez<sup>1</sup>, C. J. da Silva<sup>3</sup>, R. Saavedra<sup>4</sup>, F. Sanchez Sinencio<sup>2</sup>

<sup>1</sup>CICATA-IPN, Legaria 694, Col. Irrigación, 11500 México D.F., México

<sup>2</sup>Physics Department, CINVESTAV-IPN, A.P. 14-740, 07360 México D.F., México

<sup>3</sup>Universidade Federal de Alagoas, UFAL, Campus A.C. Simões, BR. 104 Km. 14

Tabuleiro dos Martins CEP 57072-970. Maceió, Al, Brasil

<sup>4</sup>Universidade de Concepcion, FCFM, Av. Esteban Iturra s/n, Casilla 160-C Correo 3, Concepcion-Chile

<sup>a</sup>corresponding autor: [jimenezp@fis.cinvestav.mx](mailto:jimenezp@fis.cinvestav.mx)

## Abstract

Thermal lens spectrometry (TLS) and Photoacoustic Spectroscopy (PAS) were used to obtain respectively the thermal diffusivity and optical absorption spectrum of rhodamine R6G dye aggregated with TiO<sub>2</sub> semiconductor nanoparticles, which have spherical shape with average diameter of 81.3 nm. Thorough the optical absorption spectra were possible to characterize the degradation, by U.V. light irradiation at 300 nm wavelength, of these solutions. The experimental results show that the thermal diffusivity (D) decreases with the exposure time of UV irradiation. It was also possible to observe the degradation of R6G dye through their optical absorption spectra when compared with characteristic R6G spectrum reported in the literature [1]. Complementary characterization of TiO<sub>2</sub> nanoparticles was done by SEM analysis. Our investigations are devoted to improve degradation treatments of several toxic pollutants in water.

[1] J.L. Jimenez-Pérez, J.F. Sanchez-Ramirez, R. Gutierrez Fuentes, A Cruz Orea, J.L. Herrera Pérez, Brazilian Journal of Physics, Vol. 36, p. 1025-1028(2006).

# Thermal and optical characterization of solutions containing Au nanoparticles at different pH values

*E. Navarro Cerón Juárez<sup>1</sup>, J.L. Jiménez Perez<sup>1,a</sup>, J.F. Sanchez Ramirez<sup>1</sup>, A. Cruz Orea<sup>2</sup>, J.A. Pescador Rojas<sup>1</sup>, D. Cornejo Monroy<sup>1</sup>, J.L. Herrera Pérez<sup>1</sup>*

<sup>1</sup>*CICATA-IPN, Legaria 694, Col. Irrigación, 11500 México D.F., México*

<sup>2</sup>*Physics Department, CINVESTAV-IPN, A.P. 14-740, 07360 México D.F., México*

<sup>a</sup>*corresponding autor: [jimenezp@fis.cinvestav.mx](mailto:jimenezp@fis.cinvestav.mx)*

## Abstract

Thermal lens spectrometry (TLS) and photoacoustic spectroscopy (PAS) were used to obtain respectively the thermal diffusivity and optical absorption spectra of solutions containing Au nanoparticles (diameter of 20 nm) with variable pH values. The results show that, as the pH of these nanofluids increases, the thermal diffusivity also increases. Also it was possible to observe changes in their optical absorption spectra when compared with the characteristic reported spectrum of Au nanoparticle solutions. It was observed that the pH value of the solutions influence the superficial density of charges in the nanoparticles and thus the stability of the solutions. These results will be compared with reported studies of nanofluids with variable pH [1]. These measurements were performed at room temperature. TLS was used in a mode-mismatched dual beam configuration that provides a reliable alternative for measuring, with high sensitivity, the thermal diffusivities of semitransparent materials and low thermal diffusivities. On the other hand the optical absorption spectra for these samples were obtained by using a photoacoustic spectrometer.

[1] J.F. Sanchez-Ramirez, J.L. Jimenez-Pérez, A Cruz Orea, R. Gutierrez Fuentes, A. Bautista-Hernandez, U. Pal, Journal Nanoscience and Nanotechnology, Vol. 6, p. 685 (2006).

## Viral nanostructures: *in vitro* self-assembly of Parvovirus B19-like particles

S.P. Sánchez-Rodríguez<sup>1</sup>, L. Munch-Anguiano<sup>1</sup>, O. Echeverría<sup>2</sup>,

G. Vázquez-Nin<sup>2</sup>, I. Bustos-Jaimes<sup>1</sup>.

<sup>1</sup> *Laboratorio de Físicoquímica e Ingeniería de Proteínas, Departamento de Bioquímica, Facultad de Medicina, P.O. Box 70-159, Ciudad Universitaria, México DF 04510, México.*

<sup>2</sup> *Laboratorio de Microscopía Electrónica, Departamento de Biología Celular, Facultad de Ciencias, Ciudad Universitaria, México DF 04510, México.*

e-mail: ismaelb@unam.mx

In the last years viral nanostructures have gained ground in the field of nanobiotechnology as organic templates for development of new biomaterials. This is due to their structural stability and tolerance toward manipulations to carry and display molecules from diverse nature, as well as its ability to serve as building blocks for novel nanomaterials<sup>1</sup>. Virus-like particles (VLPs) are formed by the self-assembly of the components of viruses excluding their genetic material. For this reason, VLPs are not infectious and can be used for biomedical applications such as vaccines and for systemic delivery of pharmacologically important molecules as drugs, siRNAs, genes, mRNAs, magnetic nanoparticles, quantum dots and other medical-imaging aids. In this study the heterologous expression and purification of the VP2 protein from Parvovirus B19, the only member of the *Parvoviridae* family that can infect humans, was carried out. Recombinant VP2 formed inclusion bodies in our expression system, the bacterium *Escherichia coli*. Inclusion bodies were completely solubilized in urea 8 M and the protein was renatured through urea removal. The assembly of capsid-like nanoparticles was verified by TEM and linear cesium chloride gradient. The observed VLPs displayed structure, diameter (25 nm) and density (1.29 g cm<sup>-3</sup>) similar to that reported for the native virus<sup>2,3</sup>. These results demonstrate that VP2 can be assembled *in vitro* to form VLPs of Parvovirus B19, which may be used for different nanobiotechnological applications.

### References

1. Ludwig C., Wagner R. (2007). *Curr Opin Biotechnol.* **18**, 537-545.
2. Lowin T. *et al.*, (2005). *J Vet Med B.* **52**, 348-352.
3. Kaufmann B. *et al.*, (2004). *Proc Natl Acad Sci USA.* **101**, 11628-11633.

# Two-photon Lithography for Nanofabrication of Electromechanical Devices

Naser Qureshi, Jesus Garduño-Mejía and Roberto Ortega-Martínez

*Centro de Ciencias Aplicadas y Desarrollo Tecnológico,  
Universidad Nacional Autónoma de México,  
Circuito Exterior S/N, Ciudad Universitaria, México DF 04510.*

We describe the design and implementation of a new nanolithography instrument based on the 2-photon polymerization of an SU-8 photoresist and demonstrate its use in the fabrication of nano- and micro-electromechanical devices (N/MEMS). We demonstrate the fabrication of three dimensional structures in a single processing step and a resolution better than 100nm in the fabrication of planar and dot-like polymeric structures. Unlike previous works, we show that with adequate exposure parameters this can be achieved without the use of a high-aperture immersion lens, facilitating the use of this technique in a wider range of applications. The focus of this work is on a relatively new application: the fabrication of polymer N/MEMS structures with controlled optical properties, optimized for optomechanical readout. This is particularly useful in devices where mechanical resolution is more important than speed.

Email: [naser.qureshi@ccadet.unam.mx](mailto:naser.qureshi@ccadet.unam.mx)

“Synthesis and application of carbon nanotubes by floating catalyst method using a matrix of hybrid material SBA-16/CMK”

Portales. M. B\*.<sup>1</sup>, Domínguez E. J. M.<sup>2</sup>, Reyes T. A. I.<sup>2</sup>, Cortés E. C. A.<sup>1</sup>, Melo B. J. A.<sup>3</sup>, Menendez. A. V. M.<sup>2</sup>

<sup>1</sup> *Centro de Investigación e Innovación Tecnológica (CIITEC)*

<sup>2</sup> *Instituto Mexicano del Petróleo, Área de Ingeniería Molecular, México D. F., México.*

<sup>3</sup> *Instituto Tecnológico de Cd. Madero, División de Estudios de Posgrado e Investigación.*

\*e-mail: [ben\\_portales\\_mtz@hotmail.com](mailto:ben_portales_mtz@hotmail.com)

The carbon nanotubes were synthesized using a matrix of hybrid material SBA-16/CMK, The matrix was prepared from SBA-16, it impregnated with sucrose and was pirolized in inert atmosphere, then, salts of nickel and molybdenum were impregnated, they oxidized and finally a methane and hydrogen atmosphere took to reaction in. The matrix was removed using hydrofluoric acid in aqueous solution.

Characteristically peak SBA-16 support was determinated by XRD in the 0.85 grades in the 2θ scale. The identification by DRX showed the presence of metals used like catalysts in form of carbides. Textural properties showed surface areas of 970 m<sup>2</sup>/g for SBA-16 and 49 m<sup>2</sup>/gr for carbon nanotubes, source support attributable to the presence of mesoporous of IV type and type III for the nanotubes were founded. TEM images showed a cubic arrangement in the SBA-16 and presence of nanotubes with fish-bones arrangement in their walls, the end of the nanotube has no particle, in this way it allows the perfect diffusion of matter to traverse of nanotube.

The materials were tested in hydrogen storage and reaction of reforming of methane and sulfhidric acid. Were they obtained a 3.08 % wt in hydrogen storage and has a 53 % of selectivity towards wished products.

## REFERENCES

- 1 R. Ryoo, C. Hyun Ko, M. Kruk, V. Antochshuk, M. Jaroniec, J. Phys. Chem. B 104 (2000) 11465.
- 2 Rafal M. Grudzien, Bogna E. Grabicka and Mietek Jaroniec, Effective method for removal of polymeric template from SBA-16 silica combining extraction and temperature-controlled calcinations. Journal of Material Chemistry, 2006, 16, 819–823
- 3 E. Terrés; B. Panella; T. Hayashi, Hydrogen storage in spherical nanoporous carbons, Chemical Physics Letters, 2005, 403, 363.

# **Sensibilization with Metallic Nanoparticles and Low Power Laser Treatment for Selective Modification of ABS Surfaces for Plating**

Lorena Magallón Cacho<sup>1,2</sup>, José de Jesús Pérez Bueno<sup>1</sup>Yunny Meas Vong<sup>1</sup>, ,  
Guy Stremmsdoerfer<sup>2</sup>

<sup>1</sup>*Centro de Investigación y Desarrollo Tecnológico en Electroquímica, S.C. Parque Tecnológico Querétaro Sanfandila, Pedro Escobedo Querétaro, México. CP. 76703*

<sup>2</sup>*Laboratory of Tribology and Dynamics of the Systems UMR 5513 Ecole Central de Lyon, 36 Avenue Guy de Collongue B P 163 69131 Ecully Cedex, France.*

lmagallon@cideteq.mx

This paper addresses the effect of nanometallic particles in conjunction with low-power laser radiation for the selective surface treatment of ABS to be use for plating. The nanometric scale of particles is used to amplify the thermal response to the optic stimulus, which combines bigger surface-concentration rate, as well as absorption-thermal conductivity. In this study two kind of nanoparticles were used on ABS surfaces: silver and palladium. The silver nanoparticles were deposited by the JetMetal™ technique and the adsorption of palladium nanoparticles was accomplished from colloidal suspension. Using nanometric metallic particles, the power for engraving on non-sensitized copolymer was reduced by more than one order of magnitude. Both 488 and 532 nm wavelengths were used with a power variation range of 35 to 150 mW and from 20 to 500 mW, respectively. The lowest surface power density that had a surface modification response was  $0.0815 \text{ mW}/\mu\text{m}^2$ , obtained with the former one. A reference sample without sensibilization by metallic nanoparticles, under similar conditions required 500 mW in order to observe a measurable surface modification. In the other hand, under the used experimental conditions in the study, the silver nanoparticles show a better performance with an effect at lower power. The characterization was done using the Scanning Electronic Microscopy (SEM), Energy dispersive X-ray spectroscopy (EDS) and Absorption Spectra.

# **Structural and Electronic Properties of Au and Au<sub>2</sub> on an MgO(100) Surface: Nature of the Bonding, Surface Relaxation and Charge Transfer.**

Alicia Ayala<sup>1</sup>, Reyna Caballero,<sup>1</sup> Andreas M. Köster,<sup>2</sup>  
Shiv N. Khanna,<sup>3</sup> and J. Ulises Reveles,<sup>3</sup>, and Carlos Quintanar,<sup>1,†</sup>

<sup>1</sup>Facultad de Ciencias, Universidad Nacional Autónoma de México, Ciudad Universitaria, 04510 México, D.F., México. <sup>3</sup>Departamento de Química, Cinvestav, Avenida Instituto Politécnico Nacional 2508, A.P. 14-740, México, D.F., 07000, México. <sup>4</sup>Physics Department, Virginia Commonwealth University, Richmond, Virginia, 23284-2000, USA.

† cqs@matrix.super.unam.mx

The structural and electronic properties of Au and Au<sub>2</sub> adsorbed on five coordinated oxygen and magnesium regular terrace sites, on the neutral F<sub>s</sub> color center (oxygen vacancy containing two electrons), and on the charged F<sub>s</sub><sup>+</sup> color center (oxygen vacancy containing one electron) of the MgO(100) surface have been investigated using a density functional theory and a cluster embedding approach. Our studies also examine the effect of relaxation of the substrate. We report the geometry, adsorption, and dimerization energies of the lowest energy and low energy isomers at each adsorption site, charge transfers from the MgO surface to the Au atoms of the lowest energy isomers, and compare our findings with previous theoretical studies. We found that the site with the largest adsorption and dimerization energies, and where an Au atom is most stable and can grow, is the neutral F<sub>s</sub> center. Finally, we focus on an Au<sub>2</sub> molecule, perpendicular to the surface, adsorbed at three bonding sites: a five coordinated oxygen regular terrace site O<sub>5c</sub>, an F<sub>s</sub> neutral color center (two electrons in an O vacancy), and an F<sub>s</sub><sup>+</sup> positive charged color center (one electron in an O vacancy). We found that large relaxation of the neighboring atoms and large charge transfer occurs for an Au<sub>2</sub> over the color centers. An analysis of the one-electron energy levels of the Au dimer, the MgO surface and the Au<sub>2</sub>MgO(100) complex for each absorption site allows us to rationalize the nature of the bonding, surface relaxation, calculated absorption and dimerization energies and electron charge transfers.

# Synthesis of Colloidal Titanium, Tin and Zinc Oxides Nanoparticles Under Normal Reaction Conditions with Electronic Quantum Confinement

I. Zumeta, D. Díaz

Universidad Nacional Autónoma de México, Facultad de Química, Coyoacán, C. P. 04510, México DF, México.

e-mail: intizd@gmail.com, david@servidor.unam.mx. Tel/fax 56223813

Semiconductor oxide nanoparticles have attracted the interest of the scientific community in the last decades. These oxide nanoparticles have been widely studied and applied in photovoltaic conversion [1] and different photocatalytic reactions [2,3]. Their potentialities are determined by their size and shape, that is why the synthesis process is a crucial step for the final particle properties and many methods have been published addressing that [4,5]. Due to the great importance of the synthesis process the searching for new, low cost, simple or accessible ways is still one of the main goals in nanoparticle research. In this contribution we report novel and simple synthesis methods of TiO<sub>2</sub>, SnO<sub>2</sub> and ZnO nanoparticles in quantum confinement regime. We have avoided using alkoxides due to their high hydrolysis speed and cost. The reactions take place using dimethylsulfoxide (DMSO) as solvent and different precursor salts (TiI<sub>4</sub>, SnCl<sub>4</sub>•5H<sub>2</sub>O or ZnAc (Zinc Acetate)) depending on the case. A solution of NaOH is added to produce the reaction under magnetic stirring. Absorption and Raman spectroscopies, X-ray diffraction and transmission electron microscopy (TEM,) were used for the characterization of the nanoparticles. The photocatalytic character through 1,4 dichlorobenzene (DCB) and bis(4-nitrophenyl) phosphate (BNPP) and nanoparticles interactions is discussed. The obtained particles are within 1-4 nm size range and show a “blue” shift in band gap energy (E<sub>g</sub>). Those shifts in band gap are explained based on the quantum confinement effect. Further studies are required for a straightforward explanation of the observed effects on the decomposition of the studied pollutants. New experiments are proposed for this work. (proposed for oral contribution)

We would like to thank DGAPA-UNAM and INI00907 project for supporting this work

- [1] Brian O'Regan *et. al.* [Nature](#) 353, 737-740 (1991).
- [2] Meng Ni *et. al.* [Renewable and Sustainable Energy Reviews](#) 11, 401-4025 (2007)
- [3] Anne Danion *et. al.* [Applied Catalysis B: Environmental](#) 62, 274-281 (2006)
- [4] C. H. LIANG *et. al.* [Applied physics A, Mat. Sc. & processing](#) 80 , 819-822 (2005)
- [5] N. SATOH *et. al.* [nature nanotechnology](#) 3, 106-111 (2008)

## Synthesis and characterization of Bismuth zero-valent nanoparticles and Bismuth oxide in colloidal dispersion

**Donaji Velasco Arias<sup>1</sup>, David Díaz<sup>1\*</sup>, Patricia Santiago Jacinto<sup>2</sup>, Luis Rendón<sup>2</sup>,**

<sup>1</sup>*Departamento de Química Inorgánica y Nuclear, Facultad de Química. <sup>2</sup>Instituto de Física UNAM. Av. Universidad 3000, Coyoacán, 04510, Mexico City, Mexico.*

E-mails: [donajivela@gmail.com](mailto:donajivela@gmail.com), [david@servidor.unam.mx](mailto:david@servidor.unam.mx).

Mexico is the second world producer of bismuth after China, for this reason it should be a strategic material for our country. Nevertheless, the chemistry of bismuth has not been thoroughly studied. Additionally, this element possesses the classification of "green element" (non-pollutant element or compound, or compatible with the Environment); for this reason it can substitute toxic elements such as Pb, Cd or Se in most applications in semiconductors<sup>1</sup>. The zero-valent bismuth (ZV-Bi-NPs) and bismuth oxide (Bi<sub>2</sub>O<sub>3</sub>-NPs) nanoparticles have captured the interest of the scientific community due to their potential uses in electronic, optoelectronic, sensors and magnetic devices<sup>2,3,4</sup>. In this work we obtained very stable colloidal dispersions of ZV-Bi-NPs and Bi<sub>2</sub>O<sub>3</sub>-NPs, in dimethylsulfoxide. This is a polar and aprotic reaction medium that contributes to the stabilization of the particles; in the case of ZV-Bi-NPs stabilizes the particles in the avoiding their oxidation. The methods of synthesis consist in the dissolution of either bismuth nitrate Bi(NO<sub>3</sub>)<sub>3</sub>·5H<sub>2</sub>O or bismuth acetate Bi(C<sub>2</sub>H<sub>3</sub>O<sub>2</sub>)<sub>3</sub>, followed by the addition of sodium borohydride NaBH<sub>4</sub> (as a reducing agent in the synthesis of ZV-Bi-NPs), or NaOH as a precipitating agent (in the synthesis of Bi<sub>2</sub>O<sub>3</sub>-NPs). A surface stabilizer as sodium citrate and the acetate ions (from the precursor salt of bismuth) are also added. The concentrations of the reactants in the colloidal dispersions are in are approx. 10<sup>-4</sup>M. The measurements of electric potential on the particles surface and solvodynamic size (based on light scattering) provide evidences of the stabilizing effect of the capping agents. Stability and optical properties were monitored by UV-visible electronic absorption spectroscopy. From HR-TEM and DRX of powder samples it was established the  $\alpha$ -rhombohedral phase for ZV-Bi-NPs, and cassiterite phase in Bi<sub>2</sub>O<sub>3</sub>-NPs. The synthesis methods yielded small particles, the average size of ZV-Bi-NPs was 3.3 ± 0.97 nm and ~5nm of Bi<sub>2</sub>O<sub>3</sub>-NP.

<sup>1</sup> Industrial Lubrication and Tribology. **2002**, *54*, 153. <sup>2</sup> Xia, Y.; Yang, P.; Sun, Y.; Wu, Y.; Mayers, B.; Gates, B.; Yin, Y.; Kim, F.; Yan, H. *Adv. Mater.* **2003**, *15*, 353. <sup>3</sup> Hyodo, T.; Kanazawa, E.; Takao, Y.; Shimizu, Y.; Egashira, M. *Electrochemistry*. **2002**, *68*, 24. <sup>4</sup> Adamian, Z. N.; Abovian, H. V.; Aroutiounian, V. M. *Sens. Actuators*, **1996**, *B 35/36*, 241.

# Complex Dispersion Relation of a Dielectric Stack with Thin Metallic Layers

A. Alejo-Molina<sup>1</sup>, J. J. Sánchez-Mondragon<sup>1</sup>, D. A. May-Arrijoja<sup>1</sup>, D. Romero-Antequera<sup>1</sup>, J. Escobedo-Alatorre<sup>2</sup> and O. Ibarra-Manzano<sup>3</sup>

<sup>1</sup>Instituto Nacional de Astrofísica Óptica y Electrónica, Puebla, México, CP 72840

<sup>2</sup>Center for Research in Engineering and Applied Sciences, UAEM, Mor., México, CP 62209

<sup>3</sup>Nanophotonics Group, University of Guanajuato, Salamanca, Guanajuato, México

Email: [alejo@inaoep.mx](mailto:alejo@inaoep.mx)

Metallo-Dielectric Photonic Crystals (MDPC), a single dielectric with metallic insets at filling fractions less than 1%, were first studied by Kuzmiak (*PRB* **55**, 7427 [1997]) using dispersion relations as solutions. Yablonoitch and co-workers (*JOSA A* **16**, 2294 [1999]) studied them by the transfer matrix at metallic thickness larger than 10 nm, demonstrating non perturbative features at the dielectric substrate. We discuss the complementarity of the dispersion relation and the transfer matrix method transmittance of a stack, produced by a DPC with extremely thin metallic insets with the same periodicity. Although, both types of basic structures are well known as well as their basic features, the coexistence of them, if the metallic insets are indeed thin ( $< 10$  nm for Ag), was not reported. We have carried out the analytical and numerical analysis with normal and oblique incidence. Also, we speculate that the strong absorption and the formation of a metallic band gap at high frequencies have their origin in a plasmonic interaction. The stack is two layers of different dielectric materials and metallic insets described by the Drude model, with parameters [1, 2]: plasma frequency  $\omega_p = 1.6 \times 10^{16}$  rad/s and damping coefficient  $\gamma = 0.001$ . The thickness of each layer is  $a$ ,  $b$  and  $\delta$ , and the cell period is  $L = a + b + \delta$ . The dispersion relation of the MDPC has two no-redundant equations [1], their graph is show in Fig. 1.

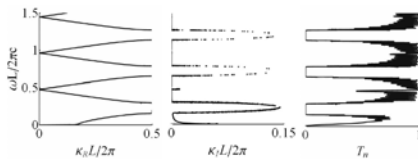


Fig. 1. Band structure, absorption and stopgap, for a MDPC with  $a = 0.1082 \mu\text{m}$ ,  $b = 0.2654 \mu\text{m}$  and  $\delta = 0.001\mu\text{m}$ .

Refractive indices:  $n_1 = 3.58$  and  $n_2 = 1.46$ .

We conclude that is possible to relate the band structure with the transmittance for 1D MDPC; it is directly related for ultrathin layers and just complementary for thin layers. We demonstrated a metallic band gap not only at the bottom but also at high frequencies.

# High-dose TL properties of nanostructured ZnO:Yb

E. Cruz-Zaragoza<sup>1,\*</sup>, U. Pal<sup>2</sup>, V. Chernov<sup>3</sup>, M. Barboza-Flores<sup>3</sup>

<sup>1</sup>Instituto de Ciencias Nucleares, Universidad Nacional Autónoma de México, A.P. 70-543, México 04510 D.F.

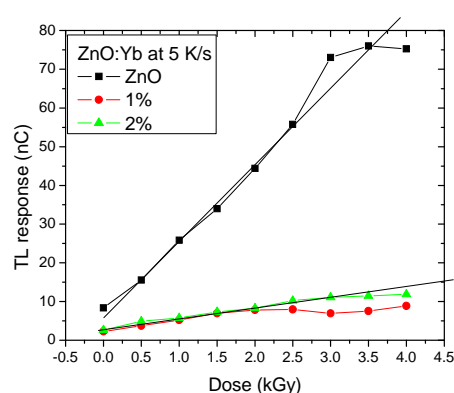
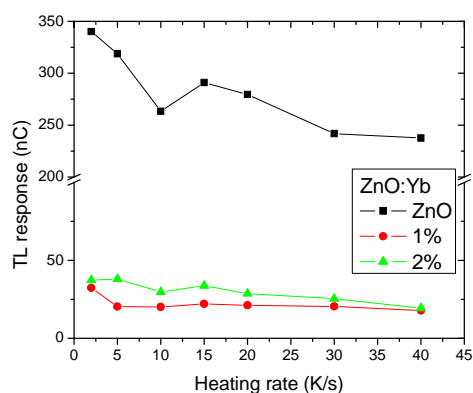
\*E-mail: ecruz@nucleares.unam.mx

<sup>2</sup>Instituto Física, Universidad Autónoma de Puebla, A.P. J-48, Puebla, 72570 México

<sup>3</sup>Centro de Investigación en Física, Universidad de Sonora, A.P. 5-088, Heromosillo, Sonora, 83190 México.

## Abstract

We report on the TL properties of nanostructured ZnO single and Yb-doped with 1 and 2 mol% concentration exposed to high 0.5 - 4 kGy doses of gamma radiation from a <sup>60</sup>Co source. The TL glow curves of undoped ZnO samples peaked around 95 °C and for ZnO Yb-doped TL structure was found at 96 - 116 °C depending on the impurity concentration. The heating rate effect on the thermoluminescent glow curves was analyzed and the maximum of the TL peaks were shifted to higher temperature as the heating rate increased from 2 to 40 C/s along with a TL intensity decrease. A linear dose-response was observed between 0.5 to 3 kGy for all samples. The impurity concentration in the ZnO powder played a major role on the glow curve shapes.



**Keywords:** Thermoluminescence; Heating rate; Glow curves; ZnO:Yb nanophosphor.

## BIODEGRADABLE NANOPARTICLES AS CARRIER FOR BRAIN DRUG DELIVERY

Gerardo Leyva Gómez, Marlen Rodríguez Cruz, Clara Domínguez Delgado, Celene Lozano Rivas, Adriana Ganem Rondero and David Quintanar Guerrero

*División de Estudios de Posgrado (Tecnología Farmacéutica), Facultad de Estudios Superiores Cuautitlán-Universidad Nacional Autónoma de México, Estado de México, C. P. 54740, México.*

*E-mail: gerardoleyva@hotmail.com*

### **Abstract.**

The nanostructured materials have shown a high impact in all areas of the technology allowing new applications. In the pharmaceutical field have been used to improve the bioavailability of a wide variety of drugs as well as to reduce its undesirable effect. In this work the functionality of two types of nanoparticles with two neuroactive drugs as carrier to the brain was evaluated. The lipidic nanospheres of Compritol 888 (lipidic matrix), clonazepam (anxiolytic drug) and poloxamer 407 (stabilizer) had a mean particle size of  $320 \pm 30$  nm and a  $\psi_z$  of -20mV (stable dispersion for six months). On the other hand the polymeric nanoparticles formed by poly (lactide-co-glycolide) 50:50 (polymeric matrix), albendazole (anthelmintic drug) and poloxamer 407 (stabilizer) had a mean particle size of  $338 \pm 6.9$  nm and  $\psi_z$  of -20mV (dispersion stable for 3 months). The maximum drug loading was 0.7 and 5.0 % w/w for lipidic and polymeric nanoparticles respectively; this was confirmed by DSC evaluations. In a preliminary study of the anxiolytic effect in rats (elevated plus-maze) it was found that the effect of clonazepam can be increased 3-fold greater in comparison to the drug dispersion. This behavior suggests that the nanoparticles administrated by oral route can increase the bioavailability of the drugs at brain level. The probable mechanism is similar to that observed when drugs are administrated with high lipid content in the diet (Trojan effect). The polymeric nanoparticles will be evaluated as a carrier to increase the brain drug concentration in order to optimize the neurocysticercosis treatment.

**References.** 1.- D. Tamayo-Esquivel, A. Ganem-Quintanar, A. L. Martínez, M. Navarrete-Rodríguez, S. Rodríguez-Romo and D. Quintanar-Guerrero, *J. Nanosci. Nanotechnol.* 6, 3138 (2006), 2.- D. Quintanar-Guerrero, D. Tamayo-Esquivel, A. Ganem-Quintanar, E. Allémann and E. Doelker, *Eur. J. Pharm. Sci.* 26, 213 (2005), 3.- P. R. Lockman, R. J. Mumper, M. A. Khan and D. D. Allen, *Drug Dev. Ind. Pharm.* 28, (2002).

# SHG of Poled Liquid Crystalline Azo-Dye Doped Hybrid Thin Films

## Prepared by the Sonogel Method.

V. Torres-Zúñiga\*, O. G. Morales-Saavedra, E. Rivera, and  
R. Ortega-Martínez.

*Centro de Ciencias Aplicadas y Desarrollo Tecnológico, Universidad Nacional Autónoma de México, CCADET-UNAM. A. P. 70-186, Coyoacán, 04510, México, D. F. MEXICO.*

\* E-mail: [vicentz@gmail.com](mailto:vicentz@gmail.com)

Three different azobenzene based compounds exhibiting liquid crystalline behavior (named here RED-PEG-7, RED-DIPEGM and RED-Me) were specially designed and synthesized to exhibit quadratic nonlinear optical (NLO)-effects like Second-Harmonic-Generation (SHG) [1]. In general, Azo-dye compounds exhibit low mechanical and thermal stability [2]; these aspects represent a serious limitation for the manufacture of functional optical prototypes for instance in nonlinear waveguiding technology. However, in order to overcome these limitations, these molecules can be inserted within an amorphous, optically neutral, highly porous and extremely pure SiO<sub>2</sub> matrix by means of the sonogel method [3-4]. In particular, the synthesis of amorphous silica via a sol-gel process induced by ultrasonic action (sonolysis) has been recently implemented as an alternative method for the fabrication of highly pure (catalyst-free) organic-inorganic hybrid composites with good structural and optical properties [3-4]. This was possible since the colloidal sol-state provide an optimal environment for the inclusion of different optically active organic dopant species. The final hybrid structure is obtained after the condensation of the sonochemical product with the dopant molecule of interest. In this work, we present the successful fabrication of sonogel based hybrid organic-inorganic thin films by the spin coating technique implementing azo-dye molecules. The organic part of these amorphous films was electrically oriented via a Corona-discharge system in order to induce a non-centrosymmetric molecular arrangement suitable for quadratic NLO-effects. Comparative characterizations between several poled and unpoled film samples reveal optimal conditions for the fabrication of active NLO-hybrid thin films with these kinds of compounds. The structural and optical properties were analyzed via AFM, Absorption Spectroscopy, and the SHG-technique.

### REFERENCES:

- 1) Omar G. Morales-Saavedra et. al. "Inclusion of liquid crystalline azo-dyes in nanometric porous anodic alumina: A comparative morphological and optical study" *Dyes and Pigments*, Vol. 78, Issue 1, 2008, pp 48-59.
- 2) Ganeev, R.A., and Usmanov, T. "Nonlinear-optical parameters of various media", *Quantum Electronics*, 37 (7), pp. 605-622 2007.
- 3) Omar G. Morales-Saavedra et. al. "Preparation and optical characterization of catalyst free SiO<sub>2</sub> sonogel hybrid materials". *Journal of Sol-Gel Science and Technology*, Vol. 41, Issue 3, pp. 277-289, 2007.
- 4) Omar G. Morales-Saavedra et. al." Linear and non-linear optical properties of 2,5-disubstituted pyrroles supported by a catalyst-free SiO<sub>2</sub> sonogel network", *Journal of Non-Crystalline Solids* Vol. 353, Issue 26, pp. 2557-2566 2007

## **A General Vision about Nano-science and Nano-technology**

E.E. Hernández-Vázquez, H.H. Cerecedo-Núñez, P. Padilla-Sosa.

Facultad de Física e Inteligencia Artificial  
Universidad Veracruzana  
Xalapa, Ver. Mex.  
hcerecedo@uv.mx

This work corresponds to a general vision about nano-science and nano-technology. The main reason that follows to develop this work is because, we still observe some confusion between nano-science and micro-science terminology, or even more, there is not clear the difference between nano-science and nano-technology. The starting point is to explain some basic concepts and differences between nano- and micro- scale; then, we mention briefly how to start the study of nano-science and nano-technology, mainly from a physics point of view; after, we mention the principal and actual nanostructures; finally, we briefly describe some applications and the future of nanostructures. Our work is based on a bibliographic review. We conclude this work mentioning that nano-science is not something new, this has several years of study and that nano-technology is early due to recent technological advances. Also, it must be distinguished between micro-science and nano-science, micro-technology and nano-technology because is not just a scale question, even more, there is a different phenomenology involved in one and other scale.

## Computational Study of silicon-doped fullerenes

Francisco J. Tenorio<sup>1</sup>, J. G. Rodríguez Zavala<sup>1</sup>, Juvencio Robles<sup>2</sup>.

<sup>1</sup>Centro Universitario de los Lagos, Universidad de Guadalajara. Enrique Díaz de León 1144 Col. Paseos de la Montaña. Lagos de Moreno, Jalisco. CP47463. <sup>2</sup> Facultad de Química, Universidad de Guanajuato. Noria Alta S/N. CP36050. Guanajuato, Gto.

ftenorio@culagos.udg.mx

Carbon –cage structures such as fullerenes have extensively stimulated a variety of scientific studies on their structure and reactivity. They have been considered as building blocks for novel and interesting materials. Fullerenes can be found both in pure and mixed state, resulting in systems which structural and electronic properties are very different. Fullerene doping can be performed out of the cage (exo), inside (endo) and instead of carbon atoms. Transition metals are frequently found as endohedral part of this kind of systems, suggesting possible applications as superconductor<sup>1</sup>. Exohedral doping has been found attractive with alkaline metals<sup>2</sup>. Substitutional doping is related with modifying the fullerene itself with a different atom than carbon. It is expected to be easier if the dopant atom has a similar electronic configuration, such as silicon<sup>3</sup>, but has been performed with other elements such as nitrogen, oxygen and some transition metal atoms<sup>4</sup>. No matter that silicon is isoelectronic to carbon, their bonding and chemical properties are different. This features would play against the substitutional doping of silicon in fullerenes; however, SiC compounds and alloys exhibit outstanding properties such as polymorphism, variable band gaps; making by themselves interesting materials subject to study and, on the other hand, Si-doped fullerenes have been already obtained by several groups<sup>3,4</sup>. In the present work, semiempirical and *ab initio* calculations have been performed to study the structure and stability of various silicon-doped fullerenes such as C<sub>70-x</sub>Si<sub>x</sub> and C<sub>82-x</sub>Si<sub>x</sub>, where x=1-3 (for example, see Figure 1). It is showed that some isomers are energetically favored. Other electronic properties are computed to assess the effect of gradual substitution of Si atoms in the cages.

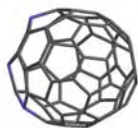


Figure1. C<sub>67</sub>Si<sub>3</sub> structure.

### References:

1. Johnson R. D., et. al., 1992, *Nature*, **355**, 239. 2.- Stephens P.W., et. al. 1994, *Nature*, **370**, 636. 3.- Pellarin M, et. al., *Chem. Phys. Lett.*, 1997, **277**, 96. 4.- Kimura, et. al., *Chem. Phys. Lett.*, 1996, **256**, 269. Fye J. and Jarrold M., *J. Phys. Chem. A.*, 1997, **101**, 1836. Ray C., et al., *Phys. Rev. Lett.*, 1998, **80**, 5365.

## Segregation and Chemical ordering in bimetallic nanoclusters.

**J. A. REYES-NAVA**<sup>1,2</sup>, J. L. Rodríguez López<sup>3</sup>, U. PAL<sup>1</sup>, H. B. Liu<sup>4</sup>

<sup>1</sup>Instituto de Física, Benemérita Universidad Autónoma de Puebla, Av. San Claudio y Blvd. 18 Sur Col. San Manuel, Ciudad Universitaria C.P. 72570, Puebla, Pue., México.

<sup>2</sup>Universidad Politécnica de Chiapas, **Calle Eduardo J.Selvas S/N entre Manuel de J.Cancino y Enriqueta Camarillo, Col. Magisterial, C.P.29010, Tuxtla Gutiérrez, Chiapas, México.**

<sup>3</sup>Advanced Materials Department, IPICYT; San Luis Potosí, S.L.P, México.

<sup>4</sup>Instituto Mexicano del Petróleo, Eje Central Lázaro Cárdenas No. 152, Col. San Bartolo Atepehuacan, C.P. 07730, México D.F., México.

E-mail: jareyesn@sirio.ifuap.buap.mx

Surface segregation mechanism in nanoalloy clusters is of great importance for controlling their morphology, composition and catalytic activities. Though, current understanding of this phenomenon, based on some theoretical calculations and discrete experimental observations highlights the general trend of this process in some particular systems, there exist no generalized convention and physical explanation to suit for all the binary systems till date.

In the present study the chemical ordering in bimetallic nanoclusters is investigated describing the surface segregation process in terms of the difference between the atomic properties of the constituent elements. Considering the attractive and repulsive contributions of the cohesive energy of an atom in a cluster, it was concluded that for adjacent elements of a row of the periodic table, the bimetallic system would be more stable if the component with smallest valence electron density is placed on the surface. On the contrary, for well separated components in the periodic table, the bimetallic cluster would be more stable if the component with the smallest core electron density is placed inside [1].

**PACS:** 61.46.Df 02.70.Ns 66.30.Pa 67.80.-s  
Acknowledgments

This work was supported by PROMEP-México and CONACyT-México, under the Project grants UPCHS-PTC-018 and FOMIX CHIS-2006-C06-45675. JARN acknowledges CONACyT for extending the postdoctoral fellowship. The authors wish to thank computational supports from the Centro Nacional de Supercómputo (CNS-IPICYT, México), IFUAP-México and UPChiapas-México.

[1] J. A. Reyes-Nava, J. L. Rodríguez-López, U. Pal, *Generalizing Segregation and Chemical ordering in bimetallic nanoclusters through atomistic view points*, <http://arxiv.org/abs/0805.1396>

## Atomic Structure of Small and Intermediate-Size Silver Nanoclusters [3].

*Alí Michel Angulo Martínez, Cecilia Noguez*

Instituto de Física, Universidad Nacional Autónoma de México, Apartado Postal 20-364,  
México D. F. 01000 MÉXICO

[ali@fisica.unam.mx](mailto:ali@fisica.unam.mx), [cecilia@fisica.unam.mx](mailto:cecilia@fisica.unam.mx).

Nanosized metal particles exhibit a wide variety of physical properties, which can be tailored by altering their size, morphology and composition. The knowledge and relationship of these parameters is relevant for the systematic synthesis of nanoparticles with uniform and reliable properties. Within this context, atomic simulations play a major role in the explanation and prediction of novel nanostructures, which are complementary ingredients for experimentalists. In metals it is well known that the stability and energy of a given cluster highly depend on its number of atoms [1]. Using a classical Molecular Dynamics method, where the interaction between atoms is simulated by a semiempirical potential [2], we have made an exploration of the lowest-energy clusters, formed with  $n$  Ag atoms with  $7 \leq n \leq 561$ . A five-fold symmetry is found in most cases, and a novel morphology for the clusters of 39 and 116 silver atoms is identified [3]. This morphology is understood in terms of decahedral and icosahedral geometries, which are somehow intercalated, as we explain in detail. These kind of structures have been observed for gold [4] and now are predicted for small and intermediate silver nanoparticles.

### References :

- [1] F. Baletto, R. Ferrando, J. Chem. Phys. **116**, 3856 (2002).
- [2] R. P. Gupta, Phys. Rev. B. **23**, 6265 (1981).
- [3] A. M. Angulo, C. Noguez, J. Phys. Chem. A, **112**, 5834 (2008).
- [4] Ascencio, J. A.; Pérez, M.; José-Yacaman, M. Surf. Sci. 2000, 447, 73.

## Synthesis of carbon nanomaterials using different methods and dextrose as carbon source

E. Hernández<sup>a</sup>, J.A. Melo<sup>a</sup>, J. M. Domínguez<sup>b</sup>, A.I.Reyes<sup>b</sup>

<sup>a</sup>*Instituto Tecnológico de Cd. Madero, División de Estudios de Posgrado e Investigación, Juventino Rosas y Jesús Urueta S/N, C. P. 89440 Tel y Fax (+52 833)215-85-44, Col. Los Mangos, Cd. Madero, Tamps, México.*

<sup>b</sup>*Instituto Mexicano del Petróleo, Área de Ingeniería Molecular, Eje Central Lázaro Cárdenas 152, C.P. 07730, México D. F., México.*

[elyhdzmdz@hotmail.com](mailto:elyhdzmdz@hotmail.com)

Nanomaterials are especially interesting because their attractive properties to be used in different fields. Many procedures have been reported about different methods for synthesizing and testing of properties for these materials. These researches reports mainly sucrose as a carbon source. In this research three different method of synthesizing and dextrose as carbon source was proposed.

Carbon nanomaterials were synthesized by nanocasting technique, using porous inorganic material SBA 15 as template. Nanomaterials were obtained via the pyrolysis of monosacaride material embedded inside the hexagonal form of SBA-15. Mesoporous support SBA-15 were prepared using the surfactant Pluronic P-123 and TEOS (Tetraethyl orthosilicate) as silica source. Textural proprieties were tested by N<sub>2</sub> physisorption (BET method) showing typical specific areas higher than 900 m<sup>2</sup>/g. Sharp reflection peaks corresponding to the periodicity were observed by X-ray diffraction (XRD), where the characteristic peaks appeared in 0.88°, 1.53° and 1.77° in 2θ for SBA-15. Structural arrangement was confirmed by Transmission electron microscopy (TEM) showing the hexagonal pore adjustment typical of SBA-15. The specific area, X-ray diffraction and structural arrangement of the carbon replicas were studied too. N<sub>2</sub> physisorption showed specific areas about 1500 m<sup>2</sup>/g. and TEM inverse replicas of SBA-15. Proprieties of carbon nanomaterials synthesized can be studied in detail in order to use it in catalysis, hydrogen storage, or another uses.

# Photoluminescence instability in Porous Silicon

T. Flores-Arroyo\*, A. Mendez-Blas, and U. Pal

*Instituto de Física, Benemérita Universidad Autónoma de Puebla, Apdo. Postal J-48,*

*C.P. 72570, Puebla, Pue., México*

[\\*tflores@sirio.ifuap.buap.mx](mailto:*tflores@sirio.ifuap.buap.mx)

Porous silicon (PS) is highly luminescent in the visible spectral range at room temperature,<sup>1</sup> in contrast to bulk crystalline silicon. However, the emission in PS is hardly stable when stored in atmospheric ambient. Depending on the preparation conditions and the nature of used wafers, electrochemically anodized PS layers can emit in different spectral ranges with different intensities.

In the present work, we have prepared PS layers of different porosities using n-type Si wafers of resistivity 0.002-0.005  $\Omega$ -cm by anodizing them at different concentrations of hydrofluoric acid (HF) in the electrolyte. The emission behavior of the PS layers was studied by photoluminescence (PL) spectroscopy at room temperature. PL emission instability in the samples was studied by recording their PL spectra at different intervals of storage time in air. It has been observed that the emission efficiency of the PS layers depend strongly on their porosity. The intensity of emission decreased exponentially with the storage time in air for all the samples. However, the rate of intensity quenching depends on the porosity of the samples. From the variation of PL intensity it is concluded that the origin of PL emission in PS is mainly due to quantum confinement of charge carriers in the nanostructures. The conclusion was supported by the Raman spectra of the samples.

*\*The work was partially supported by VIEP-BUAP (Grant # 93/EXC/2008-1), Mexico.*

1. Leigh T. Canham, *Appl. Phys. Lett.* **57**, 1096 (1990).

# Adsorption and separation of linear and branched hydrocarbons by nanoporous pyrazine pillared tetracyanonickelate

P. Vera-Cruz<sup>1</sup>, A. A. Lemus-Santana<sup>1</sup>, B. Torruco<sup>1</sup>, L. F. del Castillo<sup>1</sup>,

J. Balmaseda<sup>1</sup>

<sup>1</sup>.- *Departamento de polímeros, Instituto de Investigaciones en Materiales, Universidad Nacional Autónoma de México, D.F. C.P. 04510.*

[pauveracruz@gmail.com](mailto:pauveracruz@gmail.com), [balmaseda@iim.unam.mx](mailto:balmaseda@iim.unam.mx)

## Abstract

The material under study,  $[\text{Ni}(\text{pz})\text{Ni}(\text{CN})_4] \cdot x\text{H}_2\text{O}$  (**I**), was prepared by the separation of  $\text{Ni}[\text{Ni}(\text{CN})_4]$  layers in citrate aqueous solution to allow the intercalation of pyrazine molecules. The solids obtained were characterized from CHN elemental analyses, X-ray powder diffraction, thermogravimetry, and physical adsorption. Their crystal structure was refined by the Rietveld method. For (**I**) a tetragonal cell was obtained with lattice parameters:  $a = b = 7.174(7)$  Å, and  $c = 7.033(7)$  Å; with  $Z = 1$ . The structure consists of two-dimensional square-grid faintly waved sheets formed by the alternate linkage between square-planar ( $D_{4h}$ ) and slightly distorted octahedral ( $O_h$ ) nickel centers through cyano bridges. The  $\text{Ni } O_h$  is coordinated to four N atoms of the cyano groups and two N atoms of two pyrazine molecules. The pyrazine molecules form a vertical pillar between neighboring layers, resulting in an open three-dimensional framework where the sheets are separated a distance of  $7.033(7)$  Å.

Compound (**I**) has a framework with two types of pores, one of the pores is a cube of  $5.0730(5) \times 5.0730(5) \times 7.033(1)$  Å and the other has the same dimensions but part of its space is occupied by four carbon atoms of two neighboring pyrazine molecules. These dimensions are ideal for the adsorption and separation of linear and branched volatile organic compounds.

The TGA curve of (**I**) shows three well-defined steps. The first weight loss takes place mostly before  $100^\circ\text{C}$  and could be associated to the loss of water molecules. The second weight loss ( $250\text{--}390^\circ\text{C}$ ) can be associated to the destruction of the pillars and corresponds to one pyrazine molecule per formula unit. After  $390^\circ\text{C}$  begins the decomposition of the layers.

Inverse gas chromatography of pure hydrocarbons reveals that for linear hydrocarbons, interaction is proportional to the number of carbons in the chain. It was also found that for polar molecules the dipolar interaction is predominant. Also, their interactions are higher than those observed for linear chains. In ethanol the repulsion forces increase due to steric impediment. Furthermore, branched molecules like toluene cannot access the porosity. Therefore, the separation studies reveal that the framework is suitable for the separation of molecules with different electric and steric properties.

## Layered cylinders in 2D photonic crystals

D.L. Romero-Antequera, A. Alejo-Molina, J.J. Sánchez-Mondragón

*Instituto Nacional de Astrofísica, Óptica y Electrónica*

*Luis Enrique Erro #1, Tonantzintla, Puebla. México, C.P. 72000*

dromero@susu.inaoep.mx

Photonic crystals slabs, or 2D photonic crystals, have attracted a great deal of attention in the recent years because of their potentialities and their ease of fabrication. In this work, we propose a photonic crystal slab whose basis are common glass cylinders ( $n_c = 1.5$ ), coated with several layers of two distinct alternating dielectrics, silicon (Si,  $n_1 = 3.56$ ) and silica ( $\text{SiO}_2$ ,  $n_2 = 1.46$ ), Fig. 1. We show that this kind of structure presents a transient regime for a small number of cylinders, where the band structure as a whole shrinks because of changes in the average refractive index and the filling fraction; This allows to manipulate the structure and possibly move the full band gaps. The thick of the layers is adjusted to a quarter wavelength of optical path, according to some tuning wavelength ( $\lambda$ ), in such a way that for a sufficiently large number of full layer periods (about ten full periods), these cylinders behave as Bragg mirrors for the tuning wavelength, as reported somewhere else. We will show that we can enhance the stop gap for the tuning wavelength.

*Figure 1: Top view of the layered cylinders*

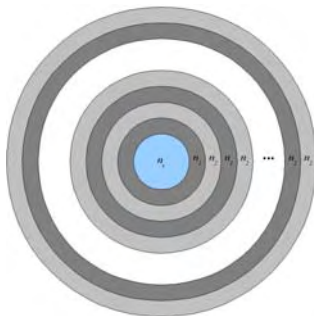


*Figure 1: Top view of the layered cylinders*

# Self- organization of Cholesterol molecules on the Au (111): An STM study

Aristeo Segura<sup>a,b</sup>, and Nikola Batina<sup>b</sup>

a) *Facultad de Ciencias Químicas. Universidad Autónoma Benito Juárez de Oaxaca, Av. Univ. S/N, Col. 5 Señores. C.P. 68120. Oaxaca, Oax., México.*

[ass@aristeosegura.com.mx](mailto:ass@aristeosegura.com.mx)

b) *Laboratorio de Nanotecnología e Ingeniería Molecular, Depto. de Química, UAM-I, Av. San Rafael Atlixco No. 186, Col. Vicentina, Del. Iztapalapa, C.P. 09340. México, D.F., México. [bani@xanum.uam.mx](mailto:bani@xanum.uam.mx)*

## Abstract

Self – organization of Cholesterol on the gold surface (111) has two important characteristics. First of All, the cholesterol molecules which were prepared on the Au (111) as a substrate and using methanol solvent, and it was to study with STM, so cholesterol molecules have high resolution molecules on surface which images are very nice quadratic architecture with angle is  $32.6^\circ$  , and they have cavity which size are 0.48 nm. Cholesterol molecules have completely organization on surface gold, and they have competitive for adsorbed on surface .Second, Cholesterol molecules have many physichemistry characteristics .For example , the cholesterol adsorbed on surface for physisorption because it only use slowly energy for adsorbed on gold surface ,and you can see high resolution image which show very clear physisorption, and the cholesterol molecules move on surface very easy, and the image show atomic gold under monolayer cholesterol, and the image show when cholesterol move on surface .The most important result in this research is how the cholesterol adsorbed on gold surface, thus cholesterol molecules use architecture from gold (111) because atomic gold has angle  $32.6^\circ$  ,so the same with cholesterol molecules which angle is  $32.6^\circ$  , and cholesterol molecules have very clear its electronic density which size is 0.2 nm, thus four electronic density is one cholesterol molecule which size is 1.08 nm and you can see two cholesterol aggregate on surface ,and it is a monolayer cholesterol molecules on surface gold , and cholesterol has a torsion on carbon 10 and 5 , but in this part adsorbed on hydrophilic surface . In conclusion, the cholesterol molecules have very nice quadratic architecture and they adsorbed for physisorption on the Au (111).

## Interaction of porphyrin molecules with metallic and semiconductor nanoparticles

Rita Patakfalvi<sup>1,2</sup>, Donaji Velasco-Arias<sup>2</sup>, Víctor Fabián Ruiz-Ruiz<sup>2</sup>, Monica Castillo-Guevara<sup>2</sup>, Héctor García-Ortega<sup>2</sup>, David Díaz<sup>2</sup>

<sup>1</sup>*Universidad de Guadalajara, Centro Universitario de los Lagos, Lagos de Moreno, México,*

<sup>2</sup>*Universidad Nacional Autónoma de México, Facultad de Química, México.*

E-mail: [rpatakfalvi@culagos.udg.mx](mailto:rpatakfalvi@culagos.udg.mx)

The optical properties and the photoactivity of the metallic and semiconductor nanoparticles are changing, if the particles are covered by dye molecules. An aromatic dye molecule, tetraphenylporphyrin was studied as possible stabilizer and surface modifier in the synthesis of Ag, ZnO and SnO<sub>2</sub> nanoparticles. The characterization of this molecule was carried out by X-ray diffraction, FTIR, Raman and UV-Vis spectroscopies. The different nanoparticles were prepared in dimethyl formamide or dimethyl sulfoxide solutions, as published earlier<sup>1-3</sup>. The porphyrin molecules have a characteristic absorption spectrum. There is an intense absorption band between 390-425 nm, called B or Soret band. At larger wavelength, there are two or four much weaker bands, called Q bands, situated between 480-700 nm. The number and intensity of these bands can give information about the porphyrin molecule: its substituents and their position, whether or not it contains a metal ion. The composites were prepared with different nanoparticle – porphyrin concentration ratios. The stabilization effect and the interaction between the Ag, ZnO or SnO<sub>2</sub> nanoparticles and the tetraphenylporphyrin was studied by UV-Vis and Fluorescence spectroscopy. Independent experiments showed that under our reaction conditions metaloporphyrins were not form.

### References:

1. R. Patakfalvi, D. Diaz, D. Velasco-Arias, G. Rodriguez-Gattorno and P. Santiago-Jacinto, *Colloid Polymer Sci* 286 (2008) 67-77
2. G. Rodríguez-Gattorno, P. Santiago-Jacinto, L. Rendon-Vázquez, J. Németh, I. Dékány, and D. Díaz, *J. Phys. Chem. B.* (2003) 107, 12597-12604.
3. D. Velasco-Arias, D. Díaz, P. Santiago-Jacinto, G. Rodríguez-Gattorno, A. Vázquez-Olmos, S. E. Castillo-Blum, Unpublished results

# Preparation and Optical Evaluation of Au-Nanoparticles Based SiO<sub>2</sub>- Sonogel Hybrid Composites

O. G. Morales-Saavedra\*, R. Zanella-Specia, J. Garduño-Mejía, F. G. Ontiveros-Barrera, V. Torres-Zuñiga, J. O. Flores-Flores and R. Ortega-Martínez. \* E-mail: [omar.morales@ccadet.unam.mx](mailto:omar.morales@ccadet.unam.mx)

*Centro de Ciencias Aplicadas y Desarrollo Tecnológico, Universidad Nacional Autónoma de México, CCADET-UNAM. A. P. 70-186, Coyoacán, 04510, México, D. F. MEXICO.*

The synthesis of SiO<sub>2</sub> based sol-gel materials induced by ultrasonic action (sonolysis) has been recently implemented as an alternative method for the fabrication of highly pure (catalyst-free) organic-inorganic hybrid composites with good monolithic and optical properties [1-2]. This was possible since the resulting SiO<sub>2</sub> glasses obtained via sonochemical reactions exhibits high nano-porosity, providing an optimal environment for the inclusion (in solution) of several optically active organic dopant species within the colloidal sol-state. However, the fabrication of inorganic-inorganic hybrid materials with this kind of “sonogels” has been a challenging task due to the poor solubility of the inorganic materials in commonly used solvents for sol-gel applications and to the slow drying process of the sonogel network. This produces the precipitation of the inorganic materials within the sol-phase, leading to the formation of inhomogeneous and low optical quality inorganic-inorganic hybrids. In this work, we show that the inclusion of nanometric inorganic particles in adequate suspensions within the sonogel matrix is possible, giving rise to mechanically stable and homogeneous hybrid composites suitable for optical characterizations. We particularly show in this case, the preparation, linear and nonlinear optical characterizations of Au-nanoparticles based hybrid sonogels, these Au-nanostructures were synthesized via the cationic adsorption of Au(en)<sub>2</sub><sup>3+</sup> (en=ethanediamine) complexes followed by thermal treatment of the sample in H<sub>2</sub> to obtain metallic gold particles supported on SiO<sub>2</sub> [3]. A model to study ultrafast electron dynamics in Au-nanoparticles based on transient optical properties is also presented [4].

## REFERENCES:

- 5) Omar G. Morales-Saavedra et. al. “Preparation and optical characterization of catalyst free SiO<sub>2</sub> sonogel hybrid materials”. *Journal of Sol-Gel Science and Technology*, Vol. 41, Issue 3, pp. 277-289, 2007.
- 6) Omar G. Morales-Saavedra et. al. “Preparation of Fullerene (C<sub>60</sub>) Based SiO<sub>2</sub> Sonogel Hybrid Composites: UV Laser Induced Photo-Polymerization, Morphological, and Optical Properties”. *Journal Of Nanoscience and Nanotechnology*, JNN; Vol. 8, Issue: 7, pp. 3582-3594, 2008.
- 7) R. Zanella, A. Sandoval, P. Santiago, V. A. Basiuk, J. M. Saniger. “New Preparation Method of Gold Nanoparticles on SiO<sub>2</sub>”. *J. Phys. Chem. B*, Vol. 110, pp. 8559-8565, 2006.
- 8) J. Garduño-Mejía, M. P. Higglett and S. R. Meech, “Modeling the influence of non-thermal electron dynamics in thin and ultrathin gold films”. *Chemical Physics*, Vol. 341, pp. 276-284, 2007.

# **Novel Photochromic Effect Amplified by the Nanosize of Titania Particles of a composite with Organic Polymers**

Ll. M. Flores Tandy<sup>1</sup>, J. J. Perez Bueno<sup>1</sup>, Y. Meas Vong<sup>1</sup>

<sup>1</sup>*Centro de Investigación y Desarrollo Tecnológico en Electroquímica, S.C. Parque Tecnológico Querétaro-Sanfandila, Pedro Escobedo, Querétaro, México. CP. 76703*

*E-mail:* lluvia7721@yahoo.com, jperez@cideteq.mx, yunnymeas@cideteq.mx

## **ABSTRACT**

A novel photochromic effect of a composite comprised of titania and organic polymers is studied in this work. The nanosize of particles, clusters and short networks enhance the effect show under UV radiation. The energy required for the change corresponds to that of the bandgap of titania. Absorption of the composite in the visible was achieved through the photochromic effect. The effect has been magnified up to be noticeable under barely sun light exposition. Both a commercial nanopowder and a sol-gel synthesized titania were used in the experimentation. The photochromic effect was observed in the composites in the form of powders, coatings and in bulk. Also, the composite was prepared from different organic polymers, some of which possesses the chromic change. The composite was characterized through HRTEM, UV-vis, reflectance and fluorescence. Based in the results, a mechanism for the photochromic change is proposed.

# **Sensibilization with Metallic Nanoparticles and Low Power Laser Treatment for Selective Modification of ABS Surfaces for Plating**

Lorena Magallón Cacho<sup>1,2</sup>, José de Jesús Pérez Bueno<sup>1</sup>Yunny Meas Vong<sup>1</sup>, ,  
Guy Stremmsdoerfer<sup>2</sup>

<sup>1</sup>*Centro de Investigación y Desarrollo Tecnológico en Electroquímica, S.C. Parque Tecnológico Querétaro Sanfandila, Pedro Escobedo Querétaro, México. CP. 76703*

<sup>2</sup>*Laboratory of Tribology and Dynamics of the Systems UMR 5513 Ecole Central de Lyon, 36 Avenue Guy de Collongue B P 163 69131 Ecully Cedex, France.*

lmagallon@cideteq.mx

This paper addresses the effect of nanometallic particles in conjunction with low-power laser radiation for the selective surface treatment of ABS to be use for plating. The nanometric scale of particles is used to amplify the thermal response to the optic stimulus, which combines bigger surface-concentration rate, as well as absorption-thermal conductivity. In this study two kind of nanoparticles were used on ABS surfaces: silver and palladium. The silver nanoparticles were deposited by the JetMetal™ technique and the adsorption of palladium nanoparticles was accomplished from colloidal suspension. Using nanometric metallic particles, the power for engraving on non-sensitized copolymer was reduced by more than one order of magnitude. Both 488 and 532 nm wavelengths were used with a power variation range of 35 to 150 mW and from 20 to 500 mW, respectively. The lowest surface power density that had a surface modification response was  $0.0815 \text{ mW}/\mu\text{m}^2$ , obtained with the former one. A reference sample without sensibilization by metallic nanoparticles, under similar conditions required 500 mW in order to observe a measurable surface modification. In the other hand, under the used experimental conditions in the study, the silver nanoparticles show a better performance with an effect at lower power. The characterization was done using the Scanning Electronic Microscopy (SEM), Energy dispersive X-ray spectroscopy (EDS) and Absorption Spectra.

# Chemical synthesis and characterization of nanostructured hydroxyapatite powder

A.B. Martínez-Valencia<sup>1,2</sup>, G. Carbajal-De la Torre<sup>2</sup>, H.E. Esparza-Ponce<sup>1</sup>, J. Ortiz-Landeros<sup>3</sup>

<sup>1</sup> *Centro de Investigación en Materiales Avanzados CIMA, Ave. Miguel de Cervantes 120 C.P. 31109 Complejo Industrial Chihuahua, Chihuahua, México.*

<sup>2</sup> *Universidad Michoacana de San Nicolás de Hidalgo UMSNH, Facultad de Ingeniería Mecánica, Santiago Tapia 403. Centro C.P. 58000. Morelia Michoacán, México.*

<sup>3</sup> *Escuela Superior de Ingeniería Química e Industrias Extractivas, Instituto Politécnico Nacional, U. P. Adolfo López Mateos, CP. 07730, México D.F., México.*

Corresponding Author: [anitvalencia@gmail.com](mailto:anitvalencia@gmail.com)

## Abstract

Synthetic hydroxyapatite  $\text{Ca}_{10}(\text{PO}_4)_6(\text{OH})$  has been widely studied and used as biomaterial because its excellent biocompatibility as much as its acceptance and osteointegration performance. Among its preparation procedures; hydroxyapatite powders can be obtained via soft chemistry methods which offer the possibility to fabricate materials with different physico-chemical properties and controlled morphologies; and several advantages such as high purity and homogeneous particle size distribution. In this work, we present a comparative study about the effects of various synthesis methods such as: sol-gel, chemical coprecipitation using ultrasonic radiation and hydrothermal technique, on the structural, microstructural and morphological properties of apatite nanoparticles powders. The characterization of synthesized materials was carried out by X-Ray Diffraction (XRD), Infrared Spectroscopy (FTIR), Scanning Electron Microscopy (SEM); Transmission Electron Microscopy (TEM) and particle size measurements.

**Keywords:** Hydroxyapatite, sol-gel, coprecipitation, chemical synthesis.

# Electronic Circular Dichroism of Single-Wall Carbon Nanotubes

A. Sánchez-Castillo, Cecilia Noguez

*Instituto de Física, Universidad Nacional Autónoma de México, Apartado Postal 20-364, México D.*

*F. 01000 México, asanchezc@fisica.unam.mx*

It is well known that the optical, electronic, mechanical and other physical and chemical properties of single-wall carbon nanotubes (SWNTs) are largely determined by their chirality and diameter. Additionally, for each chiral SWNT there are two possibilities, depending on the handedness of the enantiomers, left-handed (LH) or right-handed (RH). In a typical sample, LH and RH enantiomers are prepared in equal amounts, canceling out the optical activity of each enantiomer. However, the unbalance of a racemic mixture can show optical activity, as it was predicted for pure SWNT enantiomers [1-3]. Very recently, this unbalance has been observed experimentally by measuring the electronic circular dichroism (CD) in different samples containing SWNTs [4-6]. In a first experiment [4], optical activity was measured in a solution of mostly (6,5) SWNTs wrapped with DNA. They suggest that either (i) wrapping with DNA selects one nanotube enantiomer over the other, or (ii) the inherent chirality of DNA induces the signal in a racemic mixture of SWNTs. In a second experimental set up, Peng et al. [5-6] measured the optical activity of a mixture of SWNTs of different indices (n,m), which was obtained through the preferential extraction of LH or RH enantiomers with chiral nanotweezers. They showed that using different molecules as nanotweezers, the optical activity changes, probably caused by the selection of SWNTs of different chiral indices (n,m). In all the experiments the lack of theoretical calculations has hampered their interpretation. In this work we calculate the circular dichroism spectra of chiral SWNTs using Density Functional Theory (DFT). The calculated CD spectra show features that allow us to distinguish between SWNTs with different chirality and diameter.

[1] S. Tasaki, K. Maekawa, T. Yamabe, Phys. Rev. B **57**, 9301 (1998).

[2] G. G. Samsonidze, A. Gruneis, R. Saito, A. Jorio, A. G. Souza Filho, G. Dresselhaus, and M. S. Dresselhaus, Phys. Rev. B **69**, 205402 (2004).

[3] A. Sánchez-Castillo, C. E. Román-Velázquez, C. Noguez, Phys. Rev. B **73**, 045401 (2006).

[4] G. Dukovic, M. Balaz, P. Doak, N. D. Berova, M. Zheng, R. S. Mclean, and L. E. Brus, J. Am. Chem. Soc. **128**, 9004 (2006).

[5] X. Peng, N. Komatsu, S. Bhattacharya, T. Shimawaki, S. Aonuma, T. Kimura, and A. Osuka, Nature Nanotechnol. **2**, 361 (2007).

[6] X. Peng, N. Komatsu, T. Kimura, and A. Osuka, J. Am. Chem. Soc. **129**, 15947 (2007).

# Optical Circular Dichroism of Bare and Passivated Au Nanoclusters

Francisco Hidalgo and Cecilia Noguez

*Instituto de Física, Universidad Nacional Autónoma de México, Apartado Postal 20-364, México D.  
F. 01000 MÉXICO*

[hidalgo@fisica.unam.mx](mailto:hidalgo@fisica.unam.mx); [cecilia@fisica.unam.mx](mailto:cecilia@fisica.unam.mx)

Since the discovery of the metallic Ni<sub>39</sub> chiral nanoparticles [1], other clusters with low symmetry structures made from others elements have been found. Particularly, it has been reported chiral Au nanoparticles [2-5], bare and passivated, observing an increased and even surprising optical activity. However, the physical origin of their quiroptical signal has not been elucidated yet. In this work, the optical activity of bare and ligand protected nanoparticles is studied in detail. In recent years, the study of optical properties of nanostructured systems has grown due to its many implications in different sciences, like biology and chemistry. Chirality arises as a strong link between structural chemistry of organic molecules and inorganic clusters, where optical properties are easily measured in the laboratory. In fact, electronic circular dichroism (CD) has become a basic tool to analyze molecular and nanostructured systems, to characterize enantiomers that show chirality [1]. For instance, nature itself shows chirality in essential life molecules, like DNA, aminoacids and sugars. This property that a nanostructure can be chiral brings possibilities for future technological applications. It has been proved that metal nanoclusters, bare or passivated with chiral molecules, are attractive due to their potential nanotechnology applications in pharmacy, catalysis, etc., in addition to their fundamental interest.

## References

- [1] T. L. Wetzel; A. E. DePristo; *J. Chem. Phys.* **105**, 572 (1996);
- [2] T. G. Schaaff; R. L. Whetten; *J. Phys. Chem. B* **104**, 2630 (2000);
- [3] I. L. Garzón, *et al.*; *Phys. Rev. B* **66**, 073403 (2002);
- [4] I. L. Garzón, *et al.*; *Eur. Phys. J. D* **24**, 105 (2003);
- [5] H. Häkkinen, *et al.*; *J. Phys. Chem. B* **110**, 9927 (2006).

# Synthesis and characterization of Mg(OH)<sub>2</sub> and Ca(OH)<sub>2</sub> nanoparticles under mild reaction conditions.

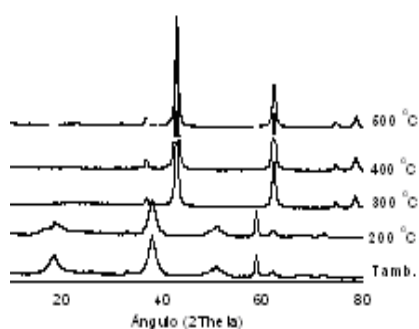
Silvia Castillo-Blum<sup>1</sup>, Yolia León-Paredes,<sup>1</sup> Alicia Díaz<sup>2</sup>, and David Díaz\*,<sup>1</sup>

<sup>1</sup> Facultad de Química. Universidad Nacional Autónoma de México. México D. F., CP 04510, México.

<sup>2</sup> Facultad de Química. Universidad de La Habana, CP 10400, C. Habana. Cuba

e-mail: [david@servidor.unam.mx](mailto:david@servidor.unam.mx)

Magnesium hydroxide and calcium hydroxide are precursors for the preparation of MgO and CaO. Magnesium and calcium oxide nanoparticles are interesting basic oxides that have many applications such as superconductor materials, bactericidal agents,<sup>3</sup> and catalysts. One of the reported methods



for obtaining metal oxides is based on the sol-gel technique.<sup>4</sup> In many cases this method requires a hypercritical drying procedure and employs hazardous metal-organic precursors. Here we present an easy synthetic method of Mg(OH)<sub>2</sub> and Ca(OH)<sub>2</sub> nanoparticles, via the spontaneous hydrolysis of magnesium acetate or calcium acetate, in DMSO and DMF.<sup>5</sup> The formation of colloids was followed by fluorescence spectroscopy. The

best conditions for the preparation of nanosized crystals of Mg(OH)<sub>2</sub>, Ca(OH)<sub>2</sub> and their corresponding metal oxide nanoparticles are reported. All these nanoparticles were characterized by fluorescence and IR spectroscopies and XRD. The XRD patterns of Mg(OH)<sub>2</sub> obtained at room and at several temperatures are shown in Figure 1. The corresponding average particle size for Mg(OH)<sub>2</sub> is close to 15 nm. In the case of Ca(OH)<sub>2</sub> was 55 nm.

<sup>1</sup> P. K. Stoimenov, R. L. Klinger, G. L. Marchin, K. J. Klabunde, *Langmuir* **2002**, *18*, 6679-6686.

<sup>1</sup>V. Štengl, S. Bakardjieva, M. Maříková, P. Bezdička, J. Šubrt, *Magnesium oxide nanoparticles prepared by ultrasound enhanced hydrolysis of Mg-alkoxides*, *Materials Letters* 57 (2003) 3998.

<sup>1</sup>G. Rodriguez-Gattorno, P. Santiago-Jacinto, L. Rendon-Vazquez, J. Nemeth, I. Dekany, and D. Diaz\*. *Novel Synthesis Pathway of ZnO Nanoparticles from the Spontaneous Hydrolysis of Zinc Carboxylate Salts*. *J. Phys. Chem. B*, 107, (2003) 12597.

# A dynamic study of interaction between fragments unit (CH<sub>2</sub>) ions and fullerene (C<sub>60</sub>) molecule

**Irineo Pedro Zaragoza<sup>4</sup>, Roberto Salcedo<sup>1</sup>**

*Instituto de Investigaciones en Materiales, Departamento de Polímeros, Universidad Nacional Autónoma de México, Circuito exterior s/n, Ciudad Universitaria, Coyoacán 04510, México D.F., México.*

[ipzaragoza@iim.unam.mx](mailto:ipzaragoza@iim.unam.mx);

**Abstract:** The interaction between CH<sub>2</sub> and fullerene (C<sub>60</sub>) allows to suggest that there is an addition reaction mechanism for the procedure, this feature is studied by means of electronic properties analysis. In this interaction are shown different effects that arise as a consequence of the particular electronic characteristics. The addition or insertion of the methylene group gives place to a reaction in which the inclusion of CH<sub>2</sub> into a fullerene bond cause the formation of several geometrical deformations. The simulation was carried out by the using of the dynamic semiclassical Born-Oppenheimer approximation. Dynamical aspects are analyzed at different speeds for the interaction between the CH<sub>2</sub> group and the two bonds CC(6,6) and CC(6,5) on the rings of fullerene (C<sub>60</sub>). The calculations were all electron type employing DFT's using exchange and correlation functionals.

**Keywords:** fullerene, addition reaction, density functional theory, molecular dynamic.

---

**Properties of  $Gd_2O_3:Eu^{3+}, Tb^{3+}$  nanopowders obtained  
by the sol-gel process**

A. de J. Morales Ramírez<sup>2</sup>, A. García Murillo<sup>1</sup>, F. de J. Carrillo Romo<sup>1,2</sup>,

M. García Hernández<sup>2</sup>, J. Moreno Palmerin<sup>2</sup>

<sup>1</sup>*CICATA, Unidad Altamira – Instituto Politécnico Nacional*

<sup>2</sup>*Depto. de Ingeniería Metalúrgica - ESIQIE -Instituto Politécnico Nacional*

*amoralesra@ipn.mx*

One of interest application field for nanostructured materials is the X-ray medical imagery, being necessary the use of dense materials enable to absorb high energy photons. Additionally, an important requirement of these materials is the emission in the UV-Vis range by X-Ray excitation, which can be influenced by the particle size. Besides, europium doped gadolinium oxide is a well known red phosphor. Moreover, nanophosphors of  $Gd_2O_3$  codoped with  $Tb^{3+}$ ,  $Eu^{3+}$  increase their light yield by energy transfer between Tb and Eu. In this work,  $Gd_2O_3$  nanopowders codoped with  $Eu^{3+}$  and  $Tb^{3+}$  ( $Eu^{3+}$  2.5 % at.,  $Tb^{3+}$  0.001-0.01% at.) were obtained via a sol-gel process using gadolinium pentanedionate, europium and terbium nitrates as precursor and doping sources. In this work we report the influence of annealing temperature on the structure, morphology and luminescent properties of  $Gd_2O_3:Eu^{3+}, Tb$  by means of TGA, XRD, TEM and X-ray emission measurements.

# Effect of Optoelectronic Doping on the Phononic modes of ZnO Nanostructures: Correlation between Structural and Vibrational Properties

A. Escobedo-Morales and U. Pal

Instituto de Física, Benemérita Universidad Autónoma de Puebla, Apdo. Postal J-48, CP, 72570, Puebla, Pue., México. E-mail: aescope@sirio.ifuap.buap.mx

Zinc oxide (ZnO) is a potential material for applications in optoelectronic technology. Its wide band gap (3.37 eV) and chemical stability make it an ideal semiconductor to fabricate light emitting devices. Through selective doping its physical properties can be modified drastically. However, understanding the role of intrinsic and extrinsic

defects on the physical properties of ZnO remains incomplete. Here we present a study of the effect of indium, antimony, and gallium doping on the phononic modes of hydrothermally grown ZnO nanostructures through Raman spectroscopy. Effect of doping on the structure and crystallinity of the materials are studied by X-ray diffraction.

It was observed that incorporation of doping elements sometimes introduces additional vibrational modes attributed to secondary phases like  $\text{In}(\text{OH})_3$  or  $\text{Sb}_2\text{O}_3$  along with some anomalous

modes not related to such secondary phases. However, those secondary phases can be successfully dissociated by thermal annealing at adequate conditions. The annealing process and doping content have strong effect on vibrational properties of the nanostructures. Vibrational properties of the nanostructures are correlated with their structural properties.

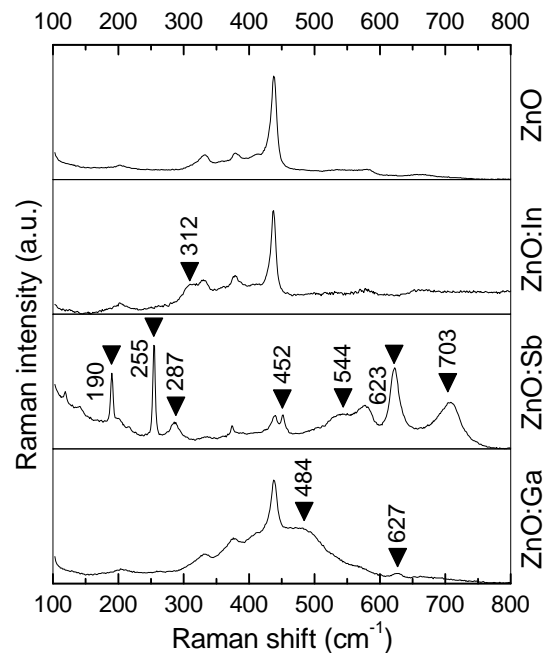


**Figure 1.** Raman spectra of as-grown heavily doped and undoped samples.

*\*The work was partially supported by VIEP-BUAP (Grant # VIEP/EXC/93/2008-1), Mexico.*

## **Synthesis of LiCoO<sub>2</sub> compound nanoparticulated by sol-gel acrylamide polymerization and microwave**

V. H. Ortiz-Iturbe, A. Ibarra-Palos, E. Chavira, C. Flores-Morales

*Instituto de Investigaciones en Materiales, Universidad Nacional Autónoma de México,  
Circuito Exterior s/n, Ciudad Universitaria, Coyoacán, Apdo. Postal 70-360, México D.F.  
04510*

E-mail: victor\_hoi@hotmail.com

The secondary lithium batteries exhibit the highest specific energy among the rechargeable batteries. The LiCoO<sub>2</sub> compound is a good material for positive electrode in lithium-ion batteries. This material displays favourable attributes that include: good power rates, low self-discharge, good capacity, and excellent cycle life. The solid-state synthesis is the technique most used, to obtain polycrystals.

In this work, we have adopted the sol-gel acrylamide polymerization method for the synthesis of nanoparticles material. By microwave radiation it was apply to obtain the corresponding xerogel. Thermogravimetric analyses were done to know the best reaction temperature to yield the nanoparticulated compound. Using the sol-gel acrylamide polymerization method; it is possible to obtain the crystalline phase at lower temperature reported by solid-state synthesis. We employ temperatures around 550 °C for several hours.

The nanocrystals of the resulting materials retain homogeneity on a nanometric scale, 80 – 120 nm. The materials synthesized by sol-gel acrylamide polymerization technique were characterized by X-Ray powder Diffraction, Transmission Electronic Microscopy and Scanning Electronic Microscopy.

This work has a partial finance support from CONACyT CB-2005-01-48883 and PAPIIT IN109308. The authors acknowledge to E. Fregoso-Israel and O. Novelo for technical support, and were PUNTA-UNAM members.

# Synthesis of metallic bismuth nanoparticles by colloidal dispersion

*Selene R. Islas-Sánchez, Silvia E. Castillo-Blum\*, David Díaz*

Depto. de Química Inorgánica, Facultad de Química, Universidad Nacional Autónoma de México, Coyoacán, México D.F. 04510 México.

\* Corresponding author: blum@servidor.unam.mx

Metal nanoparticles play important roles in several areas by virtue of their unusual chemical and physical properties, different from those of the bulk metal. Bismuth has a small energy overlap between the conduction and valence bands, highly anisotropic Fermi surface and small effective electron mass, a long carrier mean free path [1, 2]. In this work, we describe a new method for the synthesis of Bi nanoparticles using organic solvents: DMF, ethylene glycol and ethanol. The reaction is at room temperature,  $\text{Bi}^{3+}$  is reduced ( $\text{Bi}(\text{CH}_3\text{COO})_3$ ) with sodium borohydride ( $\text{NaBH}_4$ ) in the presence of ethylenediamine ( $\text{C}_2\text{H}_8\text{N}_2$ ) or pyridine ( $\text{C}_5\text{H}_5\text{N}$ ) as capping agents. The bismuth nanoparticles were precipitated and collected by centrifugation, since the bismuth colloids obtained are lyophobic. The black powder isolated was purified by washing with ethanol, methanol and a mixture of water-acetone 1:2. The diffractograms match with the hexagonal structure of bismuth (JCPDF 44-1246). The nanoparticles coated with ethylenediamine are smaller than those with pyridine. The HR-TEM micrographs indicate that mean particle diameter is about 10 nm.

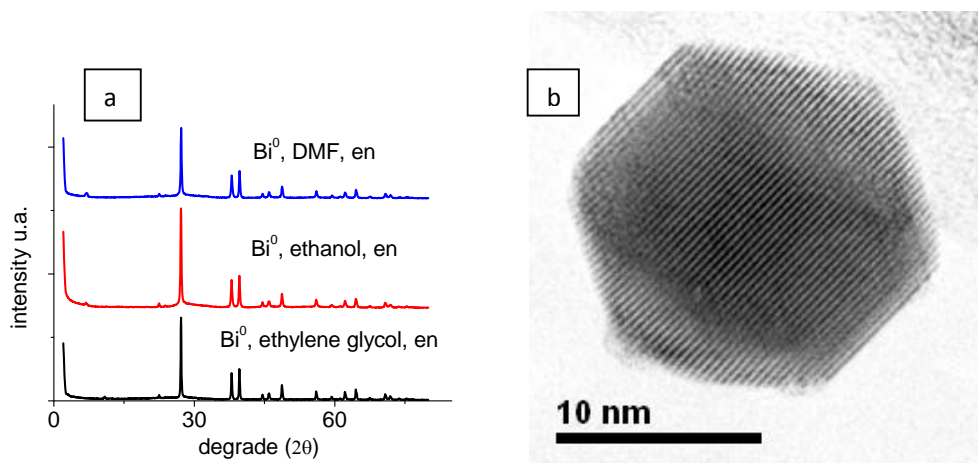


Fig. 1 a) XRD pattern of bismuth nanoparticles using from different solvents and b) HR-TEM micrograph of an isolated bismuth nanoparticle.

Acknowledgment. This work was supported by PAPIIT- UNAM IN100907.

## Reference

- [1] JY Fang, KL Stokes, WLL Zhou, et al., Chem. Commun. 18: 1872-1873 (2001).
- [2] Y. B. Zhao, Z. J. Zhang and H.X. Dang, Mater. Lett. 58 (5):790-793 (2004).

# **ESTUDIO DE OPTIMIZACIÓN DE NANOESTRUCTURAS DE CeO<sub>2</sub>, La<sub>2</sub>O<sub>3</sub> Y FASES MIXTAS OBTENIDAS APLICANDO LA SÍNTESIS HIDROTÉRMICA**

R. RANGEL<sup>1</sup>, k. ARREOLA<sup>1</sup>, P. BARTOLO-PÉREZ<sup>2</sup>

*1FACULTAD DE INGENIERÍA QUÍMICA, UNIVERSIDAD MICHOACANA DE SAN  
NICOLÁS DE HIDALGO, EDIFICIO "K", CIUDAD UNIVERSITARIA. 58060,  
MORELIA, MICHOACÁN, MÉXICO.*

*2CINVESTAV-IPN UNIDAD MÉRIDA, DEPARTAMENTO DE FÍSICA DE  
MATERIALES. MÉRIDA, YUC. MÉXICO*

El presente trabajo corresponde a la síntesis de nanoestructuras de óxidos de lantano o cerio, obtenidos a partir de sales que contienen a estos elementos. Para lograr la optimización de su producción se aplicó un diseño factorial de dos niveles. Estas nanoestructuras se obtuvieron mediante síntesis hidrotérmica en un microreactor en donde las variables en estudio fueron el pH, la temperatura y el tiempo de síntesis. Como resultado de esta síntesis se obtuvieron diversas nano estructuras tales como nano barras, nanotubos, nano alambres, etc. Posteriormente se caracterizaron mediante las técnicas de microscopía electrónica de transmisión (TEM), microscopía electrónica de barrido (SEM), espectrometría de rayos x por dispersión de energía (EDS), difracción de rayos x (XRD). Como resultado de este estudio se establecieron las condiciones para el crecimiento de algún tipo de nano estructura en particular.

## **A comparative study of nano-structured iron oxide films prepared by spray pyrolysis and laser ablation**

M.A. García-Lobato<sup>1</sup>, A.I. Martínez<sup>1,\*</sup>, R. Castro-Rodríguez<sup>2</sup>, D. Bueno-Baques<sup>3</sup>

*1 Cinvestav Unidad Saltillo, Carr. Saltillo-Mty Km 13, Ramos Arizpe Coahuila 25900, México.*

*2 Departamento de Física Aplicada, Cinvestav Unidad Mérida, 97310 Mérida Yucatán, México.*

*3 Centro de Investigación en Química Aplicada, Blvd. Enrique Reyna Herosillo 140, Apto, Postal 379, Saltillo, Coah, 25100, México.*

\* arturo.martinez@cinvestav.edu.mx

Iron oxide exhibits a great variety of polymorphs, these oxides are present in a great variety of settings, ranging from geological such as the earth minerals and in the surface of Mars, to new technological applications; they are also found in living beings such as in the brains of pigeons and the antennas of ants. Nanostructured iron oxide thin films are used in magnetoresistance devices, electrochromic and photo-electrochemical devices and as solar radiation filters [1-2]. The aim of this work is to study the nanostructured thin films of three different iron oxide polymorphs, namely hematite, maghemite and magnetite prepared by both spray pyrolysis and laser ablation. By spray pyrolysis varying the substrate temperature and the precursor salt, maghemite and hematite films were prepared at substrate temperatures ( $T_s$ ) ranging from 250 °C to 450 °C, the formation of nanostructured hematite films is promoted at higher  $T_s$  with a relative flat surface; lower temperatures promotes the formation of maghemite with a granular flake-shaped surface. Otherwise, by laser ablation from different iron oxide targets the formation of iron/magnetite mixtures and pure magnetite films is encouraged under chamber pressures near to the base pressure. At oxygen partial pressures ranging from 10 to 30 mTorr and  $T_s$  from room temperature to 350 °C, the formation of either maghemite or hematite nanostructured films were done, the proportion of one over the other depends on the substrate temperature, promoting the formation of hematite at higher pressures and higher temperatures. The characterization techniques used to correlate the magnetic, optical, structural, and morphological properties include the scanning electron microscopy, vibrating sample magnetometry, UV-vis-NIR and Fourier transform IR spectroscopy, and X-ray diffraction. The study of these iron oxide thin films is useful for the design of solar radiation filters.

[1] T. Tepper, C.A. Ross, J. Appl. Phys., **91** (2002) 4453.

[2] J.P. Hong, et al., Appl. Phys. Lett., **83** (2003) 1590.

## **Sol-gel synthesis and Structural Properties of Europium Doped Gadolinium Oxide Glass Nanoceramic Powders**

**I. Ponce<sup>1</sup>, A. Murillo<sup>1</sup>, F. Carrillo<sup>1</sup>, E. de la Rosa<sup>2</sup>, H. Terrones<sup>3</sup>**

<sup>1</sup>Centro de Investigación en Ciencia Aplicada y Tecnología Avanzada-Instituto Politécnico Nacional, Km 14.5 Carr. Tampico-Pto. Industrial, C.P.89600 Altamira, Tamps, México.

<sup>2</sup>Centro de Investigaciones en Óptica, A. C., Loma del Bosque 115, Col. Lomas del Campestre, C. P. 37150, León, Gto., México.

<sup>3</sup>Instituto Potosino de Investigación Científica y Tecnológica, Camino a la Presa San José 2055. Col. Lomas 4 sección C. P. 78216, San Luis Potosi. S.L.P., México

E-mail: iponcem0600@ipn.mx

Gd<sub>2</sub>O<sub>3</sub> is a useful host material because its crystallographic structure is a well-known host lattice for efficient phosphors. Eu-doped Gd<sub>2</sub>O<sub>3</sub> particles are excellent red-emission phosphors for display and lamp applications. Nowadays, there is a continuous searching to develop new routes of synthesis allowing a convenient configuration to optimize these scintillating properties with a better control sizes and morphology of the obtained powders. Sol-gel route offers different advantages to produce glass ceramics with high purity and homogeneity at lower temperatures and lower cost than conventional process. Therefore the aim of this study is the synthesis of Gd<sub>2</sub>O<sub>3</sub>:Eu<sup>3+</sup> nanocrystallites embedded in silica gel glass to obtain a lower cost matrix and efficient phosphor material. The Gd<sub>2</sub>O<sub>3</sub>:Eu<sup>3+</sup> powders were synthesized by the sol-gel method using gadolinium acetate, methanol, acetic acid and water as starting precursors, and europium nitrate as doping agent; silica precursor solution was prepared using tetraethylorthosilicate (TEOS), ethanol and water. Both nanoceramic Gd<sub>2</sub>O<sub>3</sub>:Eu<sup>3+</sup> powders and SiO<sub>2</sub> solution were mixed to obtain the glass ceramic matrix. The powders were thermally treated at different temperatures in order to promote the densification process and crystallinity. The evolution of organic compounds during the annealing process was studied with FTIR spectroscopy. Structural properties and morphology of the gadolinium-based ceramics embedded in silica were analyzed by XRD and HRSEM techniques. Luminescent properties of the powders were evaluated using a 254 nm excitation source, obtaining characteristic red Eu<sup>3+</sup> luminescence emission at 611 nm.

The authors thank Daniel Ramírez González for SEM measurements.

# Sol-gel BaTiO<sub>3</sub>:Er<sup>3+</sup> and BaTiO<sub>3</sub>:Yb<sup>3+</sup> powders and films: Chemical and structural studies

M. García Hernández, A. García Murillo, F. de J. Carrillo Romo,  
L. A. Cruz Santiago, A. Garrido Hernández

Centro de Investigación en Ciencia Aplicada y Tecnología Avanzada (CICATA) Unidad  
Altamira – IPN Altamira, Tamaulipas; México CP 89600

[margarciah@ipn.mx](mailto:margarciah@ipn.mx)

## Abstract

Barium titanate (BaTiO<sub>3</sub>) is a well-known material because of its good properties, such as its high dielectric constant, high charge storage capacity, good insulating properties, its chemical and physical stability and its excellent optical transparency in the visible range. Recently, in a previous work it was found that Yb<sup>3+</sup> and Er<sup>3+</sup> doped BaTiO<sub>3</sub> systems increase its optical properties.<sup>1</sup> The final shape of the material as films or powders can also affect the crystal structure which is strongly related with the particle grain size. Therefore, the luminescent properties exhibited by films constituted by particles with fine particle sizes could improve these properties. The sol-gel process was the route selected to synthesize rare earth ions (Er<sup>3+</sup> or Yb<sup>3+</sup>) doped BaTiO<sub>3</sub> system due to its numerous advantages as lower sintering temperatures than those required for direct fusion or solid state reactions, high homogeneity and purity, versatility to shaping materials as the elaboration of optical quality films. In this work, soft chemistry route and dip-coating technique has been successfully used to obtain rare-earth activated BaTiO<sub>3</sub> powders and films from barium pentanedionate [Ba(CH<sub>3</sub>COCHCOCH<sub>3</sub>)<sub>2</sub>] and titanium isopropoxide [Ti(OCH(CH<sub>3</sub>)<sub>2</sub>)<sub>4</sub>] as starting materials. The powders and films were heat-treated in a temperature range from 700 °C to 1150 °C in order to study the structural evolution. Chemical and structural properties of derived materials were investigated using infrared spectroscopy (FT-IR) revealing the presence of typical the Ti-O vibrations in BaTiO<sub>3</sub> at 565 cm<sup>-1</sup> and 414 cm<sup>-1</sup>. Structural studies carried out on earth rare doped BaTiO<sub>3</sub> powders and films showed that the characteristic diffraction peaks of cubic started at 700 °C remaining stable up to 1150 °C. The results are presented and discussed.

<sup>1</sup> M.A. Meneses-Nava et al., Opt. Mater. (2008), doi:10.1016/j.optmat.2008.04.002

# **Influence of Precursor Chemistry on the Formation of BaTiO<sub>3</sub> Ceramic Powders**

C. Damiani, A. García Murillo, F. Carrillo Romo, M. García Hernández

Centro de Investigación en Ciencia Aplicada y Tecnología Avanzada-Instituto Politécnico Nacional, Km 14.5 Carr. Tampico-Pto. Industrial, C.P.89600 Altamira, Tamps, México.

E-mail: damiani\_@hotmail.com

Nanocrystalline BaTiO<sub>3</sub> powders were prepared by sol-gel method. The influence of the starting materials on the processing, microstructure, and purity of the prepared systems has been studied using barium acetate and two different sources of titanium as tetrabutyl titanate and titanium tetraiso-propoxide was also investigated taking into account several molar ratios in function of the barium precursor (barium acetate). For the barium acetate and tetrabutyl titanate, BaTiO<sub>3</sub> powders were synthesized using (acac)H/Ba= 4/1 and H-(OAc)/Ba= 52/1, for titanium tetraiso-propoxide H<sub>2</sub>O/Ba= 40/1, PrOH/Ba= 40/1, (acac)H/Ba= 1/1 and H-(OAc)/Ba= 18/1. The decomposition process and the crystallization behavior were studied by FT-IR and XRD. BaTiO<sub>3</sub> powders synthesized with the above conditions reveal high purity ceramic and the small amount of barium carbonate phase. The high transformation temperature of this phase to the perovskite influence the crystallization and densification process of the obtained titanate ceramic powders.

# Nano-pigments: synthesis, characterization and performance

A. Fernández-Osorio<sup>1</sup>, L. Serrano<sup>2</sup>

<sup>1</sup> FES Cuautitlán Universidad Nacional Autónoma de México

<sup>2</sup> Ferro Mexicana, S.A. de C.V.

\* A. Fernández-Osorio; e-mail: ana8485@servidor.unam.mx

## Abstract

The ceramic pigments with particle size in the nanoscale have a massive potential market, because of their high surface area, which assures higher surface coverage, higher numbers of reflectance points and hence improved scattering. In this work, zirconium titanate doped with 0.2 mol % of Ni and Co and Zircon ( $ZrSiO_4$ ) doped with 0.4 mol% of Co were synthesized by the polymeric precursor method and their structural (XRD, HRTEM), optical (spectroscopy UV-Vis) and technological properties were determined to assess their potential use as ceramic pigments. Zirconium titanate can be coloured with first row transition elements, giving green and greenish yellow (Co and Ni). Zircon can be coloured with Co giving violet colour. The nano-pigments were dispersed in several ceramic glazes and glassy coatings and their colour performance compared with that of conventional micro-pigments.

## References

M. Dondi, F. Matteucci, I.Zama, G. Cruciani, Mater.Res.Bull. 42(2007)64-76

E.Ozel, S.Turan, J. Eur. Ceram. Soc., 27(2007) 1751-1757

Cavalcante P.M.T., Dondi M., Guarini G., Raimondo M., Baldi G., Dyes & Pigments 80(2009) 226-232

# **Structural and morphological properties of polycrystalline BaTiO<sub>3</sub>:Er<sup>3+</sup>, Yb<sup>3+</sup> ceramics synthesized by the sol-gel route: Influence of chelating agents**

J. Duval Lara<sup>1</sup>, J. C. Badillo Avilés<sup>1</sup>, García Hernández<sup>1</sup>, A. García Murillo<sup>1</sup>, F. Carrillo Romo<sup>1</sup>, J. Ramírez Salgado<sup>2</sup>, H. Terrones<sup>3</sup>

Mail: [jduvall0800@ipn.mx](mailto:jduvall0800@ipn.mx)

<sup>1</sup>*Centro de Investigación en Ciencia Aplicada y Tecnología Avanzada, U. Altamira-IPN Km. 14.5 Carretera Tampico-Puerto Industrial, C.P. 89600, Altamira, Tamaulipas, México.*

<sup>2</sup>*Programa de Ingeniería Molecular, Instituto Mexicano del Petróleo, Eje Lázaro Cárdenas No. 152, CP 07730, México D.F., México*

<sup>3</sup>*Instituto Potosino de Investigación Científica y Tecnológica, Camino a la Presa San José 2055. Col. Lomas 4 sección San Luis Potosí, S.L.P. México*

## **ABSTRACT**

The synthesis of co-doped BaTiO<sub>3</sub>: Er, Yb compound was investigated using alkoxide precursors using Sol-gel process. Ba (C<sub>5</sub>H<sub>7</sub>O<sub>2</sub>)<sub>2</sub> and Ti (OPr<sup>i</sup>)<sub>4</sub> were hydrolyzed under specific conditions and using [(acac) H and H-(OAc)] as complexing agents. The synthesis used allowed the elaboration of nano-size powders and films of perovskite compounds with and without complexing agents. The nanostructure materials were formed through nucleation-aggregation growth. Comparing co-doped BaTiO<sub>3</sub>: Er, Yb compounds with and without complexing agents, it was found important differences in particle shapes and sizes. In addition, the use of complexing agents during sol-gel process allowed the production of optical BaTiO<sub>3</sub>: Er, Yb thin films. The obtained results could indicate that the particle size and shape could be tailored in the current system by tailoring the simultaneous use of complexing agents and the calcination temperature; consequently a wide range of synthesizable particle size has an effect on the crystal structures.

## **ACKNOWLEDGEMENTS**

The authors gratefully acknowledge the financial support of this work by the SIP-IPN and SEP-CONACYT 47279, 59408, SIP-20082247, 20082502 Projects, respectively. The authors would also thank Daniel Ramirez Gonzalez from IPICYT for his help in the scanning electron microscopy.

# Synthesis of Carbon Nanotubes Via Microwave Heating

G. Rueda-Morales, G. Ortega-Cervantez,

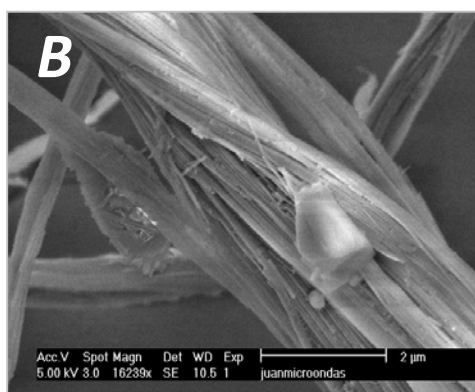
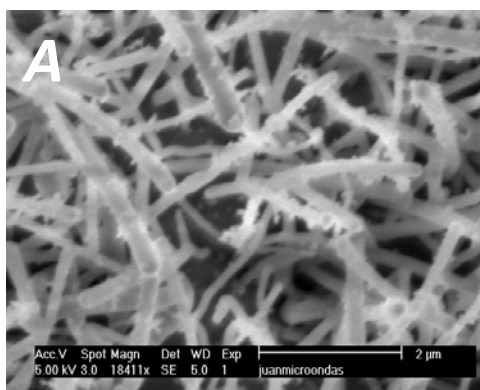
J. Ortiz-López and J.J. Vivas-Castro

*Escuela Superior de Física y Matemáticas, Instituto Politécnico Nacional*

*Edificio 9, UPALM-Zacatenco, 07738 México D.F., Mexico*

Email: [gruedamorales@yahoo.com.mx](mailto:gruedamorales@yahoo.com.mx)

Carbon nanotubes (CNTs) were synthesized with microwave irradiation heating with a domestic microwave-oven using metal acetate mixed with graphite powder. The mixture is placed inside an evacuated and sealed quartz tube and heated for 120 min. Present samples with (Fig. **A**) and without (Fig. **B**) thermal treatment for 5 min. a 800°C previous to microwave irradiation. Figure **A** shows an image of CNT “ropes” with approximate diameter 25nm. Figure **B** shows a disordered array of CNTs with diameters in the range 25 to 150nm. The obtained samples were characterized and studied by SEM and STEM.



## **Hybrid epoxy resin –silica coatings**

E. Rubio-Rosas, Itzcua G., Varela J. and V. Rodríguez-Lugo

<sup>1</sup>Centro Universitario de Vinculación, BUAP, Ciudad Universitaria,

72570, Puebla, Puebla, MÉXICO.

E-mail: efrainrubio@yahoo.com

In this work, a series of hybrid epoxy resin-silica coatings were successfully prepared. First of all, a colloidal solution were obtained by performing the conventional acid-catalyzed sol-gel reactions of tetraethyl orthosilicate (TEOS), which acts as acceded sol-gel precursor in the presence of a silane coupling agent. Subsequently, a series of hybrid solution were prepared by performing in situ thermal ring-opening polymerization reactions of epoxy resin in the presence of as-prepared colloidal solution. Finally the hybrid material was supported in the form of coating by a dip-coating procedure on glass substrate. According to SEM observations, the coatings present a plane surface free of fractures with a thickness average of 15  $\mu\text{m}$ . On the other hand, the adhesion and wear test, indicates that the coating with 50 percent silica weight presents bigger resistance to the ware and the best adhesion in glass.

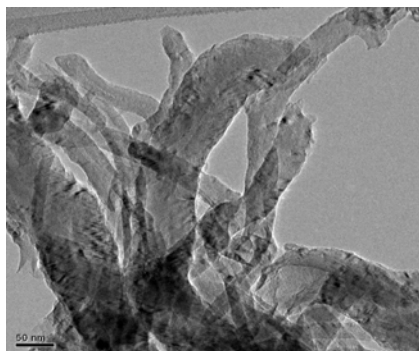
## SYNTHESIS OF NANOFIBERS OF CARBIDES Ni- Mo IN MESOPOROUS SILICATES

Adriana Isabel Reyes de la Torre\*<sup>1</sup>, Benjamín Portales Martínez, José Manuel Domínguez Esquivel<sup>1</sup>, Nicolás Cayetano Castro<sup>1</sup>, Carlos Ángeles Chávez<sup>1</sup>, José Aarón Melo Banda<sup>2</sup>

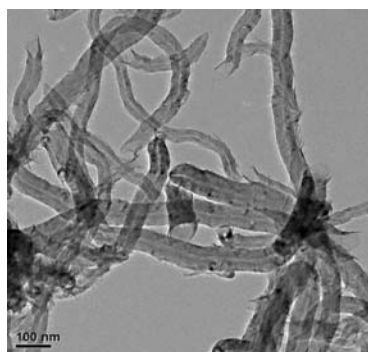
<sup>1</sup>*Instituto Mexicano del Petróleo, Programa de Ingeniería Molecular, 152 Eje Central L. Cárdenas, C.P. 07730 México D. F. Tel. 01 (55) 91758180. e-mail: [aireyes@imp.mx](mailto:aireyes@imp.mx) o [airt22@hotmail.com](mailto:airt22@hotmail.com)*

<sup>2</sup>*Instituto Tecnológico de Ciudad Madero, Juventino Rosas y Jesús Urueta S/N Col. Los Mangos, C.P. 89440, Cd. Madero, Tamps.*

The mesoporous silicates MCM-41 and SBA-15 are of interest for adsorption and catalysis because their textural properties, i.e., pore size between 35 and 50 Å and surface areas of about 1000 m<sup>2</sup>/g. These material are being investigated as support and catalysts for the processing of complex hydrocarbons<sup>1</sup>. However a low hydrothermal stability and structural degradation in presence of water have limited further applications. Thus, this work explores the structural reinforcement of the silicate walls of mesoporous MCM41 and SBA-15 material by means of coating with polymeric carbon, wich can modify their physicochemical properties as well. These materials were prepared at room temperature. The mesoporous materials were intercalated with acrylonitrile monomer (AN) and polymerized using benzoyl peroxide as the initiator (catalyst) then were pyrolized in inert atmosphere (N<sub>2</sub>) at 1000 °C. These composite materials were used as support of metallic Ni and Mo , wich were calcined over 500 °C to form the metal oxides, then futher treatments under hydrogen and methane were applied to obtain nanofibers of metallic carbides. This materials were characterized by SEM, TEM, DRX, and BET.



**NiMoC/MCM41-PAN-P by TEM**



**NiMoC/SBA15-PAN-P by TEM**

### References:

- 1) Ledoux M. J., Pham C., Guille J., Dunlop H., Journal of Catalysis, 134, (1992), 383.

# Chemical reactivity study of Fe<sub>2</sub>O<sub>3</sub> and Fe<sub>3</sub>O<sub>4</sub> nanostructures by DFT

B. Ruiz-López<sup>1</sup>, R. Esparza<sup>2</sup>, E. Rubio-Rosas<sup>1</sup>, R. Pérez<sup>2</sup> y V. Rodríguez-Lugo<sup>1</sup>

<sup>1</sup>Centro Universitario de Vinculación, BUAP, Ciudad Universitaria,

72570, Puebla, Puebla, MÉXICO.

<sup>2</sup>Instituto de Ciencias Físicas, UNAM, P. O. Box 48-3, 62251, Cuernavaca, Mor., MÉXICO.

E-mail: efrainrubio@yahoo.com

Heaviest and most polar fraction of the crude oil is called asphaltenes, and is cause of different problems during crude oil production. In a previous work, by STEM and HRTEM analysis was possible to detect the presence of Fe<sub>2</sub>O<sub>3</sub> crystalline nanoparticles inside the asphaltene obtained from Mayan petroleum. For the characteristics of these nanoparticles, is possible their participation in the mechanisms of aggregation, flocculation and deposition of the asphaltenes; in this sense, is of particular interest the study of the reactivity of Fe<sub>2</sub>O<sub>3</sub> nanostructures by DFT. The first obtained results show that the Fe<sub>2</sub>O<sub>3</sub> nanostructures has a bigger electrostatic answer (electrophilic fields) in surfaces {111} rich in Fe, that in surfaces {100} rich in O<sub>2</sub>. This answer originates a bigger absorption of characteristic functional groups of the asphalts like carboxylic, ketone, aldehydes, etc.

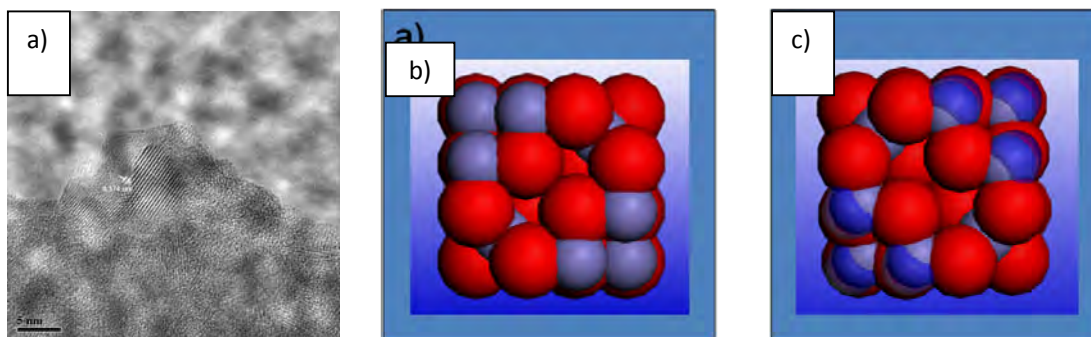


Figure 1. a) HRTEM Image of a crystalline nanoparticle present in the asphaltene. b) Fe<sub>2</sub>O<sub>3</sub> cluster, c) Electrophilic fields (Fukui functions, calculated to 0.0035 eV)

## Molecular simulation of thiol -functionalized carbon nanotubes

R. Rivera<sup>1</sup>, R. Esparza<sup>2</sup>, E. Rubio-Rosas<sup>1</sup>, R. Pérez<sup>2</sup> y V. Rodríguez-Lugo<sup>1</sup>

<sup>1</sup>Centro Universitario de Vinculación, BUAP, Ciudad Universitaria,

72570, Puebla, Puebla, MÉXICO.

<sup>2</sup>Instituto de Ciencias Físicas, UNAM, P. O. Box 48-3, 62251, Cuernavaca, Mor., MEXICO.

E-mail: efrainrubio@yahoo.com

Nanotube functionalization is a field of active investigation with innovations every week and other hand the problems of water shortages and lack of access to clean water have been and will continue to grow as major global problems. To alleviate these problems, water purification technologies are being updated. In previous work, was explored the potential of carbon nanotubes for use in decontamination. Thus, removal of hexavalent chromium from aqueous solutions by carbon nanotubes functionalized with thiols was studied. In the present work is of particular interest the study of the interaction of thiol functionalized nanotubes with different metal ions like Hg, Pb, Cr by DFT. Previous to thiol functionalization were determined the molecular orbital and electrostatic potential of the different carbon nanotubes (armchair and zigzag) to obtain the most appropriate places for the functionalization.

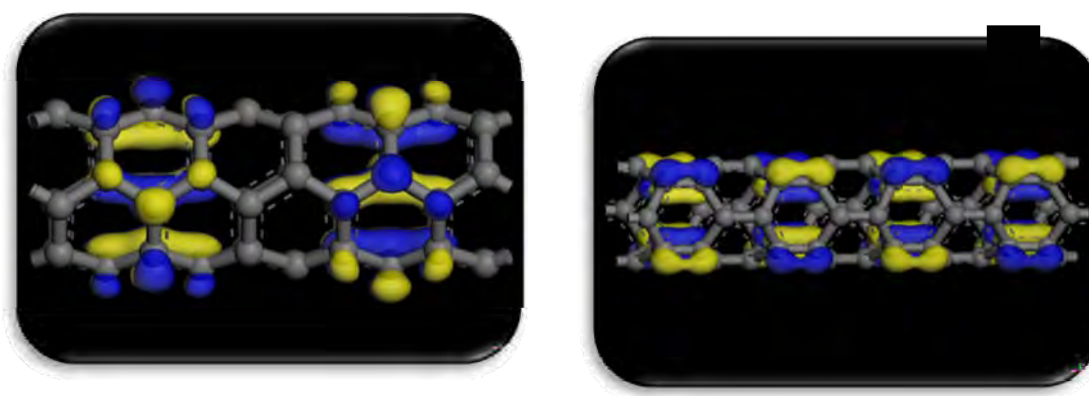


Figura 1. a) HOMO and LUMO orbital of armchair carbon nanotube. b) HOMO and LUMO orbital of zigzag carbon nanotube.

## **Reactive block copolymers as versatile compatibilizers for polymer-clay nanocomposites**

*Leticia Flores-Santos, Alberto Rosas-Aburto, Alfonso González-Montiel,  
María Dolores Baeza-Alvarado, Edgar Espinoza-Rodríguez*

*and Pablo Esparza-Hernández*

*<sup>a</sup> CID, Centro de Investigación y Desarrollo Tecnológico S.A. de C.V., Lerma, Mexico.*

It's well known that silicate-polymer nanocomposites offer a number of significant advantages over traditional silicate-polymer composites. Polymer nanocomposites can reach high tensile strength, improved heat deflection temperature and flame retardance, with typically 3-5 wt.% of the nanofiller (compared to 10-50%wt in the case of traditional fillers), producing materials with specific gravity close to that of the unfilled polymer, good surface appearance and better processability. Other properties of nanocomposites such as optical clarity and improved barrier properties cannot be duplicated by conventionally-filled resins at any loading [1]. The most common nanoclays used in polymer nanocomposites are montmorillonite and hectorite [2].

In order to obtain these improved properties an excellent dispersion or exfoliation is essential, but it's usually difficult to achieve. The present work covers the use of a series of block copolymers synthesized via CRP to enhance the dispersion and or exfoliation of nanoclays in thermoplastic or thermoset resins. The block copolymers can either be used with existing, commercially-available clays, or it can be designed as an intercalant in producing a clay nanocomposite material. The CRP technique allows fine tuning the molecular weight, the amount of functional groups and the composition of blocks, in order to obtain an optimal performance between nanofiller and the polymer. A selection of their performance as compatibilizers in several polymer-clay systems will be addressed, and a correlation of the mechanical properties with the intrinsic variables of the compatibilizer (Mn, composition, etc.) is discussed.

In summary our main result show that montmorillonite modified with the amphiphilic block copolymers is completely exfoliated and shows higher degradation temperatures compared with commercially available organoclays. This is a promising strategy for the preparation of polyolefin/clay nanocomposites, eliminating the use of maleated polypropylene and opening the possibility of using montmorillonite as nanofiller for engineering polymeric matrices.

### **References:**

- [1] P. C. LeBaron, Z. Wang, and T. J. Pinnavaia, "Polymer-layered silicate nanocomposites: an overview," *Applied Clay Science*, vol. 15, pp. 11-29, April 12 1999.
- [2] Q. H. Zeng, A. B. Yu, G. Q. (Max) Lu, and D. R. Paul, "Clay-Based Polymer Nanocomposites: Research and Commercial Development," *Journal of Nanoscience and Nanotechnology*, pp. 1574-1592, 2005.

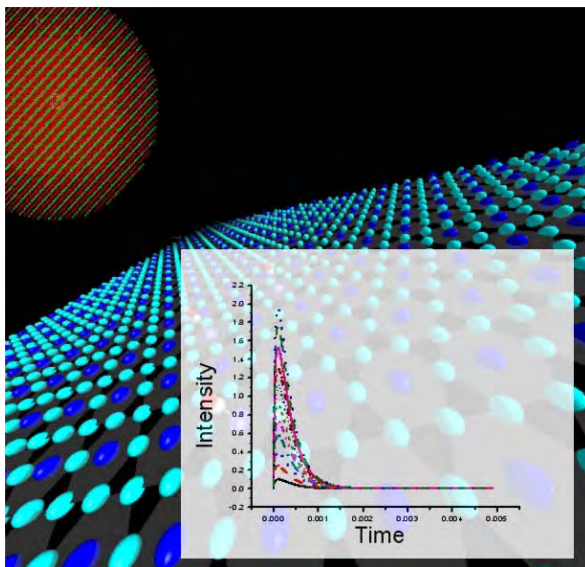
# Size and shape effect on the visible and NIR fluorescence lifetimes of nanocrystalline upconversion phosphors.

O. Meza<sup>1</sup>, and L. A. Díaz-Torres,<sup>1</sup>

<sup>1</sup>Centro de Investigaciones en Optica, A. P. 1-948, León Gto. 37160, Mexico

Mail: octaviome@cio.mx

Frequency upconversion of NIR into visible VIS light in RE doped nanocrystals has been investigated intensively due to their potential applications such as color display, optical



storage, optoelectronics, and medical applications. One of the most important parameters on luminescent materials optimization is the lifetime. One of the traditional tools to study the lifetime dependence in a dielectric crystal is solving the General Energy Transfer Master Equations (GETME) that governs the dynamics of the excitation energy among the active ions within the crystal. In this work, we study the lifetime (NIR and VIS)

as a function of size and nanocrystal shape. Our model predicts that for nanocrystallite sizes over 10 nm the luminescence life time behave has in the micro and bulk systems.

# Upconversion dynamics of the red and green emissions in $\text{ZrO}_2\text{:Er-Yb}$ nanocrystals

O. Meza,<sup>1</sup> D. Solis,<sup>1</sup> E. de la Rosa,<sup>1</sup> L. A. Díaz-Torres,<sup>1</sup> P. Salas,<sup>2</sup>

<sup>1</sup>*Centro de Investigaciones en Optica, A. P. 1-948, León Gto. 37160, Mexico*

<sup>2</sup>*Centro de Física Aplicada y Tecnología Avanzada, Universidad Nacional Autónoma de México, A.P. 1- 1010, Querétaro, Qro. 76000, Mexico*

Mail: octaviome@cio.mx

Nanocrystalline  $\text{ZrO}_2\text{:Er-Yb}$  phosphors are promising NIR to VIS upconversion emitters with applications in flat panel displays, medical biolabeling, white light generation, etc.  $\text{ZrO}_2\text{:Er-Yb}$  presents favorable photoluminescent properties as well as an ease of synthesis in the nanometer regime. In particular, these nanophosphors present color and lifetime tunability depending on concentration ratio of Yb to Er dopants. Such color tunability has been addressed as the consequence of at least to non-radiative energy transfer processes: Er cross relaxation and Er to Yb back energy transfer. Both processes are concentration dependent, the former on Er concentration and the later on Yb concentration. Here we present a rate equation model that predicts both the green to red fluorescence ratio and the fluorescence life time of the upconverted emissions. Under stationary conditions it is possible to predict with excellent agreement the red to green ratio. The presented model allows a quantification of both the cross relaxation and the back transfer coefficients. The competition among both processes is discussed, and a possible criterion to tune the overall luminescence color by carefully controlling the Yb to Er concentration is proposed.

# Detection and Light Enhancement by means of Porous Silicon Devices

G. Palestino<sup>a\*</sup>, V. Agarwal<sup>b</sup>, E. Pérez<sup>c</sup>, C. Gergely<sup>d</sup>.

<sup>a</sup>Facultad de Ciencias Químicas, Universidad Autónoma de San Luis Potosí, México;

<sup>b</sup>CIICAP-UAEM, Av. Universidad 1001, Col Chamilpa, Cuernavaca, Mor., México;

<sup>c</sup>Instituto de Física, Universidad Autónoma de San Luis Potosí, SLP, México

<sup>d</sup>GES-UMR 5650, CNRS- Université Montpellier II, Montpellier Cedex 5, France;

*palestinogabriela@fcq.uaslp.mx*

There is a great need for the development of easy-to-use, sensitive, robust and inexpensive biosensor for the detection and identification of biological substances. Porous silicon microcavity (PSiMc) is a versatile structure with a number of optical properties that can be used for biosensing applications. A PSiMc structure is characterized by a narrow resonance peak in the optical spectrum that is very sensitive to a small change in the refractive index, such as that obtained when a molecule is attached to the large internal surface of porous silicon. In this work we demonstrate the usefulness of this microcavity resonator structure as a biosensor. The obtained results reveal the penetration of the biomolecule into the central layer of the structure is necessary to obtain a microcavity optical response. However the dependence of the sensor sensitivity is strongly dependent on the pore size. Fluorescent emission of glucose oxidase (GOX) immobilized into PSi structures has been monitored by epifluorescent microscopy and enhanced light intensity has been observed when the supporting substrate of the protein was the microcavity, compared to monolayer, or mirror structure.

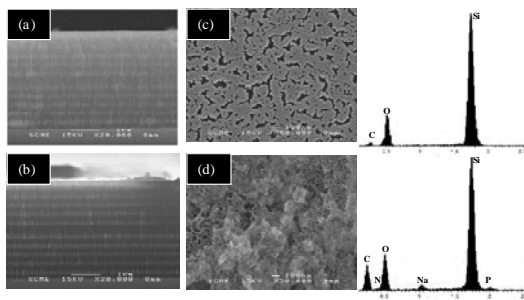


Fig 1. Cross-sectional and top view scanning electron microscopy (SEM) images before (a), (b) and after (c), (d) Silane-Glutaraldehyde-Glucose oxidase-PSi structures modification. EDX spectra show the major elements within the pores of the thermally oxidized PSiMc structures (I) and after molecular infiltration

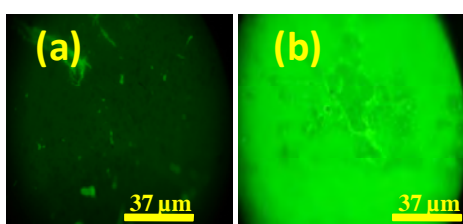


Fig 2. Fluorescence microscopy images of different PSi structures after chemical and biological modification with silane, Glutaraldehyde and GOX at 5.5 μM. The images corresponds at: (a) PSi monolayer, and (d) PSi microcavity (excitation wavelength 450 nm, 40X objective and 162 X 125 μm images size).

# Mode-Locked Fiber Laser based on Nitrogen Doped Carbon Nanotubes

I. Hernandez-Romano<sup>1</sup>, E. E. Garcia-Espino<sup>2</sup>, D. Hernandez-Cruz<sup>2</sup>,  
D. A. May-Arrijoja<sup>1</sup>, M. Terrones<sup>2</sup>, and J. J. Sanchez-Mondragon<sup>1</sup>

<sup>1</sup> INAOE, Optics Dept., Apdo. Postal 51 y 216, Tonantzintla, Puebla 72000, Mexico

<sup>2</sup> Advanced Materials Department, IPICYT, San Luis Potosí 78216, México

E-mail: dmay@inaoep.mx

Over the last few years there has been an increasing interest in Carbon Nanotubes (CNTs) both for electronic and photonics applications. From the photonics perspective, the fact that CNTs act as saturable absorbers with ultrafast recovery makes them an ideal material for the realization of passive mode-locking laser [1]. There are a couple of works about CNTs mode-lockers but they are based on single-wall CNTs (SWNTs). In this work we present an all-fiber mode-locking laser using Nitrogen doped CNTs (CNx). The laser was built using a standard ring laser configuration [2], in which we incorporate a microcapillary tube (ferrule). In this ferrule we can insert a single mode fiber (SMF) which has a small section of CNx attached to his facet, and on the other end we insert another SMF to close the ring. The tube is also filled with index matching liquid to lower the reflection when the SMF are separated.

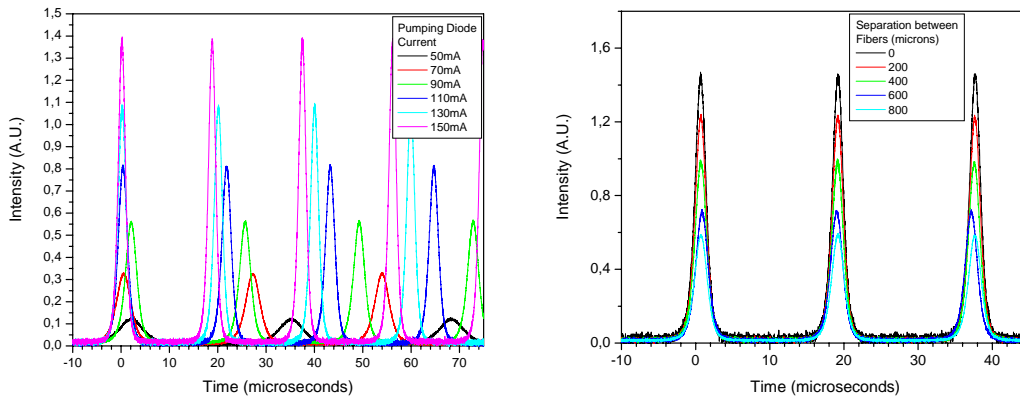


Fig. 1 Pulse train when (a) Pumping current is changed, and (b) Separation between fibers is changed.

Mode-locking is also easily achieved with CNx, and the mode-locking pulses at different pumping powers levels are shown in Fig. 1 (Left). One important feature is that as the power is increased, there is a change in the frequency of the pulses, and this can be relevant for some applications. To correct that we can keep the pumping power at maximum level, and as we separate the SMF within the ferrule losses are introduced to the cavity. This allows us to keep the frequency of the pulses, but still being able to modify the power of our mode-locking laser as shown in Fig. 1 (Right).

1. V. Scardaci et. Al., *Physica E* 37 (2007) 115–118
2. *Optics Express*, Vol. 13, No. 18, September 2005

# Toward solid-state molecular machines: crystalline steroid-based rotors

Rodríguez-Molina, B.<sup>1</sup>; Pozos, A.<sup>2</sup>; Cruz, R.<sup>2</sup>; Farfán, N.<sup>2</sup>; Romero, M.<sup>2</sup>; Méndez-Stivalet<sup>2</sup>, J. M.<sup>2</sup>; García-Garibay, M.A.<sup>3</sup>; Santillan, R.<sup>1\*</sup>

<sup>1</sup>*Departamento de Química, Centro de Investigaciones y Estudios Avanzados del IPN, México, DF.*

<sup>2</sup>*Facultad de Química, Universidad Nacional Autónoma de México, México, DF.*

<sup>3</sup>*Departamento de Química y Bioquímica, Universidad de California, Los Angeles, USA*

\*To whom the correspondence should be addressed: [rsantill@cinvestav.com](mailto:rsantill@cinvestav.com)

Nowadays the synthesis of molecules that emulate the behavior of macroscopic devices has become very popular<sup>1</sup>. We target organic covalent-linked functional structures that resemble macroscopic gyroscopes and compasses<sup>2</sup> (**fig. 1, a**). The inclusion of permanent dipoles in the core (**fig. 1, b**) could allow collective addressable behavior, under the appropriate external stimulus.

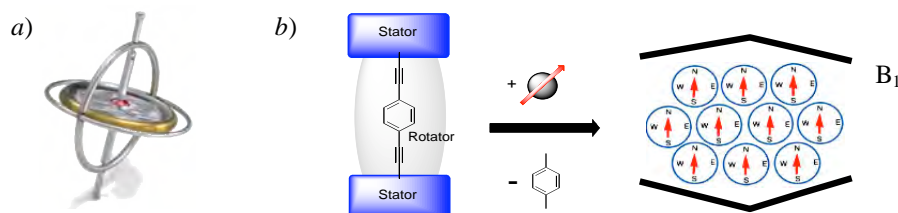


Fig. 1

As their macroscopic counterparts, our organic molecules, known as molecular rotors, are engineered to present mobile parts in the solid state and are highly promising due to their potential applications in optics and photonics<sup>3</sup>.

In the present work, we would like to present the synthesis of steroid-based molecular rotors (**fig. 2, a**). As example, mestranol rotor (**fig. 2, b**) with suitable crystals for X-ray diffraction (**fig. 2, c**) was characterized by VT <sup>13</sup>C CPMAS and VT <sup>2</sup>H spin echo (**fig. 2, d**) ssNMR.

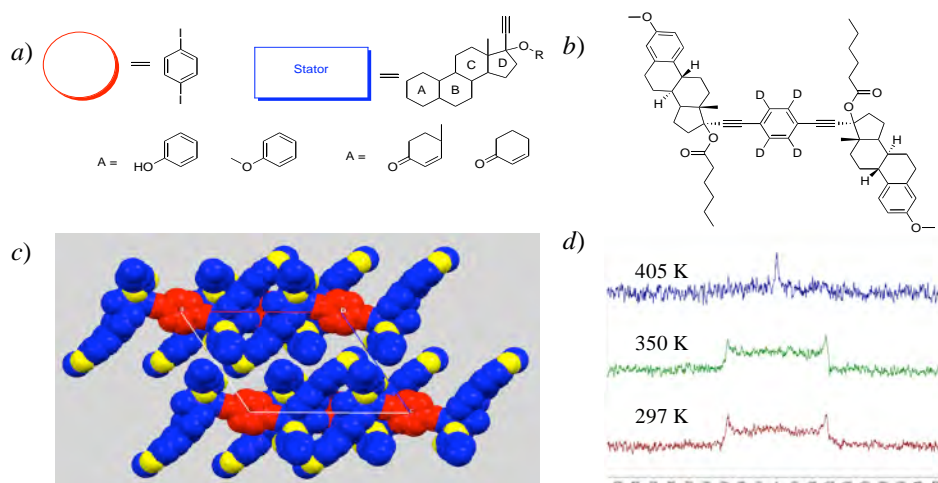


Fig. 2

## References

- 1) Leigh, D. A.; Zerbetto, F.; Kay, E. R.; *Angew. Chem. Int. Ed.* **2007**, *46*, 72–191
- 2) Horansky, R. D; Clarke, L; Winston, E; Price, J. C; Karlen, S. D; Jarowski, P. D; Santillan, R; Garcia-Garibay, M. A; *Phys. Rev. B*, **2006**, *74*, 054306
- 3) Balzani, V.; Credi, A.; Ferrer, B.; Silvi, S.; Venturi, M.; *Top. Curr. Chem.* **2005**, *262*, 1-27

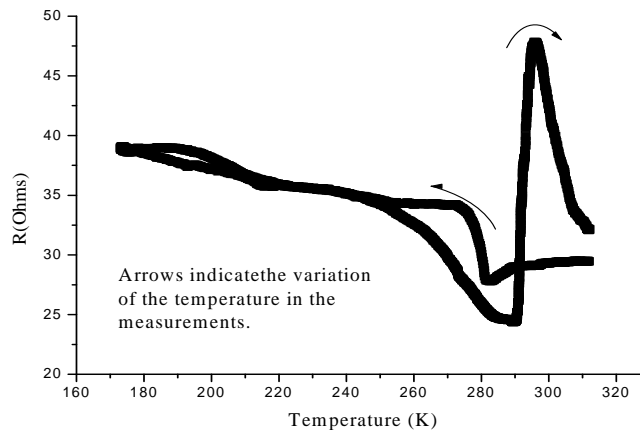
# ELECTRICAL CONDUCTIVITY ANOMALY IN SINGLE WALL CARBON NANOTUBES INDUCED BY WATER

D. Mendoza

Instituto de Investigaciones en Materiales, Universidad Nacional Autónoma de México.

[doroteo@sevidor.unam.mx](mailto:doroteo@sevidor.unam.mx)

Electrical transport properties of single wall carbon nanotubes (SWNT) have been described within the so called liquid Luttiger model for one dimensional systems, in which the electrical resistance follows a power law as a function of temperature. In this case  $R(T) \sim T^{-\alpha}$ , where the value of the exponent ranges between 0.3-0.6 [1] up to 2.2 [2]. In the present work we find a dramatic change in the electrical behavior of SWNT when the measurements are made in an environment of water vapor, such as is shown in the figure.



An hysteretic behavior as a function of temperature and an anomaly around 18°C is observed. We believe this anomaly is related to the charge transfer due to the adsorption of water molecules. A recent study on the interaction of water and SWNT shows that carbon nanotubes present a transition from hydrophilic to hydrophobic character around 18°C [3], which may be related to the anomaly observed in our experiments. In the hydrophilic state, water wets the nanotubes and the charge transfer may be more efficient than in the hydrophobic state. Detailed experiments and a suggested model for the observed anomaly will be present.

[1] M. Bockrath, et al. Nature **397**(1999)598.

[2] Z. Yao, et al. Nature **402**(1999)273.

[3] H. J. Wang, et al. Science **322**(2008)80.

## Effect of water concentration in dopamine occluded in nanostructured silica reservoirs to Parkinson treatment

T. López<sup>1,2,3</sup>, D. Esquivel<sup>4</sup>, E. Ortiz<sup>2</sup>, A. Miguel<sup>1,2</sup>, I. Sánchez-Jerónimo<sup>1,2</sup>

<sup>1</sup>Universidad Autónoma Metropolitana- Xochimilco. Health Attention Department. Calzada del Hueso 1100, C.P. 04960, Tlalpan, México D.F.

<sup>2</sup>Instituto Nacional de Neurología y Neurocirugía "MVS". Nanotechnology-Nanomedicine Laboratory. Insurgentes Sur 3877, Col. La Fama, Tlalpan México D.F.

<sup>4</sup>CIQI, Guanajuato University. Noria Alta s/n, C.P. 36050. Guanajuato, México.

Parkinson's disease (PD) is characterized by the progressive loss of substantia nigra dopaminergic neurons and the presence of cytoplasmic inclusions named Lewy bodies. Up to now only the systemic treatment is L-Dopa (natural precursor of dopamine), because the dopamine is oxidized instantly to dopaquinone. Also, dopamine not crosses the blood-brain-barrier (BBB). It is shown that after five years of treatment with L-Dopa, complications arise due to the fluctuation of the concentration level. Unfortunately, a satisfactory clinical answer has not been achieved. A local brain release reservoir to transport the chemical stabilized dopamine is the aim of this research. The molecule was stabilizing in a new nanostructured and functionalized sol-gel silica reservoir. With the purpose to obtain the adequate doses; in this work we varied the dopamine quantity occludes into SiO<sub>2</sub> reservoirs, solvent and water concentration was varied with the aim of observe the effect of this parameters in the pore size and the in vitro release profile. The SiO<sub>2</sub>-Dopamine systems obtained were characterized by N<sub>2</sub> adsorption and FTIR spectroscopy and then the release profiles were made. By the other hand the brain tissue biocompatibility tests were carried out. The textural analyses show the existence a maximum value of surface area (620 m<sup>2</sup>/g) when SiO<sub>2</sub> contained 25 % wt of dopamine in the mesoporous nanostructured solids. The stability of dopamine into the matrix was probe by FTIR; bands at 2500, 2600 and 2700 cm<sup>-1</sup> are attributed to N-H, C-H and C-O-H vibrations of dopamine. However, the characteristic vibration of  $\text{O-Si-O}^-$  species disappear, indicative to dopamine remain over the surface. Histopathological studies on the SiO<sub>2</sub>-Dopamine system material showed no changes to the tissue nearby. A fast sustained dopamine delivery was observed until 24 hours, after this time the delivery is constant. These results suggest that SiO<sub>2</sub>-Dopamine reservoirs can be a good alternative for treatment of Parkinson disease.

# ACTIVITY OF NANOSTRUCTURED TiO<sub>2</sub> OR SiO<sub>2</sub> BASED BIOCATALYSTS OVER DNA FRAGMENTATION

**T. López<sup>1,2,3</sup>, J. Bustos<sup>1</sup>, M. Alvarez<sup>2</sup>, V. Coria<sup>1</sup>, I. Meza-Mena<sup>1</sup>**

<sup>1a</sup> Departamento de Atención a la Salud, Universidad Autónoma Metropolitana-Xochimilco,  
Calz. Del Hueso 1100, Col. Villa Quietud, Coyoacán, C. P. 04960, D.F. México

<sup>2</sup> Laboratorio de Nanotecnología, Instituto Nacional de Neurología y Neurocirugía “MVS”,  
Insurgentes Sur 3877, Col La Fama, C.P. 14269, D.F. México.

<sup>3</sup> Department of Chemical Engineering, Tulane University, New Orleans, LA 70118

e-mail: tetsy3@prodigy.net.mx

Although cis-platin is a widely used anticancer drug against testicular and ovarian cancers it has a number of well-known side-effects<sup>1,2</sup>. The role of DNA in the control of cellular functions it becomes an excellent target for treating illness of genetic origin such as cancer. Most of antineoplastic drugs act over DNA, preventing cellular replication. Platinum complexes have been used since 1965 to treat cancer<sup>3</sup> and numerous organoplatinum compounds have been synthesized in order to improve its antitumor activity. Although the mechanism of action of these compounds at molecular level is still unclear, it is widely accepted that Pt coordinates to N7 sites of DNA guanine bases to form adducts with both DNA helices after hydrolysis of the Pt-Cl bonds<sup>4</sup>. In the present work, we investigated a set of biocatalysts using nanostructured biocompatible TiO<sub>2</sub> and SiO<sub>2</sub> obtained by the sol gel process, with different platinum complexes (included cisplatin) incorporated during the synthesis. In order to evaluate the interactions between biocatalysts and DNA gel electrophoresis assay was carried out. A DNA solution (500ug/mL) was mixed with 2μL of biocatalyst solution (100mg/500μL) and incubated at different times (0, 15min, 30min, 45min, 1hr, 3hr, 6hr, 12hr and 24hr). Gel electrophoresis results indicate that the most active biocatalysts were Pt(acac)<sub>2</sub>-TiO<sub>2</sub> and H<sub>2</sub>PtCl<sub>6</sub>-TiO<sub>2</sub>. It can then be proposed that the path leading to DNA fragmentation also starts by an attack of an OH linked to Pt. These results show that activity is not restricted to complexes with cis structure.

---

<sup>1</sup> H.M. Pinedo, J.H. Schornagel (Eds.), *Platinum and Other Metal Coordination Compounds in Cancer Chemotherapy 2*, Plenum Press, New York, 1996.

<sup>2</sup> L.X. Cubeddu, I.S. Hoffmann, N.T. Fuenmayor, A.L. Finn, *N. Engl. J. Med.* 322 (1990) 810–816.

<sup>3</sup> Rosenberg, B., VanCamp, L., Trosko, J. E. & Mansour, V. H. Platinum compounds: a new class of potent antitumour agents, *Nature* **222**, 385-6 (1969).

<sup>4</sup> Rabik, C. A. & Dolan, M. E. Molecular mechanisms of resistance and toxicity associated with platinating agents, *Cancer Treatment Reviews* **33**, 9-23 (2007).

## **Molecular dynamic study of the interaction vanadium oxide-HY zeolite**

Maricela Arroyo<sup>1</sup>, I. Pedro Zaragoza<sup>1</sup> and Ruben Santamaria<sup>2</sup>.

<sup>1</sup>*Instituto de Investigaciones en Materiales, Polímeros, Universidad Nacional Autónoma de México, A.P. 70-360, D.F. 045510, México*

<sup>2</sup>*Instituto de Física, Universidad Nacional Autónoma de México, A.P. 20-364, 01000, D.F. México*

The study of the interaction between vanadium oxide and the HY-zeolite using semi-classical molecular dynamics was carried out for two systems: i) when vanadium oxide penetrates the zeolite ring at its center, and ii) when vanadium oxide impacts the zeolite surface. The dynamical effects are used to investigate the reduced activity and eventual degradation of the catalyst for the vanadium oxide presence. In the first case, we observe the breaking of an OH-bond that belongs to the acid site. This is related to an initial destruction stage of the catalyst crystal structure. In the second case, vanadium oxide is adsorbed onto the zeolite surface. Density functional theory, with nonlocal exchange and correlation functionals and basis set of double numerical accuracy, is used to analyze the electronic structure. It was used in combination with Born-Oppenheimer dynamics to perform the calculations.

Keywords: Cracking of HY zeolite, vanadium oxide, molecular dynamics, Density functional theory.

[marroyo@correo.unam.mx](mailto:marroyo@correo.unam.mx)

## **Stabilization of metotrexato in sol-gel biocompatible sol-gel silica to treat brain gliomas**

T. López<sup>1,2,3</sup>, M. Alvarez<sup>1,2</sup>, E. Ortiz-Islas<sup>2</sup>, A. Miguel<sup>2</sup>, I.Sanchez-Jerónimo<sup>2</sup>

<sup>1</sup> *Universidad Autonoma Metropolitana-Xochimilco. Departamento de Microbiología. Calzada del Hueso 1100, Col. Villa Quietud, Coyoacán, C. P. 04960, México D.F,*

[tessy3@prodigy.net.mx](mailto:tessy3@prodigy.net.mx) <sup>2</sup> *Instituto Nacional de Neurología y Neurocirugía "MVS".*

*Laboratorio de Nanotecnología. Av. Insurgentes Sur 3877, Col. La Fama, Tlalpan, 14269, México, D.F.* <sup>3</sup> *Department of Chemical and Biomolecular Engineering, Tulane University,*

*New Orleans LA 70118 USA.*

estrella\_aryliz@hotmail.com

Conventional chemotherapy using Metotrexato (MTX) shows low specificity and selectivity. The undesirable side effects are the main dose limiting factors. In the last two decades, significant advances have been made in the development of biocompatible and biodegradable materials for drug local administration of several medicaments to avoid the side effects. The use inorganic nanomaterials have lead to significant advances in this field when compared to systems currently in use. In particular, biocompatible and nanostructured sol-gel silica derived materials allow the immobilization and stabilization of biologically active compounds. The aim of this kind of materials is to obtain local liberation of chemioterapic agents without secondary effects observed in traditional therapy, bypass the natural barriers and achieve high drug concentrations within the tumor. In this work, we synthesized SiO<sub>2</sub> nanoparticles by the sol-gel method and MTX was added during gelation reaction in order to encapsulate the drug. SEM studies of MTX-SiO<sub>2</sub> showed agglomerates of nanosized particles. Thermogravimetric analysis exhibit endothermic peaks below 100°C due to partial decomposition of the drug and water desorption and another endothermic peak around 250°C corresponding to the loss of residual organic groups and dehydroxylation . Infrared spectra showed bands assigned to -OH groups (3660 and 3600-3200 cm<sup>-1</sup>). Also the characteristic bands due to N-H, C=O and C-H vibrations of MTX/SiO<sub>2</sub> were observed. BET surface areas, mean pore diameter and release profile demonstrates that SiO<sub>2</sub> allow controlled sustained drug delivery in the brain for long-time periods. Biocompatibility of our nanostructured materials was probe in a group of Wistar rats for six months period. The corresponding histopathology studies show no damage in the cells around the nanostructured MTX/SiO<sub>2</sub> material.

## **Biocompatibility analysis nanostructured Pt/TiO<sub>2</sub> by histological techniques of nanostructured titania microinjection in the central nervous system**

T. López<sup>1,2,3</sup>, P. Arteaga-López<sup>1</sup>, L. Aguirre<sup>2</sup>, A. Arellano<sup>2</sup>, J. Avilés<sup>2</sup> and D. Molina<sup>2</sup>

<sup>1</sup>*Universidad Autónoma Metropolitana - Xochimilco, Health Department. Calzada del Hueso 1100, Col. Villa Quietud, Coyoacán, México, 04960.* <sup>2</sup>*Nanotechnology Laboratory, National Institute of Neurology and Neurosurgery “Manuel Velasco Suárez”. Insurgentes Sur 3877, Col. La Fama, Tlalpan, México, 14279.* <sup>3</sup>*Department of Chemical and Biomolecular Engineering, Tulane University, New Orleans, LA 70118.*

e-mail: [tessy3@prodigy.net.mx](mailto:tessy3@prodigy.net.mx)

The innovation in the area of cancer research is focusing the attention to innovative delivery systems and treatments based on nanotechnology devices that will improve the chemotherapeutics results and avoid the side effects. In a previous work we reported that the application of this technologies in the rat model, in those studies we obtained a significative reduction of the tumor size. With the aim to improve this technique in bigger species we used the dog as a model of study.

Adult intact dogs were used and then microinjected with Pt/TiO<sub>2</sub> suspension in the brain by stereotaxic method using the following coordinates: A-20, L-10 and H-20 according to the dog brain stereotaxic atlas (Diva Sharma, 1980 and Lim, 1970). Then the dog was perfused with PFA 4% and the brain with nanoparticles was extracted in cold conditions and stored in glucose/thymersal solution 1% at 4°C for one week. The brain slices were obtained using a cryostat at -17°C, with a grossor thick of 20 mm, then the brain with nanostructured biocatalyst were put in a microscope slide coated with poli-l-lisine (0.1%). The micrographs were taken with a light microscope (Olympus IX81) accopled with a digital camera. The biocompatibility analysis shown that the nanostructured Pt/TiO<sub>2</sub> material microinjected in the brain has not negative effects over the tissue and cell integrity because the histological analysis demonstrates that the membrane and nucleus are normal, the neurons and the membrane are intact. The results confirm those reported previously in our laboratory, when we used the rat brain as an experimental model. In conclusion the Pt/TiO<sub>2</sub> nanomaterial used as a vector for the cancer nanotherapy is secure because it has no effect over the system.

## **Biocompatibility study of criptomelane vs functionalized criptomelane implants in rat brain**

T. Lopez<sup>(a,b,c)</sup>, E. Ortiz-Islas<sup>(a)</sup>, P. Arteaga-López<sup>(b)</sup>, J. Manjarrez<sup>(a)</sup>,  
R. Arroyo<sup>(b)</sup>, M. Alvarez<sup>(a)</sup>, M. Montes<sup>e</sup>, P. Navarro<sup>e</sup> J. A. Odriozola<sup>f</sup>

(a) Instituto Nacional de Neurología y Neurocirugía ‘‘MVS’’, México, DF, México. (b) Depto. Ciencias Biológicas y de la Salud. Universidad Autónoma Metropolitana-Xochimilco, México. (c) Department of Chemical and Biomolecular Engineering, Tulane University, New Orleans. (e) Universidad del País Vasco. Departamento de Química aplicada, España. (f) Instituto de Ciencia de Materiales US-CSIC. Sevilla, España.

e-mail: [emma170@hotmail.com](mailto:emma170@hotmail.com)

Nanomaterials have been promoted as a revolutionary technology for cell and tissue engineering, medical device development, and the encapsulation and delivery of drugs, diagnostics, and genes. Advances in nanotechnology have led to the introduction of many nanomaterials in these areas. For long-term in vivo applications, these materials have to fulfill rigorous biocompatibility and biostability requirements. These should not induce toxicity in the surrounding tissues, and should not damage the local tissue. In the present work synthesized cryptomelane ( $\text{KMn}_8\text{O}_{16}$ ) from different manganese precursors were implanted in Wistar rat brain during one month. Other groups of rats were implanted with functionalized cryptomelane with sulphate and phosphate ions. There was no mortality in any group during the treatment. Thirty day after cryptomelane implant the animals from all groups were anaesthetized and perfused by intercardiac route with a solution of 10% paraformaldehyde in saline solution. Brains were dissected and then freezing in a criostat at  $-17^\circ\text{C}$  to obtain brain slices of 15-20  $\mu\text{m}$  at implant level. The brain slices were stained by Hematoxiline-Eosine method for histological study. A simple histological study showed that the functionalized cryptomelane presents an improvement in the material compatibility when compared with cryptomelane alone because the brain presents serious damage in tissue and cell conformation. But, the functionalized cryptomelane did not affect the tissue and cell integrity but it causes a high cicatrization tissue over the implant and a change in the cell distribution. These results suggest that functionalized cryptomelane materials can have medical applications, specifically for the treatment of cancer. Functionalized-Cryptomelane material is proposed as a photosensitizer in photodynamic therapy.

## **Biocompatibility and efficiency of nanocatalysts M/TiO<sub>2</sub> implanted in brain glioma using stereotaxic surgery**

T. López<sup>1,2,3</sup>, J. Manjarrez<sup>4</sup>, M. Calvillo<sup>5</sup>, E. Martínez<sup>1,2</sup>

<sup>1</sup>Universidad Autónoma Metropolitana - Xochimilco, Health Department. Calzada del Hueso 1100, Col. Villa Quietud, Coyoacán, México, 04960. <sup>2</sup>Nanotechnology Laboratory, National Institute of Neurology and Neurosurgery "Manuel Velasco Suárez". Insurgentes Sur 3877, Col. La Fama, Tlalpan, México, 14279. <sup>3</sup>Department of Chemical and Biomolecular Engineering, Tulane University, New Orleans, LA 70118. <sup>4</sup>Reticular Formation Physiology Laboratory, National Institute of Neurology and Neurosurgery "Manuel Velasco Suárez". Insurgentes Sur 3877, Col. La Fama, Tlalpan, México, 14279. <sup>5</sup>Neurodegenerative Diseases Laboratory, National Institute of Neurology and Neurosurgery "Manuel Velasco Suárez". Insurgentes Sur 3877, Col. La Fama, Tlalpan, México, 14279.

E-mail: [tessy3@prodigy.net.mx](mailto:tessy3@prodigy.net.mx)

Glioblastoma multiforme (GBM) is the most common malignant astrocytoma (World Health Organization [WHO] grade IV). The median survival of patients with GBM is 9 to 12 months. Current standard-of-care therapies include surgery, radiation, and chemotherapy. Recent elucidations of molecular abnormalities underlying glioma pathogenesis has led to several novel therapeutic approaches, which include strategies to enhance delivery of chemical agents into the CNS, such as Gliadel.

In this work nanostructured biocatalysts were implanted with stereotaxic surgery C6 type cells in frontal lobe / cortex of Wistar rats to generate a tumor into the parenchyma tissue. Briefly, the rats were anesthetized with ketamine and xylazine, and place in a Kopf small-animal stereotaxic instrument. The incisor bar was adjusted until the height of lambda and bregma skull points were equal. After confirmation of presence of tumor into the parenchyma, Pt/TiO<sub>2</sub> nanoparticles were put locally by minimum invasion stereotaxic surgery. One month later the rats were scarified to probe the biocompatibility of the functionalized particles. None of them showed any signs of behavioral deficits or infection over the period of the study. The microinjection of nanoparticles not produced any pathological damage in the brain tissue. According to the histopathologic study around the site, it is observed that the neurons are intact. Final tumoral volume was reduced in the follow 21 days measured by histopathologic study.

## Catalytic Nanomedicine: Dispersed Cis-Pt/TiO<sub>2</sub> activity and of support super acid in the model C6 rat Wistar.

T. López<sup>1,2,4</sup>, P. Guevara<sup>3</sup>, I. Sánchez-Jeronimo<sup>2</sup>, J. A. Odriozola<sup>5</sup>

<sup>1</sup>Universidad Autónoma Metropolitana-Xochimilco. Dept. Atención a la salud. Calzada del hueso 1100, C. P. 04960, Tlalpan, México, D. F. <sup>2</sup>Laboratorio de Nanotecnología and, <sup>3</sup>Departamento de Neuroinmunología, Instituto Nacional de Neurología y Neurocirugía "MVS". Insurgentes Sur 3877, México D. F. C. P 14269, México. <sup>4</sup>Chemistry Department and Biochemical Engineering, Tulane University, New Orleans U.S.A. <sup>5</sup>Departamento de Química Inorgánica e Instituto de Ciencia de Materiales de Sevilla, Centro Mixto Universidad de Sevilla-CSIC, Av. Américo Vespucio 49, Sevilla, Spain.

Mesoporous silica materials are promising vehicles for drug delivery applications because they are not cytotoxic, they are taken up by cancer cells, provide a versatile means of carrying a wide variety of drugs into cells; additionally, they are a high surface area, large pore volume, tunable pore size with a narrow distribution, good chemical and/or thermal stability. Cisplatin is one of the mainly active antitumor agents used for GBM central nervous system tumor in clinical treatment in the health sector around the world. However, it has several undesirable side effects such as nephrotoxicity, and nausea and vomiting, myelosuppression, neurotoxicity when is administered systemically. In this work cisplatin was stabilized in nanostructured silica biomaterial of SBA-15 type and studied its effect on rats inoculated with C6 glioma cells. SBA-15 was obtained using Pluronic P123 as structuring agent, which later was removed by calcination in air. Cisplatin was hosted within of the mesopores by immersion techniques. The materials obtained were characterized by DRX, FTIR, BET and TEM. The anti-tumoral activity of these particles, was evaluated in Wistar rats with subcutaneous glioma C6 tumor of 2 cm in diameter, they were randomly allocated in one of four groups: control group (without treatment), SBA-15 group, cisplatin complex group and cisplatin-SBA-15 group. The administration of each particle (10 mg/rat), was once at the beginning of the treatment and 21 days after the average tumor volume was obtained. The results indicate that SBA-15 had a p6mm symmetry with nanotubes packed hexagonally. The BET area was of 885m<sup>2</sup>/g, the pore size of 4.3 nm and the volume of 0.8cc. The average tumor volume (cm<sup>3</sup>) for each group was; Control (mean±s.e./cm<sup>3</sup>) (55.0±9.3; n=18); SBA-15 (49.1± 9.6; n=14); Pt(NH<sub>3</sub>)<sub>4</sub>Cl<sub>2</sub> (28.1±6.2; n=25) and SBA-15/Pt (59.0±8.3 n=21).

---

---

<sup>14</sup> H. Bollinger; "Color chemistry: Synthesis, properties and applications of organics dyes and pigments"; VCH, N.Y., 3<sup>rd</sup> revised ed. (1991).

<sup>15</sup> D. A. Skoog; J. J. Leary; "Análisis Instrumental", 4<sup>o</sup> ed.; Ed. McGraw-Hill, p. 201-219 (1994).

<sup>16</sup> D. L. Pavia, G. M. Lampman, G. S. Kriz; "Introduction to Spectroscopy: A guide for Students of Organic Chemistry", Saunders College Publishing; USA (1979).

<sup>17</sup> Ismael Reyes Torres, "Probable Rectificación en Películas Delgadas de SiO<sub>2</sub> dopadas con Rodamina 6G Y DR1 en Películas Nanoestructuradas de SDS Y CTAB"; Tesis de Licenciatura; Facultad de Ciencias; UNAM (2007).

<sup>18</sup> J. Jens Wolff, Rudinger Wortmann; "Organic materials for non-linear optics: The 2d approach"; J. Prakt. Chem., 99-11 (1998).

<sup>19</sup> Tito Trindade; "Nanocrystalline Semiconductors: Síntesis, Properties and Perspectivas"; Chem Mater. 2001,13,3846-3858 (2001)

<sup>20</sup> K. Sutter, P. J. Günter, "Photorefractive gratings in the organic cristal 2-cyclooctylamino-5-nitropyridine doped with 7, 7, 8, 8-tetracyanoquinodimethane"; Opt. Soc. Am. **7**, 2274-2278 (1990).

<sup>21</sup> Dra. Ma. Guadalupe Valverde Aguilar; "Tesis de maestria Estudio Espectroscopico de Ormosiles y Películas Mesoestructuradas"; (2003).

<sup>22</sup> Laura Angélica Romero Miranda, "Estudio de luminiscencia en películas nanoestructuradas de SiO<sub>2</sub>:DR1 y películas nanoestructuradas de PMMA:DR1, como función de la orientación dipolar por Efecto Corona"; Tesis de Licenciatura; Facultad de Ciencias; UNAM (2007).

<sup>23</sup> A. Sellinger; P. M. Weiss; A. Nguyen; Y. Lu; R. A. Assink; W. Gong; C. J. Brinker; "Continuous self-assembly of organic-inorganic nanocomposite coatings that mimic nacre"; Nature **394**, 256-260 (1998).

<sup>24</sup> J. Reyes-Esqueda, "Estudio de las propiedades ópticas no lineales de materiales sol-gel: la importancia de las interacciones moleculares en el coeficiente electro-óptico y en

---

---

la fotoconducción”; Tesis de Doctorado, Instituto de Física, UNAM (2001).

<sup>25</sup> J. Tauc, R. Grigorovichi, A. Vancu; “Optical properties and electronic structure of amorphous germanium”; *Phys. Status Solidi* **15**, 627-633 (1966).

<sup>26</sup> S. H. Jeong, B. S. Kim, B. T. Lee; “Photoluminescence dependence of ZnO films grown on Si(100) by radio-frequency magnetron sputtering on the growth ambient”; *Appl. Phys. Lett.* **82**, 2625-2627 (2003).

<sup>27</sup> R.B. Kale, Yung-Jung Hsu, Yi-Feng Lin, Shih-Yuan Lu, “Synthesis of stoichiometric flowerlike ZnO nanorods with hundred per cent morphological yield”; *Solid State Communications* **142**, 302-305 (2007).

<sup>28</sup> Y. M. Sun, Tesis Doctoral, University of Science and Technology of China, (2000).

<sup>29</sup> B.J. Jin, S. Im, S.Y. Lee, “Violet and UV luminescence emitted from ZnO thin films grown as sapphire by pulsed laser deposition”; *Thin Solid Films* **366**, 107-110 (2000).

<sup>30</sup> S. Yu, C. Wang, J. Yu, W. Shi, R. Deng, H. Zhang; “Precursor induced synthesis of hierarchical nanostructured ZnO”; *Nanotechnology* **17**, 3607-3612 (2006).

<sup>31</sup> Z.X. Fu, B.X. Lin, G.H. Liao, Z.Q. Yu; “The effect of Zn buffer layer on growth and luminescence of ZnO films deposited on Si substrates”; *J. Cryst. Growth* **193**, 316-321 (1998).

<sup>32</sup> C.L. Jiang, W.Q. Zhang, G.F. Zou, W.C. Yu, Y.T. Qian; “Precursor-induced hydrothermal synthesis of flowerlike cupped-end microrod bundles of ZnO”; *J. Phys. Chem. B* **109**, 1361-1363 (2005).

<sup>33</sup> D. H. Zhang, Z. Y. Xue, Q. P. Wang; “The mechanisms of blue emission from ZnO films deposited on glass substrate by r.f. magnetron sputtering”; *J. Phys. D: Appl. Phys.* **35**, 2837-2840 (2002).

<sup>34</sup> M. N. Kamalasanan, S. Chandra, *Thin Solid Films* **288**, 112-115 (1996).

<sup>35</sup> X. L. Cheng, H. Zhao, L. H. Huo, S. Gao, J. G. Zhao, *ensors and Act. B* **102**, 248-252 (2004).

---

<sup>36</sup> M. S. Tokumoto, V. Briois, C. V. Santilli, S. H. Pulcinelli, J. Sol-gel Sci. & Techn. **26**, 547-551 (2003).

<sup>37</sup> Z. Wang, H. Zhang, Z. Wang, L. Zhang, J. Yuan, J. Mater. Res. **18**, 151-155 (2003).

<sup>38</sup> E. A. Meulenkaamp; "Síntesis and growth of ZnO nanoparticles"; J. Phys. Chem. B **102**, 5566-5572 (1998).